

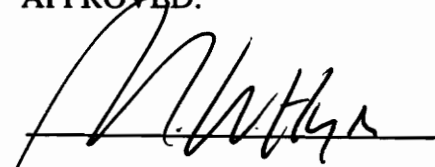
**RESPONSE OF MULTIPLE FASTENER COMPOSITE JOINTS:
NUMERICAL AND EXPERIMENTAL RESULTS**

BY

SESHU R. YALAMANCHILI

Thesis submitted to the Faculty of the
Virginia Polytechnic Institute and State University
in partial fulfillment of the requirements for the degree of
MASTER OF SCIENCE
in
Engineering Mechanics

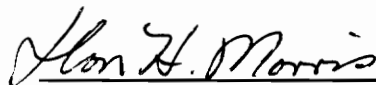
APPROVED:



M.W. HYER (Co-Chairman)



O.H. GRIFFIN, JR. (Co-Chairman)



D.H. MORRIS

May 1992

Blacksburg, Virginia.

C.2

LD
5655
V855
1992
Y342
C.2

RESPONSE OF MULTIPLE FASTENER COMPOSITE JOINTS: NUMERICAL AND EXPERIMENTAL RESULTS

by

Seshu R. Yalamanchili

M.W. Hyer, Co-Chairman

O.H. Griffin, Jr., Co-Chairman

Engineering Mechanics

(ABSTRACT)

The response of flat multiple fastener composite joints with two rows of holes and four different widths was studied. The joint geometry was very specific, and three different laminates were also considered. The laminates were loaded in a double lap fashion with steel laps. Pins were used as fasteners. All the specimens were instrumented with strain gages at critical locations, namely, around the holes. Special pins were used to measure the load reacted by each pin in the joint. This information was used to determine the percentage of the total load reacted by each pin. Most of the specimens were tested to failure, though some specimens were stopped short of failure and examined for damage initiation through X-rays. A finite-element procedure for determining the load proportioning in the multiple-fastener joints was used to complement the experiments. The commercial finite-element program ABAQUS was used to predict the load proportioning among the pins using two independent plane stress finite-element models, one representing the composite specimen, the other representing the steel laps. The models interacted through rigid circular surfaces representing the steel pins. Excellent correlation was obtained between experiments and analysis for the percentage load proportioning. For the strains, the correlation between ex-

periments and predictions was found to be excellent around the net-section region. Although predictions for other strains were not as good, they were within the range of experimental data. Distribution of contact stresses between the pins and the hole edges was also studied. Numerical analysis suggests that the prevalent assumption of radial cosine distribution of contact stress between the pin and hole edge is in substantial error. It can also be concluded that the strength of the joint is for the most part, independent of its width, though for narrower specimens, the holes were quite highly loaded.

ACKNOWLEDGEMENTS

I must first of all acknowledge the support and encouragement that my parents and my sister have given, despite being on the on the other side of the world. Without their constant encouragement this project would not have been possible. I sincerely appreciate Prof. Michael Hyer's patience in correcting my blunders and providing constant support. I also appreciate the efforts of my co-advisor Dr. O. H. Griffin, Jr. in making this study comprehensive. Dr. David Cohen of the Hercules Aerospace, Inc, has been supportive as a grant monitor, and in an advisory manner with my research. I would like to express my appreciation for funding (PO ARIB09403 with Virginia Tech) and specimen fabrication and machining for this effort from Hercules Aerospace, Inc., Bacchus Works. Also, I would like to thank Dr. Mark Shuart and Dr. C. B. Prasad of Aircraft Structures Branch at NASA-Langley Research Center for their help in instrumenting and testing of specimens. I appreciate the willingness of Prof. Don Morris , to serve on my committee and his help in reviewing my thesis. I would like to thank Mara Knott and Paula K. Davis for providing cheerful help many times. My fellow office-mates and other members of Composite Mechanics Group have been great friends, offering lots of encouragement.

TABLE OF CONTENTS

ABSTRACT..... ii

ACKNOWLEDGEMENTS.....iv

TABLE OF CONTENTS..... v

LIST OF FIGURES vii

LIST OF TABLES.....xiii

1.0 INTRODUCTION, LITERATURE REVIEW, AND OBJECTIVES 1

1.1 Introduction 1

1.2 Objectives and Approach of Present Study 6

1.3 Literature Review 11

2.0 EXPERIMENTAL SET-UP 17

2.1 Introduction 17

2.2 Specimen Preparation 18

2.3 Fixture and Testing Machine..... 19

2.4 Experimental Procedure..... 30

3.0 FINITE ELEMENT MODELING..... 32

3.1 Introduction 32

3.2 Model Description 32

3.3 Preliminary Results 40

4.0 DISCUSSION OF NUMERICAL AND EXPERIMENTAL RESULTS 46

4.1 Summary of Failure Results 46

4.2 Load Share Between the Pins 55

4.2.1 Inboard vs. Outboard Half-Hole Location 63

4.2.2 Comparison of Three Laminates 63

4.3 Strain Gage Measurements 68

4.3.1 Discussion of the 5-hole Load vs. Strain Relations and Comparisons between Inboard and Outboard Specimens 70

4.3.2 Comparisons among the Three Laminates 82

5.0 FURTHER NUMERICAL RESULTS..... 95

5.1 Introduction 95

5.2 Description of Stress Calculations..... 96

5.3 3-Hole Specimen Results..... 97

5.4 5-Hole Specimen Results 107

5.5 7-Hole Specimen Results..... 114

5.6 9-Hole Specimen Results..... 123

5.7 Summary 123

6.0 SUMMARY AND RECOMMENDATIONS..... 131

REFERENCES 136

APPENDIX A: STRAIN GAGE RESULTS FOR THE 3-HOLE SPECIMENS 139

APPENDIX B: STRAIN GAGE RESULTS FOR THE 7-HOLE SPECIMENS 144

APPENDIX C: STRAIN GAGE RESULTS FOR THE 9-HOLE SPECIMENS 168

VITA 175

LIST OF FIGURES

Figure 1.1 Cylindrical Joint.. 4

Figure 1.2 Dimensions of 3-hole and 9-hole specimens.. 7

Figure 1.3 Dimensions of 5-hole and 7-hole specimens.. 8

Figure 2.1 Schematic of a typical strain gage pattern for a 5-hole specimen. 20

Figure 2.2 Photograph of a typical strain gage pattern for a 5-hole specimen. 21

Figure 2.3 One-, 3-, 5-, 7-, and 9-hole specimens after stain gage installation. 22

Figure 2.4 Details of the instrumentation for the pin. 24

Figure 2.5 Photograph of instrumented pin. 25

Figure 2.6. Dimensional details of the steel laps for 3- and 7-hole inboard specimens 26

Figure 2.7 Dimensional details of the steel laps for 5- and 9- hole inboard specimens. 27

Figure 2.8 Specimen, steel laps, and clevis assembly. 28

Figure 2.9 Photograph of experimental set-up. 29

Figure 3.1 Quarter-model of steel laps and composite specimen. 33

Figure 3.2 Representation of the CPS8 element 34

Figure 3.3 Interaction of steel lap and composite specimen 36

Figure 3.4 Finite-element model of a 3-hole inboard specimen. 37

Figure 3.5 Deformed mesh of a 3-hole inboard specimen model 41

Figure 3.6 Deformed mesh of a 5-hole inboard specimen model 42

Figure 3.7 Deformed mesh of a 7-hole inboard specimen model. 43

Figure 3.8 Deformed mesh of a 7-hole outboard specimen model. 44

Figure 4.1 A 3-hole T45 inboard specimen after failure..... 47

Figure 4.2 A 5-hole T45 outboard specimen after failure..... 48

Figure 4.3 A 7-hole T45 outboard specimen after failure..... 49

Figure 4.4 A 9-hole T45 inboard specimen after failure..... 50

Figure 4.5 X-ray photograph of a failed 5-hole T45 inboard specimen. 53

Figure 4.6 X-ray photograph of a 5-hole T45 inboard specimen loaded to 95% of failure
load. 54

Figure 4.7 Hole numbering patterns for different specimens..... 57

Figure 4.8 Pin bending strains for pins of a 5-hole T45 inboard specimen 58

Figure 4.9 Percentage load sharing for a 5-hole T45 inboard specimen with nonconstant
load proportion 60

Figure 4.10 Percentage load sharing for a 5-hole T45 outboard specimen with load propor-
tion reversal. 61

Figure 4.11 Percentage load sharing for a 5-hole T45 inboard specimen with constant load
proportion 62

Figure 4.12 Experimentally measured load proportions for 5-hole T45 specimens..... 64

Figure 4.13 Experimentally measured load proportions for 7-hole T45 specimens..... 65

Figure 4.14 Experimentally measured load proportions for 5-hole T30, T45, and T60 in-
board specimens.. 66

Figure 4.15 Experimentally measured load proportions for 7-hole T30, T45, and T60 in-
board specimens..... 67

Figure 4.16 Strain gage numbering scheme for 5-hole inboard specimens 71

Figure 4.17 Measured and predicted net-section gage strains for 5-hole T45 inboard speci-
mens 72

Figure 4.18 Measured and predicted shear gage strains for 5-hole T45 inboard specimens ... 75

Figure 4.19 Measured and predicted bearing gage strains for 5-hole T45 inboard speci-
mens 76

Figure 4.20 Strain gage numbering scheme for 5-hole outboard specimens. 78

Figure 4.21	Measured and predicted net-section gage strains for 5-hole T45 outboard specimens	79
Figure 4.22	Measured and predicted shear gage strains for 5-hole T45 outboard specimens	80
Figure 4.23	Measured and predicted bearing gage strains for 5-hole T45 outboard specimens	81
Figure 4.24	Measured and predicted net-section gage strains for 5-hole T30 inboard specimens	83
Figure 4.25	Measured and predicted net-section gage strains for 5-hole T60 inboard specimens	84
Figure 4.26	Measured and predicted shear gage strains for 5-hole T30 inboard specimens ...	85
Figure 4.27	Measured and predicted bearing gage strains for 5-hole T30 inboard specimens	86
Figure 4.28	Measured and predicted shear gage strains for 5-hole T60 inboard specimens.....	88
Figure 4.29	Measured and predicted bearing gage strains for 5-hole T60 inboard specimens	89
Figure 4.30	Normalized joint failure loads for 3-, 5-, 7-, and 9-hole T45 specimens.	90
Figure 4.31	Comparison between 5- and 7-hole specimen joint strengths for T45, T30, and T60 specimens	91
Figure 4.32	Comparison between inboard and outboard joint strengths for 5- and 7-hole specimens.	92
Figure 5.1	Distribution of radial stress $\bar{\sigma}_r$ for 3-hole T30 inboard specimen	98
Figure 5.2	Distribution of radial stress $\bar{\sigma}_r$ for 3-hole T45 inboard specimen	99
Figure 5.3	Distribution of radial stress $\bar{\sigma}_r$ for 3-hole T60 inboard specimen	100
Figure 5.4	Distribution of circumferential stress $\bar{\sigma}_\theta$ for 3-hole T30 inboard specimen ...	101
Figure 5.5	Distribution of circumferential stress $\bar{\sigma}_\theta$ for 3-hole T45 inboard specimen	102
Figure 5.6	Distribution of circumferential stress $\bar{\sigma}_\theta$ for 3-hole T60 inboard specimen. ...	103
Figure 5.7	Distribution of radial stress $\bar{\sigma}_r$ for 5-hole T30 inboard specimen	108

Figure 5.8	Distribution of radial stress $\bar{\sigma}_r$ for 5-hole T45 inboard specimen	109
Figure 5.9	Distribution of radial stress $\bar{\sigma}_r$ for 5-hole T60 inboard specimen	110
Figure 5.10	Distribution of circumferential stress $\bar{\sigma}_\theta$ for 5-hole T30 inboard specimen . . .	111
Figure 5.11	Distribution of circumferential stress $\bar{\sigma}_\theta$ for 5-hole T45 inboard specimen. . . .	112
Figure 5.12	Distribution of circumferential stress $\bar{\sigma}_\theta$ for 5-hole T60 inboard specimen. . . .	113
Figure 5.13	Distribution of radial stress $\bar{\sigma}_r$ for 7-hole T30 inboard specimen	115
Figure 5.14	Distribution of radial stress $\bar{\sigma}_r$ for 7-hole T45 inboard specimen	116
Figure 5.15	Distribution of radial stress $\bar{\sigma}_r$ for 7-hole T60 inboard specimen	117
Figure 5.16	Distribution of circumferential stress $\bar{\sigma}_\theta$ for 7-hole T30 inboard specimen. . . .	118
Figure 5.17	Distribution of circumferential stress $\bar{\sigma}_\theta$ for 7-hole T45 inboard specimen. . . .	119
Figure 5.18	Distribution of circumferential stress $\bar{\sigma}_\theta$ for 7-hole T60 inboard specimen. . . .	120
Figure 5.19	Distribution of radial stress $\bar{\sigma}_r$ for 7-hole T45 outboard specimen	121
Figure 5.20	Distribution of circumferential stress $\bar{\sigma}_\theta$ for 7-hole T45 outboard specimen. . .	122
Figure 5.21	Distribution of radial stress $\bar{\sigma}_r$ for 9-hole T30 inboard specimen	124
Figure 5.22	Distribution of radial stress $\bar{\sigma}_r$ for 9-hole T45 inboard specimen	125
Figure 5.23	Distribution of radial stress $\bar{\sigma}_r$ for 9-hole T60 inboard specimen	126
Figure 5.24	Distribution of circumferential stress $\bar{\sigma}_\theta$ for 9-hole T30 inboard specimen. . . .	127
Figure 5.25	Distribution of circumferential stress $\bar{\sigma}_\theta$ for 9-hole T45 inboard specimen. . . .	128
Figure 5.26	Distribution of circumferential stress $\bar{\sigma}_\theta$ for 9-hole T60 inboard specimen. . . .	129
Figure A.1	Strain gage numbering scheme for 3-hole inboard specimens	140
Figure A.2	Measured and predicted net-section gage strains for 3-hole T45 inboard specimens	141
Figure A.3	Measured and predicted shear gage strains for 3-hole T45 inboard specimens	142
Figure A.4	Measured and predicted bearing gage strains for 3-hole T45 inboard specimens	143

Figure B.1	Strain gage numbering scheme for 7-hole inboard specimens	146
Figure B.2	Measured and predicted net-section gage strains for 7-hole T45 inboard specimens	147
Figure B.3	Measured and predicted net-section gage strains for 7-hole T45 inboard specimens	148
Figure B.4	Measured and predicted shear gage strains for 7-hole T45 inboard specimens	149
Figure B.5	Measured and predicted shear gage strains for 7-hole T45 inboard specimens	150
Figure B.6	Measured and predicted bearing gage strains for 7-hole T45 inboard specimens	151
Figure B.7	Measured and predicted net-section gage strains for 7-hole T30 inboard specimens	152
Figure B.8	Measured and predicted net-section gage strains for 7-hole T30 inboard specimens	153
Figure B.9	Measured and predicted net-section gage strains for 7-hole T60 inboard specimens	154
Figure B.10	Measured and predicted net-section gage strains for 7-hole T60 inboard specimens	155
Figure B.11	Measured and predicted shear gage strains for 7-hole T30 inboard specimens	156
Figure B.12	Measured and predicted shear gage strains for 7-hole T30 inboard specimens	157
Figure B.13	Measured and predicted shear gage strains for 7-hole T60 inboard specimens	158
Figure B.14	Measured and predicted shear gage strains for 7-hole T60 inboard specimens	159
Figure B.15	Measured and predicted bearing gage strains for 7-hole T30 inboard specimens	160
Figure B.16	Measured and predicted bearing gage strains for 7-hole T60 inboard specimens	161
Figure B.17	Strain gage numbering scheme for 7-hole outboard specimens	162

Figure B.18 Measured and predicted net-section gage strains for 7-hole T45 outboard specimens 163

Figure B.19 Measured and predicted net-section gage strains for 7-hole T45 outboard specimens 164

Figure B.20 Measured and predicted shear gage strains for 7-hole T45 outboard specimens 165

Figure B.21 Measured and predicted shear gage strains for 7-hole T45 outboard specimens 166

Figure B.22 Measured and predicted bearing gage strains for 7-hole T45 outboard specimens 167

Figure C.1 Strain gage numbering scheme for 9-hole inboard specimens 169

Figure C.2 Measured and predicted net-section gage strains for 9-hole T45 inboard specimens 170

Figure C.3 Measured and predicted net-section gage strains for 9-hole T45 inboard specimens 171

Figure C.4 Measured and predicted shear gage strains for 9-hole T45 inboard specimens 172

Figure C.5 Measured and predicted shear gage strains for 9-hole T45 inboard specimens 173

Figure C.6 Measured and predicted bearing gage strains for 9-hole T45 inboard specimens 174

LIST OF TABLES

Table 1.1 Layup Sequence Information for 3 Laminates 10

Table 2.1 Multiple Fastener Joint Test Matrix 18

Table 3.1 Smeared Engineering Properties of the Three Laminates 39

Table 4.1 Summary of Multiple Fastener Joint Tests..... 52

Table 4.2 Pin Load Shares for Different Joints of T45 Laminate: Numerical vs. Experimental 56

Table 4.3 Pin Load Shares for 5-, 7-hole Inboard Specimens, Comparison of Three Laminates 68

1.0 INTRODUCTION, LITERATURE REVIEW, AND OBJECTIVES

1.1 Introduction

Because of the obvious advantages of high specific strength, high specific stiffness, and tailorability, composites are being considered for extensive use in structures, particularly in large scale structures. As it is not practical to make the entire structure in one piece, it is imperative to join the different segments of the structure through efficient joints. Joining of composites has been one of the weak links in large scale composite structures. Use of bonded joints is limited by the problems associated with inspection of the integrity of the bond for large load capacity joints, and complications involved in disassembly. This leaves the designer with the only other option, namely that of relying on mechanical fastening using pins or bolts. The present work deals with large-scale composite joints which rely on mechanical fasteners, in particular, pins.

When large loads are involved, high load concentrations in the joints can be avoided by having multiple fasteners in multiple rows. Rocket booster casings, deep submergence pressure hulls, and splices in the primary structure of aircraft are but a few of the numerous applications of this kind of joints. In these applications the loads may be as simple as pure tension, or the joint may be subjected to combined loads. Whichever the case, the complex joint geometries lead to multiaxial stress states, stress concentrations, and a number of other

complicating features in the material around the hole. The major challenge for the designer is to predict, in the presence of these complicating features, the limits of joints designed for large load capacities. Additionally, for the designer and the composites community at large, it is necessary to verify these predictions. With composite materials, knowing the limit load means not only knowing the magnitude of the load, but also the failure mode at the limit load. Though both the prediction and verification of joint design are important, verification of full-scale prototype design could be impossible. For applications like the aforementioned, the loads required are generally beyond the capacity of most existing testing equipment. In addition, the cost of fabricating full-scale test articles for empirical parameter studies would be prohibitive. Testing of scaled components is an option. However, scaling laws for strength calculations are not fully developed at this time, though work is being done. One of the recent works by Kellas and Morton¹ reported only limited success in the prediction of full scale strength, despite other encouraging results. For joints, the role of hole diameter, hole spacing, laminate thickness, laminate properties, and other geometric and material properties in scaling need to be fully understood for the realistic testing of sub-scale joints. This present work addresses another option to full scale testing, namely, the testing of segments of a full-scale joint, and then translating the results from the testing of segments to the determination of the capacity of the full joint. Here the studies focus on the segments. The translation to full-scale results is not addressed. In addition, the work here addresses a specific joint. However, the concepts can be applied to other situations, and as will be seen, there are many interesting results even though the study is limited to segments.

The specific joint at hand was a design posed by Hercules Aerospace Company, under their Advanced Case Technology-Failure Criterion/Joint IR&D 91105-5 Program. This program is involved in the design of large, multiple-segment rocket boosters. The primary

task of the program is to understand and predict the strength of a cylindrical joint like the one shown in fig. 1.1. In this figure, one of the two cylinders to be joined is shown. The end of this cylinder is to be joined to the end of another cylinder by butting the two cylinders together. As can be seen in the fig. 1.1, in the enlarged detailed view, the specific joint being investigated here has two rows of holes. Also, it can be seen that the two rows are offset, or staggered, relative each other. Cylindrical inner and outer steel laps, acting in a double lap fashion, with multiple fasteners extending through the cylinder walls, join the two cylinders. Single-fastener composite joints typically exhibit one of three primary failure modes: shearout, bearing, or net tension. Multiple-fastener joint failures, however, tend to occur from a combination of the above modes. These modes of failure are complex and often are not readily determined by simple analytical approaches. Many issues are involved, both in formulating the analytical or numerical model, and in determining how values of joint parameters such as material properties, hole diameter, hole spacing, and load proportioning among the holes influence joint response. For the particular joints under consideration, the inner and outer laps are also important to the problem. The compliance of these laps could control the percentage of total load reacted by each fastener in the joint. Joint performance and failure depend on all of these factors, some having more influence than others.

For the joint under consideration, because only segments are being considered, there is another important issue. Testing of segments of a cylinder raises the important issue of specimen width. How large should the included angle be to accurately represent the stress state in the complete cylinder? Stated differently, how many holes should the specimen include? In a complete cylinder, the joint is essentially of infinite width. When testing a segment of the cylinder, the specimen width is finite. There are boundaries present in a finite-

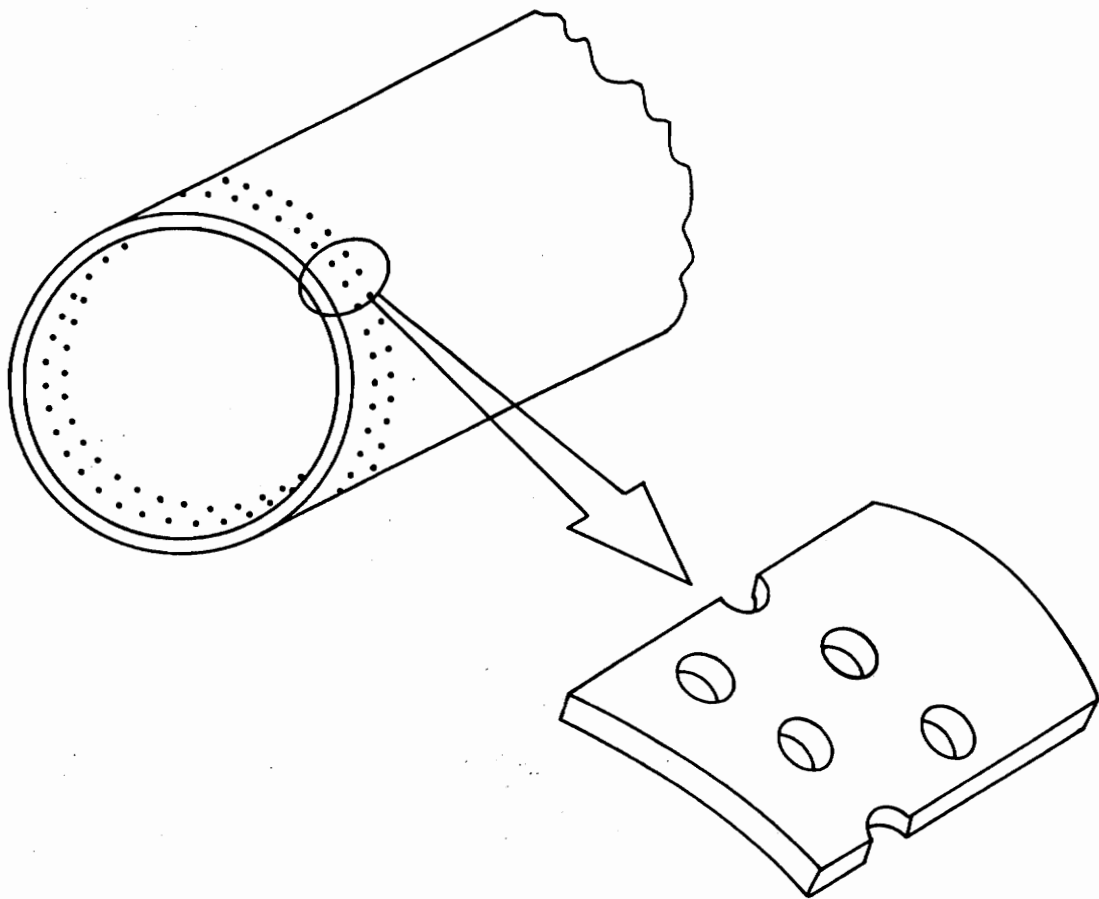


Figure 1.1. Cylindrical joint

width specimen that are not present in a complete cylinder. There may be a bias to the stress state because of these boundaries. It is important to know how failure data gathered from finite-width specimens with specific geometric characteristics translate to failure predictions for complete cylinders. Determination of the stresses in finite-width multiple-hole specimens, and understanding how the number of fasteners influence the stresses, are important in addressing this issue. Though the need for large load frame capacities is eliminated with the testing of segments rather than the complete cylinder, and though the cost for specimen preparation is but a fraction of cost for a complete cylinder, curvature in the segment poses another difficulty. Fabrication of curved test specimens and design of a test fixture to ensure the loads are being properly transmitted to the specimen, add to the complexity and cost of the problem.

In summary, design of multiple-fastener joints for applications such as the joining of cylindrical segments is a many-faceted problem involving analysis and testing. Analysis is necessary for estimating the state of stress in the vicinity of the fasteners for the expected loading conditions. With the particular joints under consideration, inclusion of the effects of the inner and outer laps is important. In the past, these portions of a joint have not generally been included in the analysis. Inclusion of these components would mark an advancement of the state of analysis. The testing is necessary to verify the analysis. Since it is not practical, nor perhaps even possible, to test the complete cylindrical joints, the testing of segments represents an important alternative. Testing issues include the number of holes in the segment, as well as how to accommodate the curvature.

1.2 Objectives and Approach of Present Study

For the present study, inclusion of curvature is felt to be an unnecessary complicating feature. The issue of determining the stresses in double-lapped multiple-hole joints can still be pursued with a flat specimen, as well as the issue of determining the influence of the number of fasteners in a specimen. Clearly, if one cannot predict the stresses in a flat specimen, changing the geometry by making it curved will not make up for the lack understanding. Thus, the philosophy being used here is to concentrate on flat specimens.

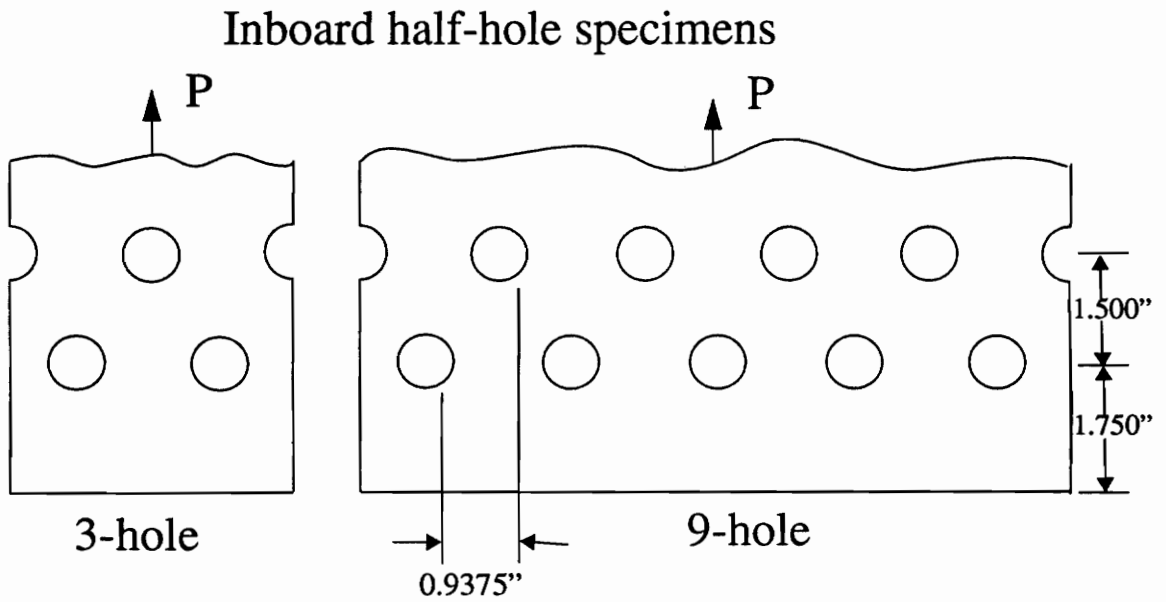
The primary objectives for the current work are to:

a. Develop an analysis to determine the state of stress in multiple-fastener double lapped specimens. The double laps will be included as part of this analysis, and the proportion of load reacted by each fastener will be determined. This information can be used in a failure analysis.

b. Verify the predictions of the analysis by conducting experiments. Key responses will be measured and compared with predictions, including the proportioning of the total load.

c. Using both the analytical and the experimental results, determine the influence of specimen width on the stresses in the joint, and determine the minimum specimen width that can be used represent the response of the complete cylindrical joint, yet provide accurate information regarding failure.

To accomplish these objectives, particularly the establishment of the width of flat multiple-fastener joint that can be used for failure prediction of complete joint, four specimen widths were considered. These four different widths are shown in figures 1.2 and 1.3. In



(Note: All the holes are of $0.750''$ diameter, and all specimens are $1.008''$ thick)

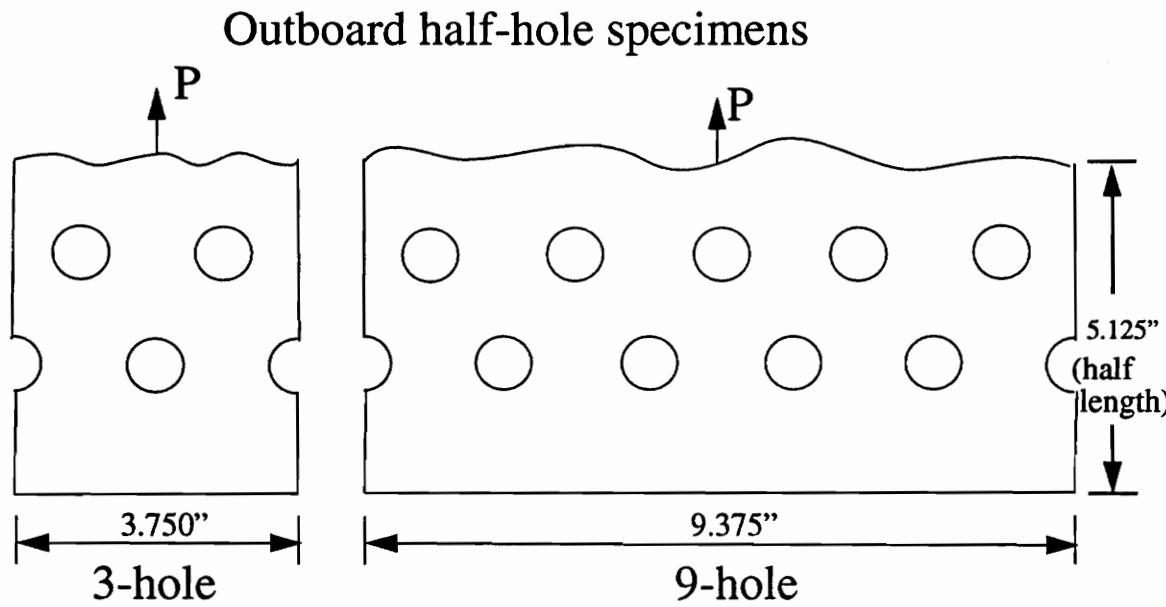
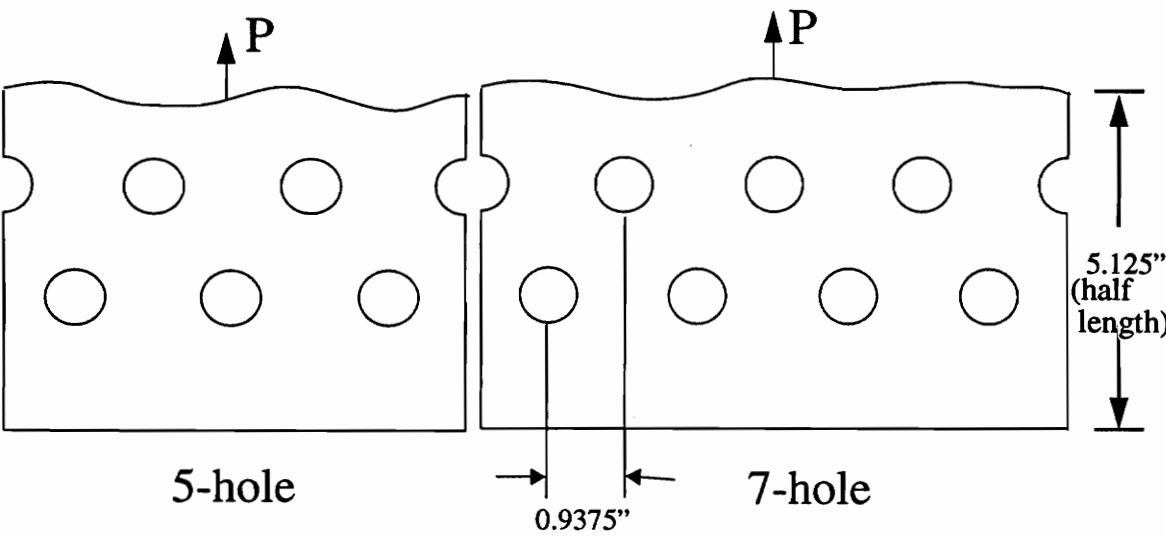


Fig. 1.2. Dimensions of 3-hole and 9-hole specimens



(Note: All the holes are of 0.750" diameter, and all specimens are 1.008" thick)

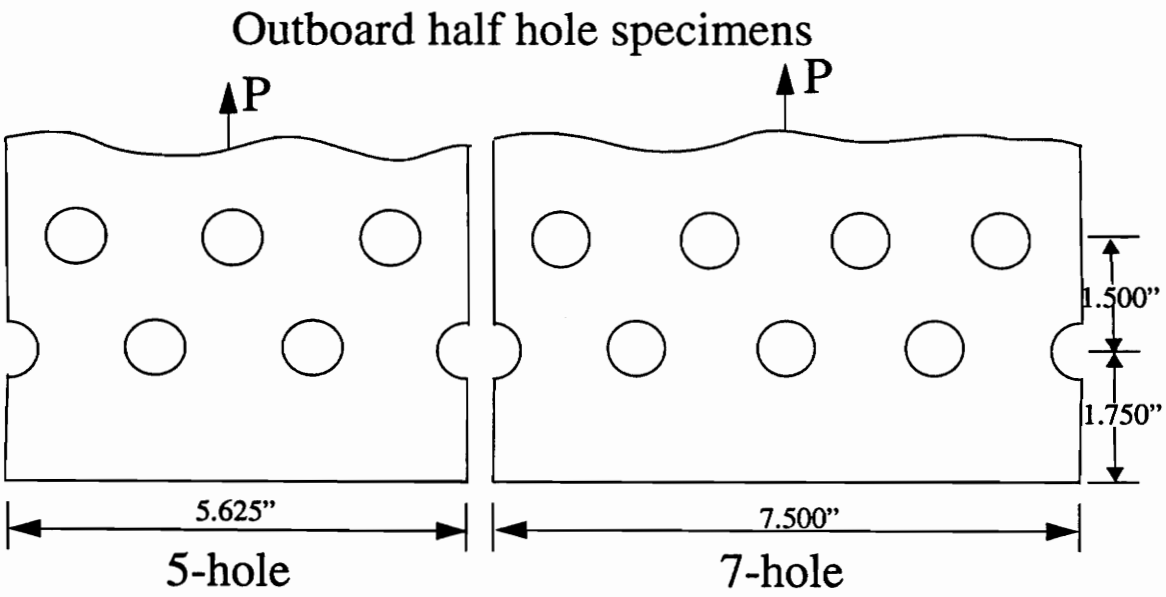


Fig. 1.3. Dimensions of 5-hole and 7-hole specimens

these figures, only one end of the joint specimens is shown. The other end of each specimen (i.e., the top end) is identical. The widths are indicated by the number of complete holes included in each end of the specimen namely, 3-hole, 5-hole, 7-hole, and 9-hole. The odd number of holes is the result of staggered rows. The staggering also results in an unloaded half hole on either the inboard or outboard row of the hole. Note that the term 'outboard row' refers to the row closest to the end, while the term 'inboard row' refers to the other row. Having half holes in either the outboard row or the inboard row means that for each width of the specimen, it is possible to have two different geometries. One geometry would have the unloaded half hole on the inboard row, the other geometry would have the unloaded half hole on the outboard row. The analysis and testing concentrated on specimens with the half hole on the inboard row (hereafter referred as inboard specimens), though a few specimens having the half hole on the outboard row (referred to as outboard specimens) were also tested to observe the effect of half hole location. Nomenclature, geometry, and dimensions of the specimens are shown in figures 1.2 and, 1.3. In fig. 1.2 one end of a 3-hole and one end of a 9-hole specimen for both inboard and outboard half hole configurations are shown. In fig. 1.3 one end of the 5-hole and one end of the 7-hole specimens are shown for both half-hole configurations. As seen, the specimen width varied from 3.750 in. (3-hole) to 9.375 in. (9-hole). The hole diameters were 0.750 in. The width-wise distance between holes was 0.938 in. and the lengthwise distance was 1.500 in. The distance from the center of the outboard row of holes to the end of the specimen was 1.750 in. The specimens were 1.008 in. thick. The overall length of each specimen was 10.250 in.

Three different laminate layups were considered. Stacking sequence and percentage content of plies of each angle are shown in Table 1. 1. As indicated, the laminate denoted as T45 is dominated by $\pm 45^\circ$ plies, and the laminates denoted as T60 and T30 by $\pm 60^\circ$ and

$\pm 30^\circ$ plies, respectively. The subscript R6 indicates there are 6 repeats of the sublaminates in the layup sequence.

Table 1. 1. Layup Sequence Information for 3 Laminates

T45: $\{[(\pm 15^\circ)_3 / 90^\circ_2 / 0^\circ / \pm 45^\circ / 0^\circ / \pm 45^\circ / 0^\circ / \pm 45^\circ / 0^\circ / \pm 45^\circ / 0^\circ / 90^\circ_3]_{R6} / (\pm 15^\circ)_3\}$				
T60: $\{[(\pm 15^\circ)_3 / 90^\circ_2 / 0^\circ / \pm 60^\circ / 0^\circ / \pm 60^\circ / 0^\circ / \pm 60^\circ / 0^\circ / \pm 60^\circ / 0^\circ / 90^\circ_3]_{R6} / (\pm 15^\circ)_3\}$				
T30: $\{[(\pm 15^\circ)_3 / 90^\circ_2 / 0^\circ / \pm 30^\circ / 0^\circ / \pm 30^\circ / 0^\circ / \pm 30^\circ / 0^\circ / \pm 30^\circ / 0^\circ / 90^\circ_3]_{R6} / (\pm 15^\circ)_3\}$				
Fiber Orientation	Total number of plies	Ply Thickness (in.)	Total Thickness (in.)	Fiber Orientation (%)
$\pm 15^\circ$	42	0.006	0.252	25
90°	30	0.006	0.180	18
$\pm \theta^\circ$	60	0.006	0.360	36
0°	36	0.006	0.216	21
Total	168		1.008	100

The stresses are computed by considering both the composite and the steel inner and outer laps. The pins connecting the two laps are also considered in the analysis. For the multiple-hole joints, as mentioned before, such an analysis has not been conducted before. The analysis here properly accounts for the influence of the compliance of both the steel laps and the composite on the proportioning of load reacted by each hole. In addition, no a priori assumption is made regarding the distribution of the stresses due to the pin contacting the hole. These contact stresses are determined by the interaction between the steel laps and the composite, the percentage of load reacted by each hole, by the influence of neighboring holes, and the influence of the joint boundaries. The analysis is based on the commercially available finite element code ABAQUS².

To study the accuracy of the analysis, computed strains are compared with strains mea-

sured in a series of experiments. Also, the percentage of total load shared by each pin is estimated from experimental data by specially instrumented pins, and this percentage is compared with finite element predictions.

Finally, to study the influence of joint width on joint response, and to some degree on failure, the stresses as computed from the finite element analysis, and the strains and failure loads as measured in the experiments, are examined and compared on the basis of joint width.

To follow is a review of some of the important literature regarding mechanically fastened joints. Some of the early work is included for an historical perspective.

1.3 Literature Review

A vast amount of literature is available regarding single-hole bolted or pinned joints. Not much work is reported on the issues pertinent to multiple-hole joints, namely the load distribution between the holes and the interaction between different holes. The focus of the present review will be on what work has been done on multiple-hole joints.

Although work on single-hole joints can be traced to as far back as 1928, studies of multiple-hole joints were not reported until late seventies. Pyner and Matthews³ were among the first to report on multiple-hole composite joints. They experimentally investigated the strength of multiple-hole joints for a variety of geometries, and compared the results to the strength of single-hole joints. They found that hole interaction effects became significant in multiple-bolt connectors if specimen and bolt spacing dimensions were selected such that single-bolt bearing strengths could not be achieved. They concluded that the load capacity per bolt decreases as the geometry becomes increasingly complex. They

also concluded that strength data determined from tests on single-hole specimens becomes less relevant when applied to joints of increasing complexity. Although this study provided insight into the response of multiple-hole joints, it failed to address some important issues. For instance, no investigation was done on the load sharing of each row when there was more than one row transverse to the load direction. Also, load sharing between the holes was not studied when the rows were staggered with respect to each other. The reported average maximum load per bolt did not provide a clear picture of load sharing and the interaction between the holes.

Hart-Smith^{4,5} presented a study, the main objective of which was to determine the nature of the stress interactions in a multiple-bolt joint. He concluded that multiple-bolt joints have increased strength relative to single-bolt joints only when bearing failure governs. Hart-Smith further concluded that a direct superposition of stress fields caused by the individual holes can be assumed in tensile loading cases. Hart-Smith also concluded that the capacities of the joints with bolts are about twice that of joints with simple pins.

Wong and Matthews⁶ carried out two-dimensional finite-element analyses of single and two-hole bolted joints, and compared the results with experiments. Like many other authors working with joints, they applied a cosinusoidal radial stress around the hole boundary. In the two-hole model the holes were transverse to the load direction, parallel to loaded edge. Hence, in this case, the load was equally shared between the holes and the question of sharing of load between the holes didn't arise.

Godwin⁷ et al, conducted an experimental study of multi-bolt joints in graphite-reinforced plastics. Their conclusions were as follows: When the distance between two rows of bolts is small (less than 6 hole diameters), in a wide panel an increase in strength may be gained by increasing the end distance to suppress the shear-out failure. Staggering rows of

bolts does not improve the strength of the joint substantially. However, staggered row joints results in very large zone of damage at failure, which may be of significance in situations where high energy absorption at failure is important.

Garbo and Ogonowski⁸ used the anisotropic two-dimensional theory of elasticity in conjunction with laminated plate theory and the point stress failure hypothesis of Whitney and Nuismer⁹ on a ply-by-ply basis in their program BJSFM (Bolt Joint Stress Field Model). Stress distributions and the ultimate strengths of pin-loaded laminates were predicted assuming a cosinusoidal radial stress distribution for the pin - plate interaction. Load sharing between the rows was not addressed.

Through experiments and finite-element analyses, Rowlands, and Rahman, et al¹⁰, studied the effects of load distribution among the bolts, material properties, friction, etc., for single- and two-hole joints in orthotropic materials. They assumed different proportions of loads between the two bolts in series and studied the effects of different proportions. They found that substantial changes in joint strength can occur, depending on the load distributions between the bolts. However, the load share between the holes was never measured or predicted through analysis. They found that large increases in radial contact stress occur due to increased bolt tolerances.

Collings¹¹ investigated the effects of laminate orientation, bolt clamping pressure, and laminate thickness on the ultimate strength of single- and multiple-hole joint configurations for various widths and hole diameters in graphite-epoxy laminates. The load capacity of multiple-hole joints was predicted from single-hole data for the graphite-epoxy materials. The load share between rows or the different holes was not addressed. It was found that in case of multiple-hole joints there is no adverse interaction between holes and therefore, no loss in efficiency as the number of holes increased. This conclusion seemingly contradicts

the conclusions of Pyner and, Matthews³ but the two papers actually considered different hole patterns. In the context of the hole patterns studied in each paper, the conclusions for each paper were verified experimentally. Thus it appears that making general statements regarding the efficiency of multiple-hole joints can be dangerous.

Garbo and Becker¹² devised a method for simulating a multiple-hole stress state through testing a single-hole specimen by subjecting it to a combined fastener bearing and tension bypass loading. Strength predictions were obtained using a ply-by-ply failure analysis. Good correlation between experiments and analysis was reported but extensions of these data to specific multiple-hole joints was not fully understood.

Similar bearing-bypass loadings on bolted composite joints were studied by Crews and Naik¹³. A combined experimental and analytical study was conducted to investigate simultaneous bearing and bypass loading on graphite-epoxy laminate. They found an unexpected interaction of the effect of the bypass and bearing loads for the onset of the compression-reacted bearing damage. This interaction was caused by a decrease in the bolt-hole contact arc and a corresponding increase in severity of the bearing loads.

Chang et al¹⁴ assumed a cosinusoidal radial stress distribution around the hole to obtain the stress distribution in various pin-loaded laminates. Failure was predicted using the Yamada-Sun failure criterion along the chosen characteristic failure curve which had a locus that was determined experimentally. This approach was extended to evaluate two-hole tandem and two-hole side-by-side bolted configurations¹⁵ for three different laminates with various hole diameters, edge distances, and widths. With a side-by-side hole arrangement, the holes each reacted 50% of the load. The paper was not clear as to how load proportioning was accomplished for the case of tandem holes. Results for quasi-isotropic laminates revealed that predicted strengths were conservative by 10-40%. Chang et al¹⁶ modified

their analysis to include nonlinear intralaminar shear stress-strain behavior in hopes of reducing their conservative predictions. This new analysis reduced the predicted strength values to 10-25% level and resulted in more realistic failure mode predictions. In an attempt to understand the progressive nature of failure in laminated composites, Chang et al¹⁷ altered their two-dimensional nonlinear finite-element analysis to include an incremental loading and failure approach. The ultimate strength of tensile specimens with a central circular hole was predicted for various laminate orientations. Model verification was done by experimentally obtaining the ultimate strengths. Predicted results agreed with experimental values to within 20%. Failure mode prediction was accurate.

Hyer and Chastain¹⁸ studied the issue of adjusting the proportion of load transmitted by each hole in a multiple-hole composite joint so that the joint capacity is maximum. The joints considered had two holes in tandem. An algorithm which included a two-dimensional finite-element stress analysis and a failure criterion was developed to determine the load proportion at each hole which resulted in the maximum capacity of the joint. By proportioning the load it was found that the capacity could be increased generally from 5 to 10%, though in some cases a greater increase is possible.

As seen in the review, the important issues for the current problem, namely the load share between the two rows and among the holes in the same row, has not been addressed by anyone. To begin any analytical work in the area of multiple-hole joints, load sharing must be addressed. Furthermore, any predictions need to be substantiated with experiments. The chapters to follow deal with these topics as they are addressed in the present work. In the next chapter, the experimentation will be discussed. Specimen preparation, specimen strain gaging, and the instrumenting of pins to measure load proportioning will

be described. Photographs of some of the specimens are provided. Then the details of the fixture and test machine will be presented. These considerations will provide motivation for the finite-element modeling. Finally, the failure loads of the 31 specimens tested are tabulated, and photographs of some of the failed specimens are shown.

The third chapter discusses the development of the ABAQUS two-dimensional plane-stress finite-element analysis of the steel laps and the composite specimen. The boundary conditions, symmetry conditions, meshes used, and the modeling philosophy are discussed. The material properties for the three laminates, and illustrations of the deformed meshes of selected specimen models will be presented.

Comparisons between the numerical predictions and the experimental results are the subject of the fourth chapter. Specifically, the method used to reduce the experimental data to ascertain the proportioning of the total load reacted by each hole will be presented, along with the proportions themselves. Measured and predicted strains around the holes are also presented. Since there are considerable data from the testing and analysis of the 31 specimens, in the main text only the 5-hole specimens will be discussed. Information for 3-, 7-, and 9-hole specimens is in Appendices.

Further numerical results are presented in the fifth chapter, where radial and circumferential stress distributions around the holes of the different specimens are addressed. It is these radial stresses that are often assumed to vary cosinusoidally around the hole edge. The variation of the stress distributions with changes in laminate properties is also discussed. Chapter 6 summarizes the entire work and conclusions are drawn from the preceding five chapters.

2.0 EXPERIMENTAL SET-UP

2.1 Introduction

As described in the preceding chapter, the experimental phase of the study consisted of testing 3-, 5-, 7-, and 9-hole specimens. The 5- and 7-hole specimens were tested for three different laminates and also for two different half-hole configurations, namely the inboard and outboard half-hole configurations. The number of specimens of each kind of laminate tested is given in the Table 2.1. The specimen nomenclature in the table is as follows: The first three letters represent the laminate stacking sequence, as described in the first chapter in conjunction with Table 1.1. The fourth letter 'H' simply specifies that it is a specimen with holes. The fifth letter indicates the location of the unloaded half hole, 'I' for inboard and 'O' for outboard. The sixth letter in the notation stands for the number of complete holes in the specimen. For example, T45HI3 indicates that the laminate is of the stacking sequence including $\pm 45^\circ$ layers (T45), with the unloaded half hole on the inboard row, and it has 3 complete holes in it. From the table it is clear that the testing was concentrated on 5- and 7-hole inboard specimens, and on the T45 laminate. A few single-hole specimens were also tested for calibration purposes. This pattern to the testing was dictated solely by time and the expense of specimen manufacture and preparation.

Table 2.1. Multiple Fastener Joint Test Matrix

Test Condition	Laminate Type		
	T30	T45	T60
3-hole half-hole inboard row	*	T45HI3 3	*
5-hole half-hole inboard row	T30HI5 3	T45HI5 4	T60HI5 3
7-hole half-hole inboard row	T30HI7 3	T45HI7 2	T60HI5 3
9-hole half-hole inboard row	*	T45HI9 3	*
5-hole half-hole outboard row	*	T45HO5 3	*
7-hole half-hole outboard row	*	T45HO7 3	*

*, Not Tested

Number indicates the number of specimens tested

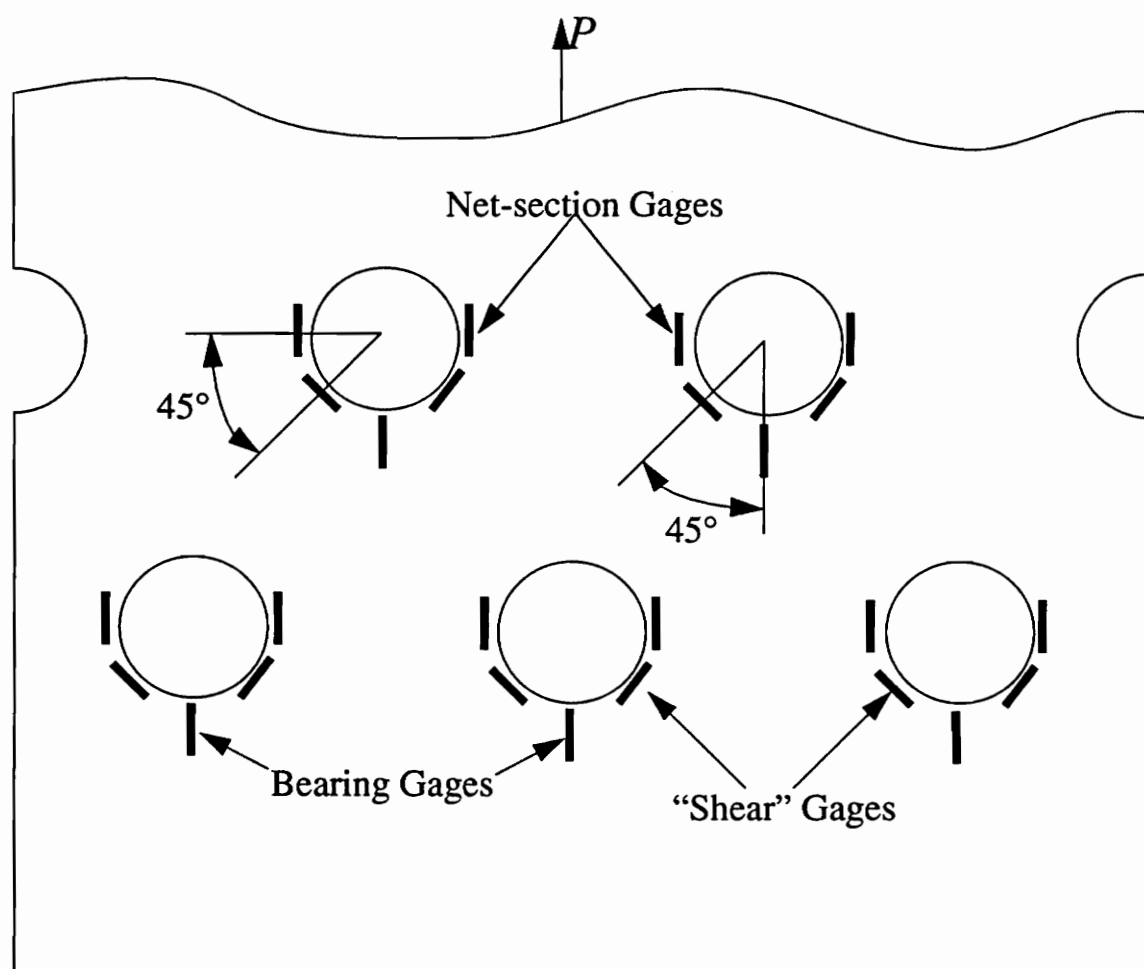
2.2 Specimen Preparation

All three laminates were manufactured by Hercules Inc., using Magnamite IM7G graphite fiber with 8551-7a resin. The specimens were layed up flat by hand and cured in an autoclave. As mentioned in the first chapter, only one end of the complete joints is shown in figs. 1.2 and 1.3. Hence for testing there were double steel laps on each end. Both ends of the specimen were identical as far as could be detected. All the specimens were instrumented with strain gages in a pattern shown in figure 2.1. As shown in the figure, gages were placed at the net section and bearing regions around the hole edge. There were also

gages halfway between these two gages, or at the 45° location relative to both the net-section and the bearing gages. These gages at 45° will be referred to as “shear” gages. In addition to being 45° away from either the net-section or bearing gages, the centerlines of a shear gages were at an angle of 45° to the loading direction. The gages shown in fig. 2.1 were installed only on one side of the specimen, and only around bottom half (loaded half) of the hole. Although for explanation purposes gages were shown around all five holes of the specimen in fig. 2.1, in reality gages were installed only around the centerline hole and the holes to the left of it, taking advantage of the symmetry about the vertical centerline. A close-up view of an instrumented specimen is shown in figure 2.2. The numbering scheme for the strain gages varied from specimen to specimen, depending on width and hole configuration of the specimen. This will be discussed in the later chapters. In Figure 2.3 specimens of five different widths, namely the 1-, 3-, 5-, 7-, and 9-hole specimens, are shown with strain gages mounted and lead wires attached.

2.3 Fixture and Testing Machine

Since a point of interest in these experiments was not only the final failure load, but also the proportion of load reacted by each hole, special pins were used¹⁹ which measured pin bending as they were loaded by the double steel laps and the composite specimen. Such a pin is shown in Figure 2.4. These special pins had a strain gage mounted on a flat recess on the shank at the center of the pin. This gage responded to pin bending when the joint was loaded and the amount of bending in the pin was taken as a measure of the load reacted by the pin. By comparing the amount of bending in all the pins, the share of load each pin reacts could be determined. In addition to this gage on the shank, a leaf spring with back-to-back strain gages was also mounted on the flat recess. The spring was mounted on the shank



5-Hole Inboard Specimen

Figure 2.1. Schematic of a typical strain gage pattern for a 5-hole specimen

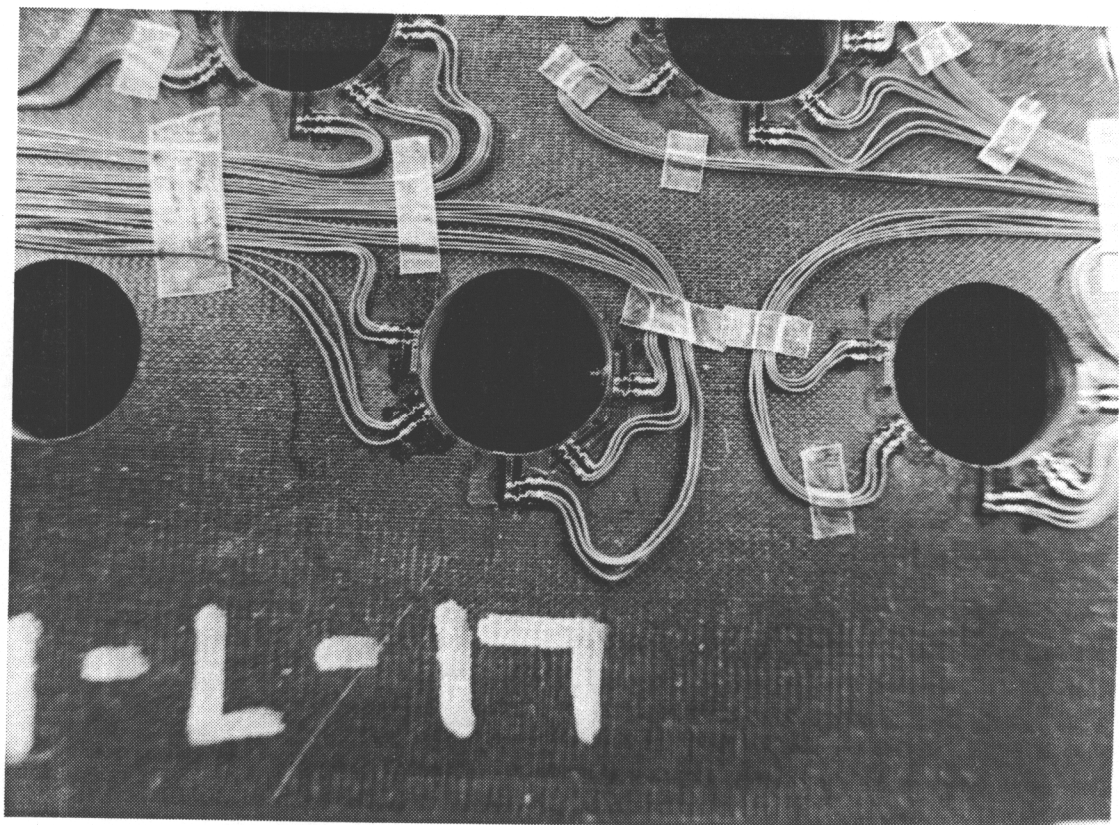


Figure 2.2. Photograph of a typical strain gage pattern for a 5-hole specimen

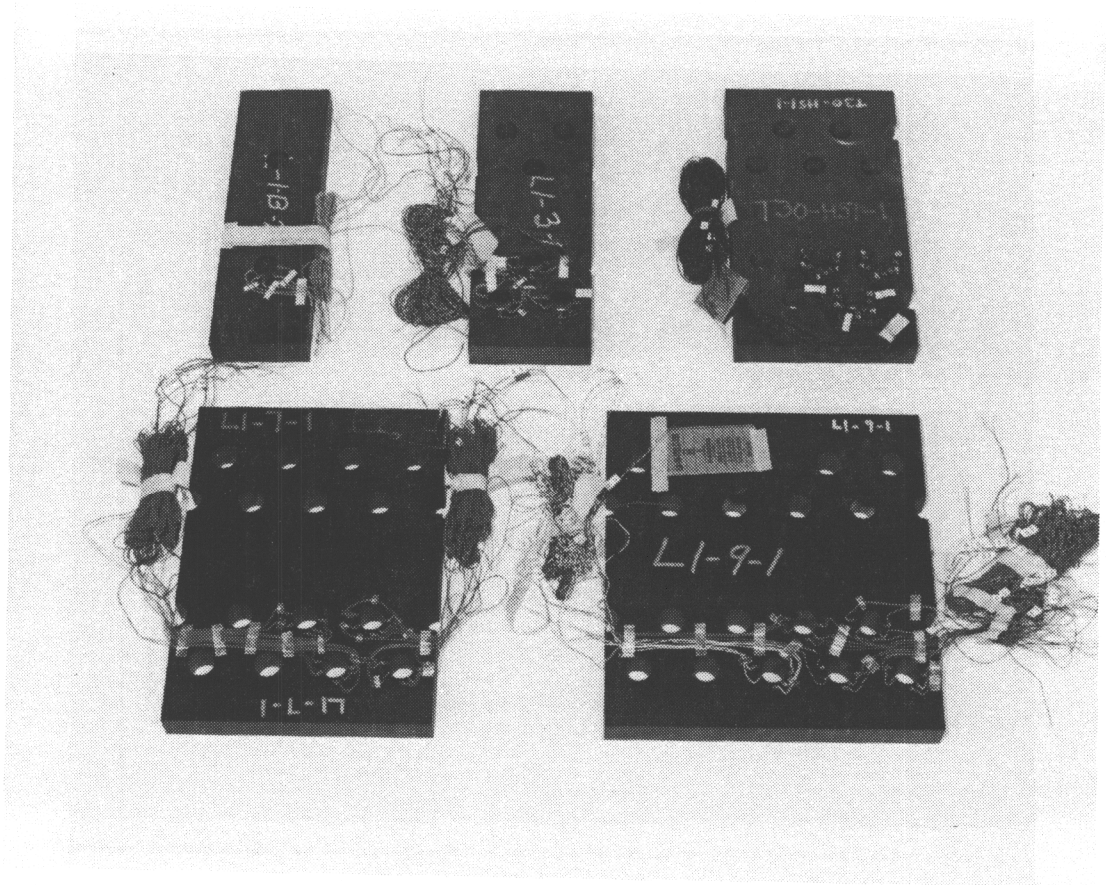


Figure 2.3. One-, 3-, 5-, 7-, and 9-hole specimens after strain gage installation

with adhesive. This spring measured the hole deformation and hence should be useful in determining the hole elongation for each hole in the joint. Strain data from the spring was to be used to provide a direct comparison between the measured hole elongation in a single-hole specimen and that in a multi-hole specimen, and also between analysis and experiment. Unfortunately, difficulties with the spring mounting prevented the measurement of useful data regarding hole elongation. The results of these measurements will not be discussed. Details of the instrumentation are shown in figure 2.4, and a photograph of a pin is shown in fig. 2.5.

The specimens were loaded through specially made steel plates, the plates acting in double-lap fashion. The steel lap plates are shown in figs. 2.6 and 2.7, there being two sets of these plates, four plates per set. One set of four plates was for testing 3-hole and 7-hole inboard specimens, and the other set was for testing 5-hole and 9-hole inboard specimens. For testing outboard specimens, the plates were switched. The need for two separate sets of plates, and the switch for testing outboard specimens, becomes clear upon looking closely at the hole geometry of various specimens. Dimensions of a plate from each set are shown in figs. 2.6 and 2.7. As seen in the figures, the plates have a 3 in. diameter hole on the end opposite the specimen holes. The 3 in. hole accommodates a steel pin which connects the steel laps to the loading frame used in the testing. The end which fastens to the specimen is thinner relative to the other end and is about 0.875 in. thick. Four of these plates were used as outer laps, two laps being used on each end of the specimen. The composite specimens are attached to the steel laps with bolts, and the steel laps in turn attached to the load frame with the 3 in. pin and a large clevis arrangement. A diagram of the pin-lap-specimen set-up is shown in fig. 2.8. Figure 2.9 is a photograph of the loading set-up.

The machine used for testing was a Southwark - Emery vertical testing machine. The

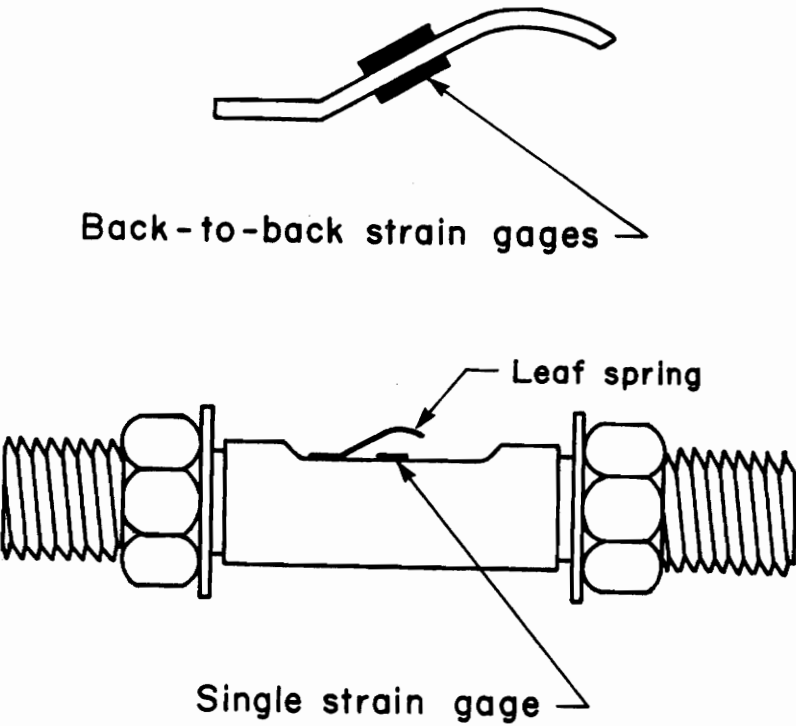


Fig. 2.4. Details of the instrumentation for the pin

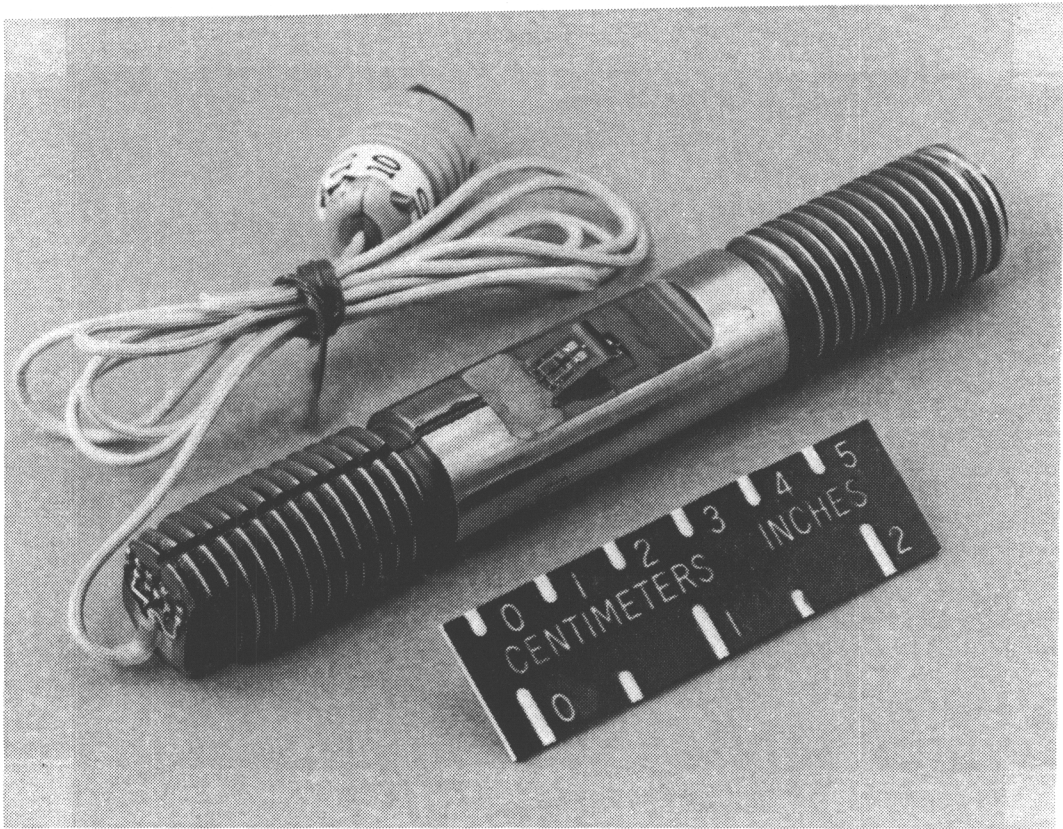


Figure 2.5. Photograph of the instrumented pin

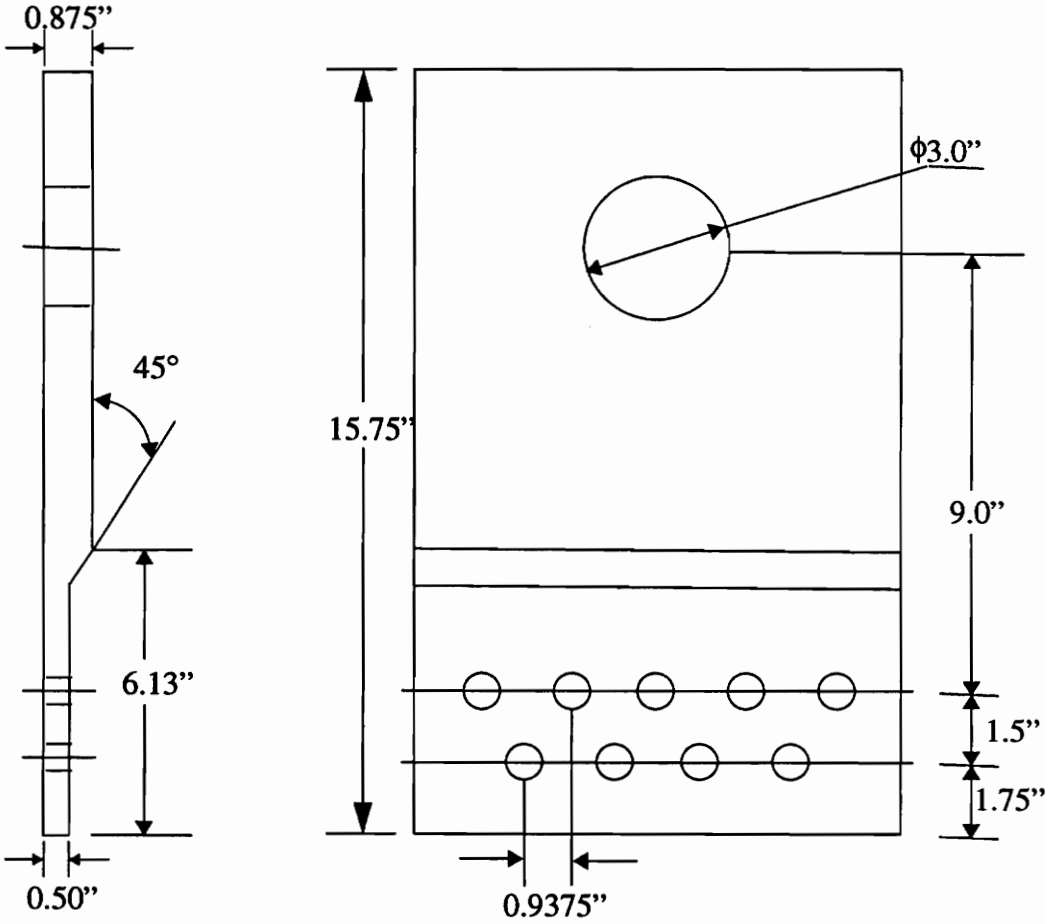


Figure 2.6. Dimensional details of the steel laps for 3- and 7-hole inboard specimens

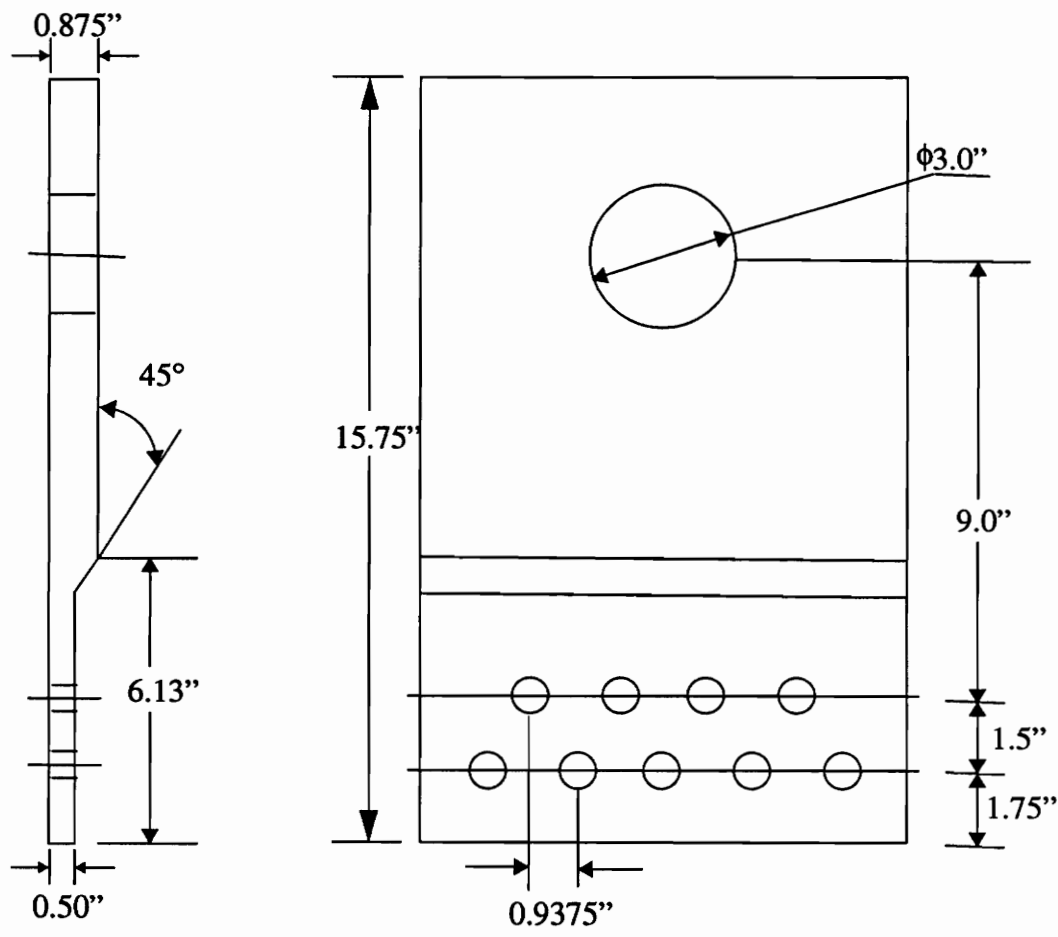


Figure 2.7. Dimensional details of the steel laps for 5- and 9-hole inboard specimens

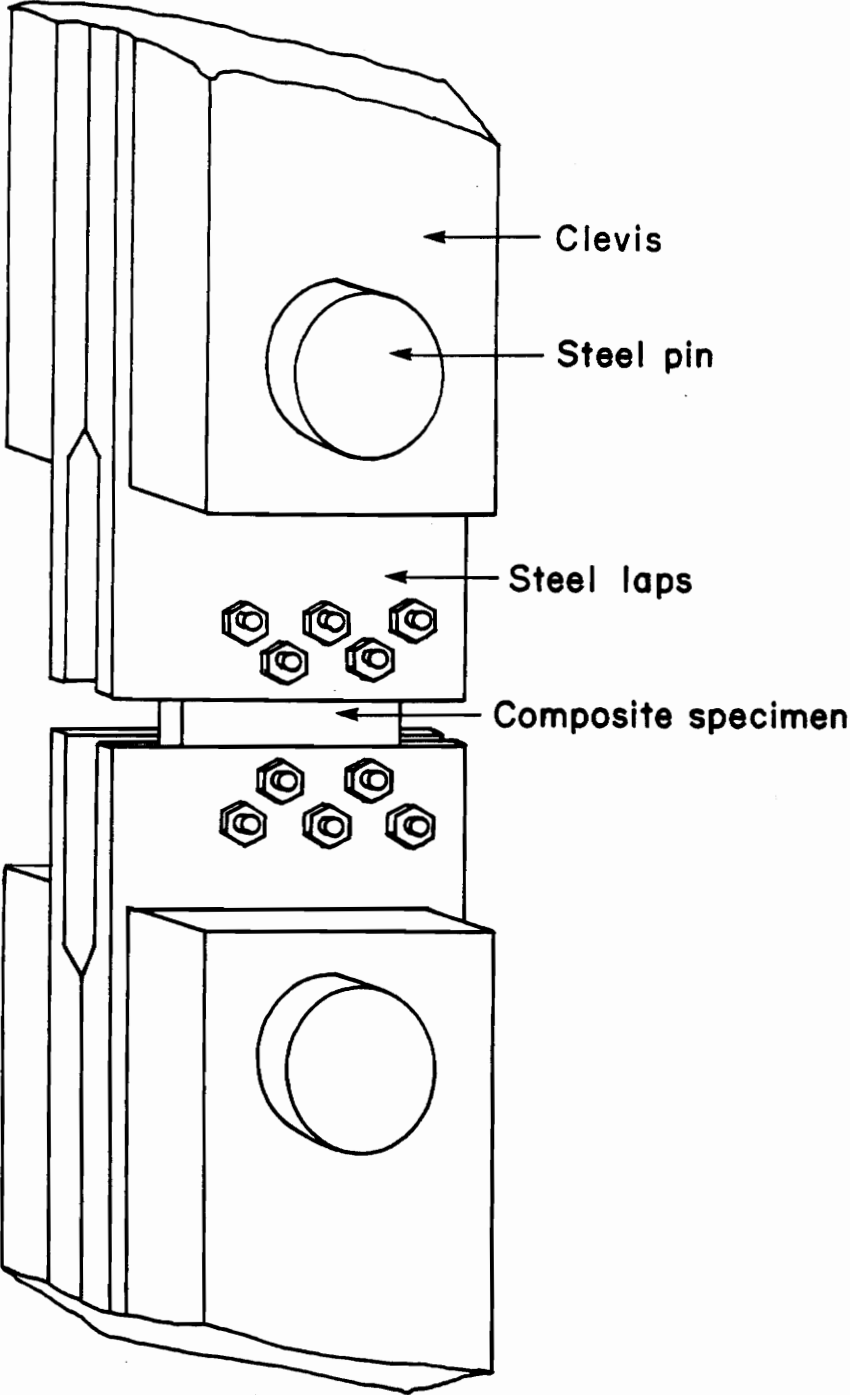


Figure 2.8. Specimen, steel laps and clevis assembly

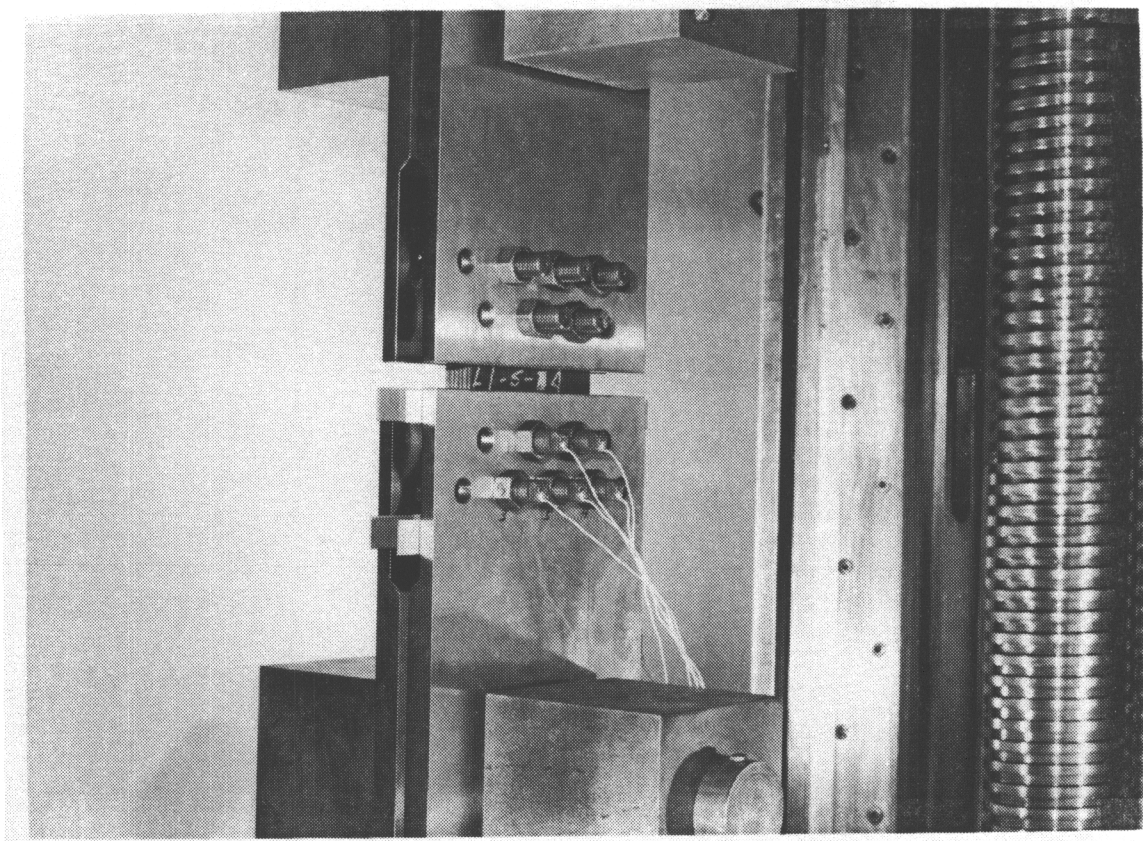


Figure 2.9. Photograph of experimental set-up

machine is owned by the NASA-Langley Research Center and has a capacity of 1.2 million lbs. in both tension and compression. The machine is located at the NASA-Langley Research Center and is composed of two elements, namely, the testing machine proper and the control cabinet. The testing machine includes the sensitive and tension crossheads, the tension screws, columns, and an elevator which rises to a height of 27 ft. above the base of the machine. The control cabinet provides housing for all the mechanisms for measuring and recording the loads, for controlling the loading, and for controlling the mechanical movement of the sensitive crosshead.

2.4 Experimental Procedure

As can be seen in figure 2.9, with the wires coming only from the bottom end of the specimen, only one end of each specimen was instrumented. To accommodate the strain gage wires from gages around the holes on the bottom end of the specimen, a gap of 0.125 in. was maintained between the outer steel laps and the composite inner lap. This gap was maintained with steel shims. The bolts on top end were torqued to 50 ft-lb to produce a through-the-thickness clamping force on the composite specimen. This was important because it was desirable to have the failure at the lower, instrumented end of the specimen. It was confirmed through earlier tests that failure is likely occur at the untightened end. In addition, earlier tests at Hercules¹⁹ on similar joints indicated that the gap between the steel laps and the composite specimen should not effect joint strength, provided there are no delaminations present around the holes prior to the test. This was also confirmed during the present tests, as number of specimens failed at the end with the torqued bolts (top end in fig. 2.9) rather than the unclamped end.

Most of the specimens had two replicas, making a total of 3 specimens for each lami-

nate and hole geometry. Two specimens were tested to failure. The third was loaded to 95% of the average failure load of the other 2 specimens. This specimen was then unloaded. Some specimens were X-rayed to examine for evidence of the initiation of failure.

Data was collected using the standard data acquisition system at NASA-Langley Research Center. The system consists of a Beckman signal conditioning unit which has four signal conditioning boxes, each with 50 channels. Output from these signal conditioning boxes is routed to a NEFF 620/600 data acquisition unit. The NEFF data acquisition unit is a high speed device that measures and records multi-point low level analog signals. Two separate types of software operate on the data acquisition system. The first type of software is the operating acquisition program. The operating acquisition program is a real - time executive program which operates in conjunction with a MODCOMP MAX computer to acquire, display, and record the test data. The second type of software is applications oriented. This software is responsible for converting voltage to engineering units, for real-time plotting, and other functions. Although separate, the two types of software work in tandem and constitute a complete data acquisition system.

The next chapter describes the finite-element model that was used to predict the response of the joint specimens. Since strain gages were used to monitor response, strains from the finite-element model are discussed. In addition, load proportioning among the holes is predicted.

3.0 FINITE ELEMENT MODELING

3.1 Introduction

A two-dimensional finite-element model of the outer steel laps, the pin, and the inner composite specimen was developed using PATRAN,²⁰ a commercial software package for formulating finite-element models and post-processing finite-element results. As mentioned earlier, the actual finite-element analyses were done with ABAQUS². After formulating the joint model with PATRAN, PATRAN provided a file which was used as input for ABAQUS. Details of the analyses are given in the following section.

3.2 Model Description

Taking advantage of the two-planes of symmetry in the problem, only the lower left quadrant of the problem was modeled. This quarter model is shown in the fig. 3.1. The finite elements used were 8-node quadratic plane stress elements denoted as CPS8 in the ABAQUS library. These elements were used for modeling both the composite specimen and the steel laps. This element is shown in fig. 3.2. Node and Gauss point numbers are as indicated in the figure. As shown, results can be calculated at nine integration points and eight nodes. It should be mentioned at this time that because the problem was being modeled as planar, the influence of the two steel laps was represented by one mesh. Since in

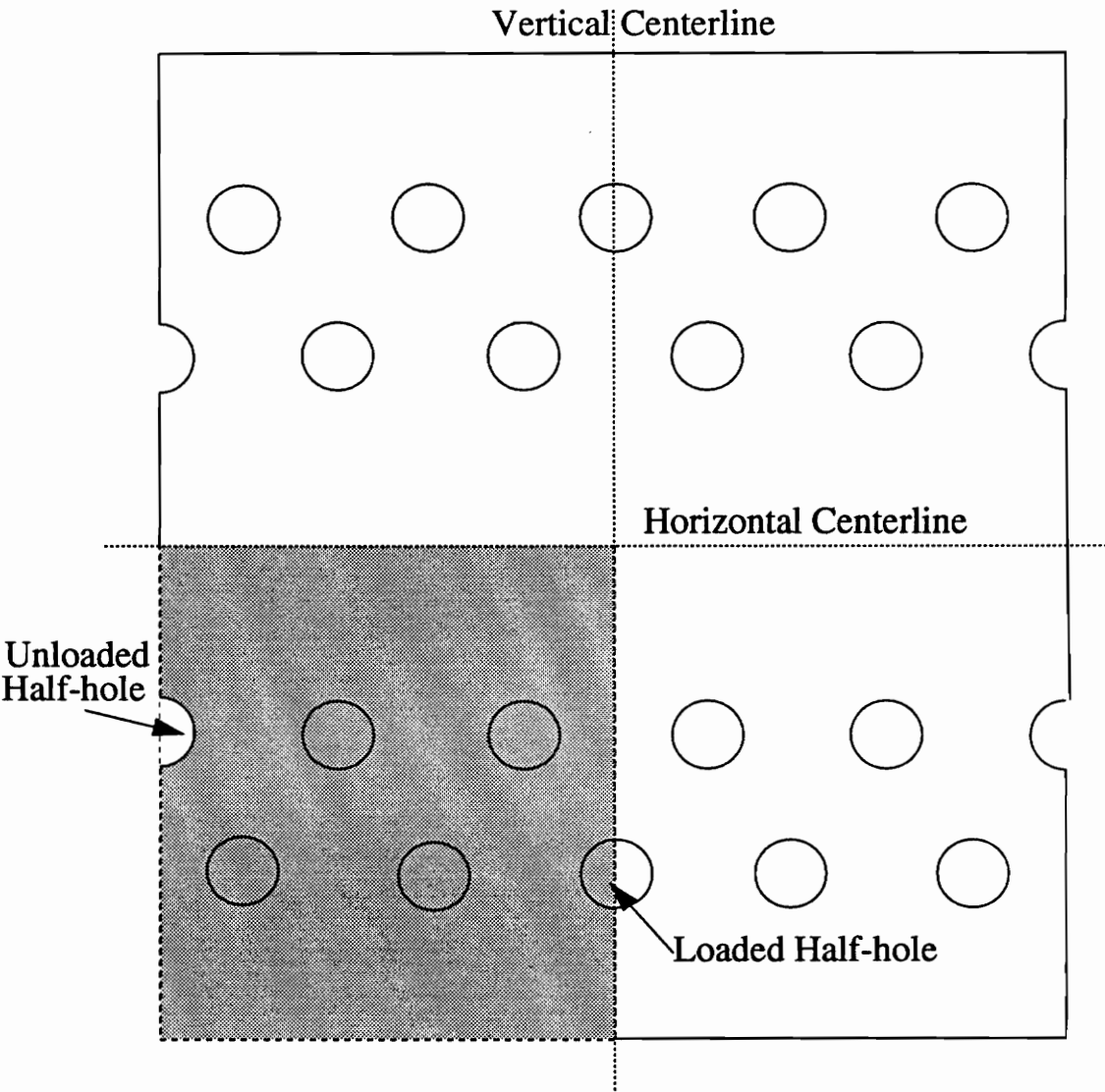


Figure 3.1. Quarter model of the steel laps and composite specimen

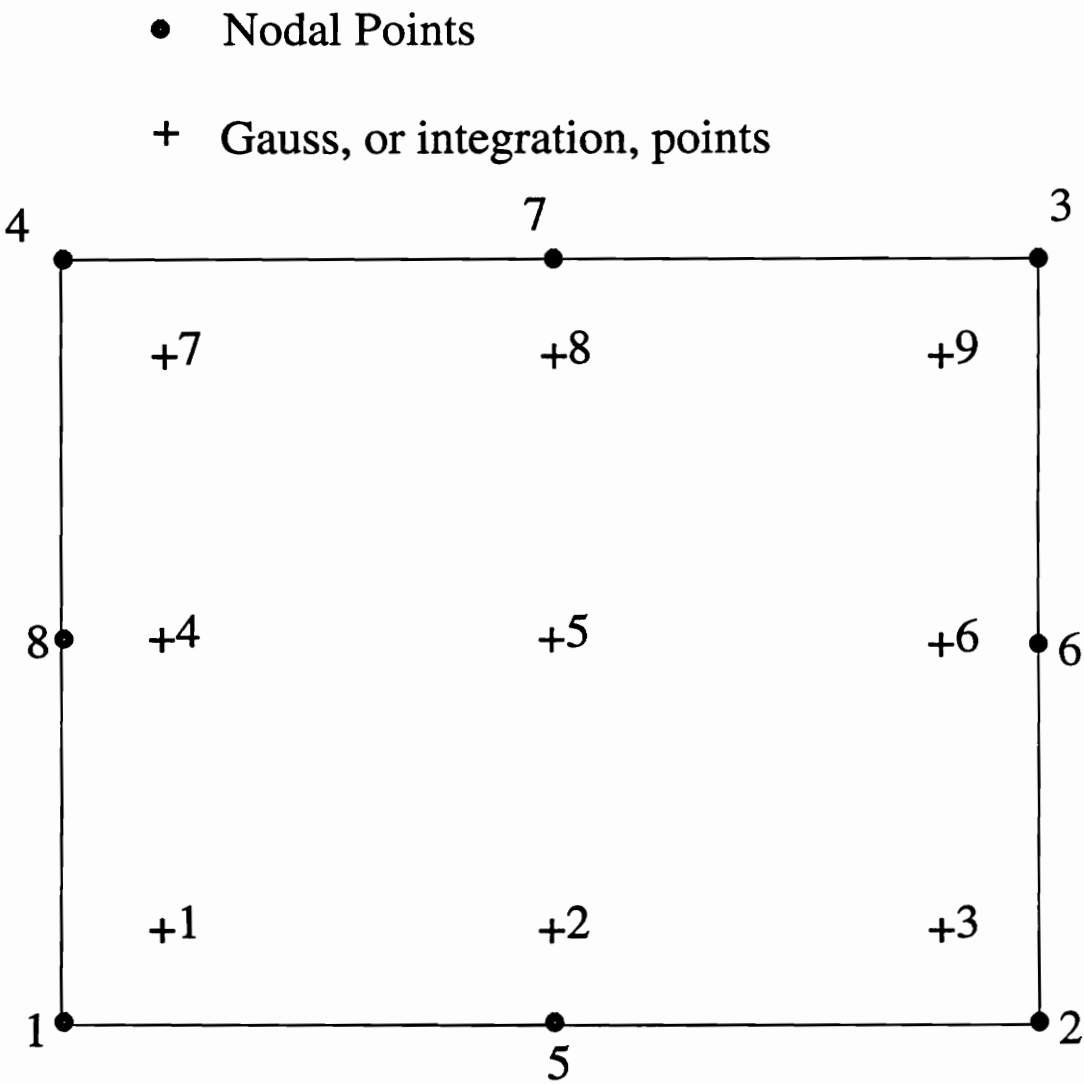


Figure 3.2. Representation of the CPS8 element

this planar model the location of the laps in the thickness direction was irrelevant to the outcome, the two laps were combined and modeled as a single lap with appropriate thickness. Hence, the model involves two interacting meshes, one mesh representing the composite specimen, the other representing the steel laps. The interaction of the two meshes was accomplished through the use of rigid circular surfaces on the hole boundaries. The circular surfaces represented the pins. The independent (no common nodes or degrees of freedom) steel lap and composite specimen models were made to interact through these rigid circular surfaces with centers initially at the centers of the holes. Different components of a typical model, and the way they are put together and interact through the circular surface, are shown in fig.3.3. This is shown for only one hole as an example. In this model the circles were referenced to the centers of the holes and were free to move in the plane. This freedom to move represented the motion of one hole relative to the others due to the compliances of the steel and composite. Neither the steel nor the composite was allowed to penetrate the rigid circular surfaces. This was accomplished by using the gap elements available in ABAQUS. The gap element is an element which has no dimensions and here were added to the surface of the hole edge where interaction with the rigid circular surface representing the pin was expected. The surfaces were forced to stay circular and hence represented rigid pins. Neither friction nor hole clearance were modeled, but with care in the experiments, the latter would not be an issue. Previous studies indicate that while the inclusion of friction and pin compliance can influence the predicted stresses, for nominal levels of friction and clearances, they are not first order effects^{21,22}.

The model for a 3-hole inboard specimen is shown in fig.3.4. Recall that in the experiments the steel laps were made to accommodate more than one specimen width, the 3-hole specimen being the narrowest specimen. Modeling the steel to be wider than the composite,

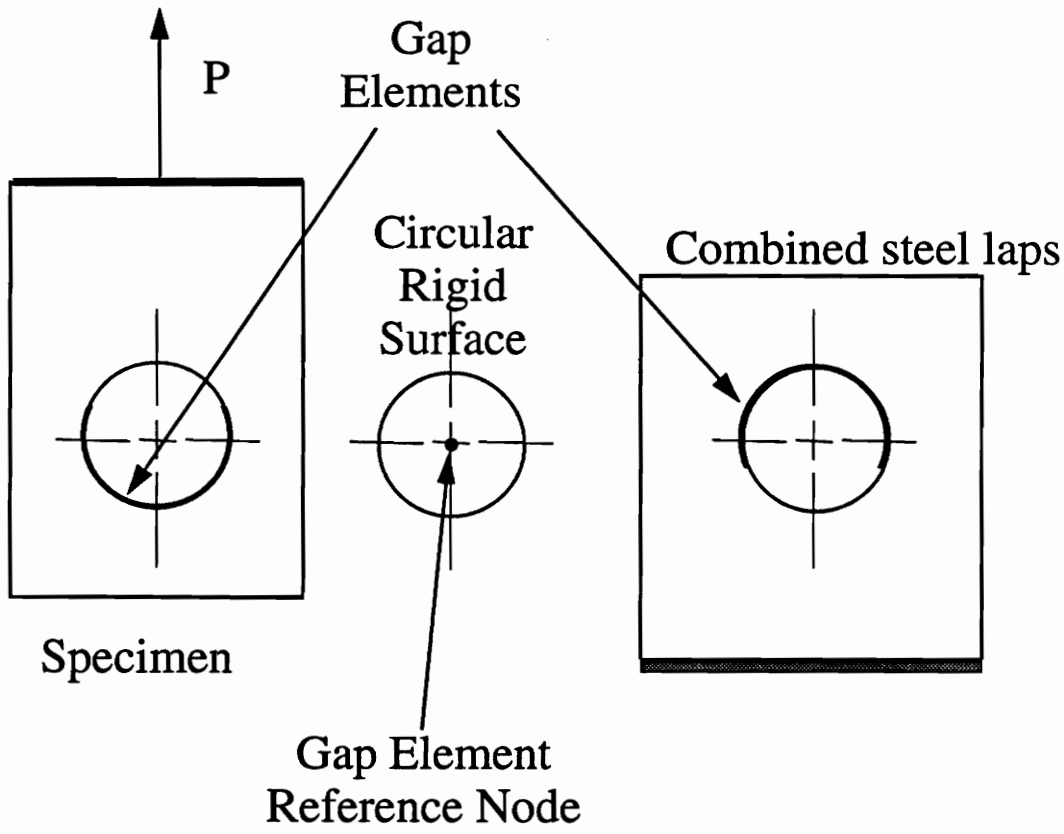


Figure 3.3. Interaction of steel lap and composite specimen

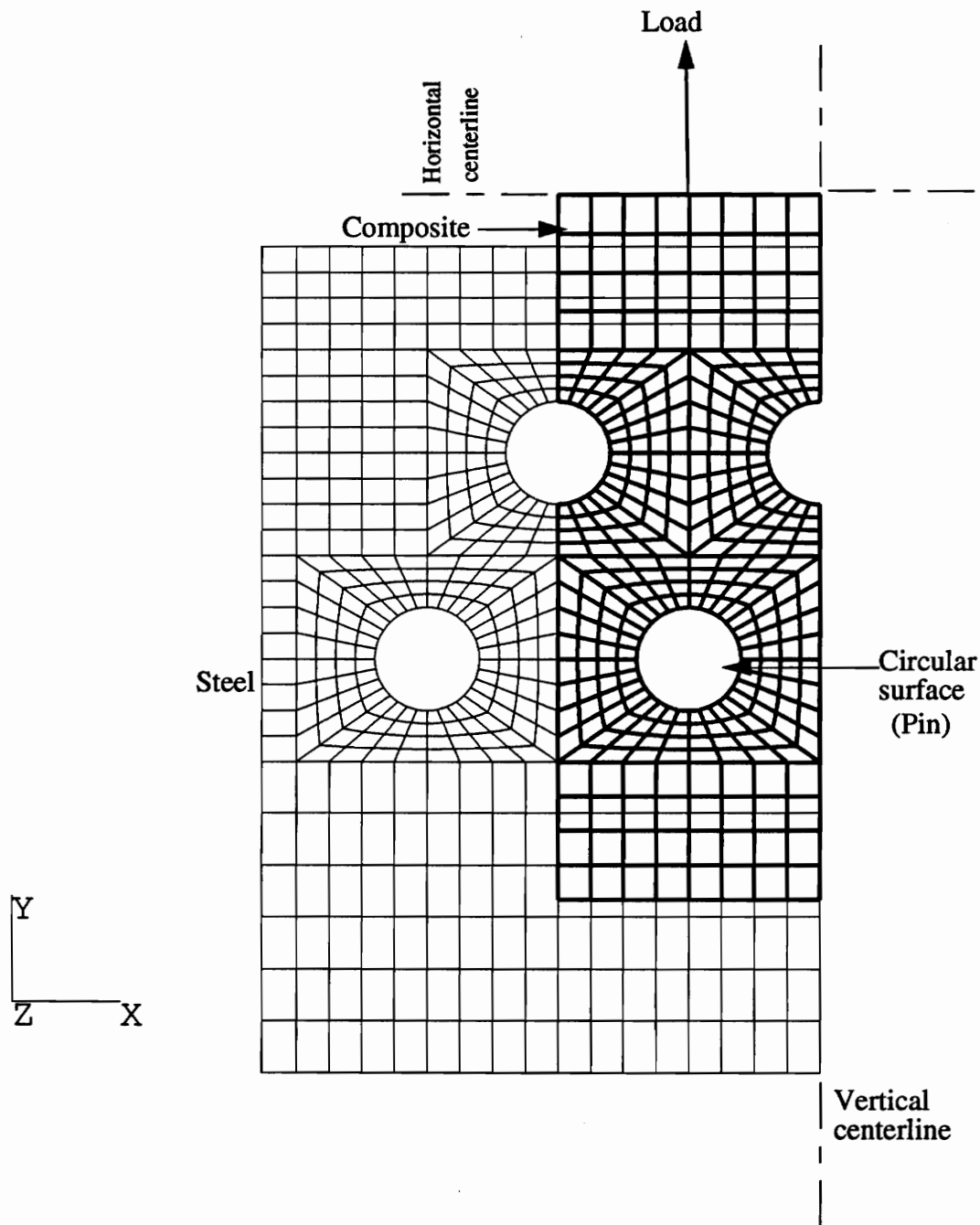


Figure 3.4. Finite-element model of a 3-hole inboard specimen

as shown in fig. 3.4, simulates the actual experimental set-up. Because of the modeling, the finite-element mesh representing the steel lap and the mesh representing composite specimen coincide for the most part. Note the x-y-z coordinate system in fig. 3.4. As indicated in fig. 3.1, the half hole on the centerline is actually loaded, while the half hole on the left edge of the specimen is unloaded.

Regarding the boundary conditions, first consider the steel lap. The length of the steel is not modeled completely in the analyses. As was seen in figs. 2.6 and 2.7, the thickness of the steel laps nearly doubled away from the specimen. In the model the steel lap was considered only to the point where its thickness increased. The point of the thickness increase was approximated as being rigid. Hence, referring to fig. 3.4, the lower boundary of the steel lap was prevented from any displacement. To be consistent with symmetry, the vertical centerline (right edge of the fig. 3.4) was constrained from displacement in the x direction. The upper boundary of the composite specimen namely, the horizontal centerline, was constrained to remain straight and horizontal by means of a multi-point constraint. This enforced the symmetry condition in the crosswise direction of the specimen. The force applied to the joint was applied to the composite at the node in the upper right corner, i.e., on the vertical centerline

The rotation of the nodes at the pin centers (the centers of the circular surfaces) was restrained from rotation about the z axis. To be consistent with the symmetry, the center of the pin on the centerline was further constrained from displacement in the x-direction. Nodes at the other pin centers were not constrained from translation, thus allowing the pins to translate in accordance with the elastic deformations of the two interacting laps.

The analysis for each specimen geometry and lamination sequence was carried out at two different load levels, one at 50% and another at 75% of the failure load recorded in the

experiments for that particular specimen configuration. These failure loads will be presented in the next chapter.

The properties of steel were assumed to be

$$E=30 \times 10^6 \text{ psi,}$$

$$\nu=0.3$$

and the properties of a ply were assumed to be

$$E_1=24.3 \times 10^6 \text{ psi,}$$

$$E_2=1.01 \times 10^6 \text{ psi,}$$

$$G_{12}=0.764 \times 10^6 \text{ psi,}$$

$$\nu_{12}=0.26,$$

with a ply thickness of 0.006 inches.

The smeared engineering properties of the three different laminates were calculated using classical lamination theory and are shown in Table 3.1. A close examination of the three lamination sequences reveal that they are actually unsymmetric laminates. However, the classical laminate theory analysis indicated that the laminates do have a negligibly small B matrix (bending-extension coupling matrix). It was thus ignored, even at the failure loads.

Table 3.1: Smeared Engineering Properties of the Three Laminates

	T30	T45	T60
E_x	5.59 E6 psi	7.00 E6 psi	9.70 E6 psi
E_y	15.2 E6 psi	12.5 E6 psi	11.3 E6 psi
G_{xy}	2.56 E6 psi	3.05 E6 psi	2.56 E6 psi
ν_{yx}	0.352	0.342	0.206

In ABAQUS the isotropic material option was used for the steel. For the laminates, the LAMINA option was used. Both the materials were assumed to be linear elastic. The RIGID SURFACE option in ABAQUS was used to define the surfaces which interacted with the cylinders representing the pins. For a given hole the rigid surface interacting with the

steel was referenced to the same node as was the rigid surface interfacing with the composite. Thus the finite-element models of the steel lap (as stated earlier, the two laps were assumed to be a single lap with thickness equal to the two laps) and the composite specimen interacted only through the gap elements and the rigid cylindrical surfaces, which were in turn connected to a common nodal point at the hole center. (Further details of this model are given in reference 23). The resulting problem was solved for displacements, strains, and stresses. With the gap option in effect, ABAQUS uses nonlinear strain-displacement relations. The problem, however, falls within the domain of linear elasticity.

3.3 Preliminary Results

A representative deformed finite-element mesh of a 3-hole specimen is shown in fig. 3.5. It must be noted that the rigid surfaces or 'pins' have controlled the coupled response of the steel laps and composite specimens. This is noted in the figure by the fact that even after deformation, the contact surface of the composite with the pin can be represented by semi-circle on the lower half of the hole, and the contact surface of the steel lap with the pin can be represented by a semi-circle on the upper half of the hole. Though the term 'semi-circle' has been used, the contact regions are not quite semi-circular, or 180° . It should be noted that the original full circle representing the rigid pin can be identified after deformation. The circle is identified in fig. 3.5. It can be seen in fig. 3.5 that the full hole on the outboard row is skewed towards the unloaded inboard half hole on the left edge. This skewing is very important, as will be seen in the upcoming discussions. Similarly, as shown in figs. 3.6 and 3.7, the corresponding holes in the 5-hole and 7-hole specimens are also skewed towards the unloaded inboard half hole. When the specimens have unloaded half-holes outboard, the skewing is not quite as conspicuous, as seen in fig. 3.8.

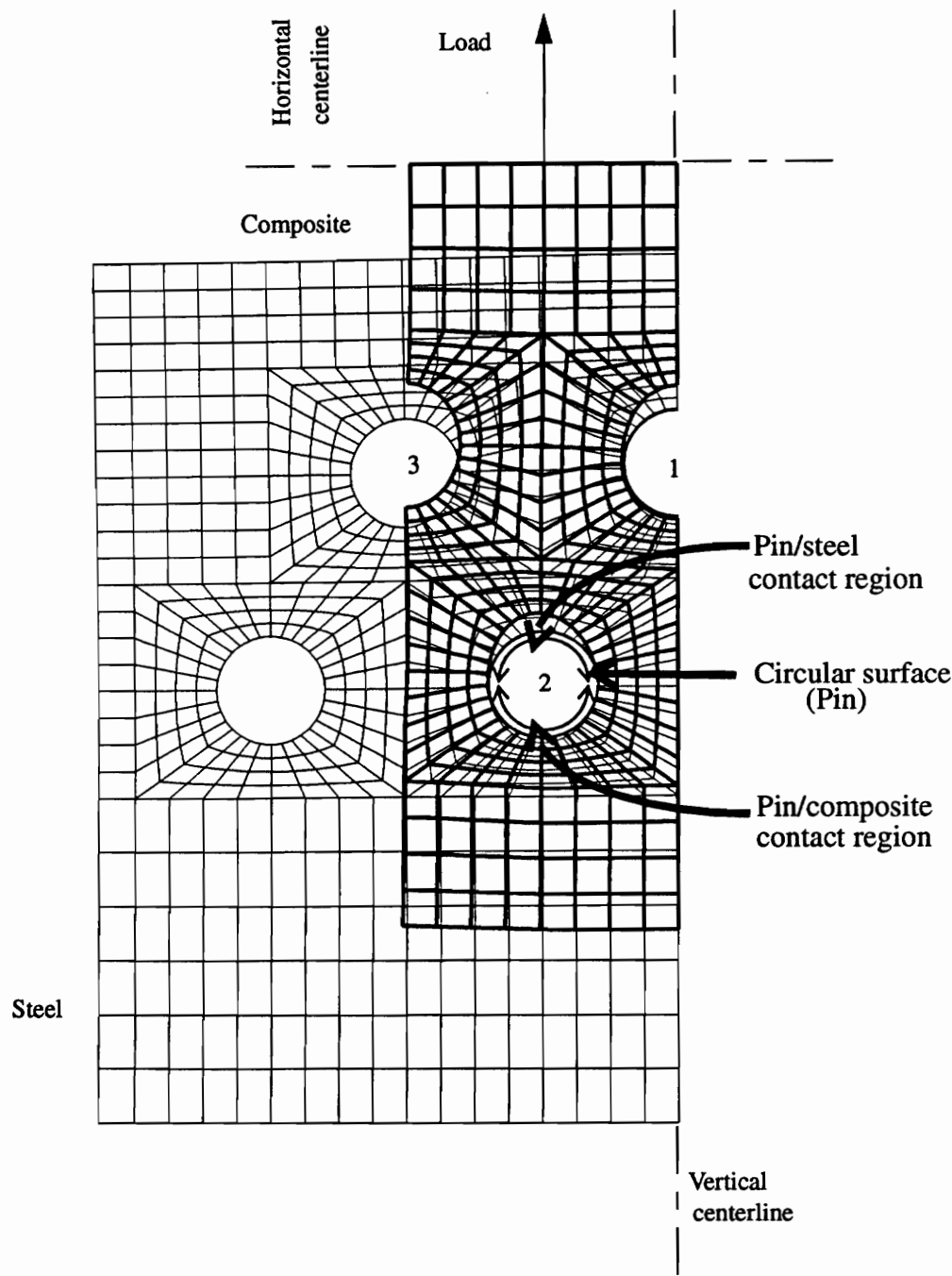


Figure 3.5. Deformed mesh of a 3-hole inboard specimen model

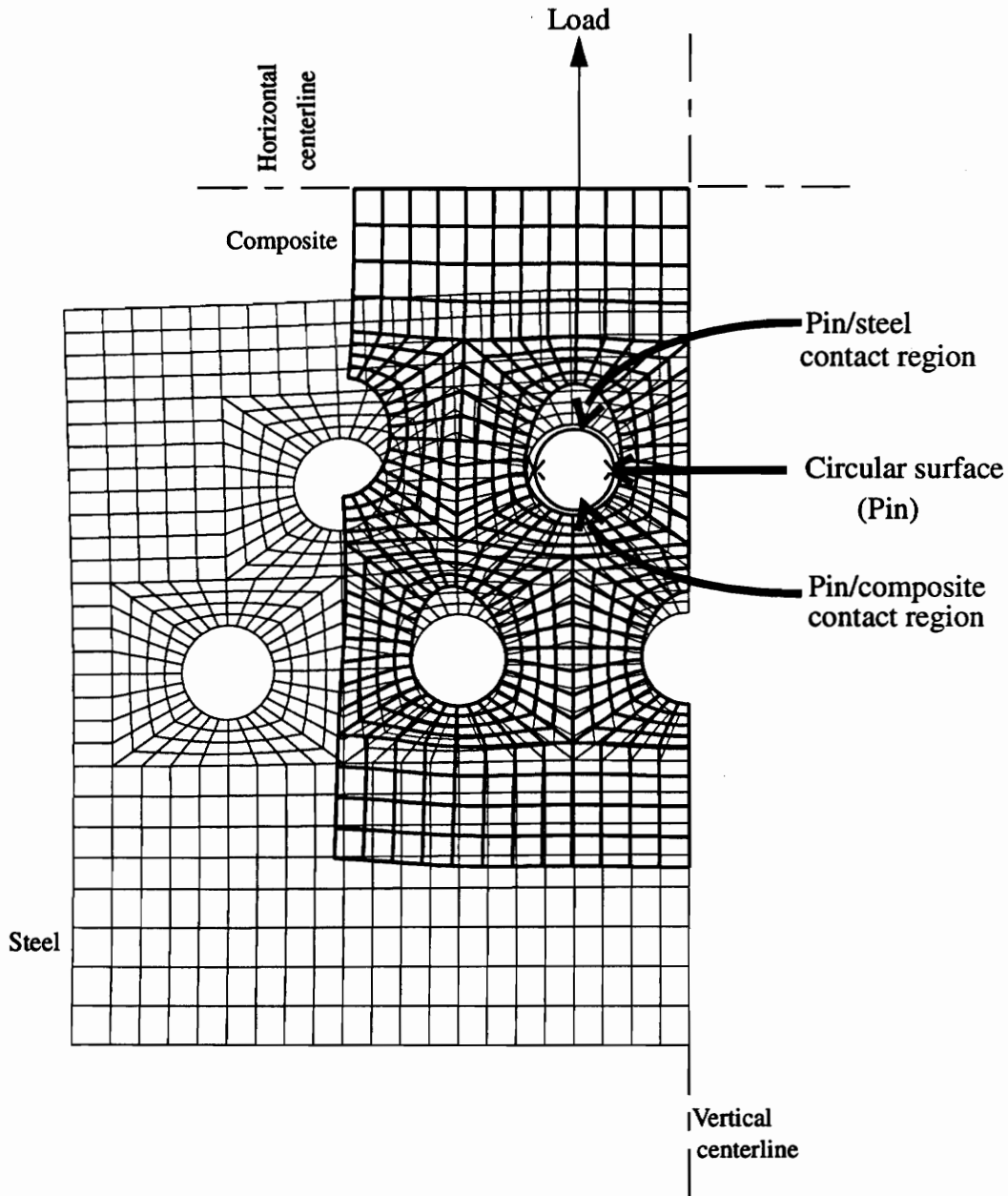


Figure 3.6. Deformed mesh of a 5-hole inboard specimen model

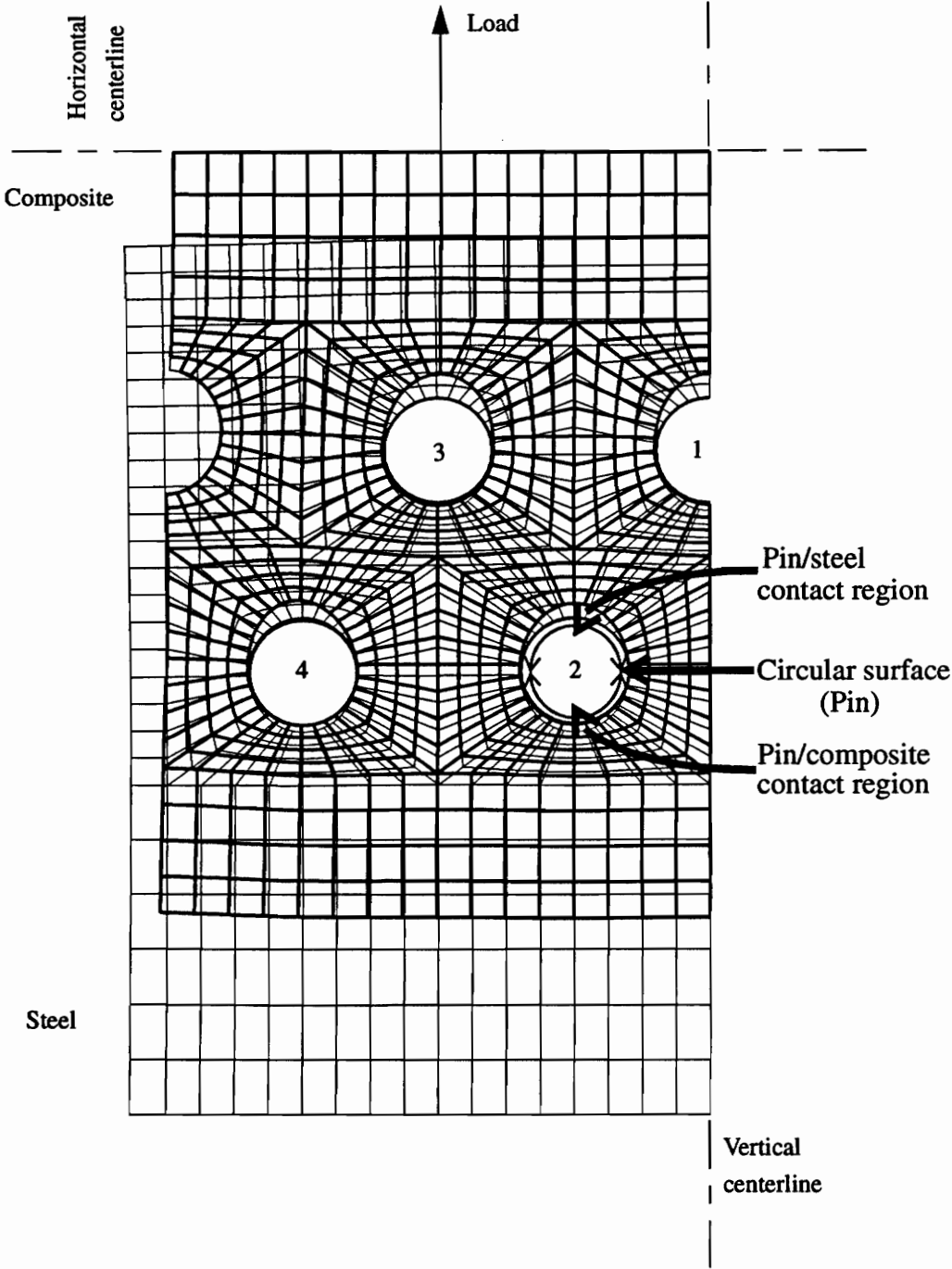


Figure 3.7. Deformed mesh of a 7-hole inboard specimen model

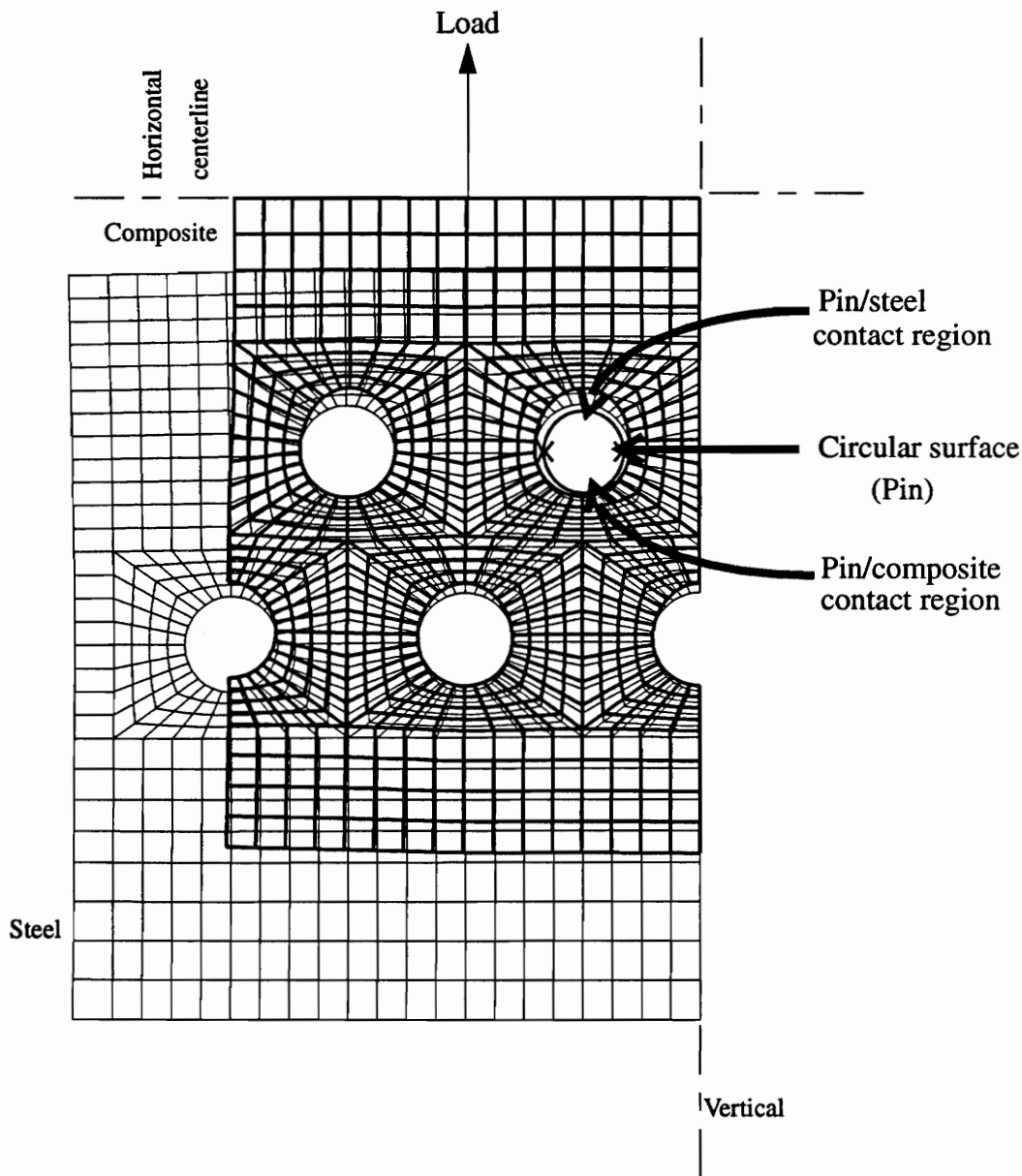


Figure 3.8. Deformed mesh of a 7-hole outboard specimen model

The procedure of this analysis has some unique features. The first is the incorporation of stiffness effects of the steel laps on the joint response. The feature is the accurate modeling of pin-to-hole contact load distribution. Generally this load is idealized, for example, by an assumed cosine radial stress distribution. In the present case, the load (a) will not follow the cosine distribution (in particular, for the off-center-line holes due to the aforementioned skewing), (b) will not be distributed along the entire 180° hole's circumferential angle, as is typically idealized, and (c) will not be symmetrically distributed around the hole for holes that are located on either side of the specimen center. The third unique feature of the analysis is the proper accounting for the proportioning of the total load reacted by each pin. This analysis provides a method by which the load share per pin can be determined accurately. This approach can be extended to other geometries, e.g., three rows of holes.

The next chapter correlates the results from the testing with the predictions of the just-described finite element model. Though some responses of interest cannot be directly measured, good correlation between the predicted results and measurements for the responses that can be measured gives some degree of confidence in the prediction of quantities that cannot be measured directly.

4.0 DISCUSSION OF NUMERICAL AND EXPERIMENTAL RESULTS

In this chapter, results from the experimental testing are presented and discussed. Correlation with the finite element analysis is considered as the experimental results are discussed. As will be seen, the overall agreement between the experimental results and the analytical predictions was found to be quite good. In certain cases where the response of the gages was nonlinear or erratic, although the correlation was not good, the numerical predictions were within the range of the experimental data among the three replicate specimens. In the latter part of this chapter, the majority of the results are from 5-hole specimens. Results from other specimens are presented in appendices. The discussions in the present chapter can be considered to cover the specimens included in the appendices. Because of the large amount of data from both the experiments and the finite element analysis, it was decided to consider only the results from the 5-hole specimens in the main text. The 5-hole specimens were chosen because the 5-hole specimens were studied for the most possible combinations of parameters, e.g., inboard vs. outboard half-hole, and the three laminates, T45, T60, and T30 (see table 2.1).

4.1 Summary of Failure Results

A 3-hole T45 inboard specimen, a 5-hole T45 outboard specimen, and a 7-hole T45 out-

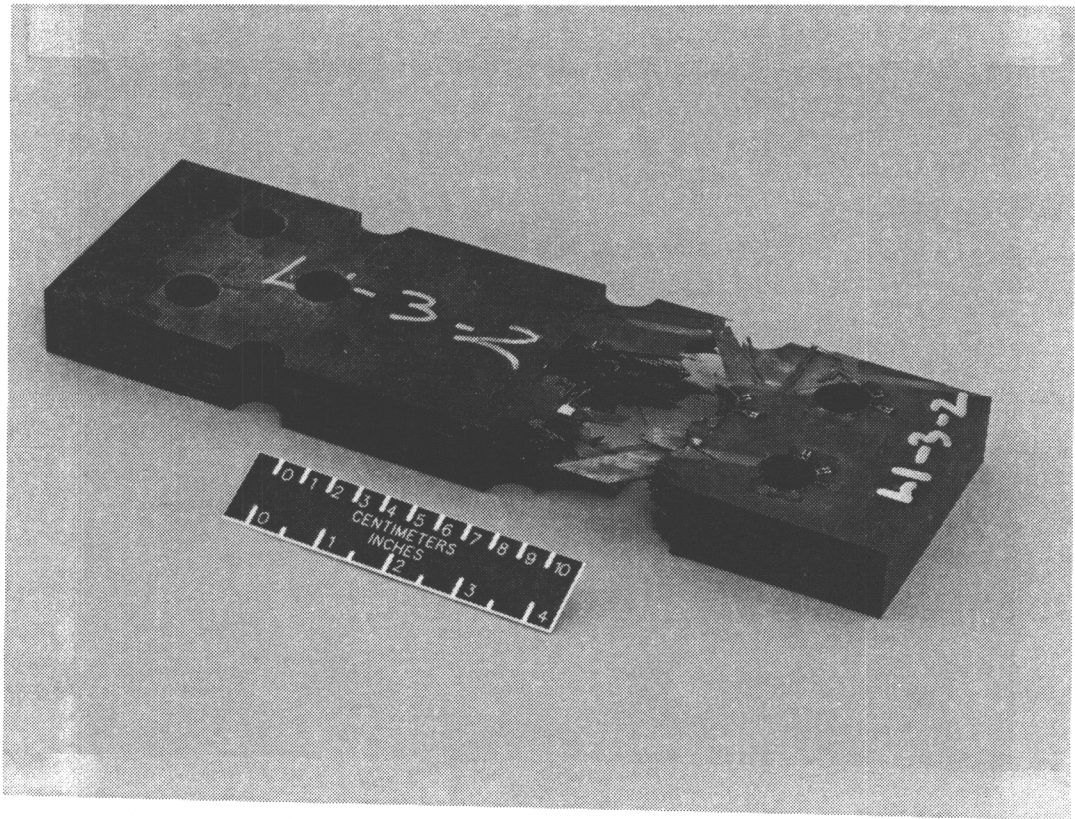


Figure 4.1. A 3-hole T45 inboard specimen after failure

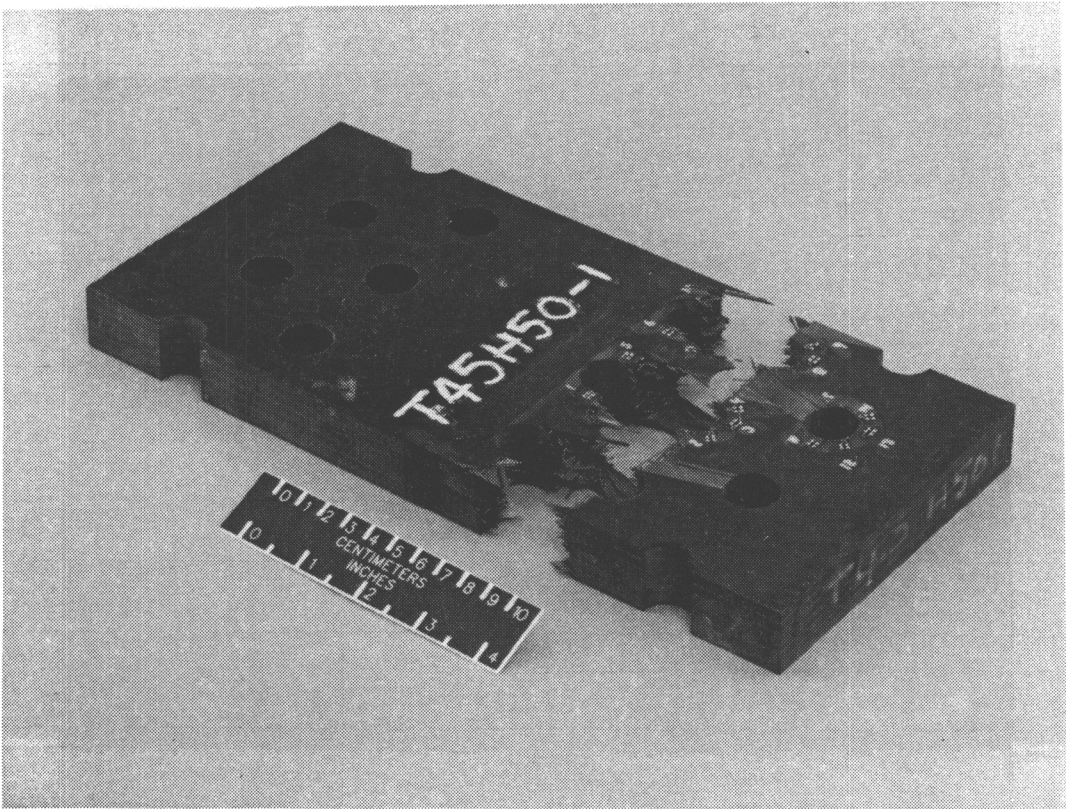


Figure 4.2. A 5-hole T45 outboard specimen after failure

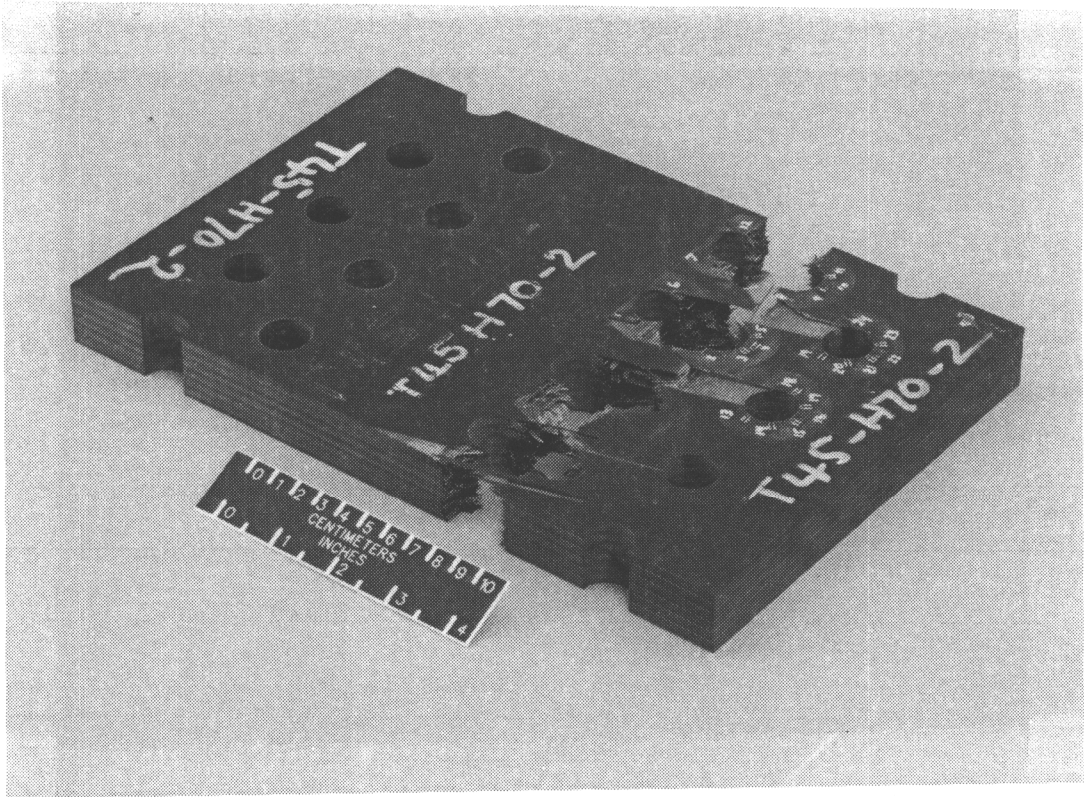


Figure 4.3. A 7-hole T45 outboard specimen after failure

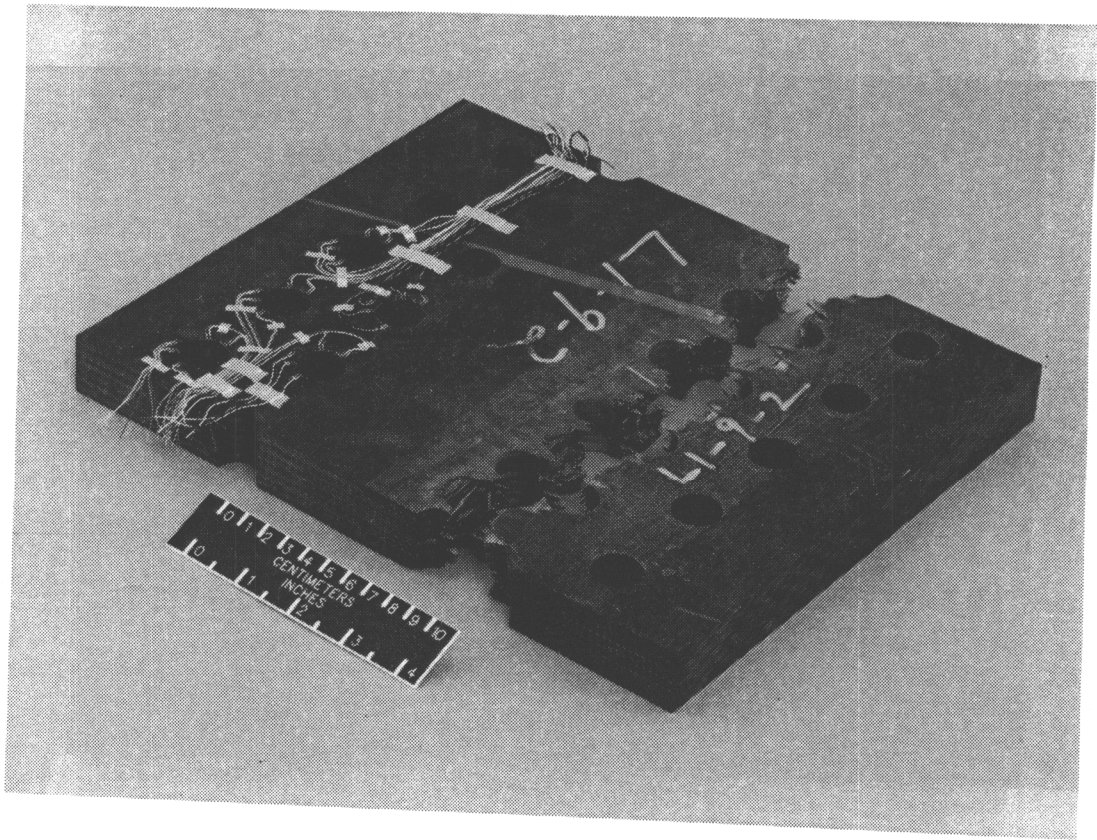


Figure 4.4. A 9-hole T45 inboard specimen after failure

board specimen after failure are shown in the figures 4.1, 4.2, and 4.3, respectively. A 9-hole inboard specimen after failure is shown in fig. 4.4. It can be seen that most of these specimens failed at the inboard net section on the instrumented end of the specimen. The failure data from all multiple-hole specimens is summarized in Table 4.1. This table provides the failure load for each specimen, and the gross-section strength. Gross-section strength is simply the failure load divided by the gross area, i.e., the specimen overall width times the specimen thickness. It can be seen that in Table 4.1, compared to earlier notation, the specimen designation has an additional number appended to the end. This additional number indicates the various replicas of the same specimen. For instance, T45HI3-1, T45HI3-2, and T45HI3-3 denote three replicate 3-hole specimens. Details of the results from testing the various specimens are discussed in the following chapter, where they are discussed in the context of the numerical predictions. For calibration purposes, a few single-hole specimens were also tested.

Figures 4.5 and 4.6 show the X-ray photographs of 5-hole T45 inboard specimens. One photograph, fig. 4.5, was taken after the failure of the specimen, while the other photograph, fig. 4.6, was taken from a specimen which was loaded to the 95% of the estimated failure load. In fig. 4.5 the damage (lighter portion) is clearly visible around the holes on the inboard row of holes on the unfailed end, while it is not so clear in case of fig. 4.6, though with a close look there is some evidence of damage. This damage is concentrated around the net-section region and appears to be associated with transverse failure of the 90° plies, i.e., the plies with fibers perpendicular to the loading direction. A close examination of the failed specimen like the one in fig. 4.5 reveals that although the failure occurred near the net-section region, it is not a net-section failure mode.

Table 4.1 . Summary of Multiple Fastener Joint Tests

Specimen Designation	Number of Holes	Laminate Type	Half-hole Location	Failure Load (kips)	Gross-Section Strength (ksi)
T45HI3-1	3	T45	Inboard	145	38.7
T45HI3-2	3	T45	Inboard	149	39.7
T45HI3-3	3	T45	Inboard	139*	37.1*
T45HI5-1	5	T45	Inboard	220	39.1
T45HI5-2	5	T45	Inboard	228	40.5
T45HI5-3	5	T45	Inboard	219	38.9
T45HI5-4	5	T45	Inboard	210*	37.3*
T45HO5-1	5	T45	Outboard	207	36.8
T45HO5-2	5	T45	Outboard	200	35.6
T45HO5-3	5	T45	Outboard	195*	34.7*
T60HI5-1	5	T60	Inboard	176	31.3
T60HI5-2	5	T60	Inboard	180	32.0
T60HI5-3	5	T60	Inboard	170*	30.2*
T30HI5-1	5	T30	Inboard	207	36.8
T30HI5-2	5	T30	Inboard	194	34.5
T30HI5-3	5	T30	Inboard	190*	33.8*
T45HI7-1	7	T45	Inboard	309	41.2
T45HI7-2	7	T45	Inboard	300	40.0
T45HO7-1	7	T45	Outboard	274	36.5
T45HO7-2	7	T45	Outboard	264	35.2
T45HO7-3	7	T45	Outboard	260*	34.7*
T60HI7-1	7	T60	Inboard	239	31.9
T60HI7-2	7	T60	Inboard	227	30.3
T60HI7-3	7	T60	Inboard	220*	29.3*
T30HI7-1	7	T30	Inboard	269	35.9
T30HI7-2	7	T30	Inboard	257	34.3
T30HI7-3	7	T30	Inboard	220*	33.3*
T45HI9-1	9	T45	Inboard	378	40.3
T45HI9-2	9	T45	Inboard	386	41.2
T45HI9-3	9	T45	Inboard	368*	39.3*

* Test stopped at 95% of the estimated failure load for purpose of X-raying.

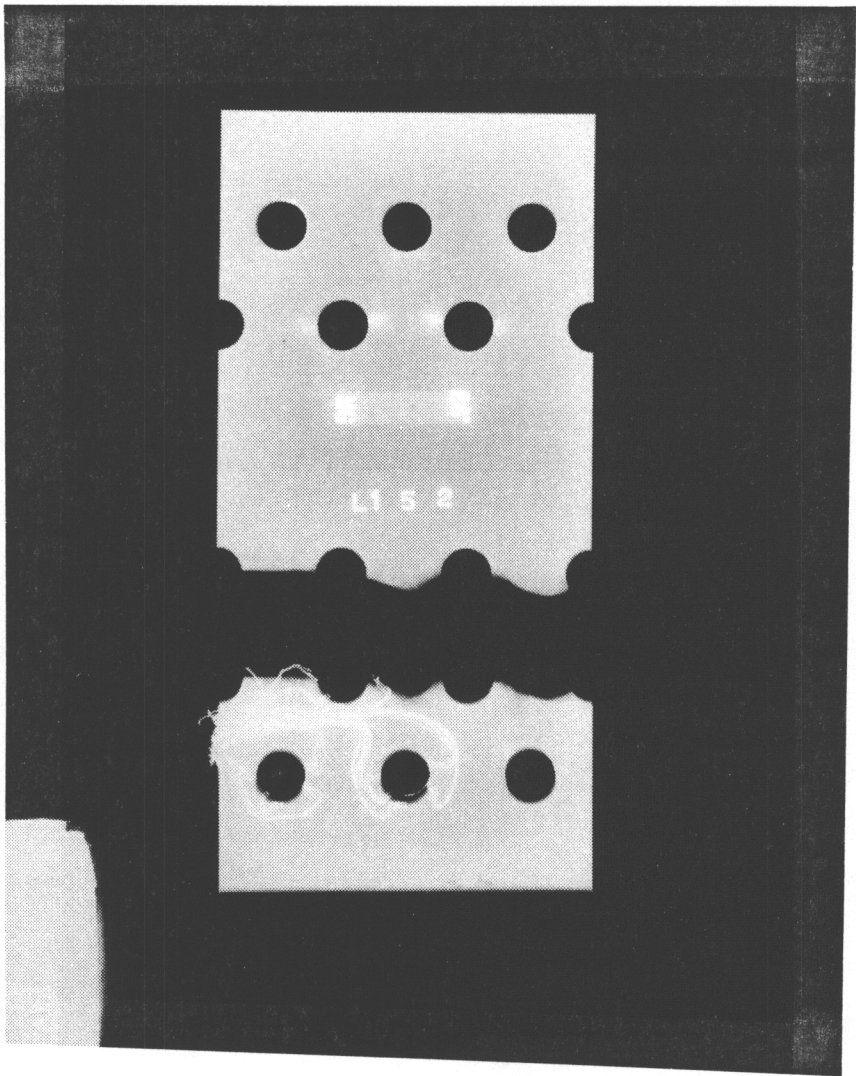


Figure 4.5. X-ray photograph of a failed 5-hole T45 inboard specimen

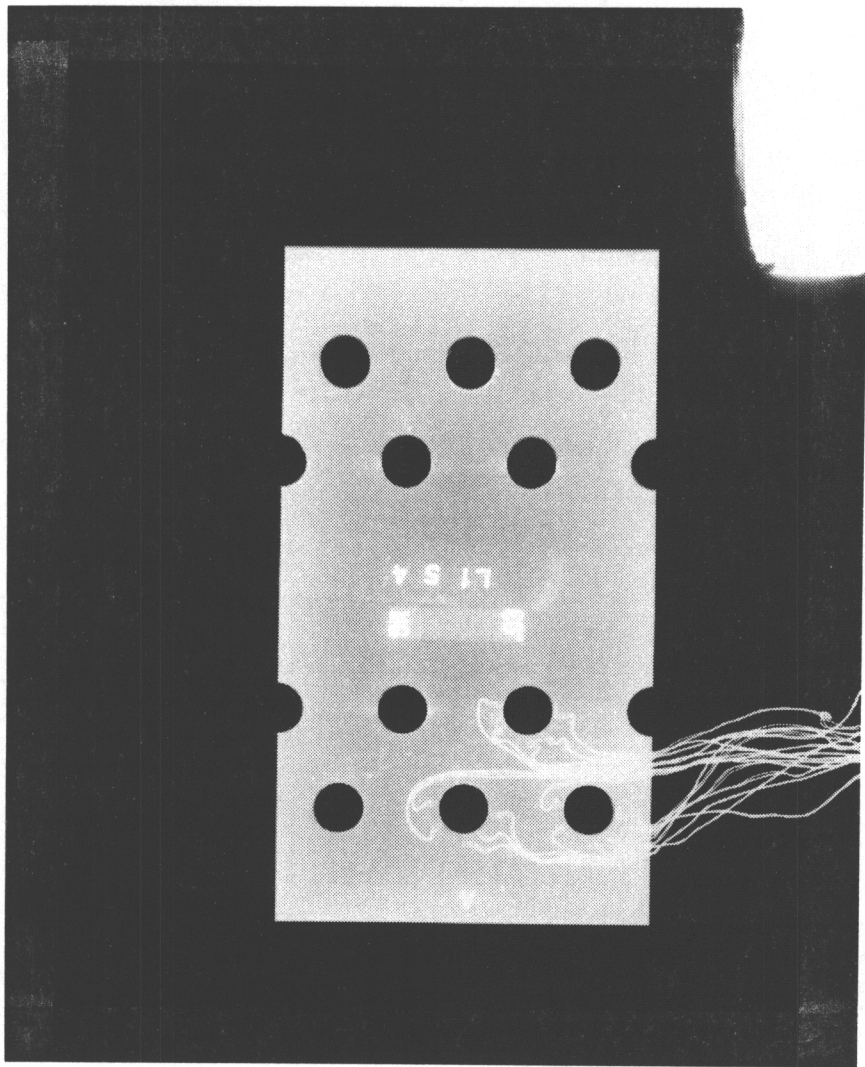


Figure 4.6. X-ray photograph of a 5-hole T45 inboard specimen loaded to 95% of failure load

The failure surface actually originated from the hole edge a small distance around the hole circumference from the net-section. Such a failure could be categorized as a combination of shear-out and net-section failure modes. In general, it is felt that the primary failure was not associated with large progressive damage, rather, the failures for the laminates tested were essentially brittle, fiber-dominated failures

4.2 Load Share Between the Pins

One of the most significant contributions of the present work is providing a clear picture of the load sharing between holes in multihole joints. As has been described, the percentage of load reacted by each hole was measured in the experiments and compared with the values obtained from the analysis. The results from both the experiments and analyses for various specimens of the T45 laminate are presented in Table 4.2. The hole numbering scheme used to identify the holes for the various specimen geometries is shown in fig. 4.7. As can be seen, the numbering starts at the centerline hole (hole no. 1) and the subsequent numbers are reflected on either side of this centerline hole, taking advantage of symmetry. As the experiments were conducted with an instrumented pin in every hole, the experimental data from, say, both holes numbered with a 3 were averaged for the comparison with the analysis. By examining Table 4.2 it can be seen that the present analysis predicts the load sharing between the holes with good accuracy.

Before going on to further discussions regarding load sharing, it is worth considering the method used to compute the load sharing. As described in the previous chapter, the gages on the shank of the pins was used to measure the bending of the pins. The response of these gages were an indirect measure of the load reacted by the pins. The relation between of pin bending strain and applied load for one of 5-hole inboard specimens, specimen

T45HI5-2 to be exact, is shown in fig. 4.8. In this figure, there is a slight deviation of hole numbering notation.

Table 4.2. Pin Load Shares for Different Joints of T45 Laminate: Numerical vs. Experimental

Specimen	Hole 1 (%of total load)		Hole 2 (%of total load)		Hole 3 (%of total load)		Hole 4 (%of total load)		Hole 5 (%of total load)	
	num	exp	num	exp ^a	num	exp ^a	num	exp ^a	num	exp ^a
3-hole inboard	41	38	30	32						
5-hole inboard	13	14	24	24	20	19				
5-hole outboard	20	20	14	17	26	23				
7-hole inboard	15	15	10	12	18	16	15	15		
7-hole outboard	9	10	15	16	11	11	20	16		
9-hole Inboard	8	8	12	13	8	8	14	13	12	12

a. Indicates average value of load percentage from holes symmetric about centerline



Indicates value not applicable.

A suffix of L (for left) or R (for right) was added to the hole numbers to denote their position with respect to the centerline hole, as opposed to earlier notation where the holes were numbered without any suffixes. This identification of pin location with respect to the center hole facilitates the detection of inplane bending, if there was any. It should be noted that this deviation in notation is only for this section and subsequent discussions do not include the suffixes. As the load increases, the pin bending strain increases accordingly. The

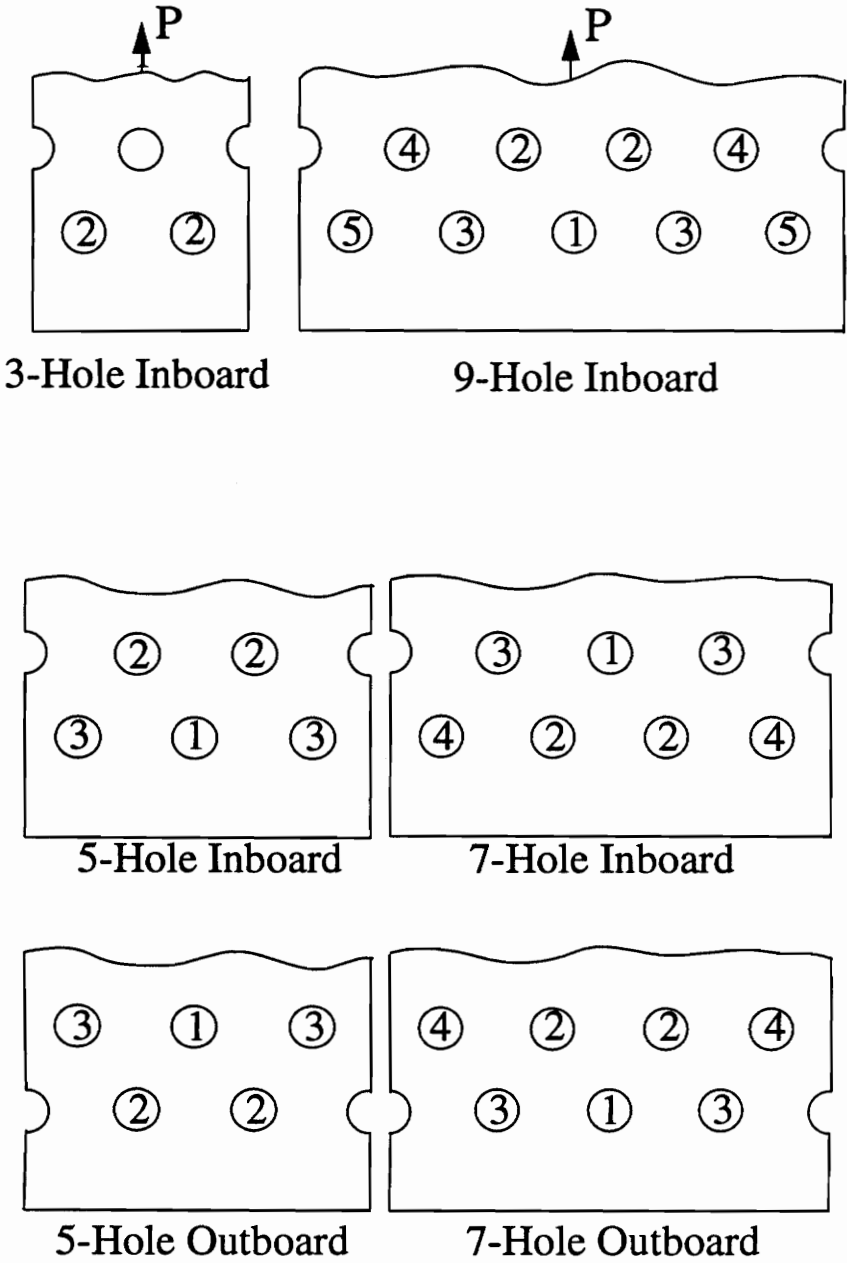


Figure 4.7. Hole numbering pattern for different specimens

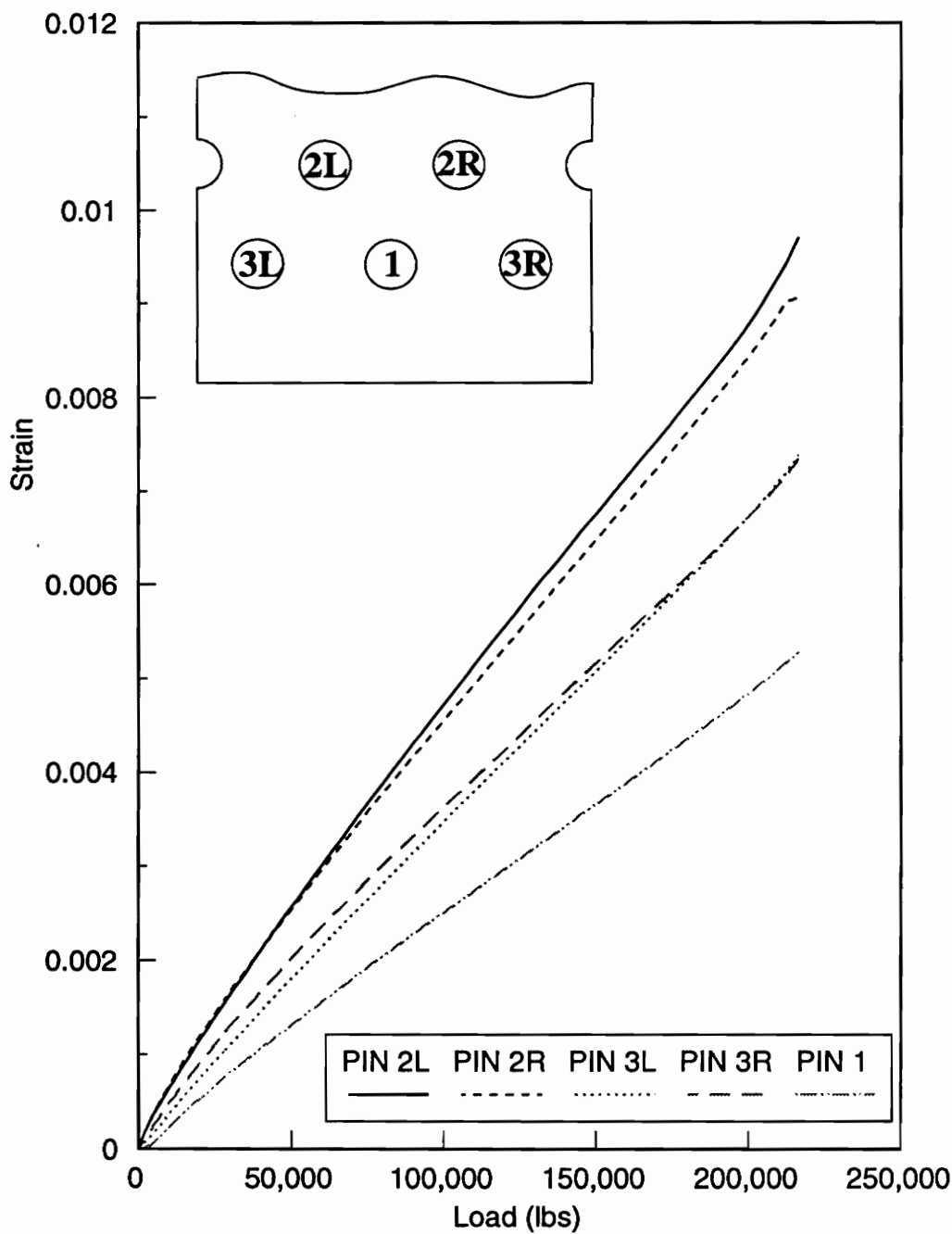


Figure 4.8. Pin bending strains for pins of a 5-hole T45 inboard specimen

relationship between pin strain and the load is nearly linear and there is significant symmetry to the left-right response of the joint. For example, the response of pin 2 to the left of the centerline and the response of pin 2 to the right of the centerline are very similar. Figure 4.9 shows the plot of the same data transformed into percentage strain. These data are determined as follows: At a given load level the strains for the pins are summed. Then at that load the strain for each pin is divided by the sum of the strains. The percentage load for the i^{th} pin is assumed to be given by that ratio or,

$$\text{Percentage load for } i^{\text{th}} \text{ pin} = \frac{\epsilon_i}{\sum_{k=1}^{N_{\text{pin}}} \epsilon_k} \times 100\% \quad (4.1)$$

where N_{pin} is the number of pins.

It can be seen that for this particular specimen, after about 50,000 lbs the pins react a percentage of load that remains the same to failure. The response below 50,000 lbs can be attributed to any of the following: (a) hole misalignment; (b) small differences in diameters of the different holes; or (c) slight eccentricities in the load fixture. These irregularities are sometimes serious and result in drastic changes in percentage load sharing, as illustrated by fig. 4.10. The figure represents the pin bending response for a 5-hole outboard specimen, specifically specimen T45HO5-3. In other cases, anomalies are almost non-existent, as can be seen in fig. 4.11 for another outboard 5-hole specimen, specifically, T45HO5-2. The percentages of load sharing shown in the Table 4.2 were calculated by taking the average of each pin's reaction for all the replicate specimens of a given type at 75% of the failure load, a load for which the percentages are fairly stable and constant.

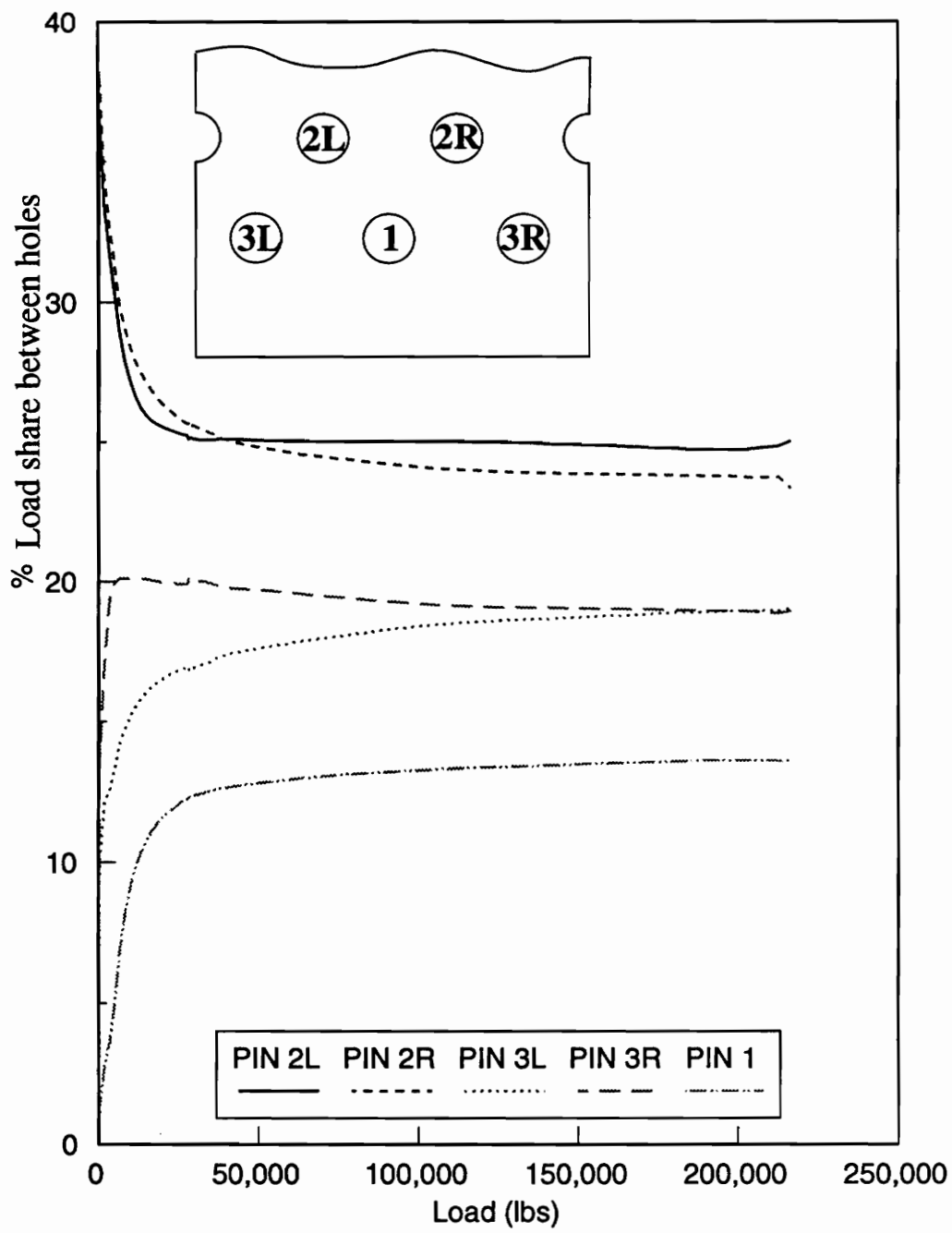


Figure 4.9. Percentage load sharing for a 5-hole T45 inboard specimen with nonconstant load proportion

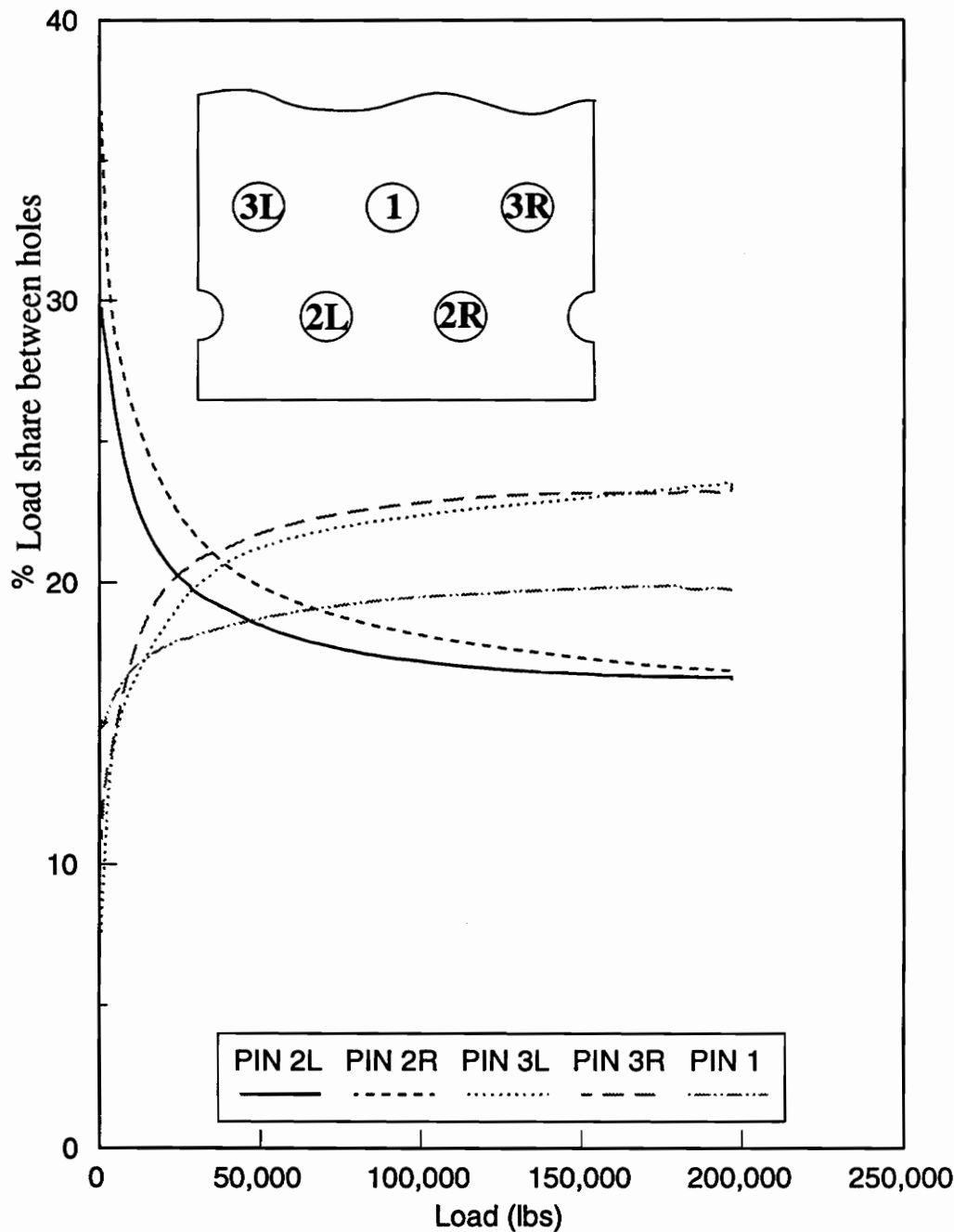


Figure 4.10. Percentage load sharing for a 5-hole T45 outboard specimen with load proportion reversal

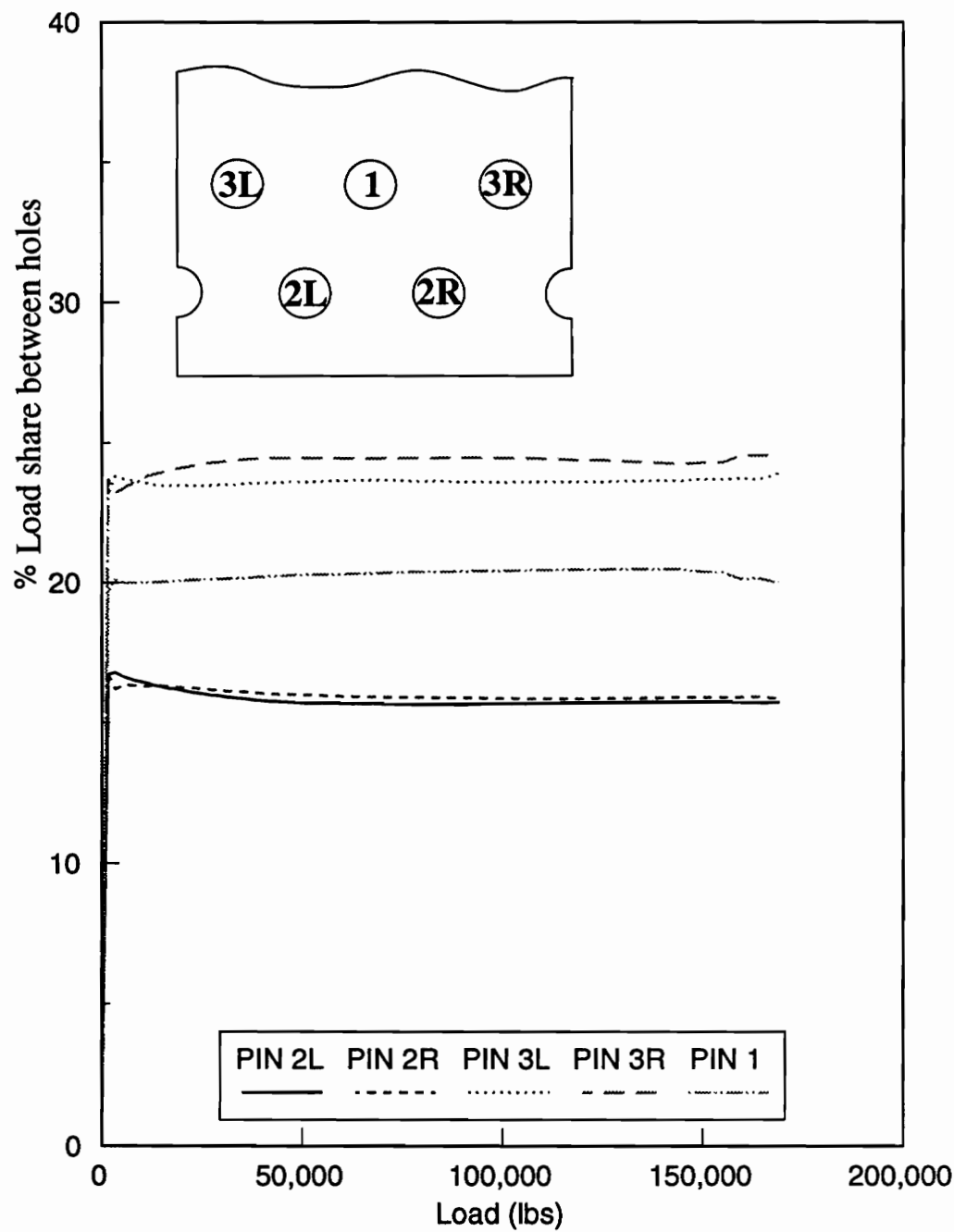


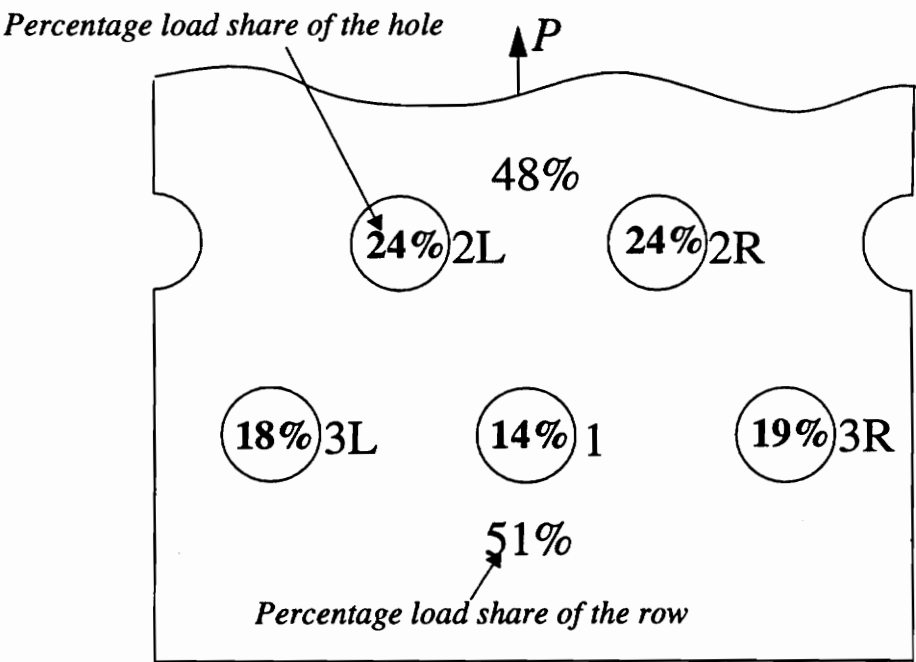
Figure 4.11. Percentage load sharing for a 5-hole T45 outboard specimen with constant load proportion

4.2.1 Inboard vs. Outboard Half-Hole Location

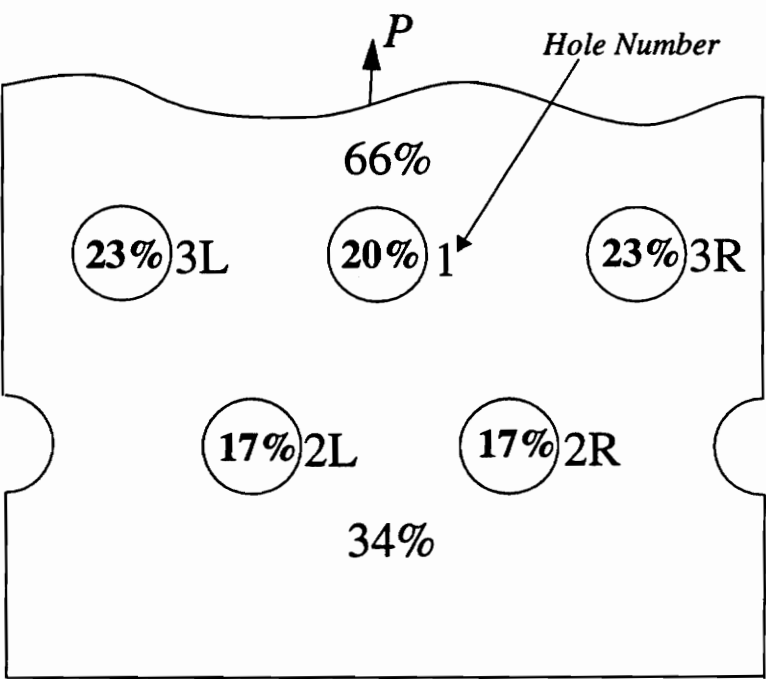
One of the primary objectives of the current study was to determine the effect of the location of the half-hole, i.e., inboard or outboard, on load capacity. From Table 4.1 it is clear that for both the 5-hole and 7-hole T45 specimens the inboard configuration reacts about 10% more load than the outboard configuration. The details of this difference in strength can be seen upon a closer look at the percentage load sharing between different holes. Details of the load sharing for these T45 specimens are shown in figs. 4.12 and 4.13. It is noticed that irrespective of the half-hole location, each hole on the inboard row reacts at least as much load as any one on the outboard row. Additionally, when the half hole is outboard, the inboard row reacts considerably more load than the outboard row. In fact, for the 5-hole and 7-hole specimens, when the half-hole is outboard, the inboard row reacts about twice as much load as the outboard row. Finally, for the inboard specimens, the percentage of load per row for the 5-hole specimen is nearly identical to the percentage of load per row for the 7-hole specimen. The same is true for the 5-hole and the 7-hole outboard specimens. As might be expected, the row with more holes shares a greater percentage of the total load than the row with less holes. With the half hole on the inboard row, and this row then having less holes, the inboard row shares somewhat less of the total load than the outboard row. However, with the half hole on the outboard row, and thus the inboard row having more holes, as pointed out above, the inboard row reacts almost twice as much load as the outboard row. Hence, having the half hole on the outboard row appears to shift the load disproportionately to the inboard row, and hence reduces total load capacity somewhat.

4.2.2 Comparison of Three Laminates

The experimentally determined load proportioning for 5- and 7-hole T30, T45, and T60



5-Hole Inboard



5-Hole Outboard

Figure 4.12. Experimentally measured load proportions for 5-hole T45 specimens

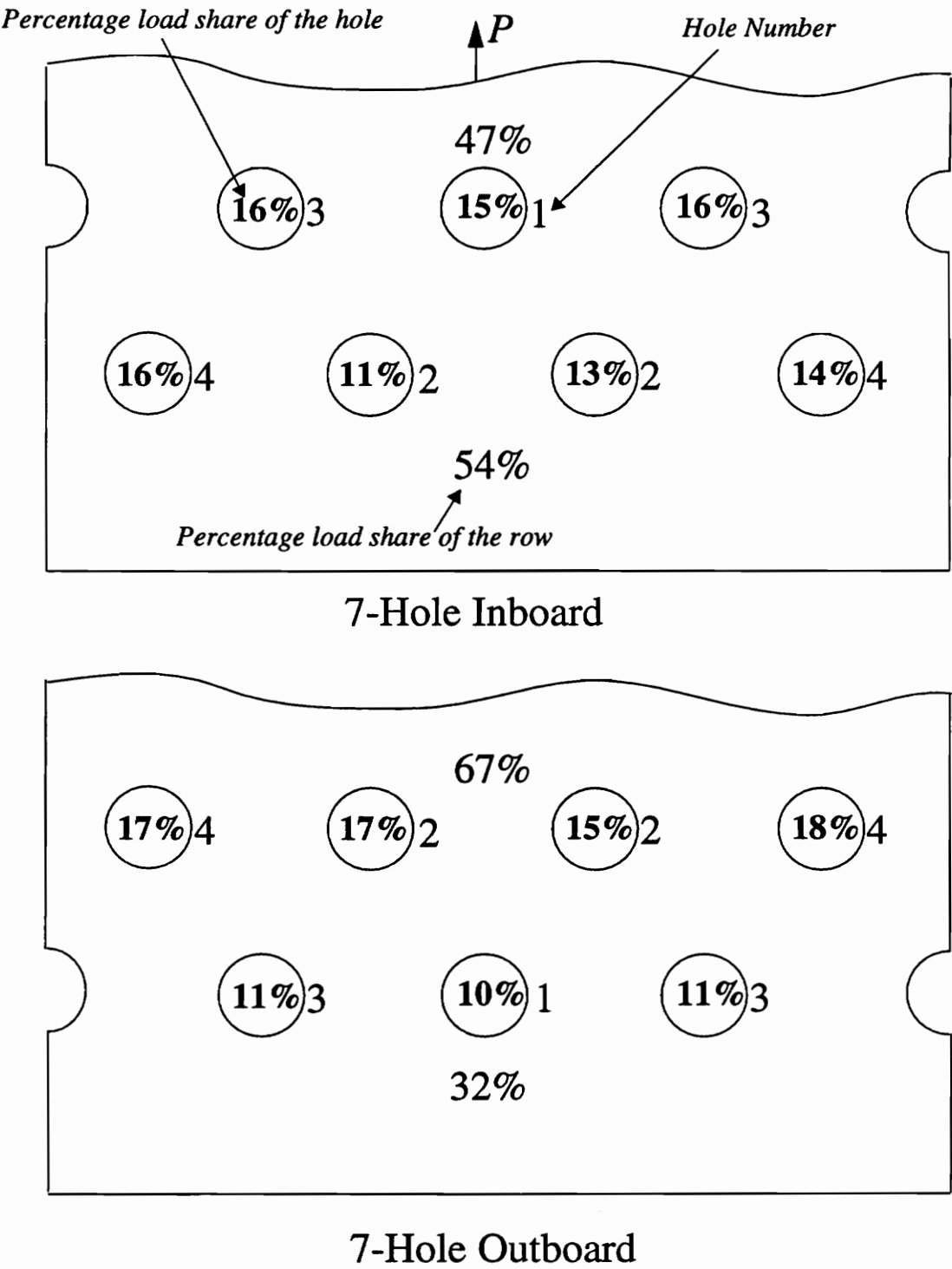


Figure 4.13. Experimentally measured load proportions for 7-hole T45 specimens

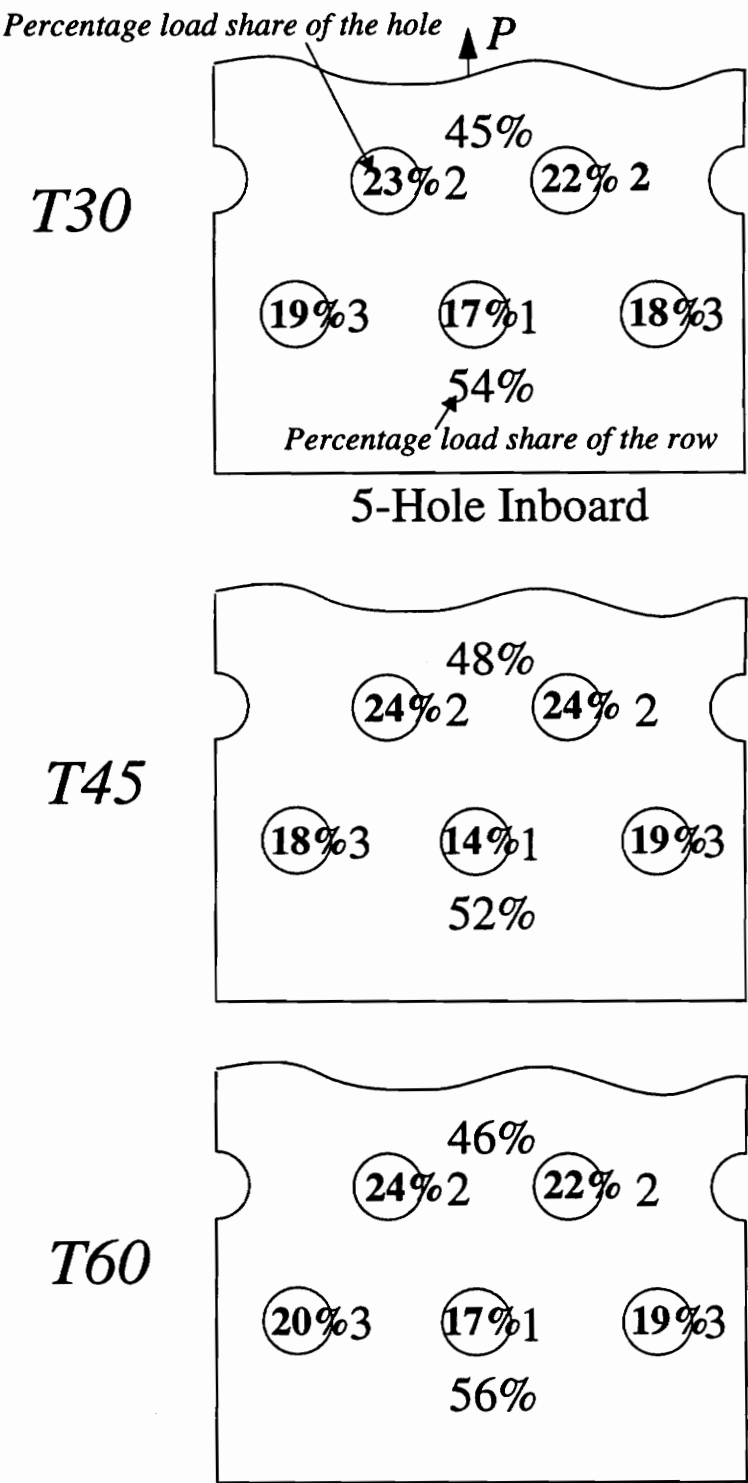


Figure 4.14. Experimentally measured load proportions for 5-hole T30, T45, and T60 inboard specimens

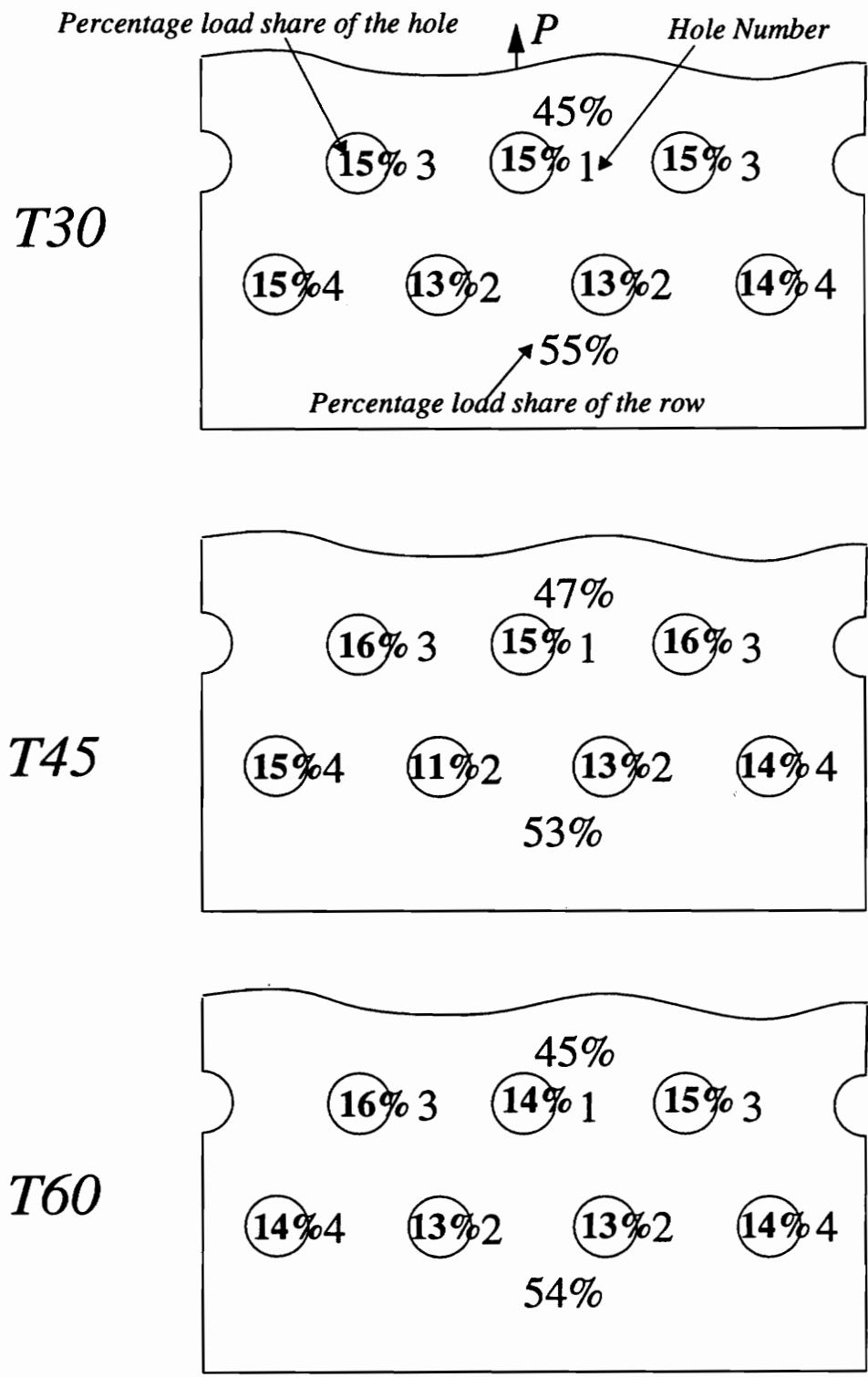


Figure 4.15. Experimentally measured load proportions for 7-hole T30, T45, and T60 inboard specimens


inboard specimens are compared in figs. 4.14. and 4.15. It can be seen that the percentage of the total load shared by the each row for the 5-hole T45 specimen is close to 50%, with the inboard row's share somewhat under 50%, and the outboard row's share somewhat over 50%. The same is found to be true in case of 7-hole T45 inboard specimen. For the other two laminates, the load proportions are not as close to 50% for either the 5- or 7-hole specimens. These differences in percentages are within the experimental error. However, if these differences exist in reality, the disproportional load sharing between the rows could be one of the reasons for lower strength of the specimens of T30 and T60 laminates.

Comparisons between the numerically predicted and experimental measured load proportions for the 5- and 7-hole T30, T45, and T60 inboard specimens are shown in Table 4.3.

Table 4.3. Pin load shares for 5-, 7-hole Inboard Specimens, Comparison of Three Laminates

Specimen	Hole 1 (%of total load)		Hole 2 (%of total load)		Hole 3 (%of total load)		Hole 4 (%of total load)	
	num	exp	num	exp ^a	num	exp ^a	num	exp ^a
5-hole T30	16	17	23	22	19	18		
5-hole T45	13	14	24	24	20	19		
5-hole T60	17	17	22	23	20	19		
7-hole T30	14	15	12	13	16	15	16	14
7-hole T45	15	15	10	12	18	16	15	15
7-hole T60	16	14	12	13	17	16	15	14

a. Indicates average value of load percentage from holes symmetric about centerline.

 Indicates values not applicable

4.3 Strain Gage Measurements

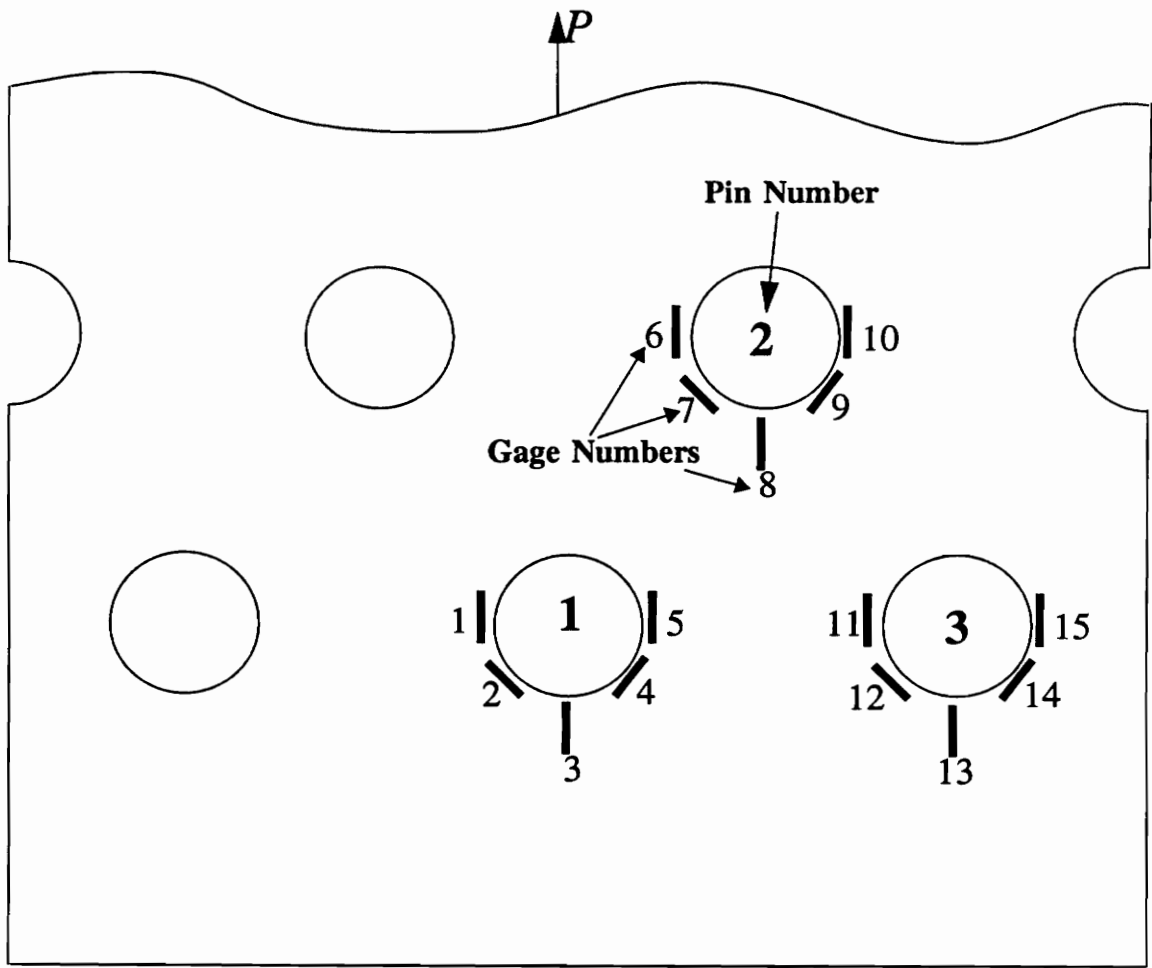
Load proportioning provides an overall view of the response of the joint specimens. Strain gages provide a more detailed view. Comparisons among geometries, for a given laminate, and among laminates for a given geometry, provide insight into what variables are important in determining specimen response. In this section, the strains measured during the experiments and the strains predicted from the numerical analysis are compared by examining strain vs. load relations. The locations of the strain gages were discussed in Ch. 2. In the figures to follow, the load (ordinate of the plots) is normalized by the failure load of the corresponding specimens. A horizontal line representing the failure load is drawn at the ordinate value of unity. As the failure load is determined by taking average of the failure loads of similar specimens, the load for any one of the specimens may go beyond the normalized failure level of unity, while the loads for another may fall short of unity. Hence the ordinate of all the figures has a range from 0 to 1.2. This normalization by the average failure load makes comparisons between different specimens straightforward, even for specimens having different numbers of holes, or different lamination sequences.

In the figures to follow, within a figure there are a number of subfigures, the subfigures being separated by gage number. As mentioned in Ch. 2, three replicate specimens were tested for each kind of specimen. This results in three distinct load vs. strain relations for a gage at a given location on a given specimen type. The three different relations pertaining to three different specimens are indicated by S1, S2, and S3 in the legends of the subfigures corresponding to specimen 1, specimen 2, etc. The predicted strains from the analyses are shown on the subfigures. Though in the experiments the strains were measured as a continuous function of load, the ABAQUS analyses were not printed for a continuous spectrum

of loads. Rather the analyses were printed at 50% and 75% of the failure load. In general, contact problems cannot be solved numerically in direct fashion. Rather, they require specification of a load level and iteration to achieve a satisfactory solution at that load level. In the figures to follow, the predicted strains at the 50% and 75% load levels are indicated by asterisks. The two asterisks and the zero load-zero strain point are connected with straight lines. As will be seen, the predicted strain response vs. load is practically linear. Thus, while connecting the three points with a straight line is not entirely correct, a straight line closely represents the predicted load vs. strain response. The load vs. strain relations for other specimens are presented in the appendices, Appendix A for the 3-hole specimen, Appendix B for the 7-hole specimens, and Appendix C for the 9-hole specimens. Much of the discussion in this chapter extends to those relations as well.

4.3.1 Discussion of the 5-hole Load vs. Strain Relations and Comparisons between Inboard and Outboard Specimens

To understand the figures to follow, the numbering scheme of the strain gages must be introduced. The numbering scheme for the 5-hole inboard specimens is shown in fig.4.16. It should be noted that the numbering pattern for gages is not necessarily related to the numbering pattern for the holes. Also, as mentioned earlier, for economic reasons, gages were installed around only three of the five complete holes, taking advantage of the left-right symmetry of the problem. Unfortunately, any left-right inplane bending in the specimen would remain undetected, though it would strongly influence the strains. It can be seen that gages 1, 5, 6, 10, 11, and 15 were located at the net-section regions of the holes and hence were the net-section gages. Gages 2, 4, 7, 9, 12, and 14 were the shear gages. It is important to note that these gages recorded only extensional strains at angle of 45° , not the shear strains. Gages 3, 8, and 13 were the bearing gages, recording the compressive bearing



5-Hole Inboard Specimen

Figure 4.16. Strain gage numbering scheme for 5-hole inboard specimens

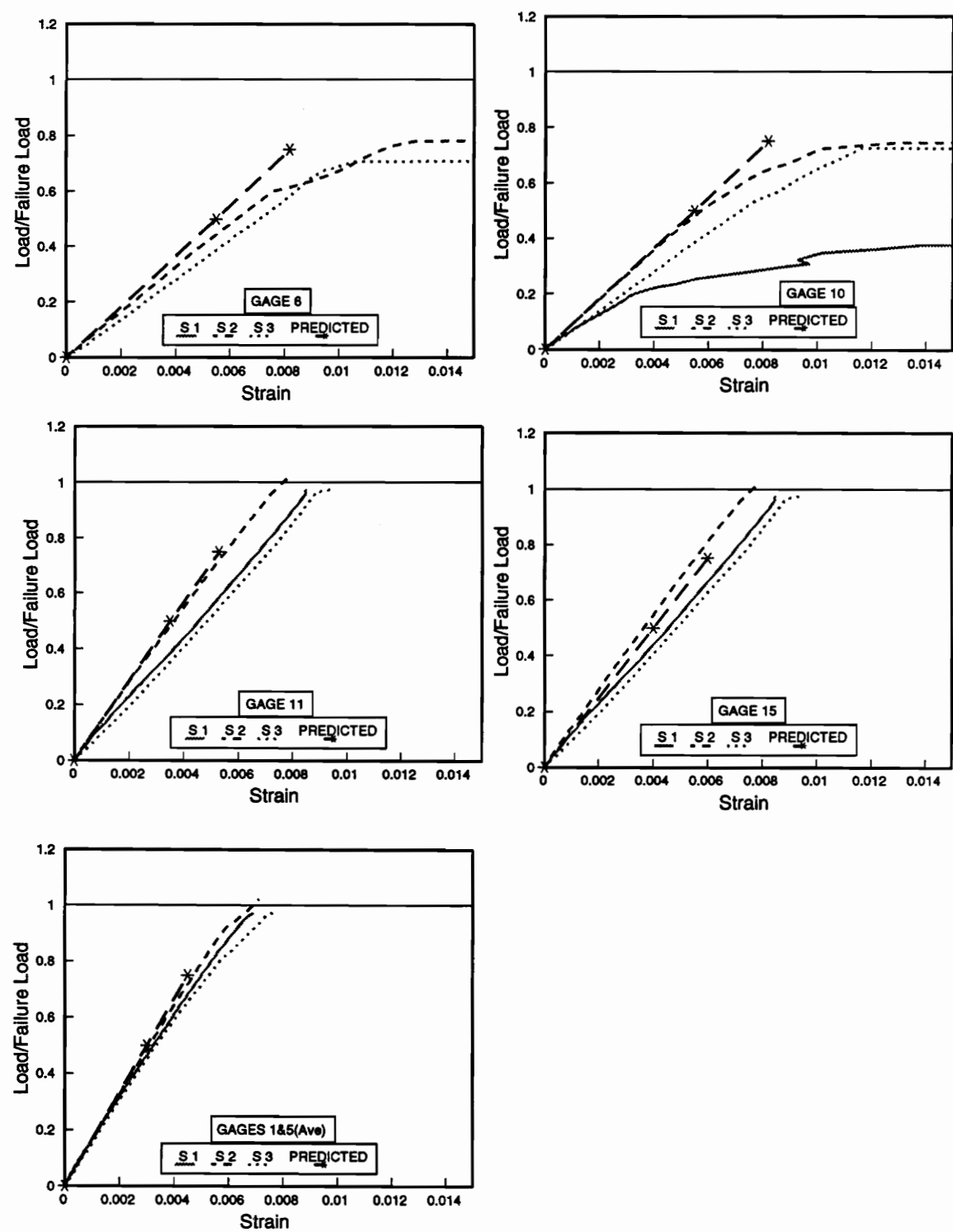


Figure 4.17. Measured and predicted net-section gage strains for 5-hole T45 inboard specimens

strains at the lower edge of the hole.

The predicted and measured strains for all the net-section gages for 5-hole T45 inboard specimens are shown in fig. 4.17. As mentioned previously, the ordinate value of unity represents the average failure load for these specimens. The average failure load is based on results from specimens S1 and S2. Gages 1 and 5 are on the most lightly loaded hole (see fig. 4.12 or 4.14, or Table 4.2 or 4.3). Gages 1 and 5 were symmetrically located about the centerline and hence should have shown identical readings. Indeed, the individual responses of the gages was found to be very similar. For this reason, the average response of these two gages is shown rather than showing the responses of individual gages. As can be seen, the correlation between the predictions and measurements for these strains is quite good, the strains becoming somewhat nonlinear just prior to the failure. Gages 6 and 10 are on the inboard hole, the most heavily loaded hole. The response of these two gages is not expected to be identical. Unfortunately, because hole 2 is at a greater distance from the specimen centerline than hole 1, the strains around that hole are more susceptible to side-to-side bending in the specimen biasing strain responses. Gage number 10 on specimen S1 failed prematurely, as can be seen in the subfigure for that gage. Gages 11 and 15 are even farther from the specimen centerline and even more susceptible to side-to-side bending.

Overall, the correlation between the experiments and predictions for the net-section gages was good. Specimen 2 correlated almost perfectly with numerical predictions. For gages 1 and 5, all specimens correlated well with the prediction. Side-to-side bending could have influenced the responses of gages 6, 10, 11, and 15 and influenced the correlation between experimental results and numerical predictions. With the format of these figures, the slopes of the load vs. strain relations can be used to compare load sharing of the various holes. Shallower slopes correspond to more loading. In this regard, as discussed earlier,

holes on the inboard row take more load than the ones on the outboard. This is confirmed to some degree by the fact that the two gages on the inboard hole, gages 6 and 10, consistently show higher net-section strains (shallower slopes) than the others. The gages on the outboard holes are also consistent with the load sharing data that was shown in the earlier section. The load proportion was less for the holes close to the centerline of the specimen compared to the holes close to the edge (see fig. 4.12 or 4.14, or Table 4.2 or 4.3). This trend is reflected in the load vs. strain relations. The net-section strain was least around the center hole and increased as the holes became closer to the specimen edge. It is interesting to note that nonlinear load vs. strain behavior appeared to begin at strain levels of 0.008.

The strains recorded by the shear gages are shown in fig. 4.18. These gages, for the most part, showed nonlinear behavior, though there was an initial linear trend. The repeatability from specimen to specimen was poor, except for the gages on the centerline hole. Since gages 2 and 4 are symmetric about the centerline, their average was compared with the predicted results. Overall, the shear gage responses followed the trend indicated by the net-section gage response and the load sharing percentages. The correlation between the experimental and predicted values was still reasonably good, although not as good as with the net-section gages. This is primarily because of the poor repeatability of the experimental values. The predicted values, however, are within the experimental scatter.

The load vs. strain relations for the bearing gages is shown in fig. 4.19. The bearing gages almost never showed linear response. The repeatability for the bearing gages was worse than in the case of shear gages. To be sure, however, the predicted response was within the range of measured responses among the three specimens. Since the bearing gages were in close proximity to the high contact stresses and susceptible to crushing, and since they were susceptible to erratic behavior due to the top layer of the laminate possibly buckling, some

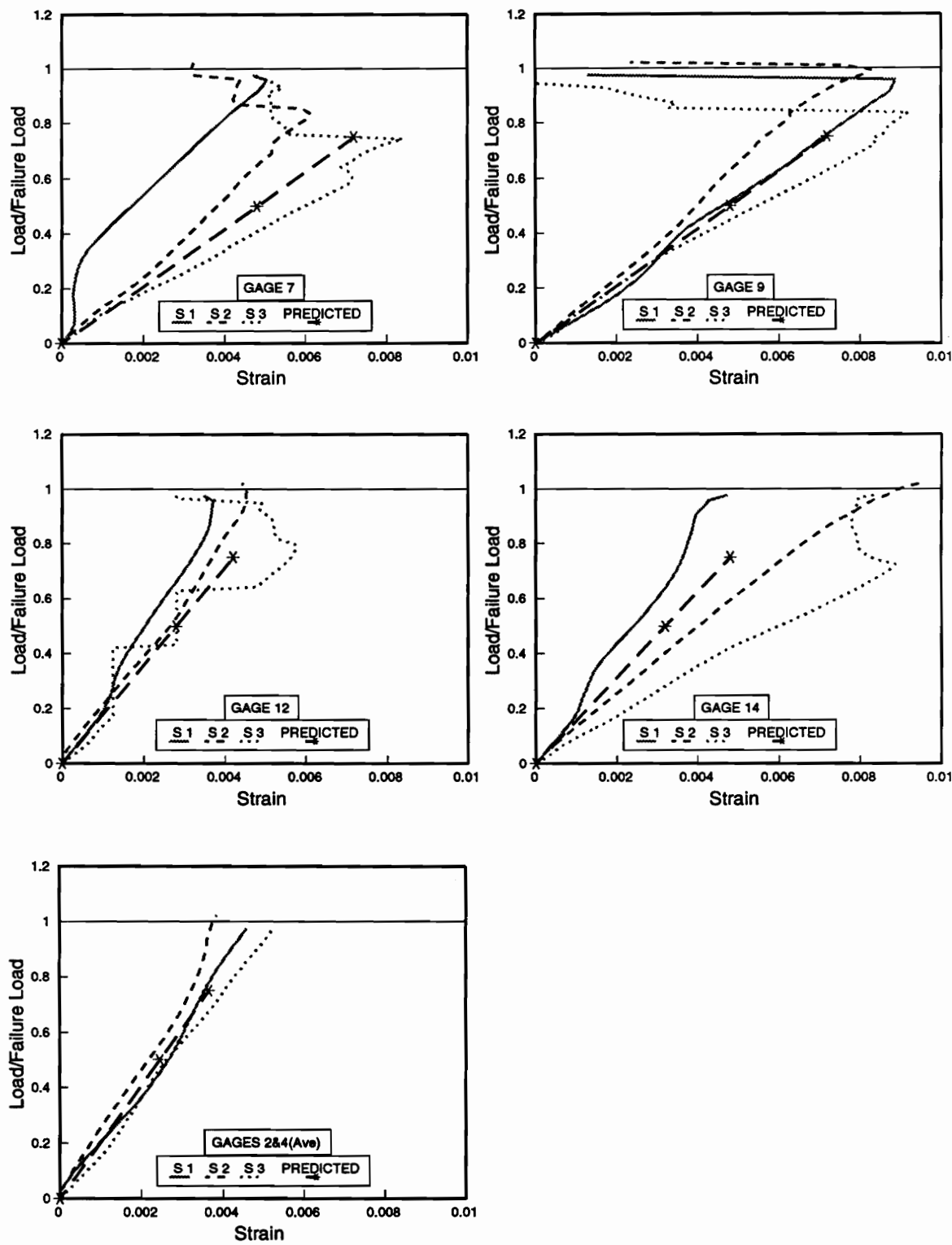


Figure 4.18. Measured and predicted shear gage strains for 5-hole T45 inboard specimens

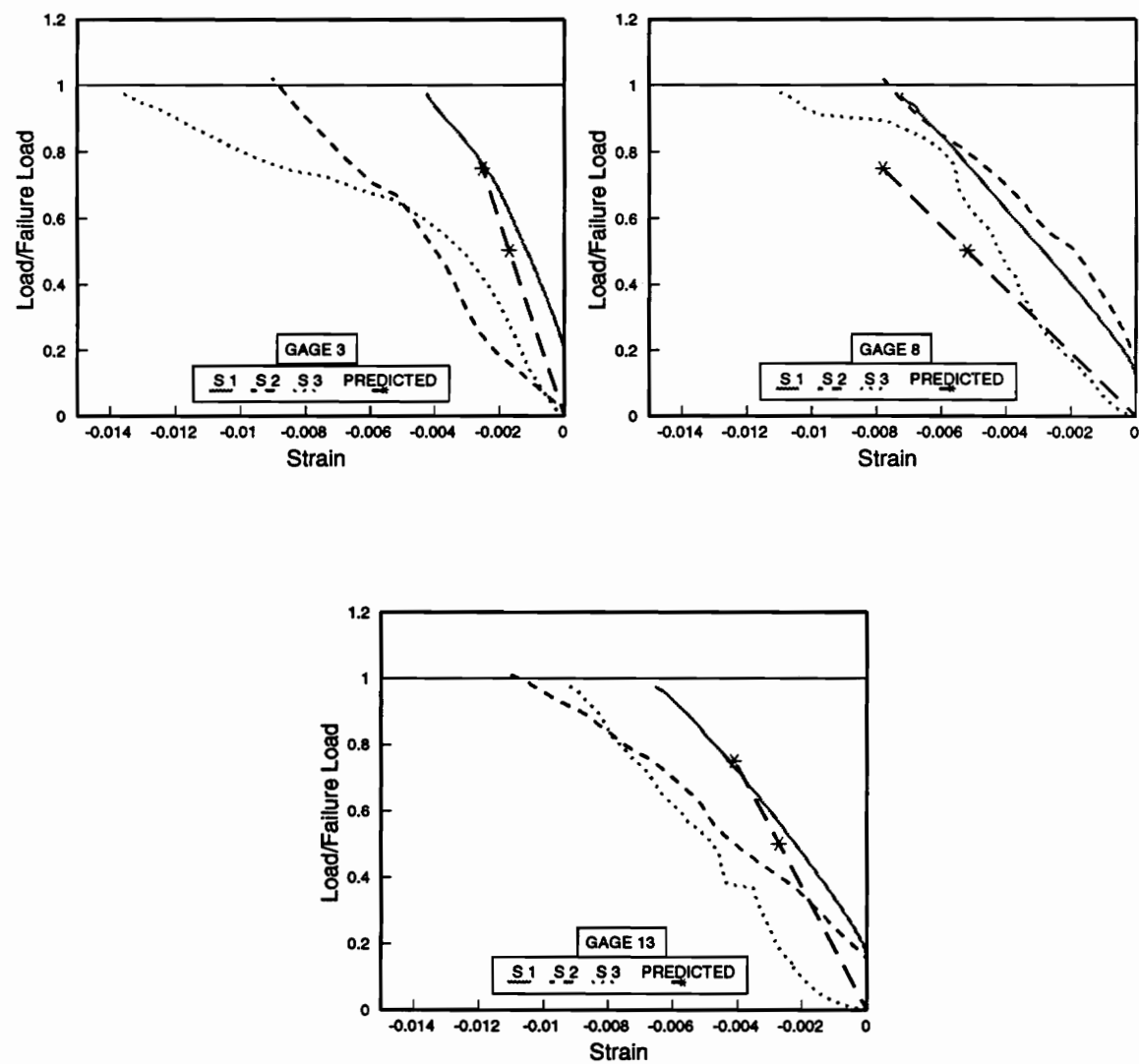
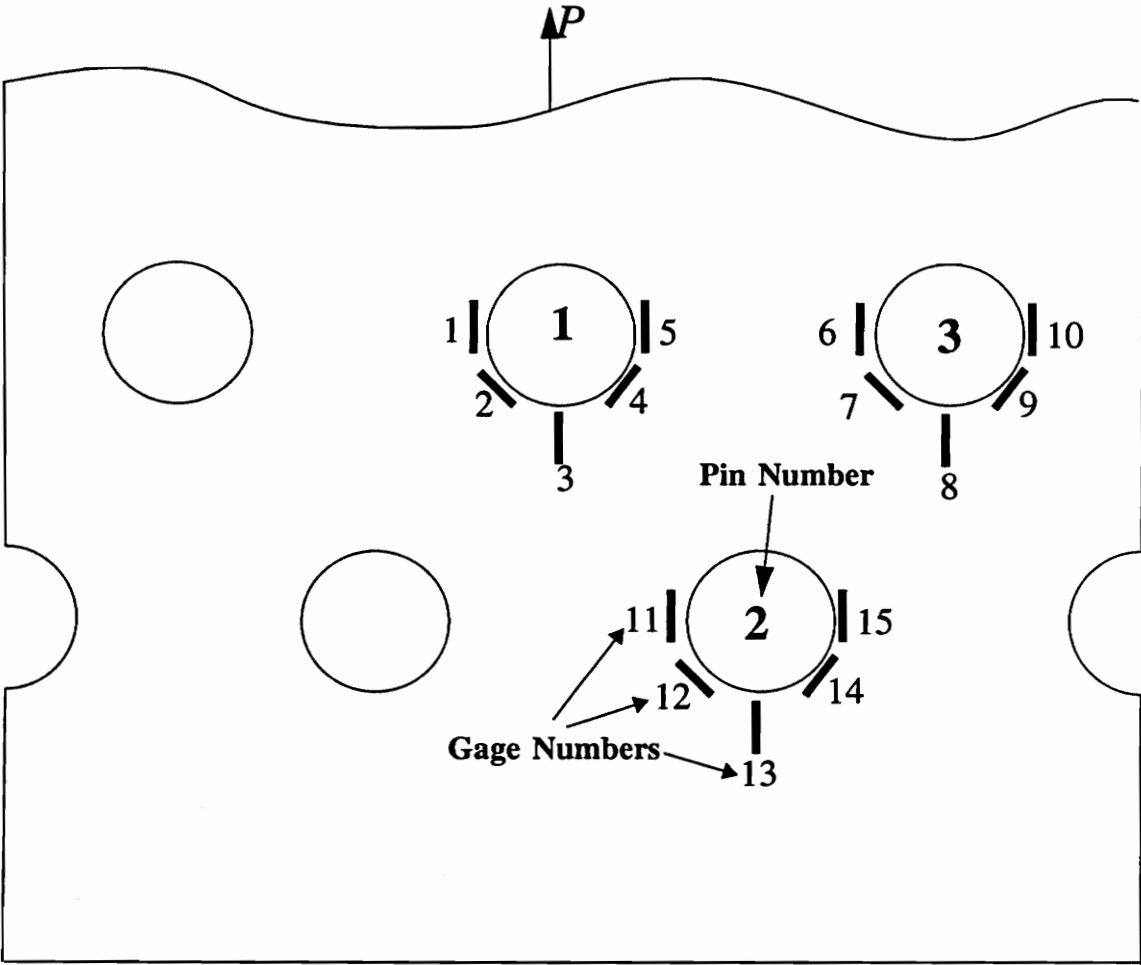


Figure 4.19. Measured and predicted bearing gage strains for 5-hole T45 inboard specimens

nonlinear behavior was expected. The measured bearing strains were generally less than the predicted bearing strains.

The numbering scheme for the strain gages on the 5-hole outboard specimens is shown in fig. 4.20. The response of the net-section, shear, and bearing gages, for the 5-hole outboard T45 specimens is shown in figs. 4.21, 4.22, and 4.23, respectively. Overall, the strain data for these net-section gages is of the same quality and level of repeatability as the strain data from the net-section gages on the 5-hole inboard specimen just discussed, fig. 4.17. Repeatability is good, the response is generally linear, and the correlation between the prediction and measurements was good as long as the gage accurately recorded the strains. It is not possible to determine whether the nonlinearity in the load vs. strain relation for, say gage 6, was due to material nonlinearity, or due to the strain gage disbonding from the specimen. The figures, however, again confirm the conclusions drawn from the load share data in the earlier sections, namely, the holes on the outboard row, gages 11 and 15, show less strains relative to the ones on the inboard row. Specifically, for this outboard specimen, the slopes of the load vs. strain relations for the inboard holes are significantly less than the slopes of the load vs. strain relations for the outboard holes. This reflects the factor of two in the amount of the total load shared by the inboard row compared to the outboard row for the outboard specimens (see figs. 4.12 and 4.13). This is in contrast to the somewhat similar slopes for the inboard specimens, fig. 4.17, reflective of the fact that for the inboard specimens the two rows share roughly the same percentage of load. The significantly greater strain on the inboard row of the outboard specimens is indicative of why the outboard specimens failed at lower total load when compared to the inboard specimens.

As with shear gages for the 5-hole T45 inboard specimens, fig. 4.18, for the 5-hole T45 outboard specimens the responses of the shear gages, fig. 4.22, were more erratic than the



5-Hole Outboard Specimen

Figure 4.20. Strain gage numbering scheme for 5-hole T45 outboard specimens

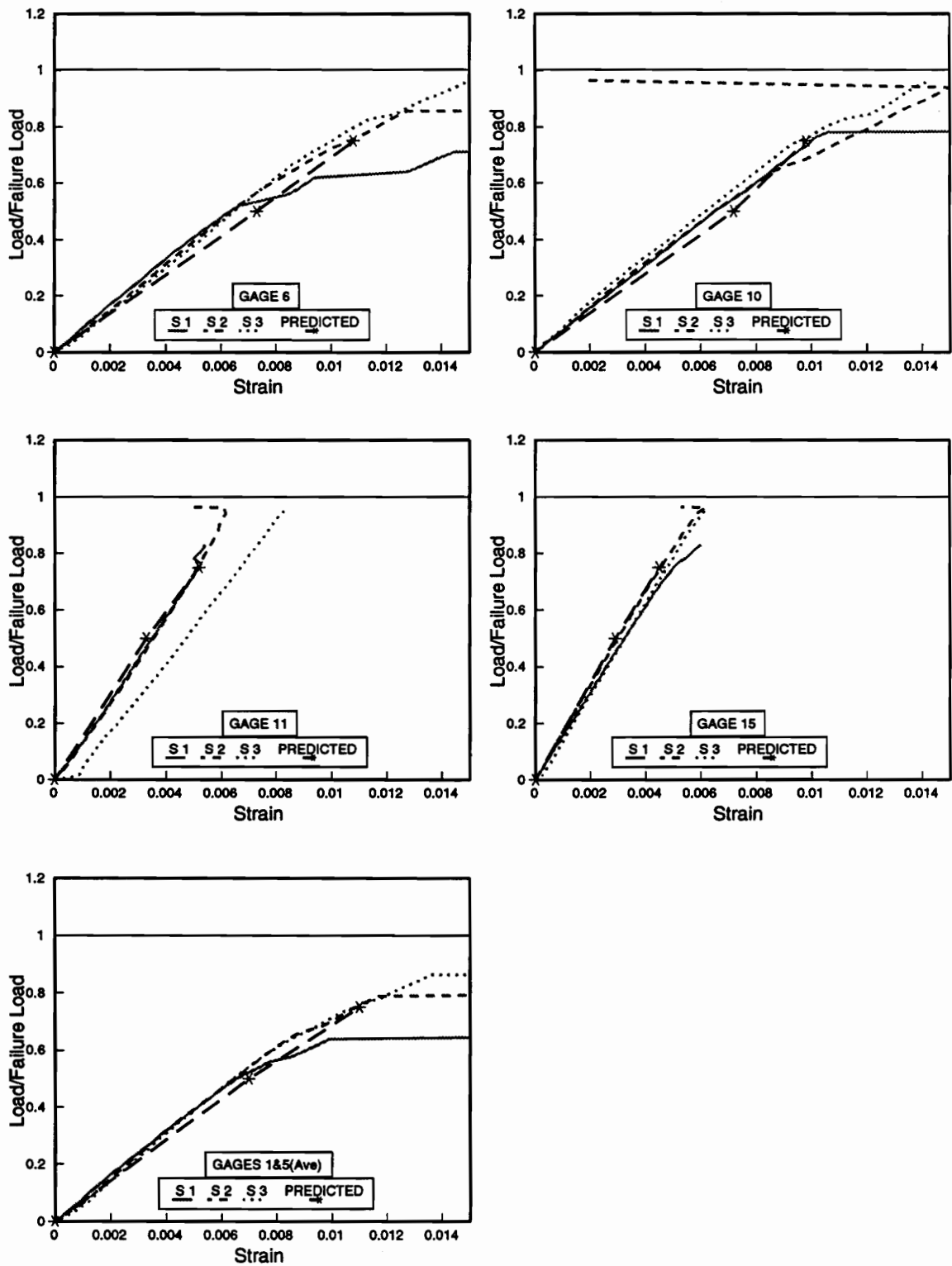


Figure 4.21. Measured and predicted net-section gage strains for 5-hole T45 outboard specimens

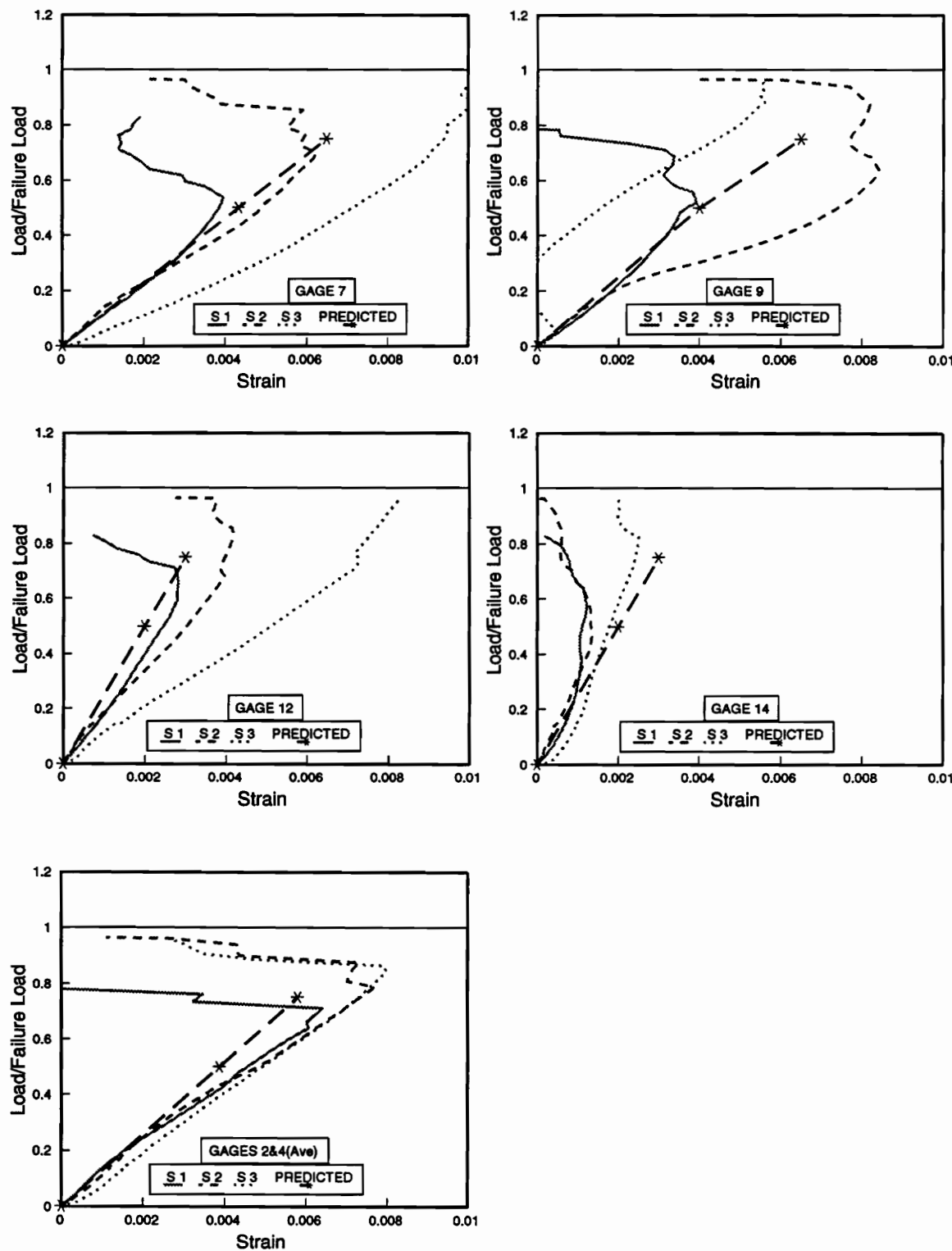


Figure 4.22. Measured and predicted shear gage strains for 5-hole T45 outboard specimens

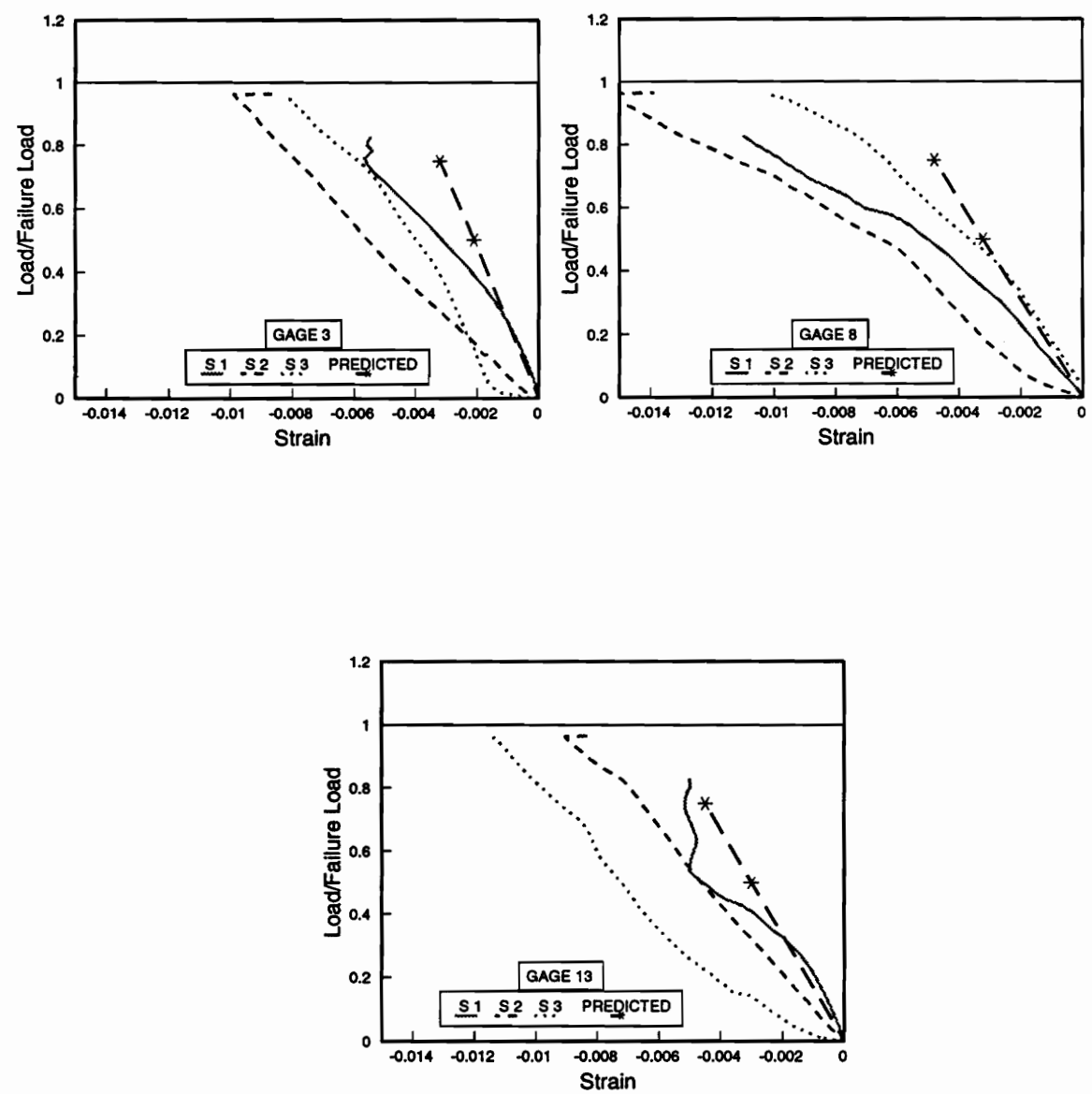


Figure 4.23. Measured and predicted bearing gage strains for 5-hole T45 outboard specimens

responses of the net-section gages. It is not clear what causes this problem, but like the bearing gages, though to a lesser degree, the shear gages are in the vicinity of pin/hole contact, whereas with the net-section there is no pin/hole contact. The gages on the centerline hole do appear to be less erratic than the gage response at other holes. Hence, side-to-side bending may be a factor.

The response of the bearing gages, fig. 4.23, are again somewhat erratic but show an overall trend that is reflected by the prediction. The measured bearing strains, however, are much less than the predicted bearing strains. While the correlation is reasonably good for shear gage and bearing gage strains, the data showed wide range of scatter and rather poor repeatability, similar to the case of inboard specimens, fig. 4.19.

4.3.2 Comparisons among the Three Laminates

The load vs. strain relations for the net-section gages on the T30 and T60 laminates, for the inboard configuration, are shown in figs. 4.24 and 4.25 respectively. These results are the counterparts to the results in fig. 4.17 for the T45 laminate. Reasonably good correlation between the numerical and experimental values was found for most gages, except for gages 1 and 5, where the numerical results seem much too stiff. These numerical results follow the trend that was shown by other specimens, i.e., namely the gages around the centerline hole showing less strains compared to those holes which are off the centerline. The above confirmation of numerical results strongly suggests a possibility of a data collection error during experiments for these two particular gages. Repeatability of the gage responses among the three specimens confirms this possibility. Though difficult to detect with the non-dimensional form of the figures, for a given load level the net-section strains for the T45 laminates were less than for the T30 or T60 laminates. This is consistent with the fact that the failure loads for the T45 specimens were larger than the failure loads for the other

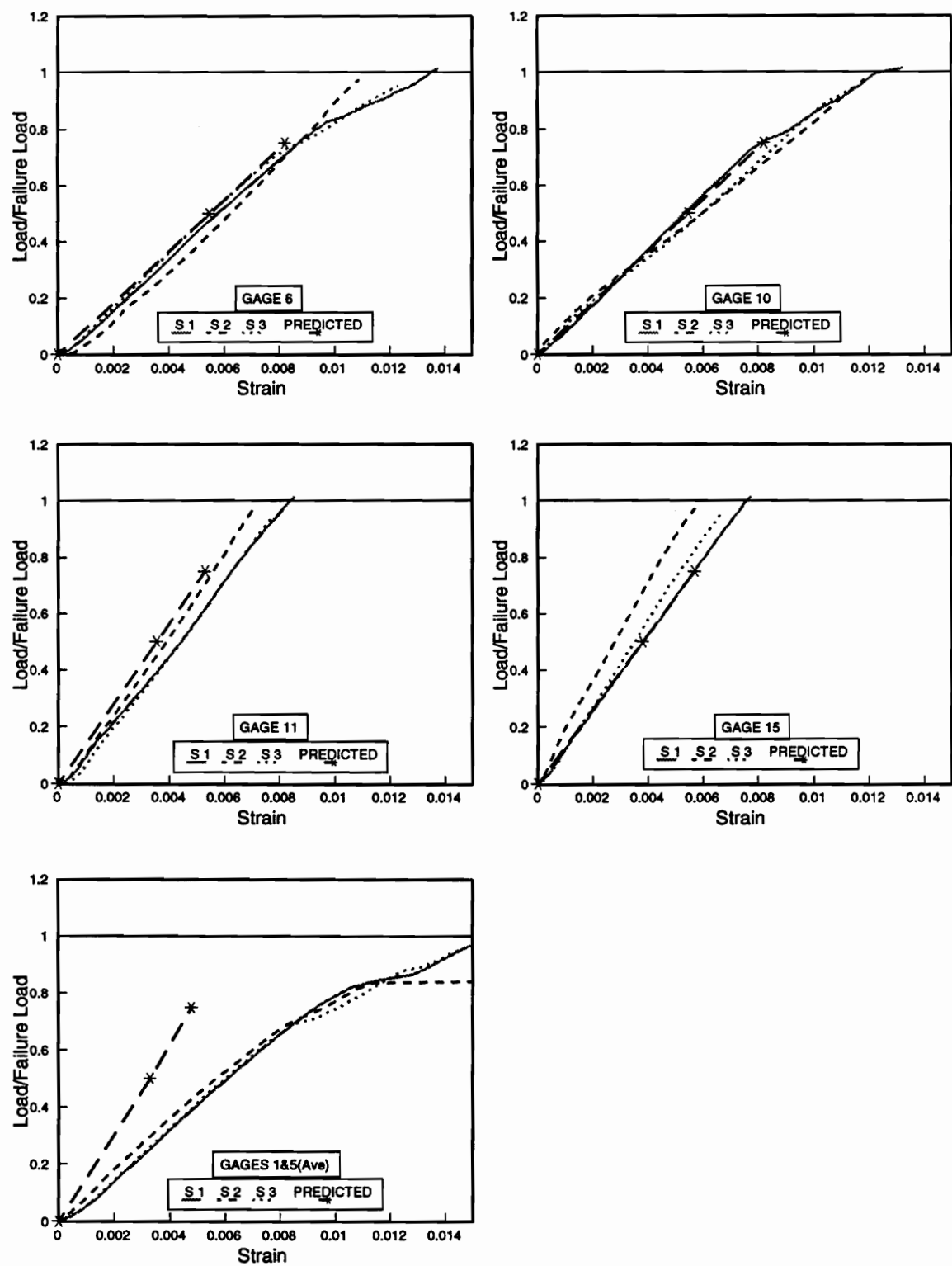


Figure 4.24. Measured and predicted net-section gage strains for 5-hole T30 inboard specimens

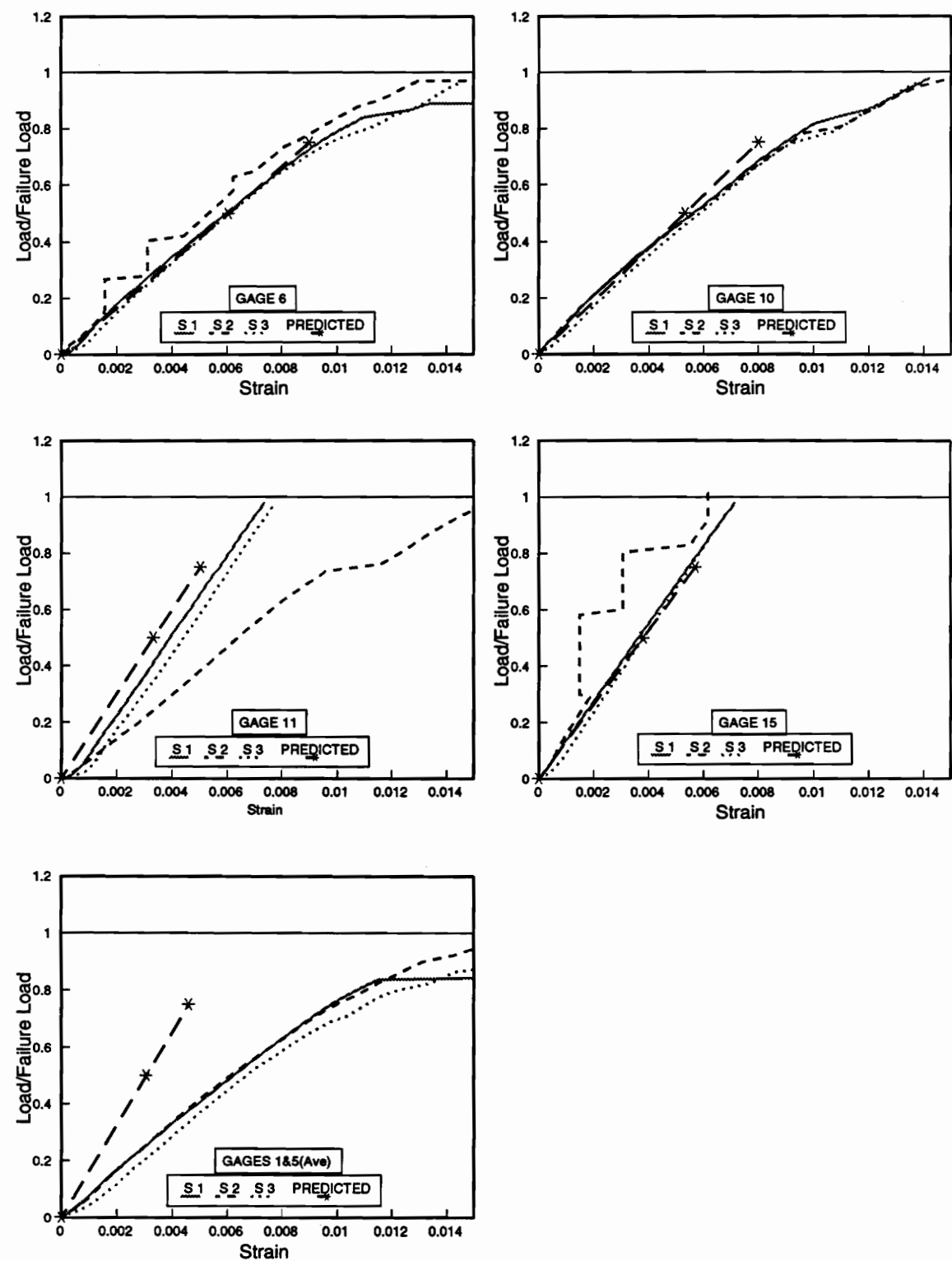


Figure 4.25. Measured and predicted net-section gage strains for 5-hole T60 inboard specimens

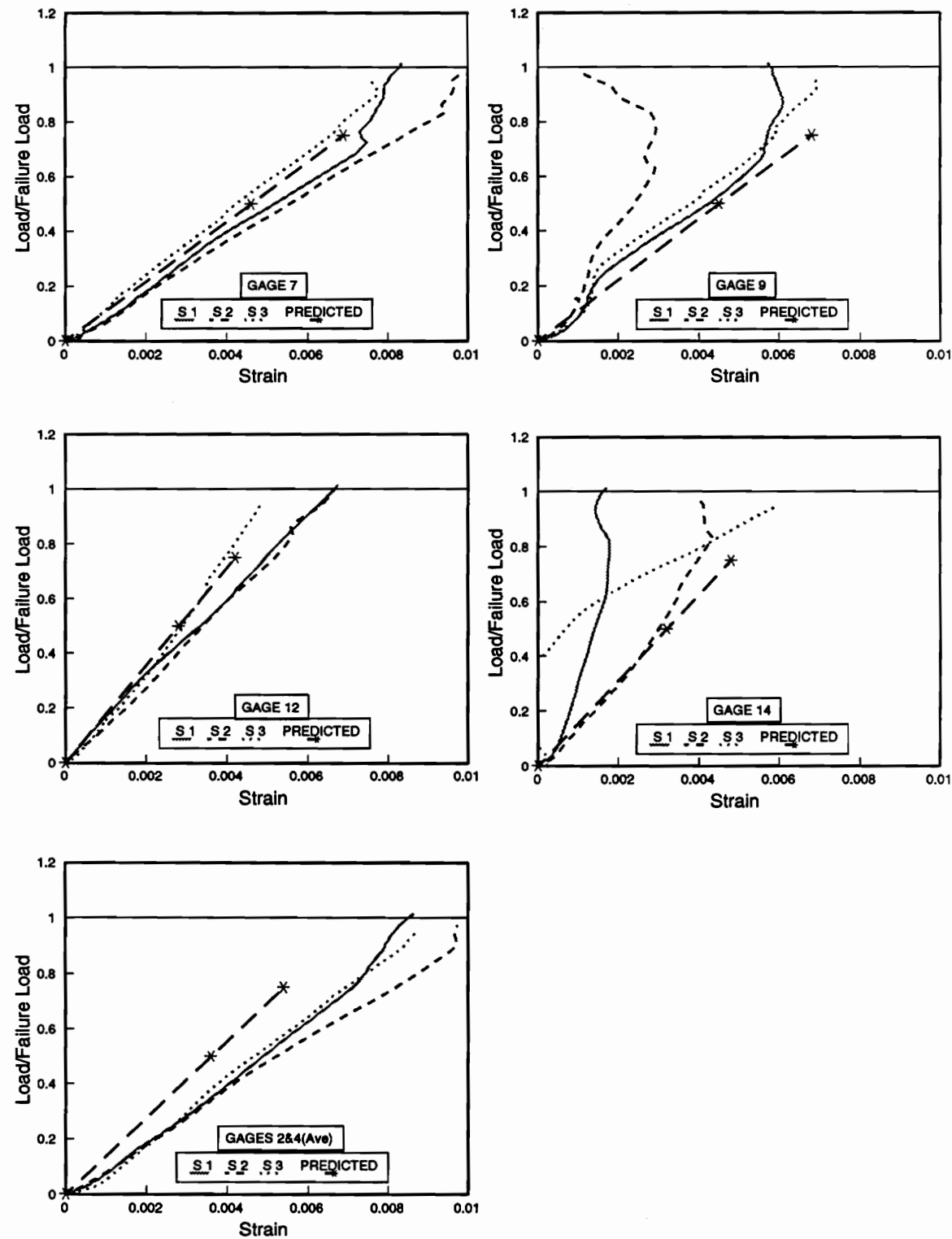


Figure 4.26. Measured and predicted shear gage strains for 5-hole T30 inboard specimens

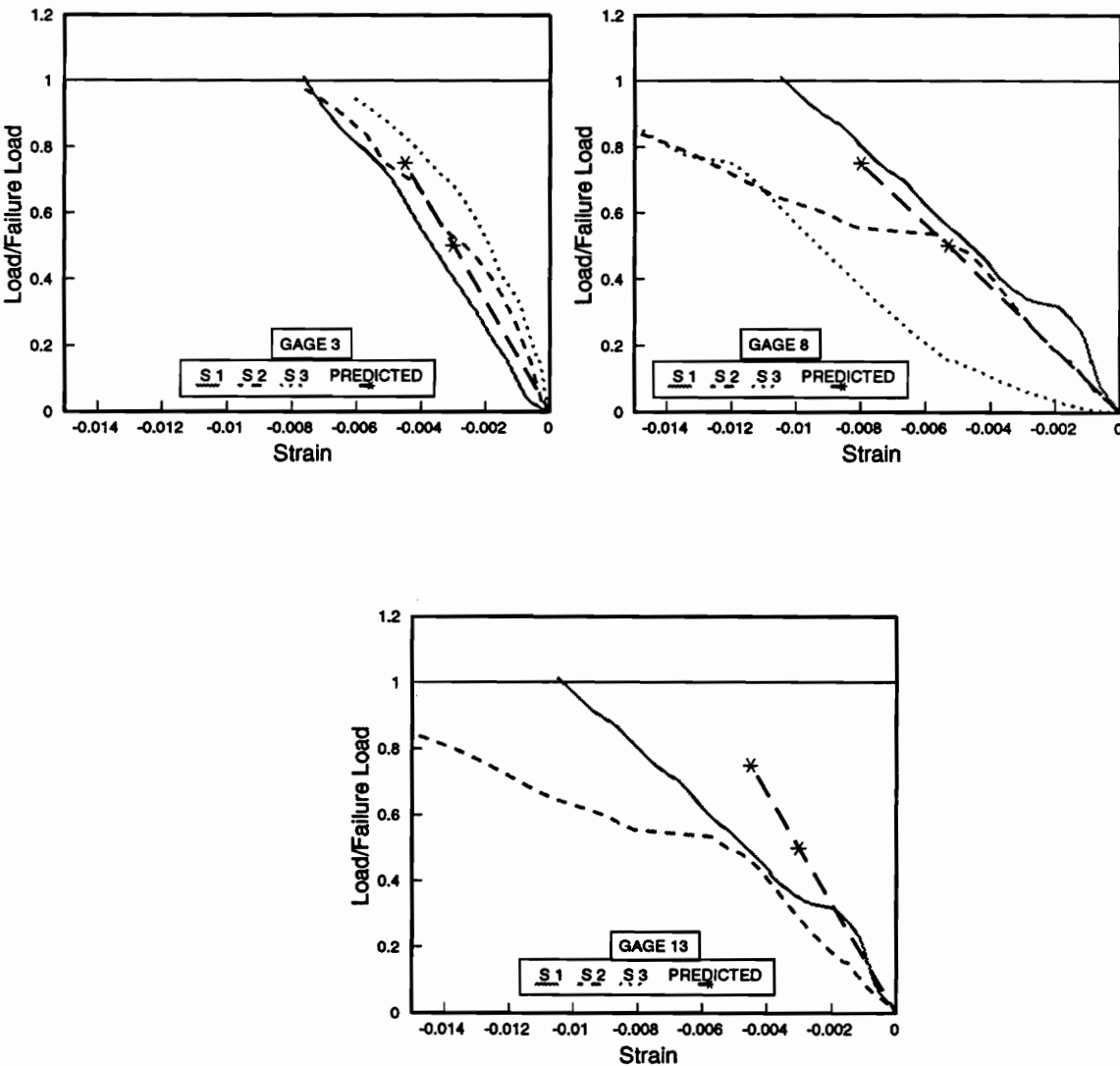


Figure 4.27. Measured and predicted bearing gage strains for 5-hole T30 inboard specimens

two laminates. This leads to the conclusion that perhaps strain-to-failure is an important criterion.

Responses of shear and bearing gages are shown in figs. 4.26 and 4.27, respectively, for the 5-hole T30 inboard specimen. These figures are analogous to figs. 4.18 and 4.19, figures which show the shear and bearing gage responses for T45 specimens. The same discussion can be extended to the current figures. However, in case of fig. 4.26, more shear gages showed linear response than in 4.18. The response of bearing gages in fig. 4.27 did not seem to differ from the bearing gage response of the other specimens. In general, the strains of some gages in the T30 specimens tended to show more strain than the corresponding gages on the T45 specimens, although the difference was not substantial. The differences can be related to the difference in strength between the two laminates. The response of the shear gages, fig. 4.28, and the bearing gages, fig. 4.29, for T60 specimens seem to follow a pattern similar to the shear and bearing gage responses of the other laminates. However, in many cases the value of strains seem to be significantly higher than for the other two laminates. This again, explains the reason for the least strength of the T60 specimens among the three lamination sequences considered in the study.

4.4 Comparison of Strengths of Different Widths, Hole Configurations, and Laminates

To have a clearer picture of the relative strengths of the different specimens, the gross-section strengths of the various specimens are compared. These strengths are illustrated in figs. 4.30, 4.31, and 4.32. The figures afford various comparisons among the specimens. In particular, the strengths for 3-, 5-, 7-, and 9-hole T45 inboard half-hole specimens are shown in the fig. 4.30. From the figure it is seen that there is only a marginal increase in

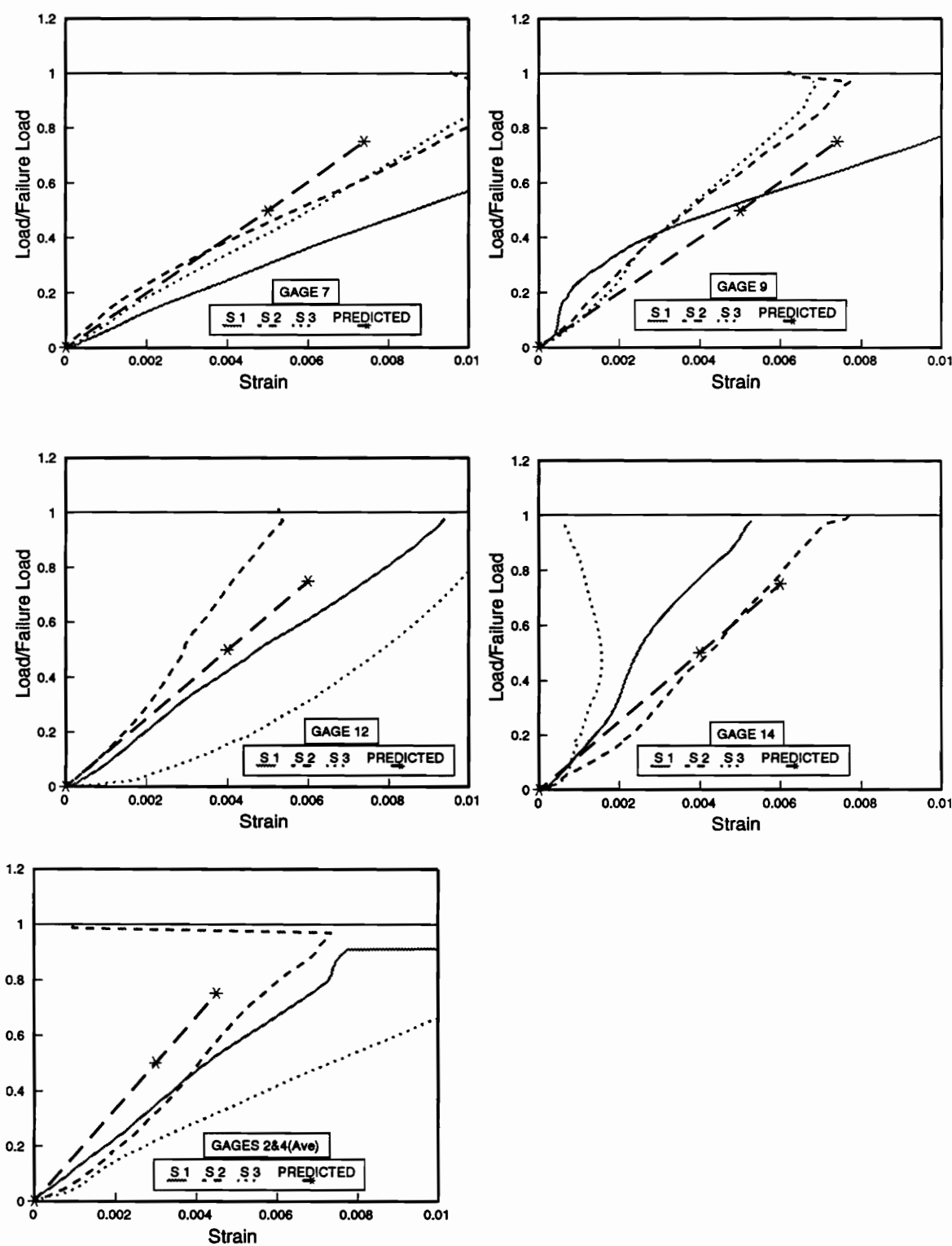


Figure 4.28. Measured and predicted shear gage strains for 5-hole T60 inboard specimens

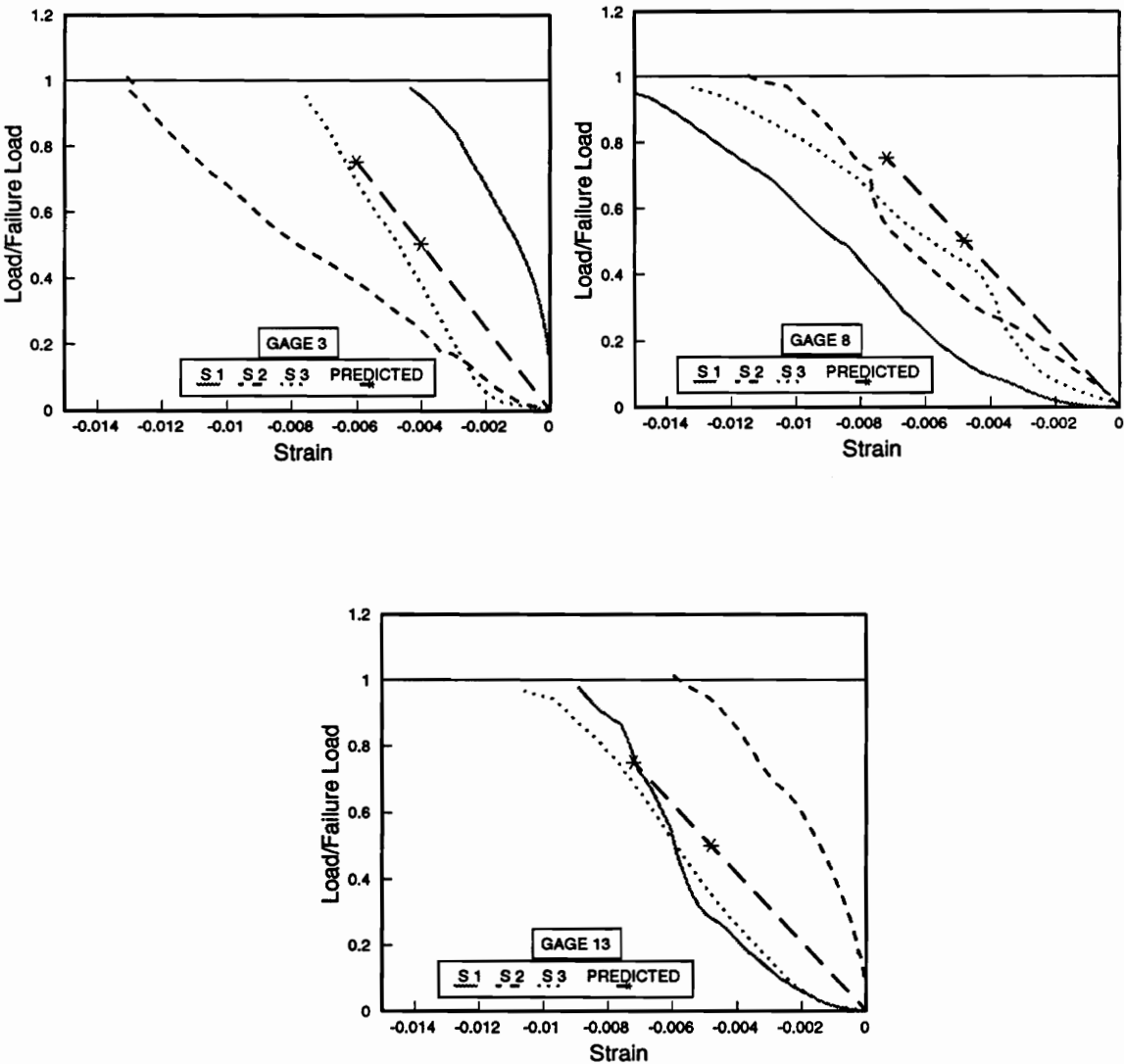


Figure 4.29. Measured and predicted bearing gage strains for 5-hole T60 inboard specimens

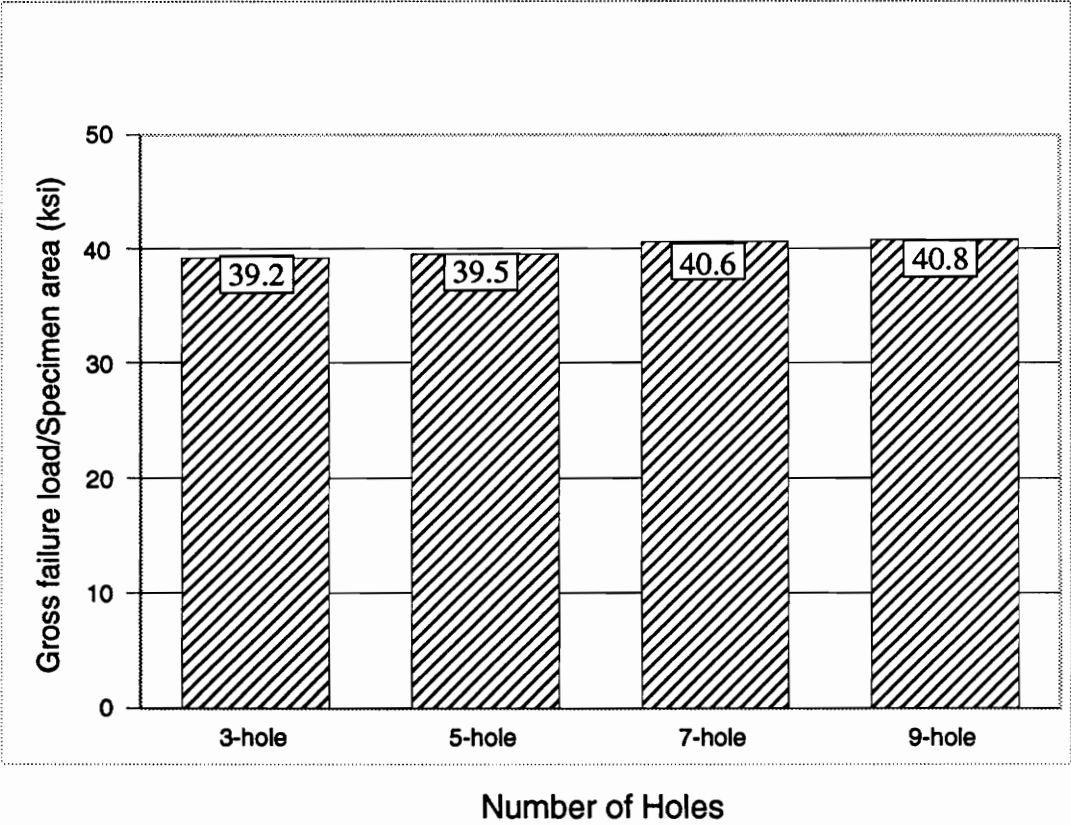


Figure 4.30. Normalized joint failure loads for 3-, 5-, 7-, and 9-hole T45 specimens

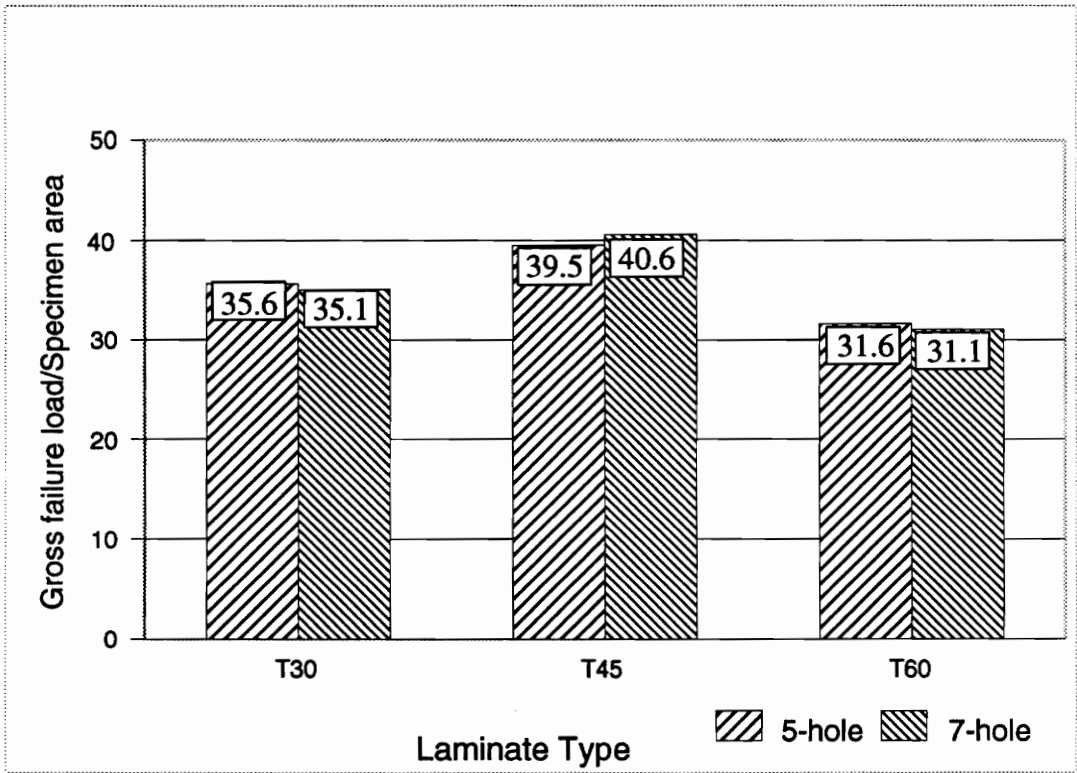


Figure 4. 31. Comparison between 5- and 7-hole specimen joint strengths for T45, T30, and T60 specimens

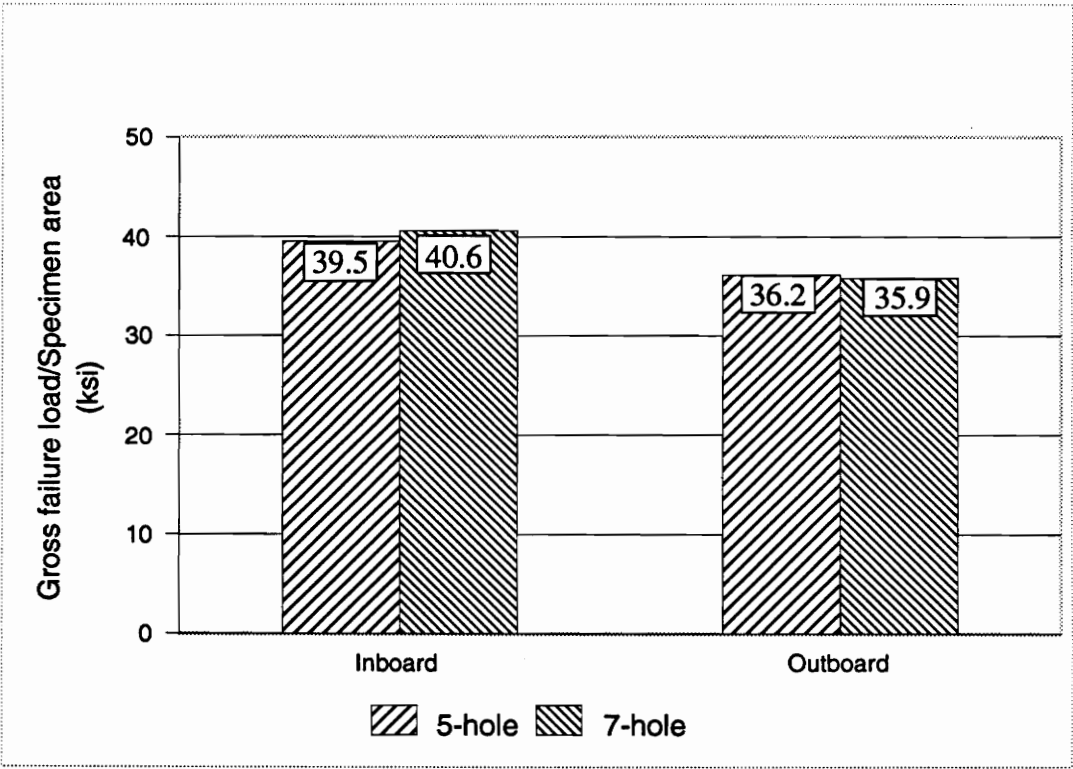


Figure 4.32. Comparison between inboard and outboard joint strengths for 5- and 7-hole specimens

gross-section strength with the increase in the number of loaded holes in the specimen. Also it can be concluded that among the inboard specimens, a 3-hole specimen will yield most conservative joint strength design value. A comparison of the overall net-section strain levels for the T45 inboard specimens (figs. 4.17, A.2, B.2, and C.2- C.3) shows that the single inboard hole of 3-hole specimen, hole 1, is among the most highly strained. Thus it is not surprising that the 3-hole specimen fails at the lowest load level.

Figure 4.31 shows the joint strengths for 5- and 7-hole inboard specimens for the three different laminates. As expected, because of the results in fig. 4.30, the difference in the joint strength between 5- and 7-hole specimens was marginal for all the three laminates. The gross strength of the T60 laminate was noticeably less than that of other two laminates, while the difference in strengths between the T45 and T30 laminates was not as great, though the T45 laminate showed the highest strength. The lower strength of the T60 laminate correlates with the higher strains, as compared with the T45 laminate, as was discussed in connection with fig. 4.25.

The joint strengths of 5-hole and 7-hole joints fabricated of the T45 laminate for both inboard and outboard half hole configurations is shown in fig. 4.32. It is evident from the figure that the difference in strengths between inboard and outboard specimens is significant. This difference and the reasons for it have been discussed. Inspection of this figure also shows the slight difference between the 5-hole and 7-hole specimens for a given configuration.

4.5 Conclusions

From the results presented, it is clear that the analysis and the experiments correlate well as regards overall response of the joints. The load sharing among the holes was pre-

dicted with high accuracy. For the 5-hole and 7-hole specimens, it was found that the inboard row of the inboard specimens reacts slightly more load than one-half the total load, while the outboard row reacts somewhat less than one-half the load. Interestingly enough, an earlier finding by Hercules Aerospace, Inc.¹⁹ with a thicker joint inboard specimen showed the inboard row reacted 52% of the total load while the outboard row reacted 48%. The results obtained here also indicate that as the number of holes increases, the load per hole within a joint becomes more uniform. However, the outermost hole always reacts more load, independent of whether it is an inboard or outboard specimen.

The net-section gage strains measured in the experiments agreed quite well with the predicted values. Repeatability among the three replicates was good. The correlation between experiments and predictions for the shear and bearing gage strains was not good. Repeatability of these results in the experiment was also not particularly good. One possible explanation for the poor repeatability and poor correlation with predictions was the close proximity of these gages to the contact of the pin with the composite.

Finally, it was shown from the experiments that, as measured by gross-section strength, the T45 specimens were the strongest. The T60 specimens were the weakest. In regards to strength of the T45 specimens, the 3-hole specimens were the weakest and the 9-hole specimens were the strongest. Finally, for the 5- and 7-hole T45 specimens, the inboard specimens were stronger than the outboard specimens. From the economic standpoint, a 3-hole specimen may be the best for estimating strength. It requires less material than the other specimens, and gives conservative results. With the smaller number of holes, details of the response around the holes, however, are distorted and could be misleading. Hence the 5-hole specimen may be a satisfactory compromise.

5.0 FURTHER NUMERICAL RESULTS

5.1 Introduction

As mentioned in Ch. 1, the current problem has not been previously addressed to the degree that it has been here. In the literature review most of the significant investigations of the response of multiple fastener joints were discussed. It was seen that none of them investigated details such as the distribution of contact stresses around each hole, or the degree of load proportioning. In most cases it was assumed that the contact stresses are cosinusoidal, while some did not investigate those aspects at all. The need for the accurate prediction of the contact stresses becomes important in the prediction of failure modes and failure loads of the joint. The standard practice is to assume that the radial stresses vary as the cosine of the angle measured from the bottom of the hole, and then compute the local stresses from that distribution. Failure predictions would then be based on some criterion and these stresses. While this approach may work reasonably well for the cases where the holes in different rows are not staggered with respect each other, for the cases where they are staggered, the approach may not work. A close look at the deformed meshes of different specimens, shown in the Ch. 3, provided an indication of possible deviation from the cosinusoidal distribution. On further investigation, it was found that the contact stress distribution around holes at certain locations indeed deviated substantially from this assumption. These results are discussed in this chapter.

5.2 Description of Stress Calculations

The finite element analysis used herein can directly provide information about the interaction between the pin and the hole edge. The radial contact stress $\bar{\sigma}_r$ between the pin and the hole edge is a function of the radial component of the stress resultant at the hole edge. It should be noted that this contact stress is averaged over the laminate thickness. This is opposed to the layer level stress σ_r . The stress resultant can be calculated at the Gauss points closest to the hole edge. The radial stress distribution around the hole can also be calculated from the stresses obtained from the ABAQUS gap elements. The two approaches, as expected, yielded very similar results. However, the results obtained from the gap elements are not shown here as they seem to be less smooth than the data from the Gauss points. The lack of smoothness was felt to be due to numerical effects associated with the contact mechanism. More elements around the hole could be used to increase smoothness. Here the contact stresses are normalized by dividing them with the corresponding bearing stress, σ_b . The bearing stress is defined as

$$\sigma_b = P/d t$$

P = load reacted by each pin, lbs.

d = diameter of the hole (0.75 in.)

t = thickness of the specimen (1.008 in.)

The circumferential stress in the laminate at the edge of the hole, $\bar{\sigma}_\theta$, can be computed by taking the circumferential component of the same Gauss point stress resultant. Again, the circumferential stress is averaged over the laminate thickness rather than taking the value at the layer level.

The stresses $\bar{\sigma}_r$ and $\bar{\sigma}_\theta$ are shown in the following figures. The stresses are shown as a

function of θ , $\theta=0^\circ$ being at the bottom of the hole, the location expected to have large compressive radial stresses. The stresses are calculated over a region of about $\theta=190^\circ$, starting around $\theta=-95^\circ$ and going to $\theta=+95^\circ$, as will be shown in the figures. Using a 190° range was done to illustrate the complete nature of the radial stress distribution, i.e., starting from a value of zero near one net-section, passing through a maximum value, and then returning to zero again near the other net-section. In the case of the circumferential stresses, the distribution will be exactly opposite, i.e., maximum occurring at the net-section, gradually decreasing towards the center of the hole, and returning to a maximum near the other net-section. Although the bearing stress σ_b is compressive in nature (negative value), only its magnitude is taken into account while normalizing the stresses. This is done in order to retain the original sign of the stresses, i.e., negative for $\bar{\sigma}_r$ and positive for $\bar{\sigma}_\theta$.

5.3 3-Hole Specimen Results

The hole edge stresses for the 3-hole inboard specimens are shown in figs. 5.1 - 5.6. This specimen has only two different hole edge stress distributions, as the stress distributions around the two outboard holes on either side of the vertical centerline are similar. Since in the analysis only half of the centerline hole was modeled, taking advantage of symmetry, the stress distribution was obtained for only one-half of the centerline hole. To make comparisons and to make the picture complete in itself, those values from the half hole on the centerline are reflected about $\theta=0^\circ$ and the figures show the stress distribution around the complete hole. Care should be taken when observing the stress distributions for the holes off the centerline. The analysis was conducted for the holes to the left of the centerline, and hence skewing of the stress distributions is peculiar to holes on that side of the

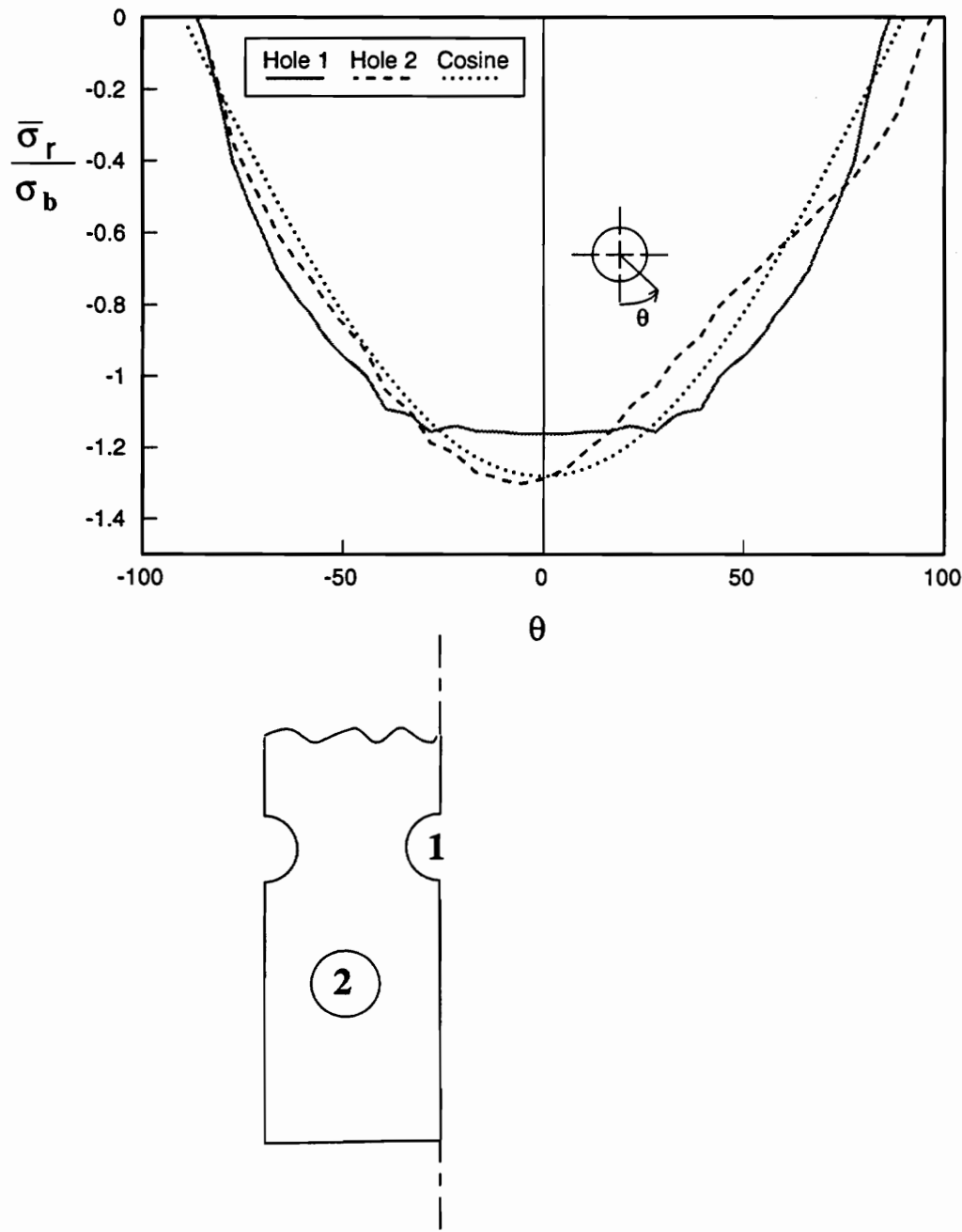


Figure 5.1. Distribution of radial stress $\bar{\sigma}_r$ for 3-hole T30 inboard specimen

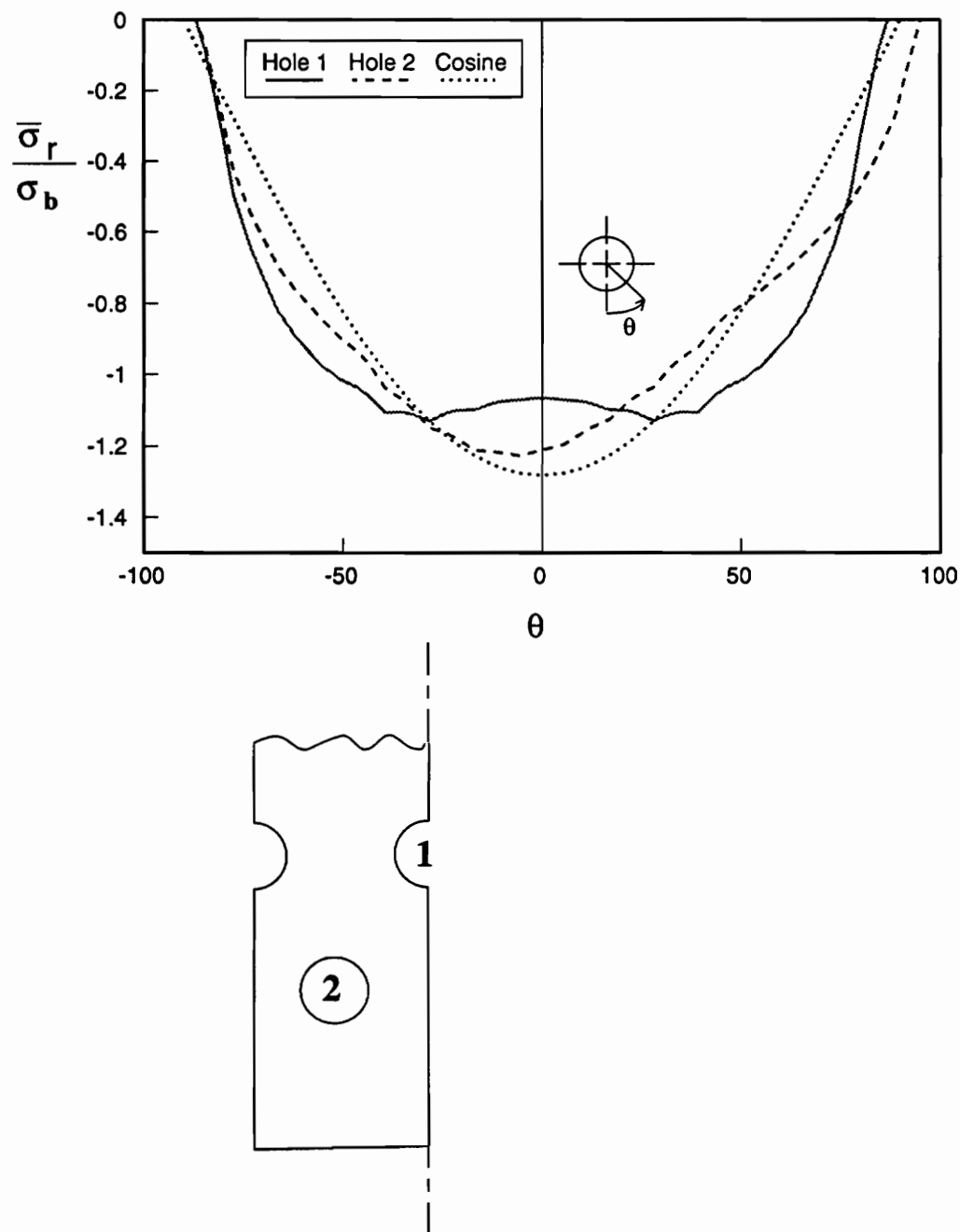


Figure 5.2. Distribution of radial stress $\bar{\sigma}_r$ for 3-hole T45 inboard specimen

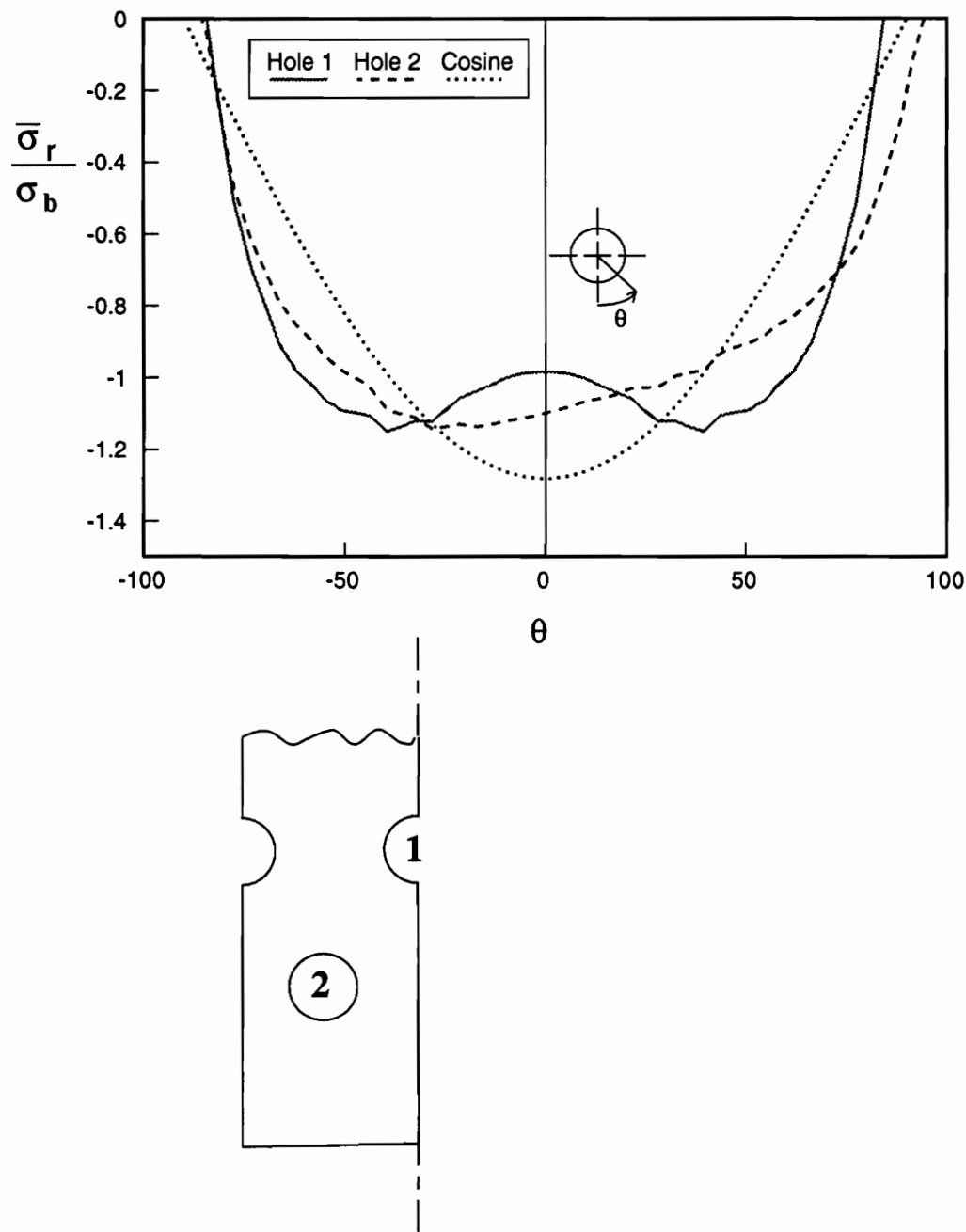


Figure 5.3. Distribution of radial stress $\bar{\sigma}_r$ for 3-hole T60 inboard specimen

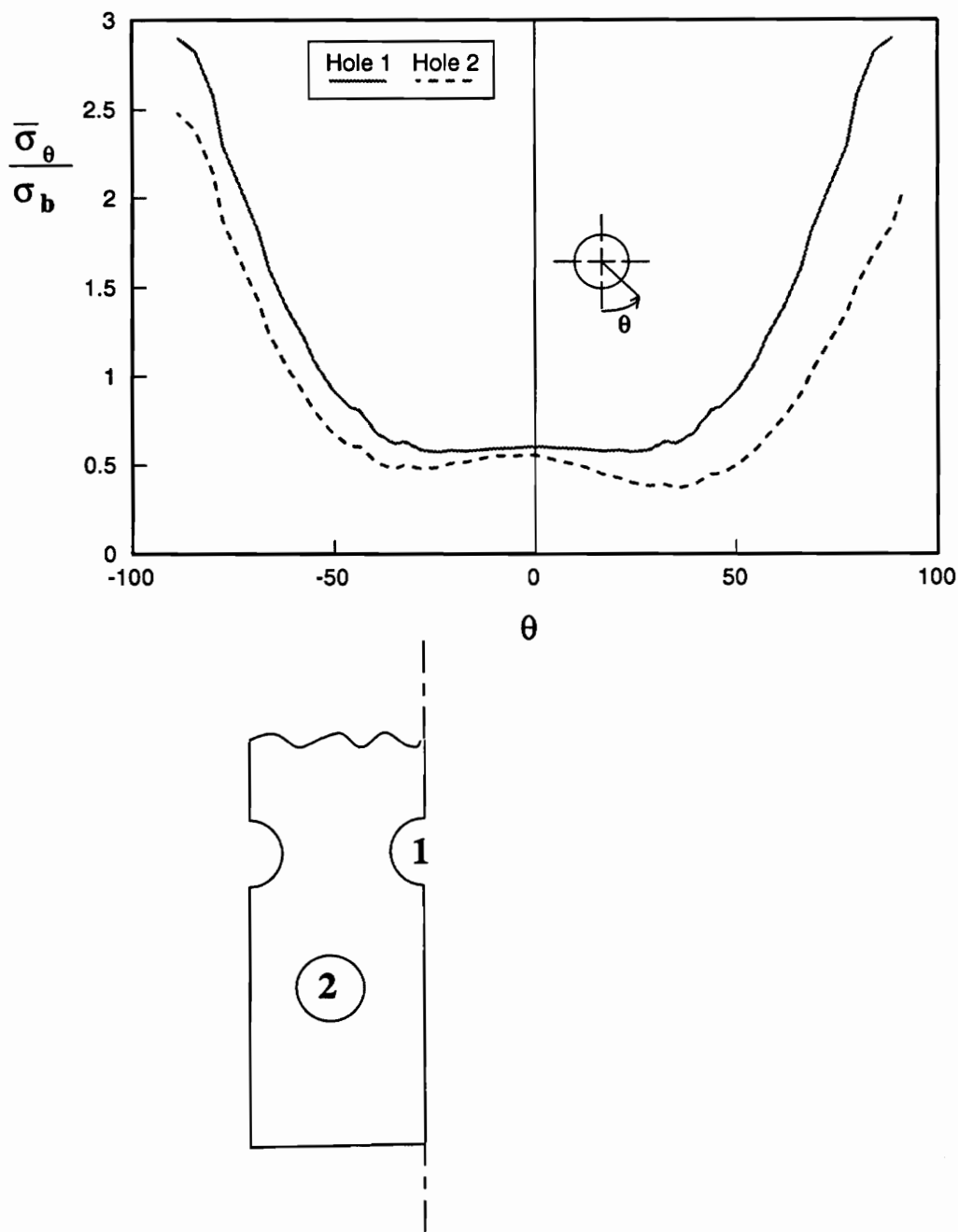


Figure 5.4. Distribution of circumferential stress $\bar{\sigma}_\theta$ for 3-hole T30 inboard specimen

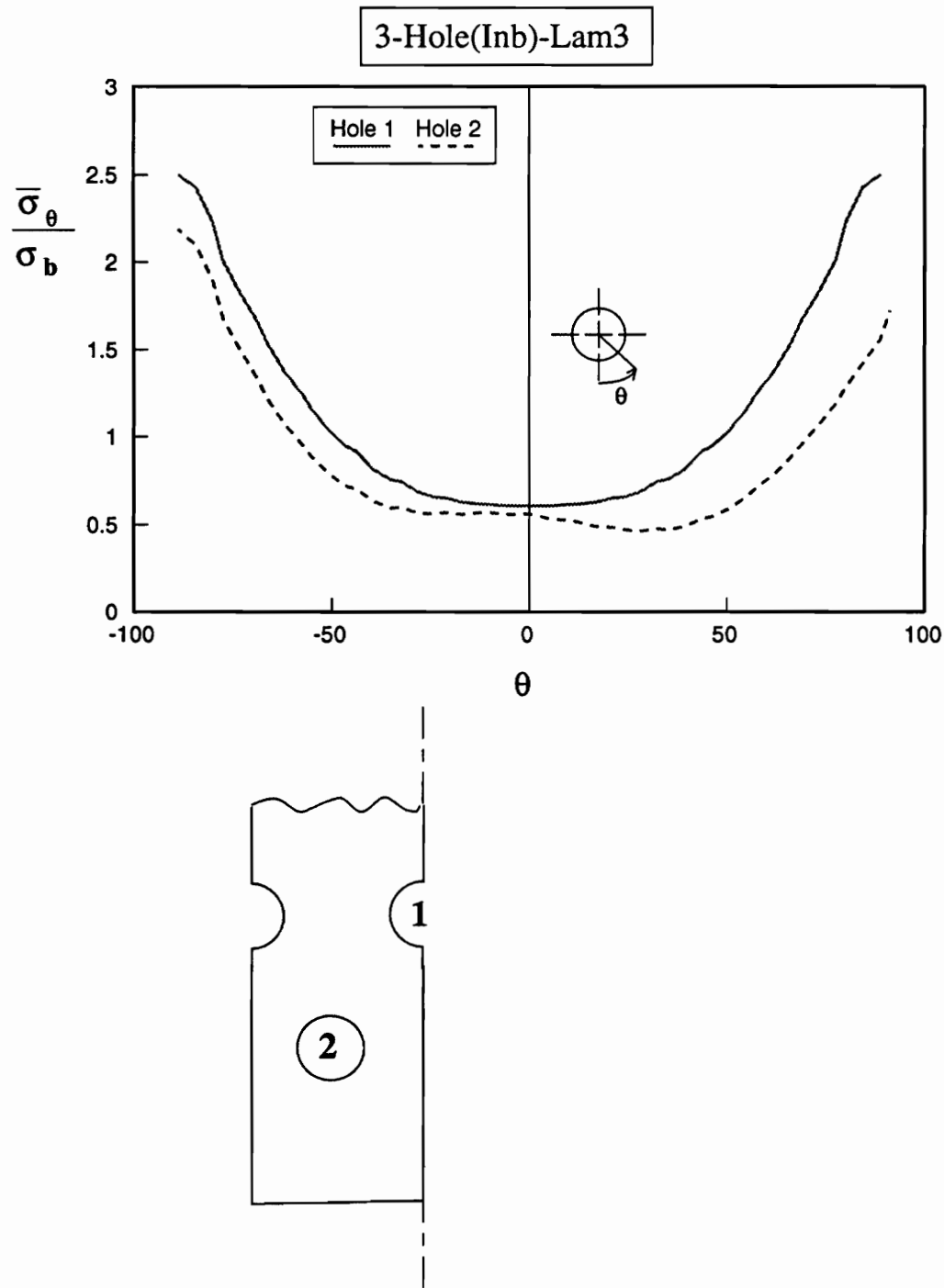


Figure 5.5. Distribution of circumferential stress $\bar{\sigma}_\theta$ for 3-hole T45 inboard specimen

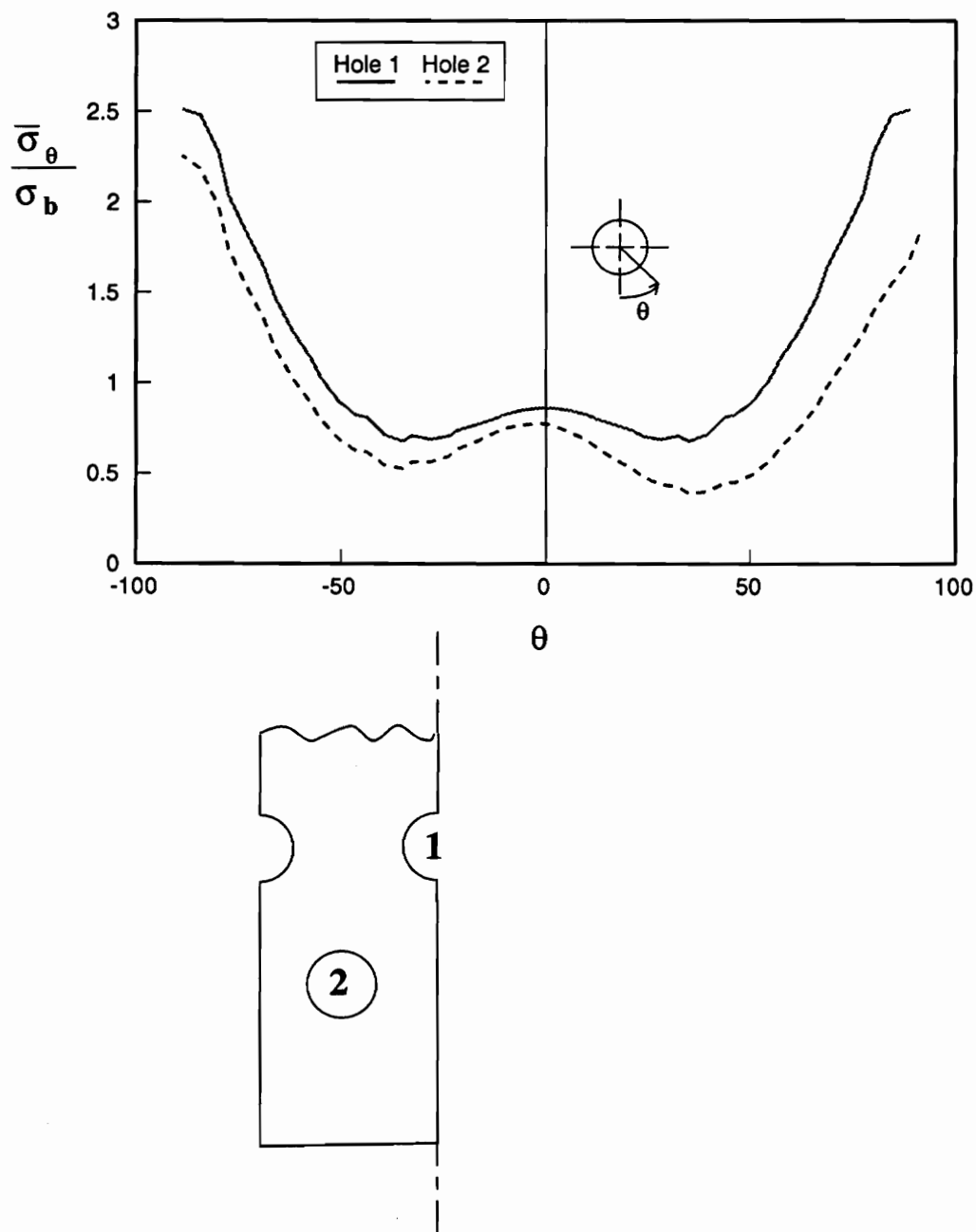


Figure 5.6. Distribution of circumferential stress $\bar{\sigma}_\theta$ for 3-hole T60 inboard specimen

specimen. For mirror-image holes on the right side of the specimen, skewing will be in the opposite direction. For comparison, the often used cosinusoidal stress distribution, normalized by σ_b , is shown in some of the figures to follow.

Figure 5.1 shows the radial stress distribution around the holes for a 3-hole inboard T30 specimen. In this figure, as just mentioned, in addition to the two lines representing the distribution around the two holes, a third line representing ideal cosinusoidal distribution is also shown. With the normalization used here, the cosinusoidal distribution, if used, would be the same for each hole. The hole numbering scheme and the measurement of θ are also shown in the figure. From the figure it can be seen that the stresses around the outboard hole (hole 2) somewhat follow a cosinusoidal relation with θ , whereas for the inboard hole (hole 1) the stress distribution flattens at the bottom of the hole. It should be noted that the single inboard hole is straddled by two loaded outboard holes. This fact does not seem to be of much importance at this stage but will be a factor governing the shape of the stress distributions, and becomes more evident in the cases involving additional holes. As can be seen in the figure, the stress distribution for hole 1 is not perfectly smooth. There are cusps in the stress distribution near $\theta = \pm 40^\circ$. This lack of smoothness was alluded to earlier in regard to determining stresses from the Gauss points and from the ABAQUS gap elements. As mentioned, a finer mesh around the hole might alleviate this problem.

Though the stress distribution for hole 2 could be approximated by a cosinusoidal distribution, a cosinusoidal distribution would be symmetric with respect to $\theta = 0^\circ$. As seen in the figure, the actual distribution for the hole 2 is skewed somewhat to left of its centerline, the peak occurring slightly away from $\theta = 0^\circ$, further from the centerline of the specimen. The stress distribution around hole 3, which is reflection of hole 2 about the centerline, would be skewed to the right of its centerline. An important point to be noted at this stage

is that the laminate under consideration, the T30 case, is the stiffest in the loading direction of the three laminates under consideration. To follow is an examination of the other laminates in the order of decreasing stiffness in the loading direction.

The radial stress distribution around the holes for 3-hole T45 inboard laminate is shown in fig. 5.2. Here again the stresses around hole 2 follow a relationship with θ which is approximately cosinusoidal. However, the stress distribution for hole 1 takes a more severe dip at the bottom of the hole than for the T30 laminate. It seems that the outboard holes straddling the this inboard hole relieve somewhat radial stresses around the bottom of the hole. This effect seems to be more pronounced for the specimens which are softer in the loading direction. A look at the figure 5.3, where the radial contact stress distribution for a 3-hole T60 specimen is shown, confirms this trend. The stress distribution around hole 1 shows a decrease at the bottom of the hole which is even more pronounced than the decrease for the other laminates. In fact, reexamining figs. 5.1- 5.3, it is seen that the stress distribution around hole 2 tends to flatten somewhat at the bottom of the hole for the more compliant laminates. These decreases in radial stress at the bottom of the hole are contrary to intuition. A close look at the deformed meshes of the 3-hole specimen (fig. 3.5) shows a distortion of the outboard holes towards the unloaded inboard holes. The upper end of the major axis of the ellipse outlining the deformed hole is rotated toward the unloaded inboard half hole. This no doubt causes skewing of the almost-cosinusoidal radial stress distribution of the outboard hole (hole 2). The fact that the radial stress distribution decreases near $\theta=0^\circ$ for the inboard holes can be interpreted as follows: It is not that the radial stress decreases near $\theta=0^\circ$, rather, the radial stress increases away from the $\theta=0^\circ$ location, say at $\theta=\pm 30^\circ$ to $\pm 50^\circ$. This increase is due to the fact that the unloaded portion of hole 2 ($\theta \geq 90^\circ$ for that hole) moves toward hole 1 due to the lack of any tractions on that portion of the edge of

hole 2 pulling material away from hole 1. This deviation of distribution from cosinusoidal distribution, although unexpected, has some precedences in the literature. Sun and Sankar^{24, 25} reported that for an indenter pressing into an orthotropic material, as the indenter contact length increases (or the contact surface wraps around the indenter), the contact stresses tend to have peak values at the edges and smaller values at the center. Although their problem dealt with indentation of beams with a rigid cylinder, an analogy can be drawn for the present case. In the current problem, the hole of the specimen may be getting wrapped around the indenter due to effect of the loaded hole on the outboard. This could be the reason for the decrease in stresses at the bottom of the hole.

The circumferential stress distribution $\bar{\sigma}_\theta$ for the 3-hole T30 inboard specimen is shown in fig. 5.4. It can be seen that the maximum circumferential stress is occurring at the net-section region, and gradually decreases towards the center of the hole, forming a trough-like shape to the distribution. Again, the distribution for hole 2 is not symmetric about the centerline. Although not very conspicuous for this laminate, the value of $\bar{\sigma}_\theta$ appears to have a local maximum at the bottom of hole, or near $\theta=0^\circ$, for the outboard holes. The stress distribution for the inboard holes flattens at the bottom. The circumferential stresses show a pronounced local maximum near the bottom of the hole for 3-hole T45 specimen for outboard holes, as seen in fig. 5.5. The holes on the inboard showed no increase in stresses at the bottom of the hole. As seen in fig. 5.6, this trend continued with the most compliant laminate under consideration, namely T60, where local maxima clearly occurred at the bottom of the holes for both holes. Interestingly, for the softest laminate under consideration, this local maximum effect does not seem to be limited to the inboard hole (hole 1). Unlike the radial stress distribution, where significant decreases in the stresses occurred mainly in cases of inboard holes, the circumferential stress distributions seem to have local maxima

for both holes. Again, this effect is noticeable in both holes only in case of T60 laminate.

5.4 5-Hole Specimen Results

The 5-hole specimens have one more hole than the 3-hole specimens and thus there is more chance to observe the stress distributions, as shown in figs. 5.7 - 5.9 for the T30, T45, and T60 specimens, respectively. These specimens have three outboard holes (1 and 3) and two inboard holes (2). The stress distributions in the following figure follow the same trends that were observed for the 3-hole specimens, in particular, the flattening or decrease in the distribution for the inboard holes near $\theta=0^\circ$ with decreasing load-direction stiffness. For both the outboard holes the stress distribution resembles a cosinusoidal distribution. It should be noted that the skewing of the stress distribution with respect to $\theta=0^\circ$ for the outboard holes is not as conspicuous as it was in case of 3-hole specimens. The peak of the distribution occurs close to $\theta=0^\circ$. This again can be understood by observing the deformed mesh of a 5-hole specimen in fig. 3.6. This figure shows less tendency, relative to the 3-hole case, of the ellipse representing the deformed holes to rotate away from the loading direction. With the 5-hole specimen it is clear that for inboard holes straddled by two outboard holes, the stress distribution flattens or decreases near $\theta=0^\circ$, the magnitude of the effect being related to the load-direction stiffness.

Turning to distribution of the circumferential stresses for 5-hole inboard specimens, figs. 5.10 - 5.12, the same trends observed for the three 3-hole specimens continued. The distribution of $\bar{\sigma}_\theta$ for the outboard holes (1 and 3) in the T30 and T45 specimens showed a mild maximum at the bottom, while the distribution for the inboard hole (2) tended to be flat at the bottom. For the T60 specimens, fig. 5.12, the local increase in the circumferential stresses at the bottom of the holes is quite evident for all the holes.

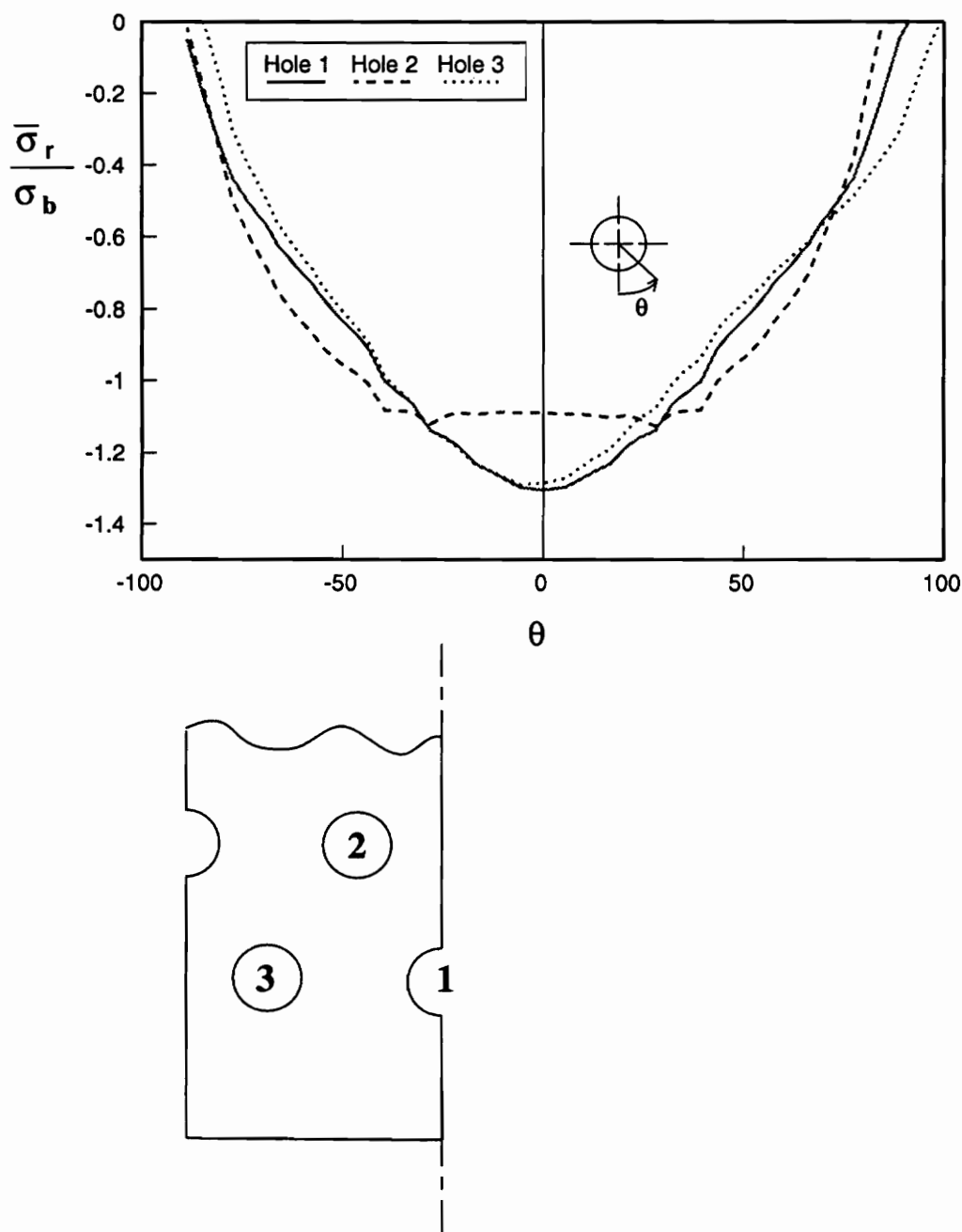


Figure 5.7. Distribution of radial stress $\bar{\sigma}_r$ for 5-hole T30 inboard specimen

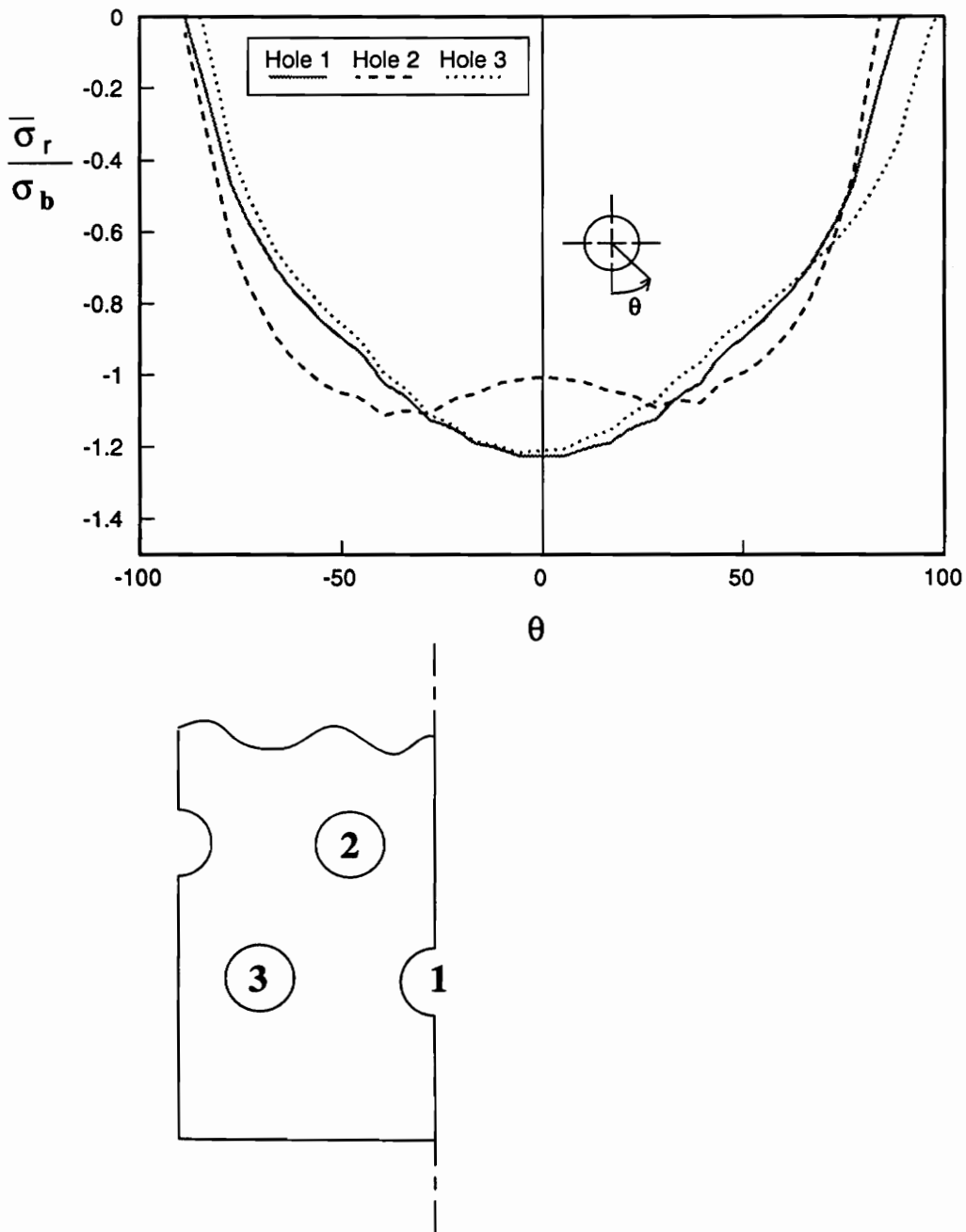


Figure 5.8. Distribution of radial stress $\bar{\sigma}_r$ for 5-hole T45 inboard specimen

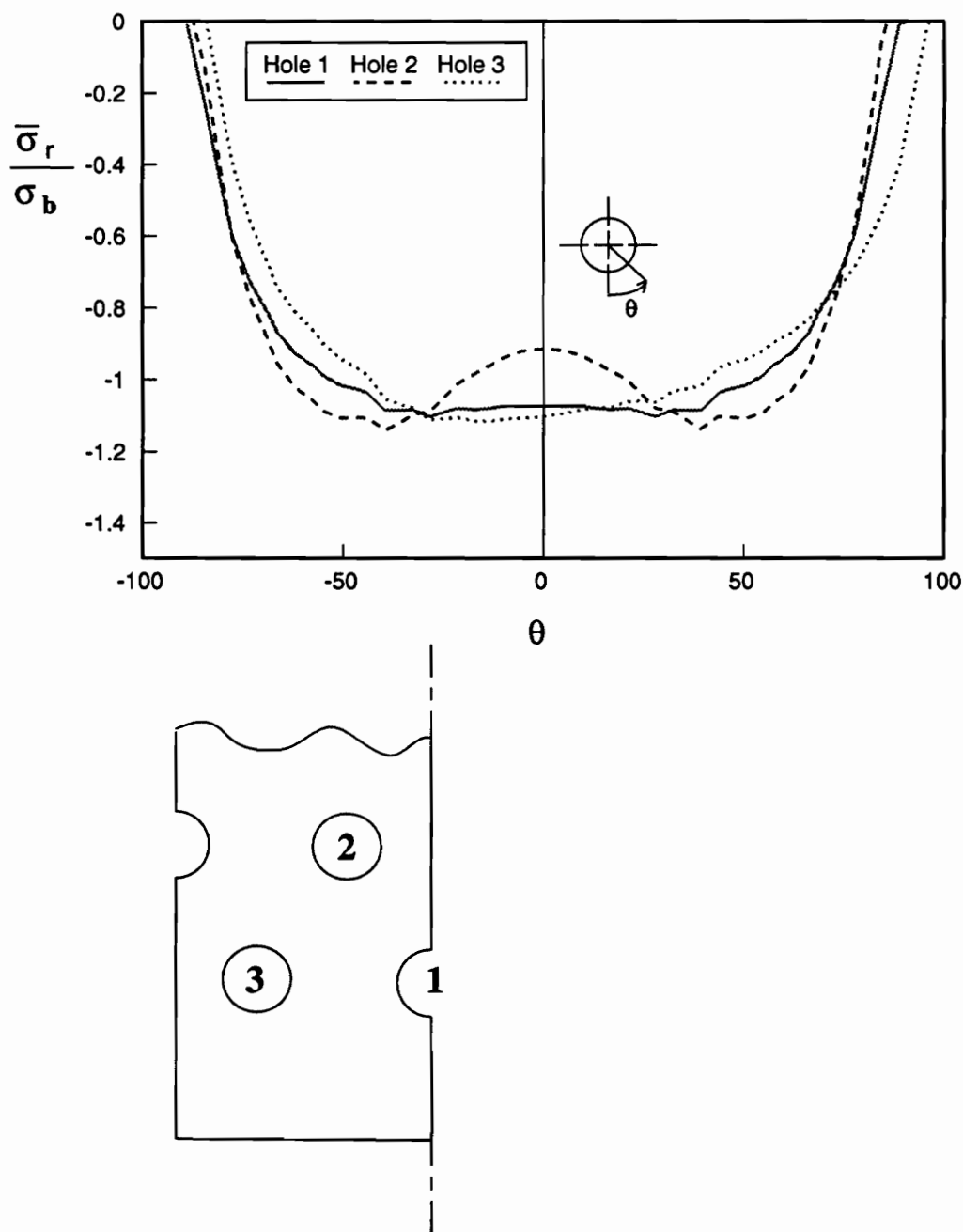


Figure 5.9. Distribution of radial stress $\bar{\sigma}_r$ for 5-hole T60 inboard specimen

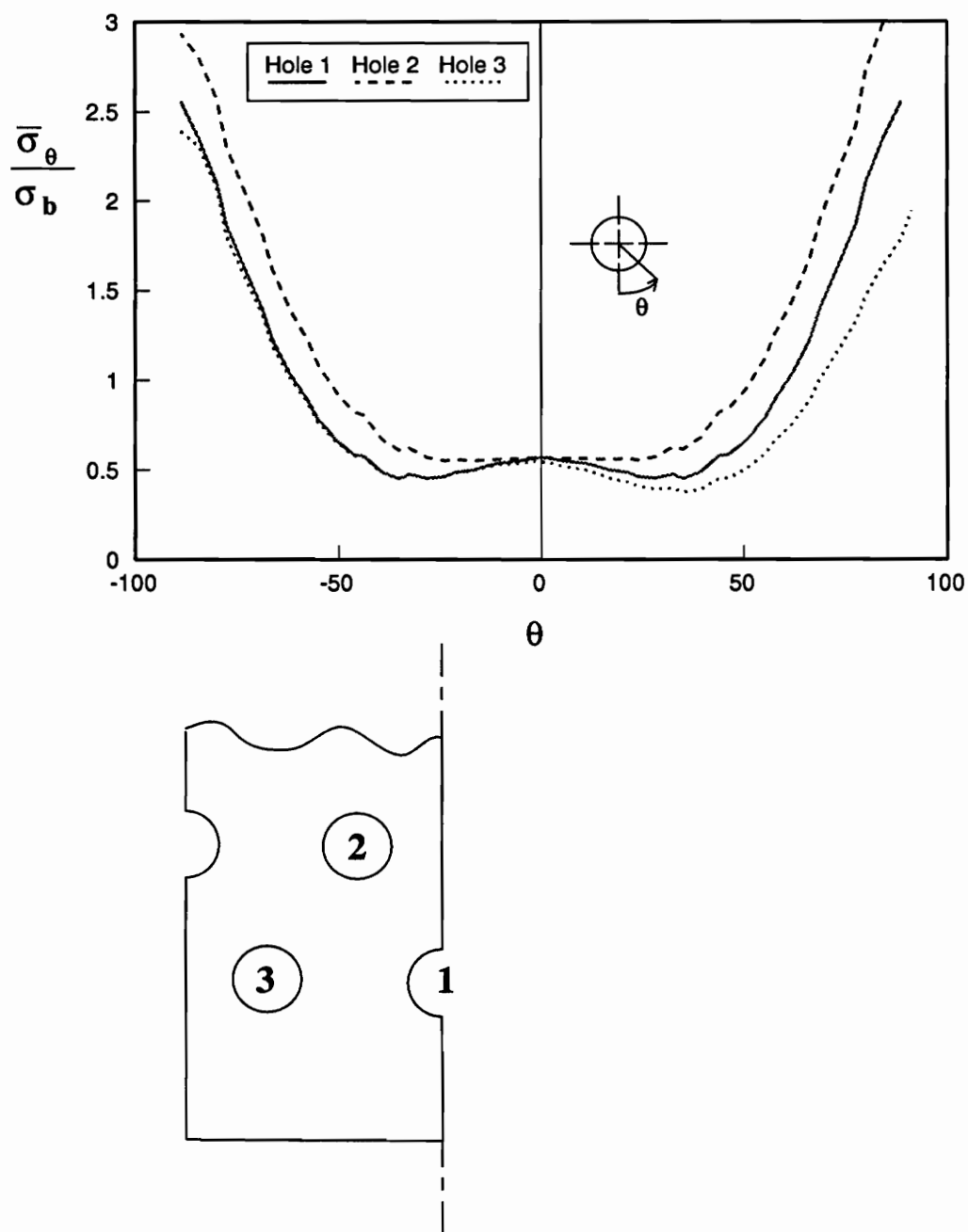


Figure 5.10. Distribution of circumferential stress $\bar{\sigma}_\theta$ for 5-hole T30 inboard specimen

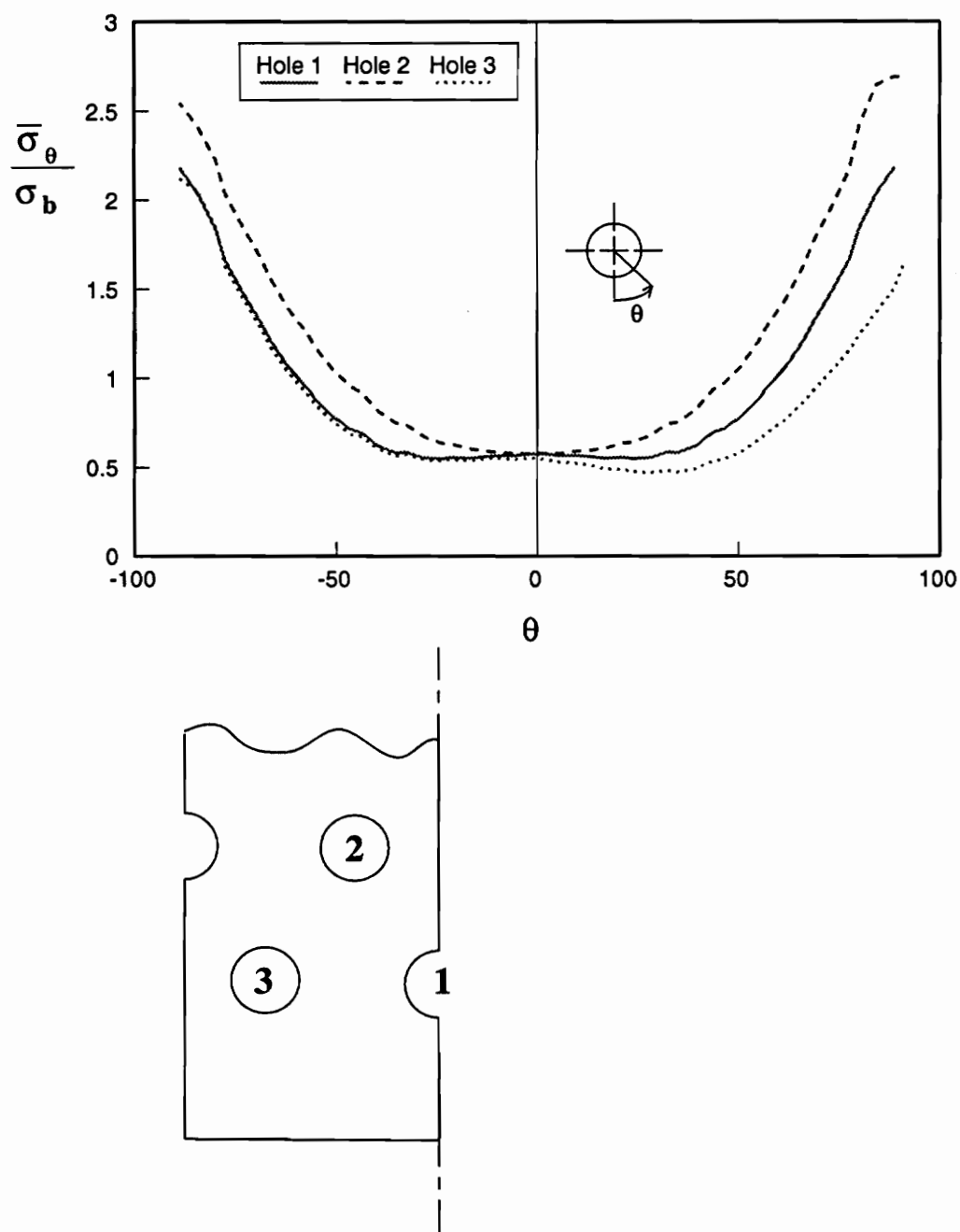


Figure 5.11. Distribution of circumferential stress $\bar{\sigma}_\theta$ for 5-hole T45 inboard specimen

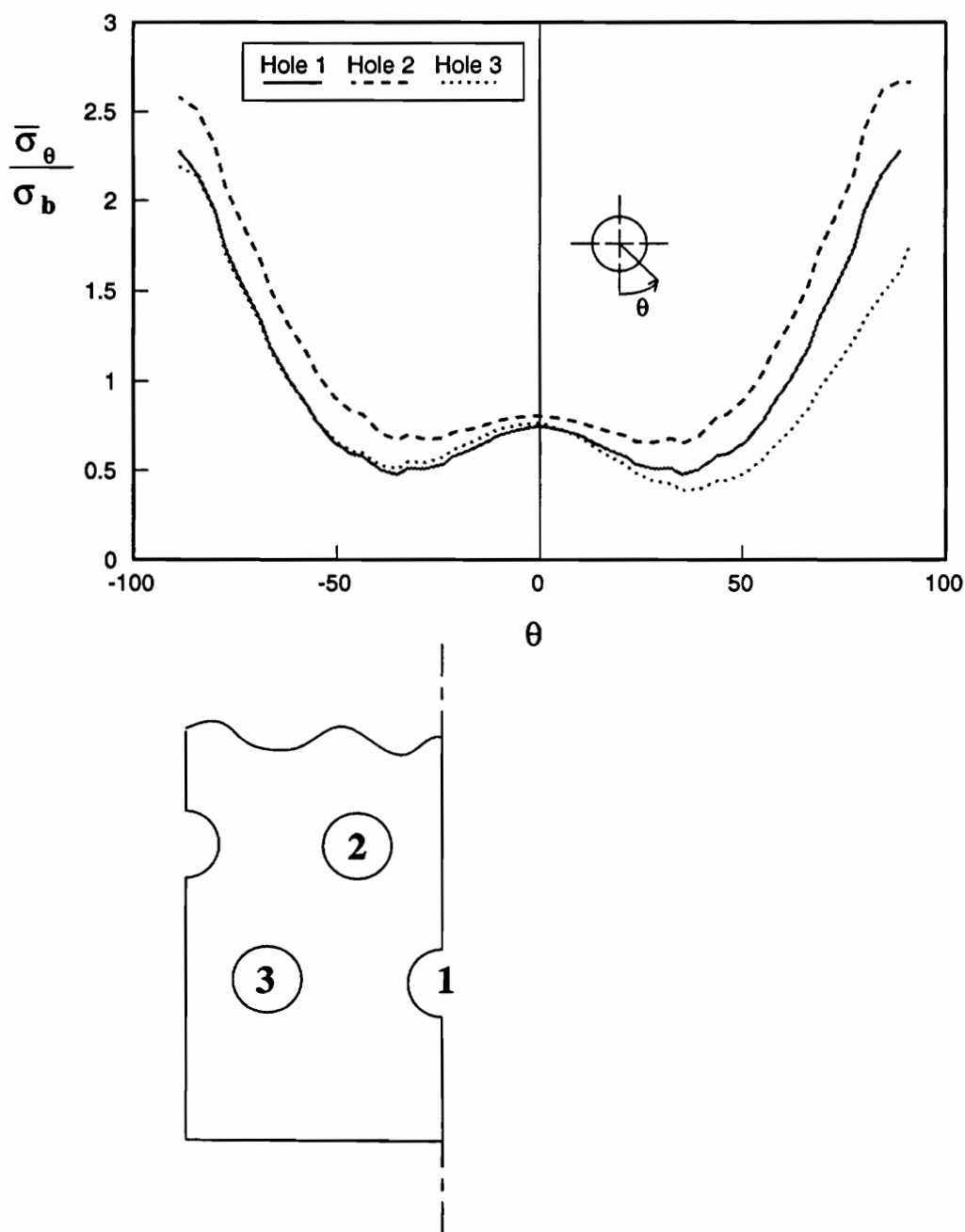


Figure 5.12. Distribution of circumferential stress $\bar{\sigma}_{\theta}$ for 5-hole T60 inboard specimen

5.5 7-Hole Specimen Results

The 7-hole specimens have three inboard holes and four outboard holes. This makes this geometry quite useful for general observations. Here again for the 7-hole inboard specimens, the inboard holes are each straddled by two loaded outboard holes. As expected, the stress distribution at the bottom of the hole decreases, the decrease becomes more pronounced as the material gets softer in the direction of loading. This can be seen in the figures 5.13 - 5.15 respectively, where the radial stress distributions for 7-hole T30, T45, and T60 inboard specimens, respectively, are shown. The stress distributions follow the other trends that were observed for the specimens with less of holes, though the distributions are more complex. Likewise, the trends observed for the circumferential stresses for the 3-, and 5-hole specimens continues with the T30, T45, and T60 7-hole specimens, as confirmed by figs. 5.16 - 5.18, respectively.

The situation becomes more interesting in case of a 7-hole outboard specimen. This is shown in figs. 5.19 and 5.20 for the T45 specimen. For the 7-hole outboard specimen, one of the inboard holes is not straddled by two loaded outboard holes (hole 4). Instead, the one inboard hole has only one loaded outboard hole on one side, while on the other side is the unloaded outboard half-hole. Figure 5.19 shows the radial stress distribution around the holes for a 7-hole T45 outboard specimen. Here again the hole 2, which is an inboard hole straddled by two outboard holes shows a decrease in the stress distribution close to the bottom of the hole, while the stress distributions around the outboard holes, as usual, follow a cosinusoidal-like distribution. In contrast to the other inboard holes, for hole 4, the stress distribution follows a path which is close to cosinusoidal and does not show any decrease in the values of stress at the bottom of the hole near $\theta=0^\circ$. This confirms that the decrease

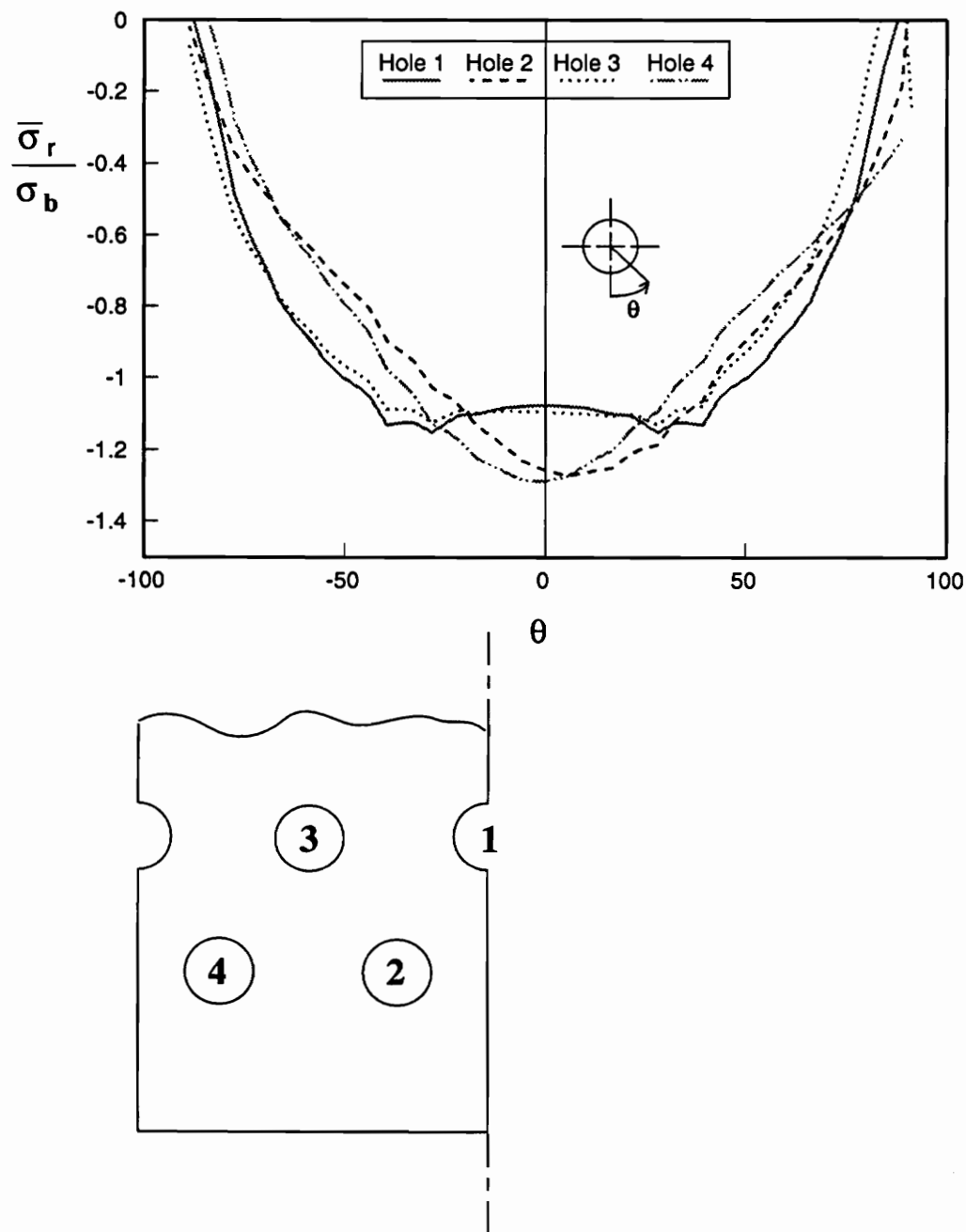


Figure 5.13. Distribution of radial stress $\bar{\sigma}_r$ for 7-hole T30 inboard specimen

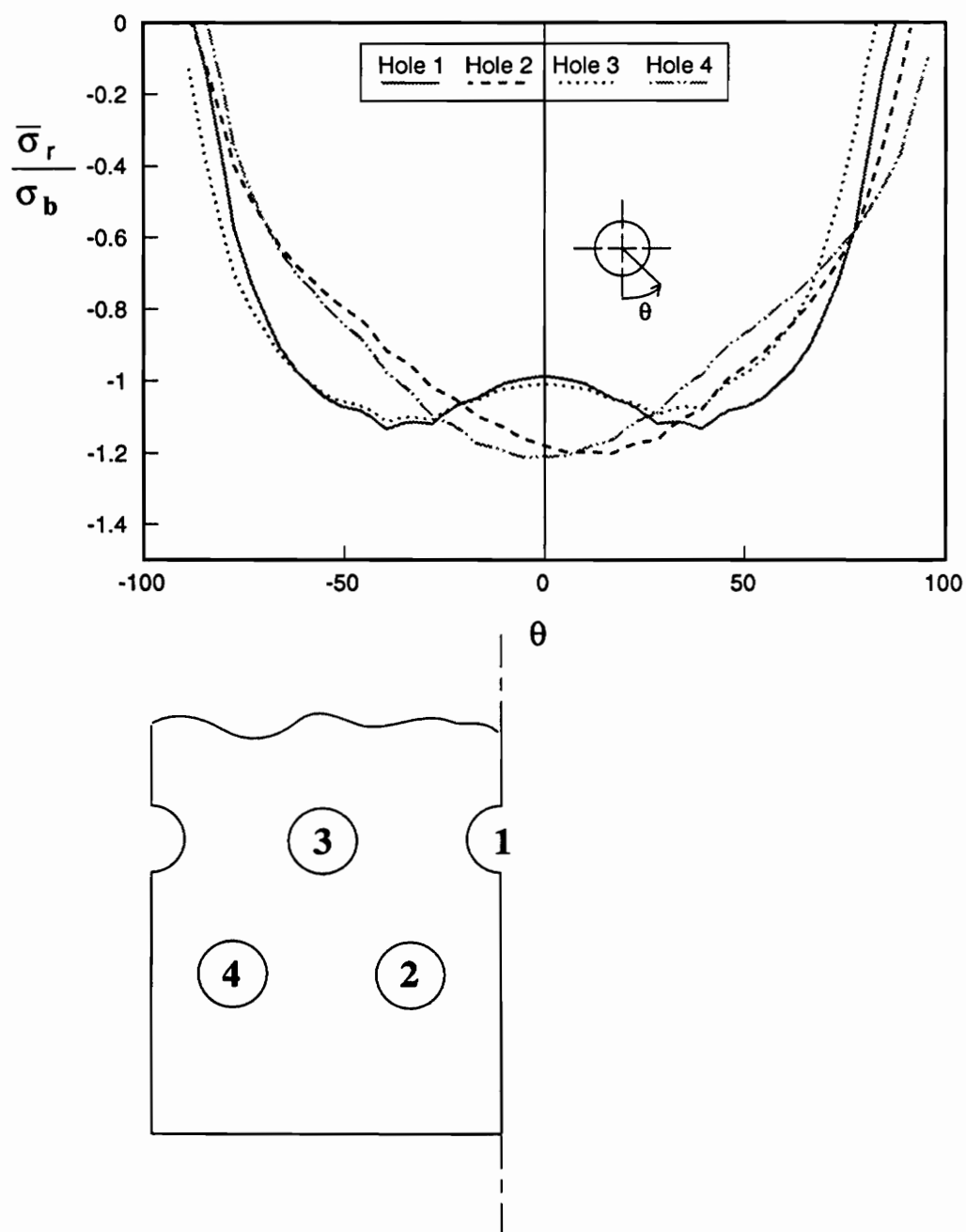


Figure 5.14. Distribution of radial stress $\bar{\sigma}_r$ for 7-hole T45 inboard specimen

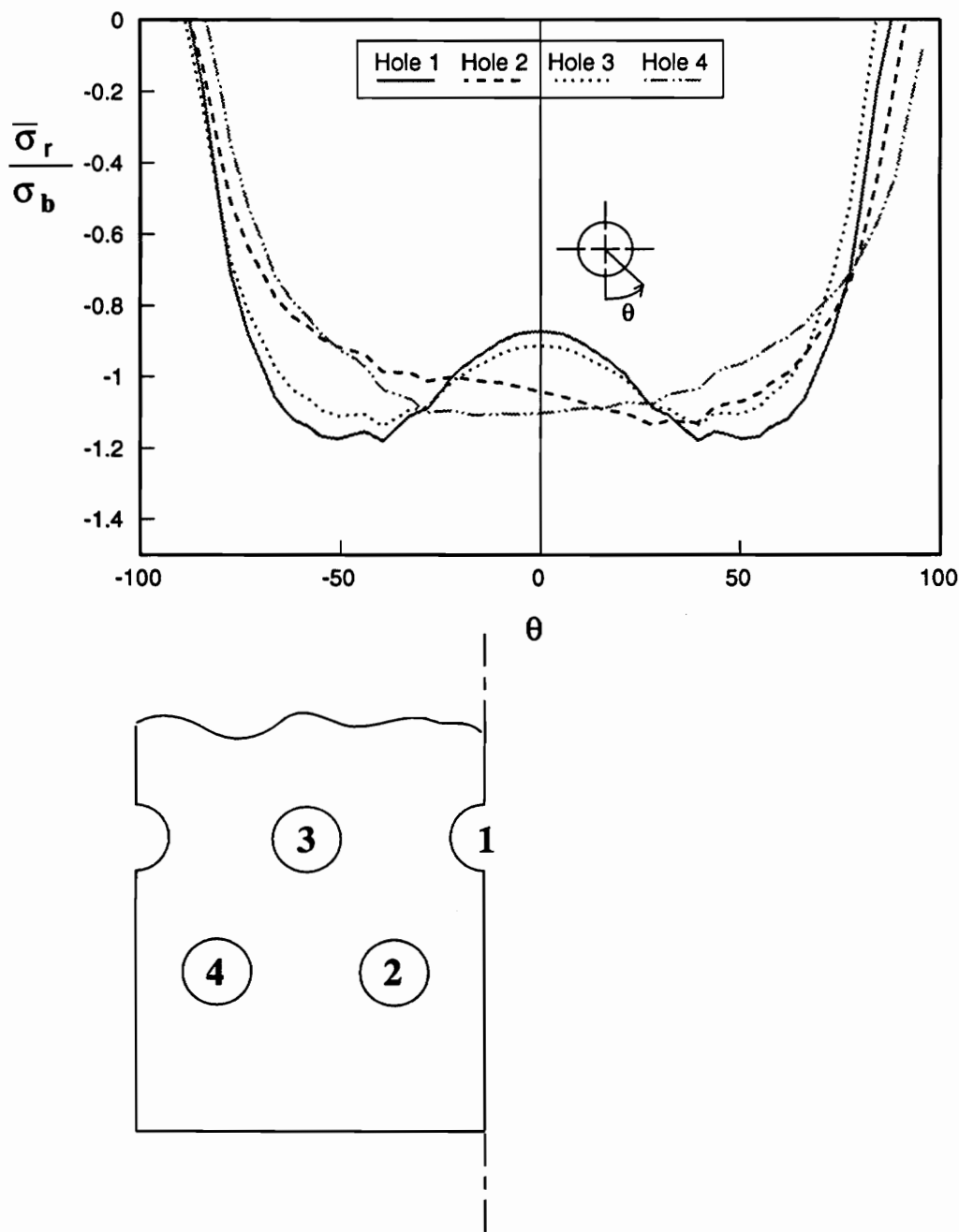


Figure 5.15. Distribution of radial stress $\bar{\sigma}_r$ for 7-hole T60 inboard specimen

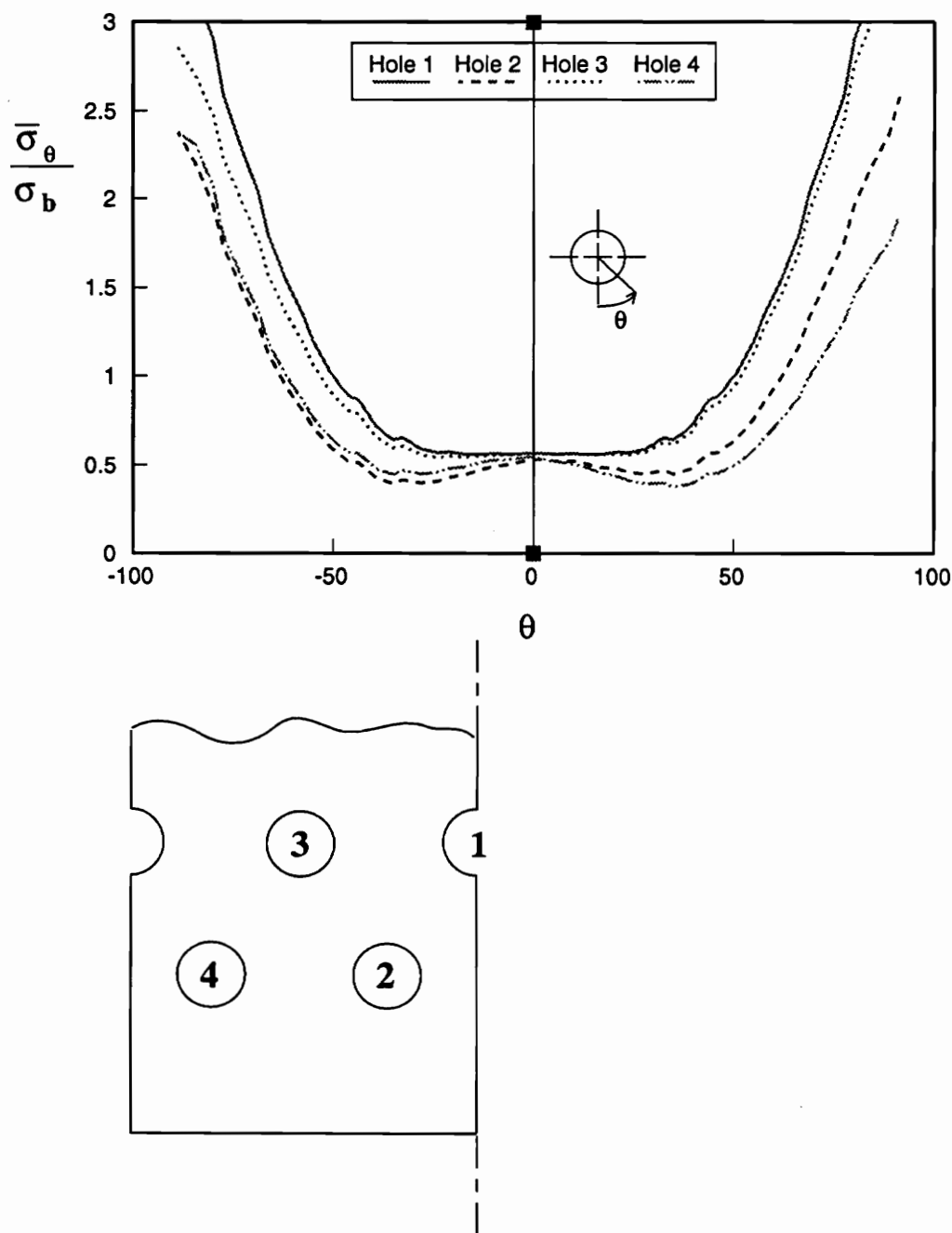


Figure 5.16. Distribution of circumferential stress $\bar{\sigma}_\theta$ for 7-hole T30 inboard specimen

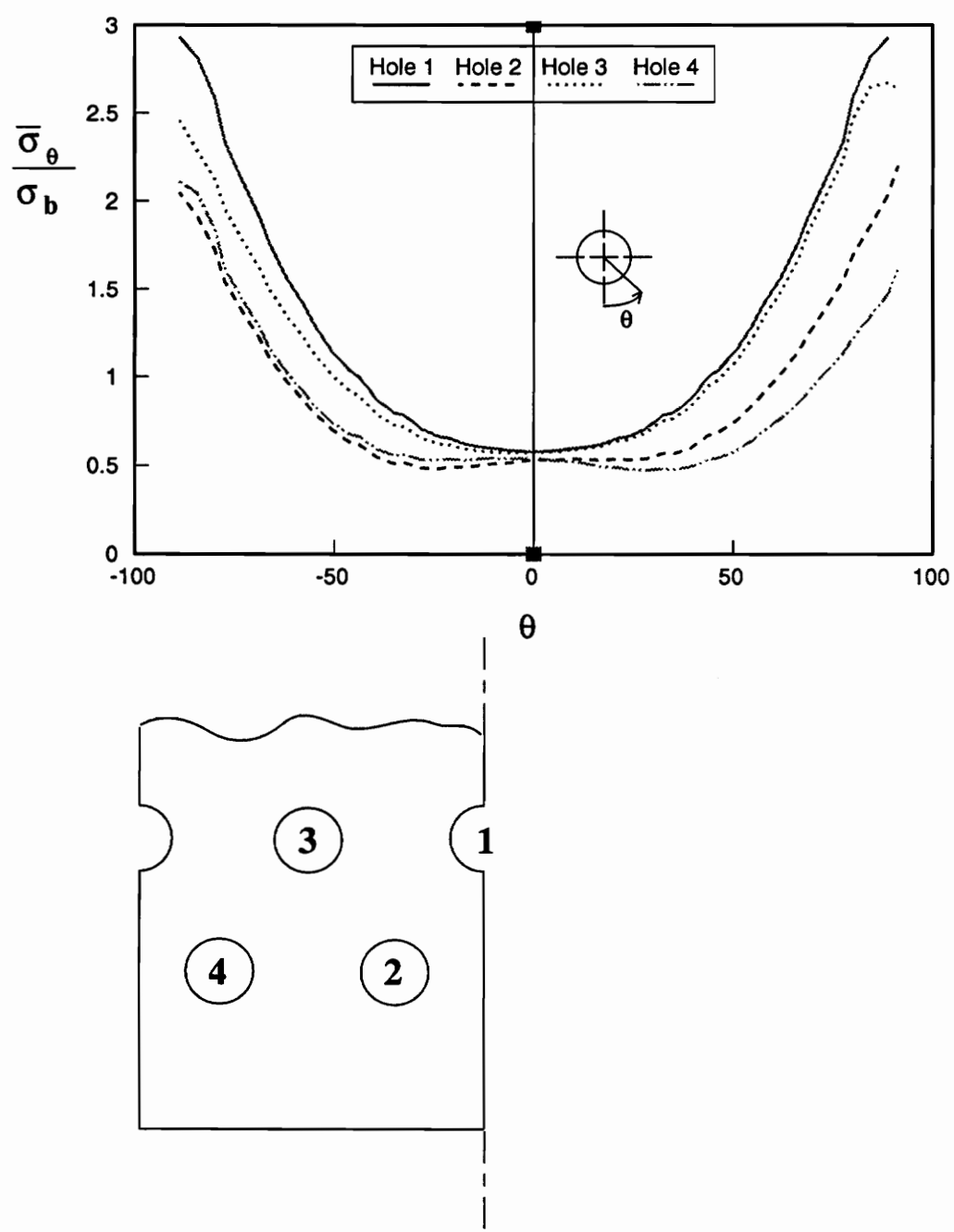


Figure 5.17. Distribution of circumferential stress $\bar{\sigma}_\theta$ for 7-hole T45 inboard specimen

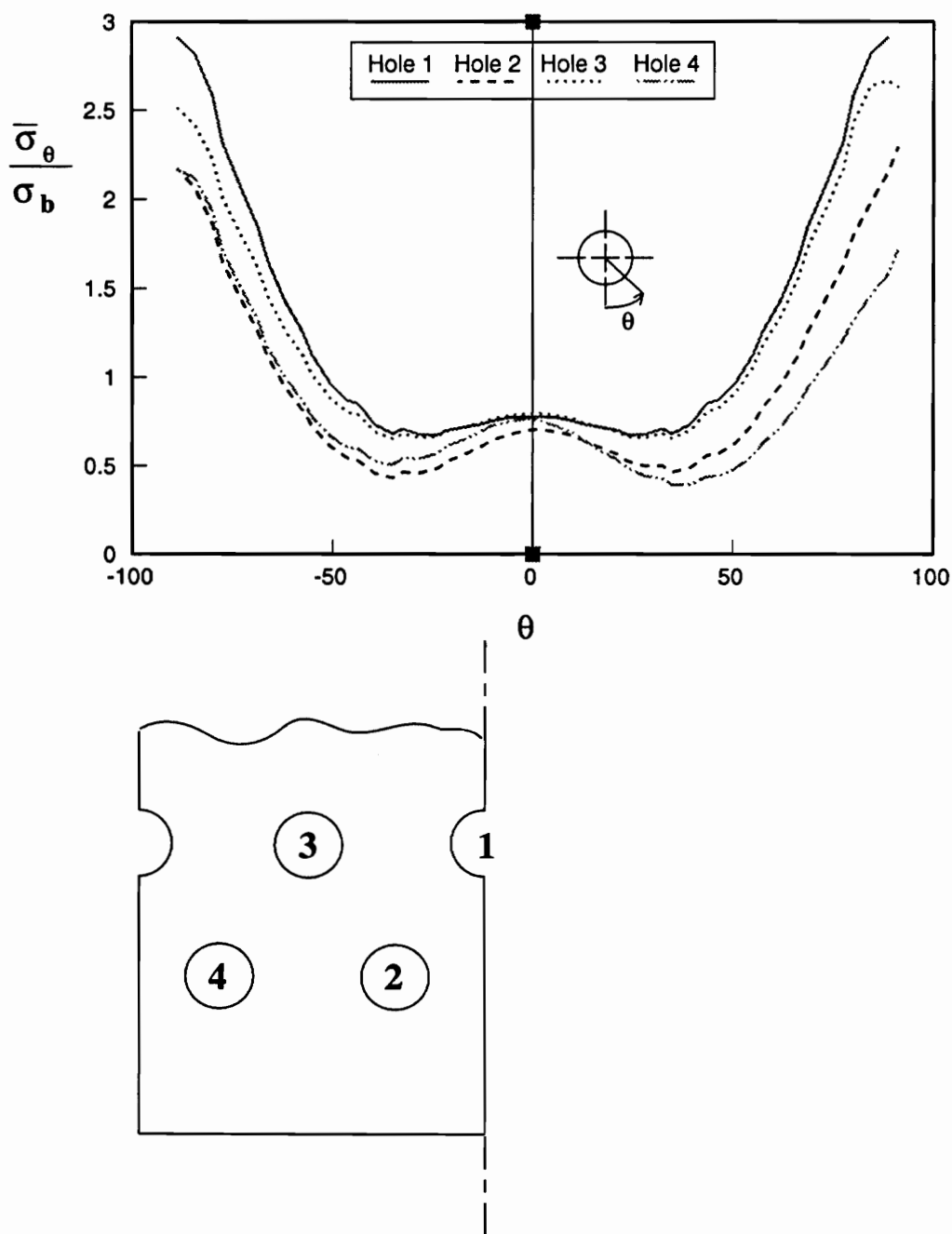


Figure 5.18. Distribution of circumferential stress $\bar{\sigma}_\theta$ for 7-hole T60 inboard specimen

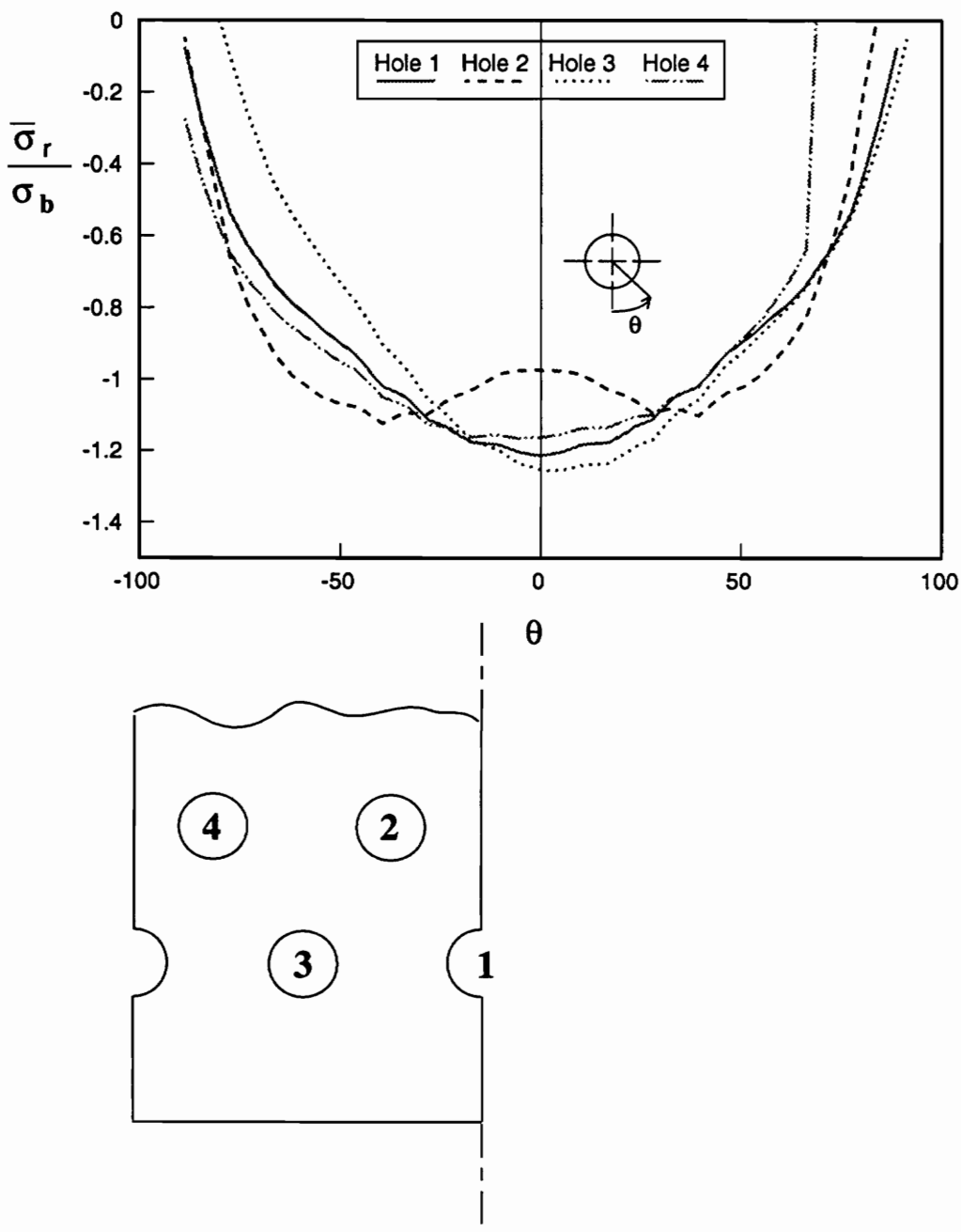


Figure 5.19. Distribution of radial stress $\bar{\sigma}_r$ for 7-hole T45 outboard specimen

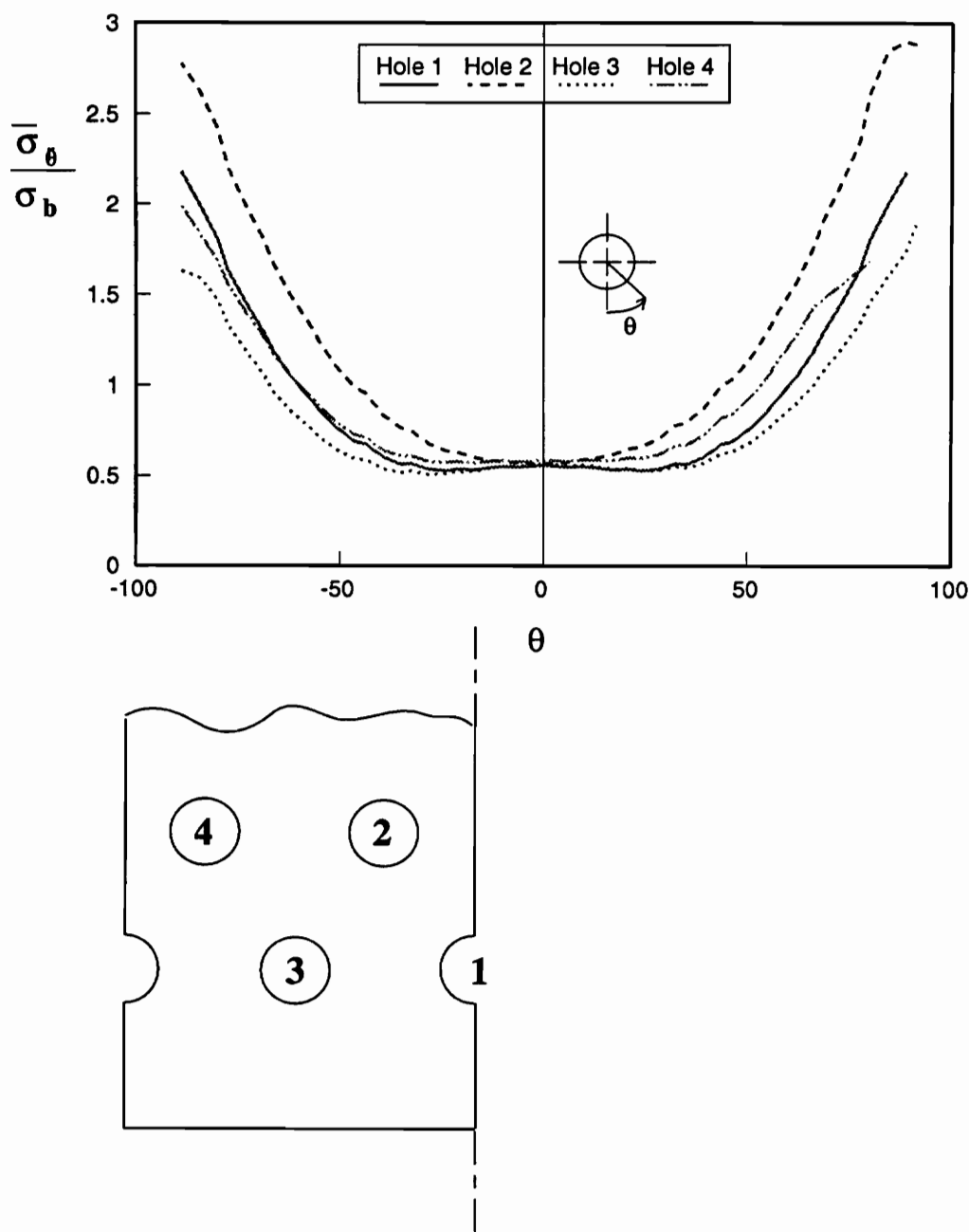


Figure 5.20. Distribution of circumferential stress $\bar{\sigma}_\theta$ for 7-hole T45 outboard specimen

in stress near the bottom of the hole occurs only for inboard holes which are straddled by two loaded outboard holes. It confirms the idea that load path in the specimens, especially as affected by the unloaded half hole, determines the distribution of the stresses around the holes. In case of 7-hole specimens, the skewing of the cosinusoidal-like stress distribution becomes even less that for corresponding 5-hole specimen.

Similarly, for the distribution of the circumferential stress $\bar{\sigma}_\theta$, the inboard hole is not straddled by two outboard holes (hole 4) responds more like an outboard hole by showing a local maximum at the bottom of the hole, although it is not very conspicuous in case of T45 specimen.

5.6 9-Hole Specimen Results

The trends established with the 5- and 7-hole specimens continue with the 9-hole specimens. This can be seen in figs. 5.21 - 5.23, where the radial stress distribution, and figs. 5.24 - 5.26, where the circumferential stress distributions for T30, T45, and T60 inboard 9-hole specimens are shown, respectively.

5.7 Summary

In summary, some general rules governing the contact stress distributions can be established as follows: The first rule is the straddle effect. When a hole on the inboard row is straddled by two complete loaded holes on the outboard row, the radial stresses are relieved somewhat at the bottom of the hole, resulting in a decrease in the distribution of $\bar{\sigma}_r$ at the bottom of the hole. However, if the inboard hole has one loaded outboard hole on one side and unloaded outboard half-hole on the other side, the radial stress distribution will follow

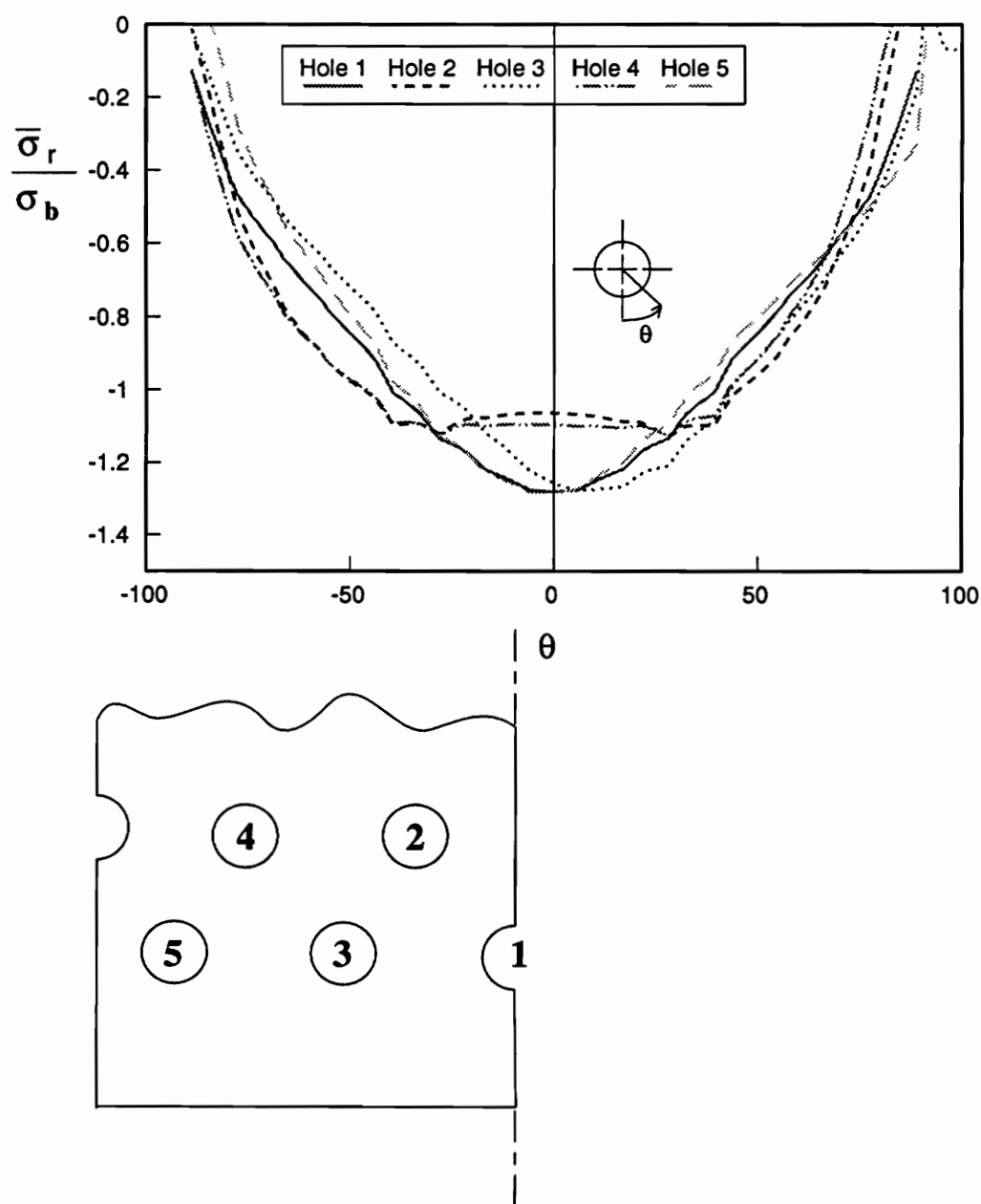


Figure 5.21. Distribution of radial stress $\bar{\sigma}_r$ for 9-hole T30 inboard specimen

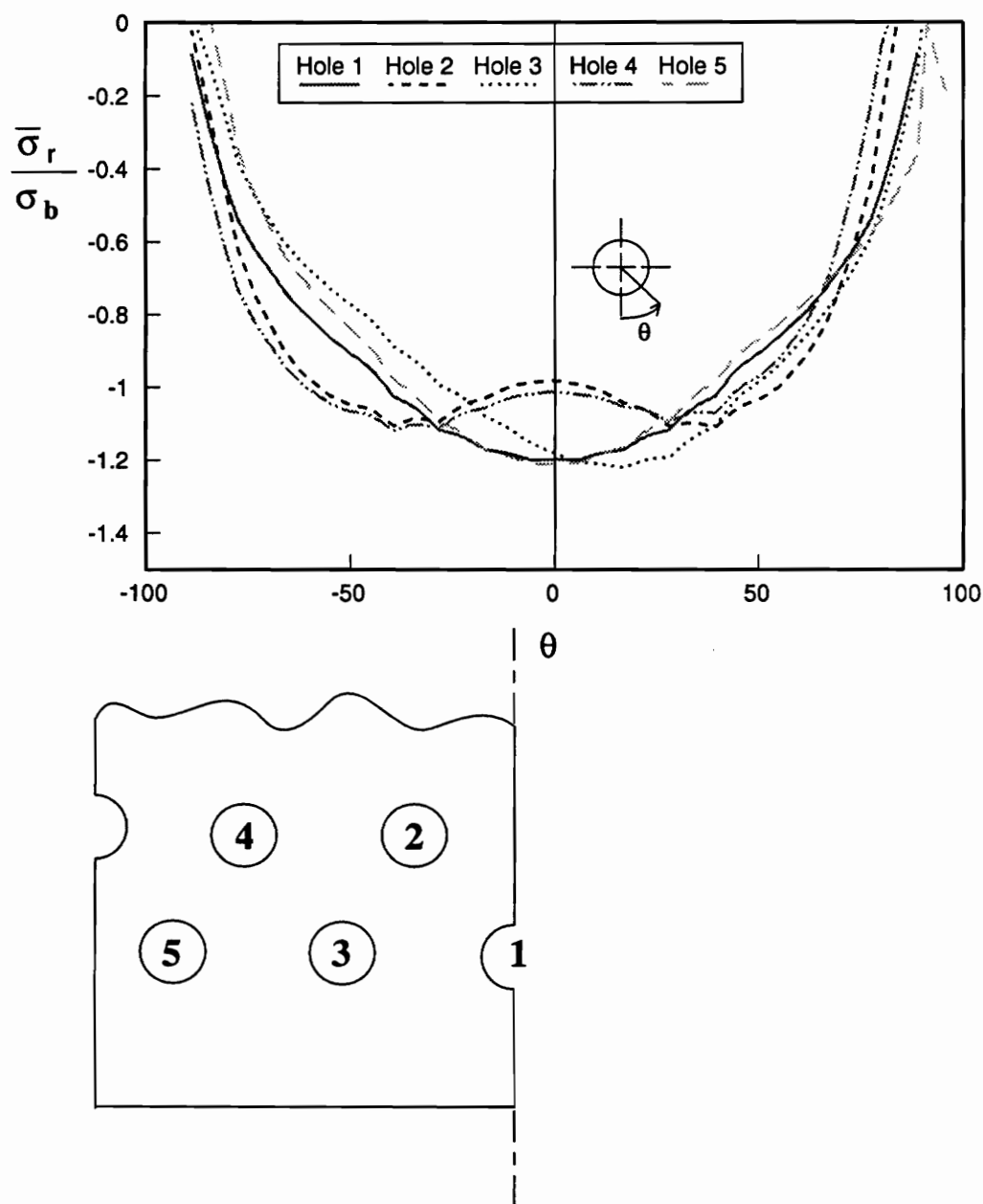


Figure 5.22. Distribution of radial stress $\bar{\sigma}_r$ for 9-hole T45 inboard specimen

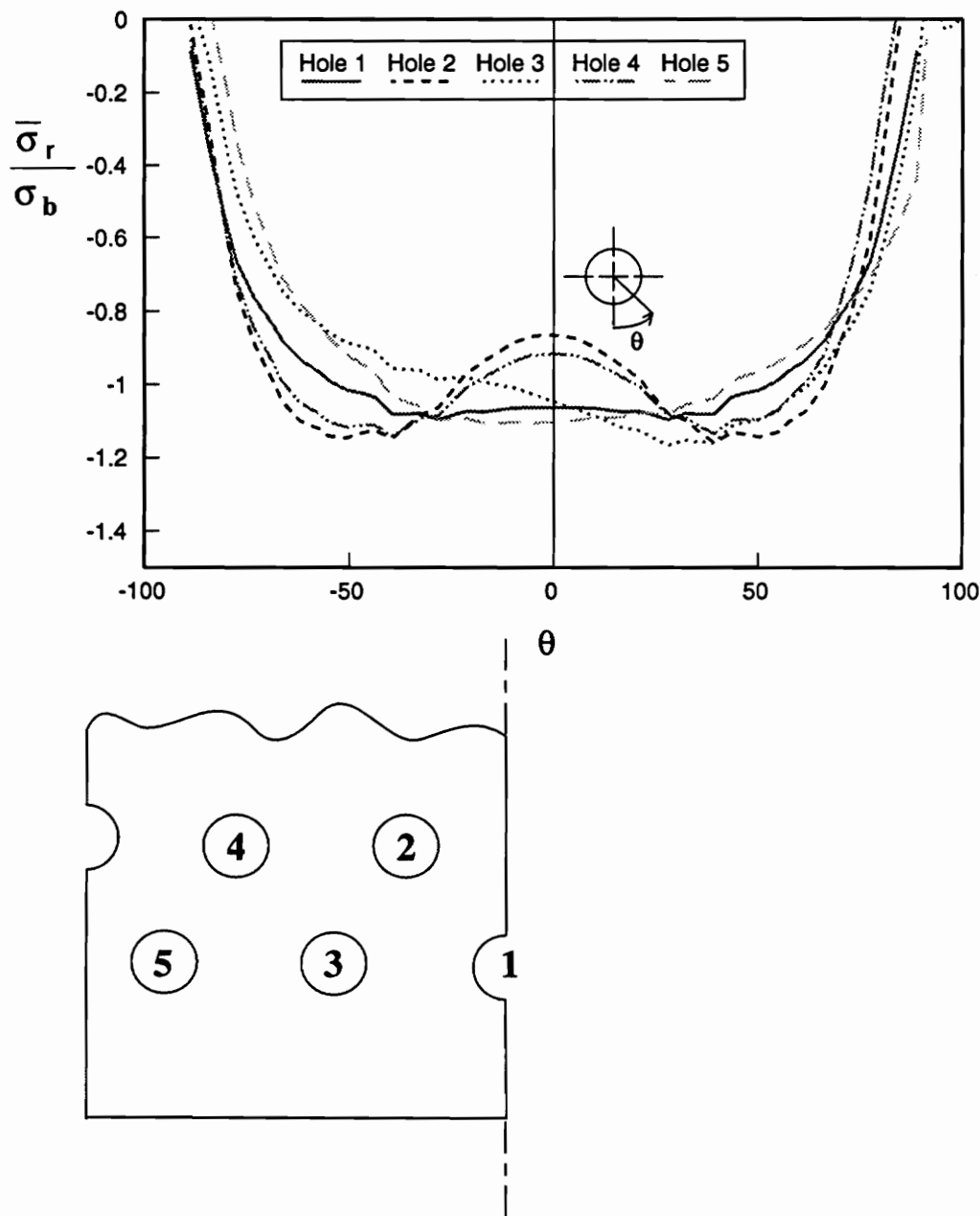


Figure 5.23. Distribution of radial stress $\bar{\sigma}_r$ for 9-hole T60 inboard specimen

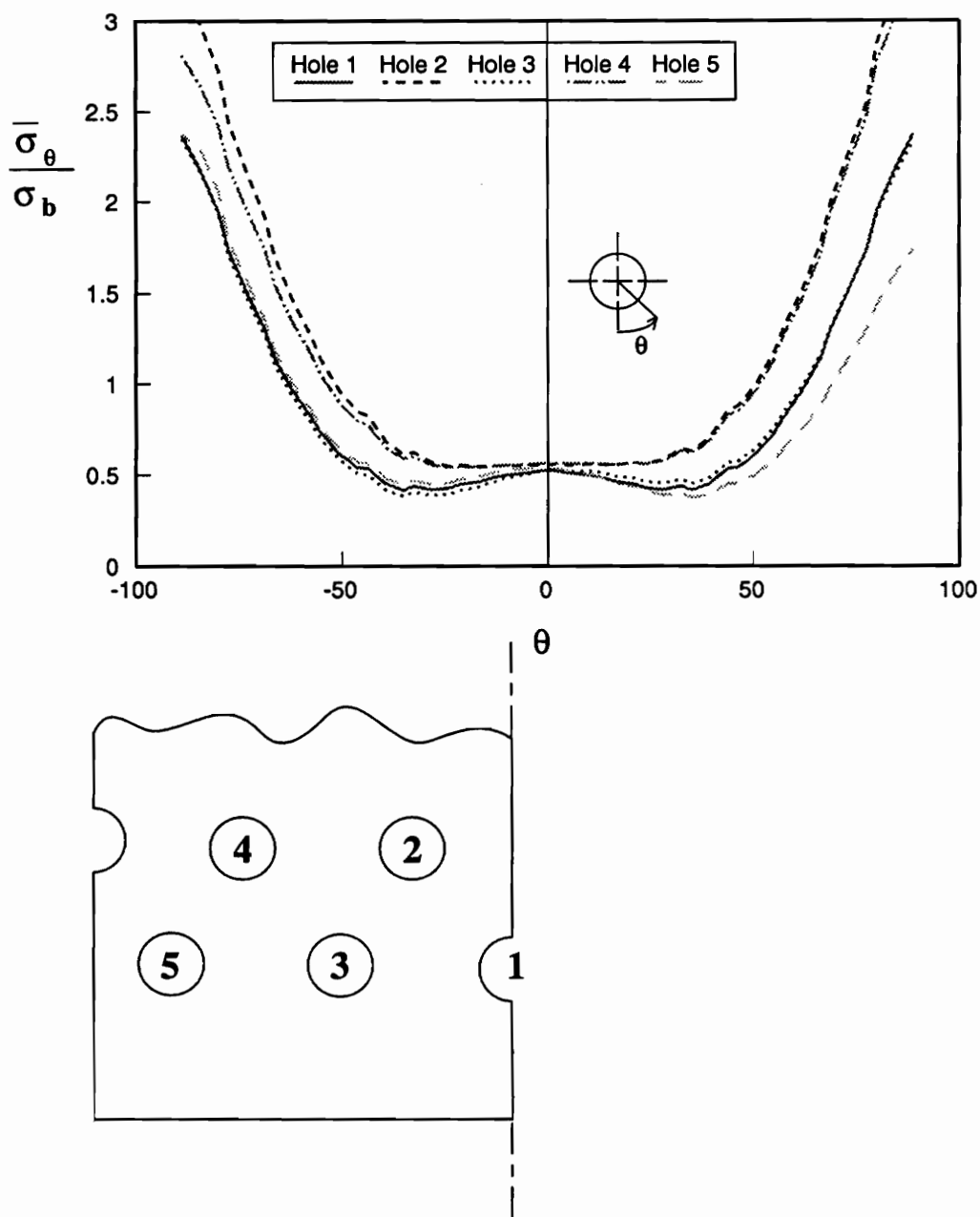


Figure 5.24. Distribution of circumferential stress $\bar{\sigma}_\theta$ for 9-hole T30 inboard specimen

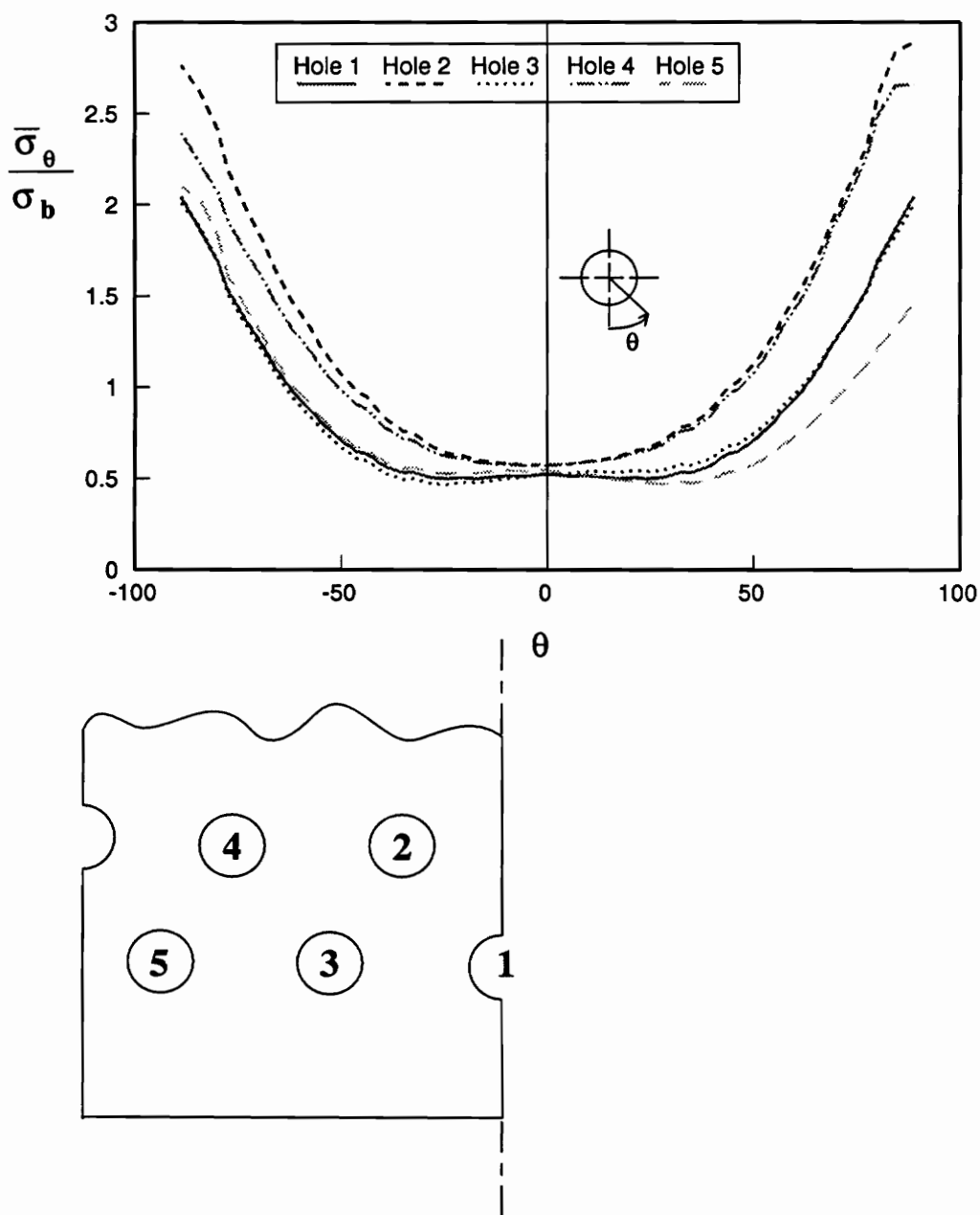


Figure 5.25. Distribution of circumferential stress $\bar{\sigma}_\theta$ for 9-hole T45 inboard specimen

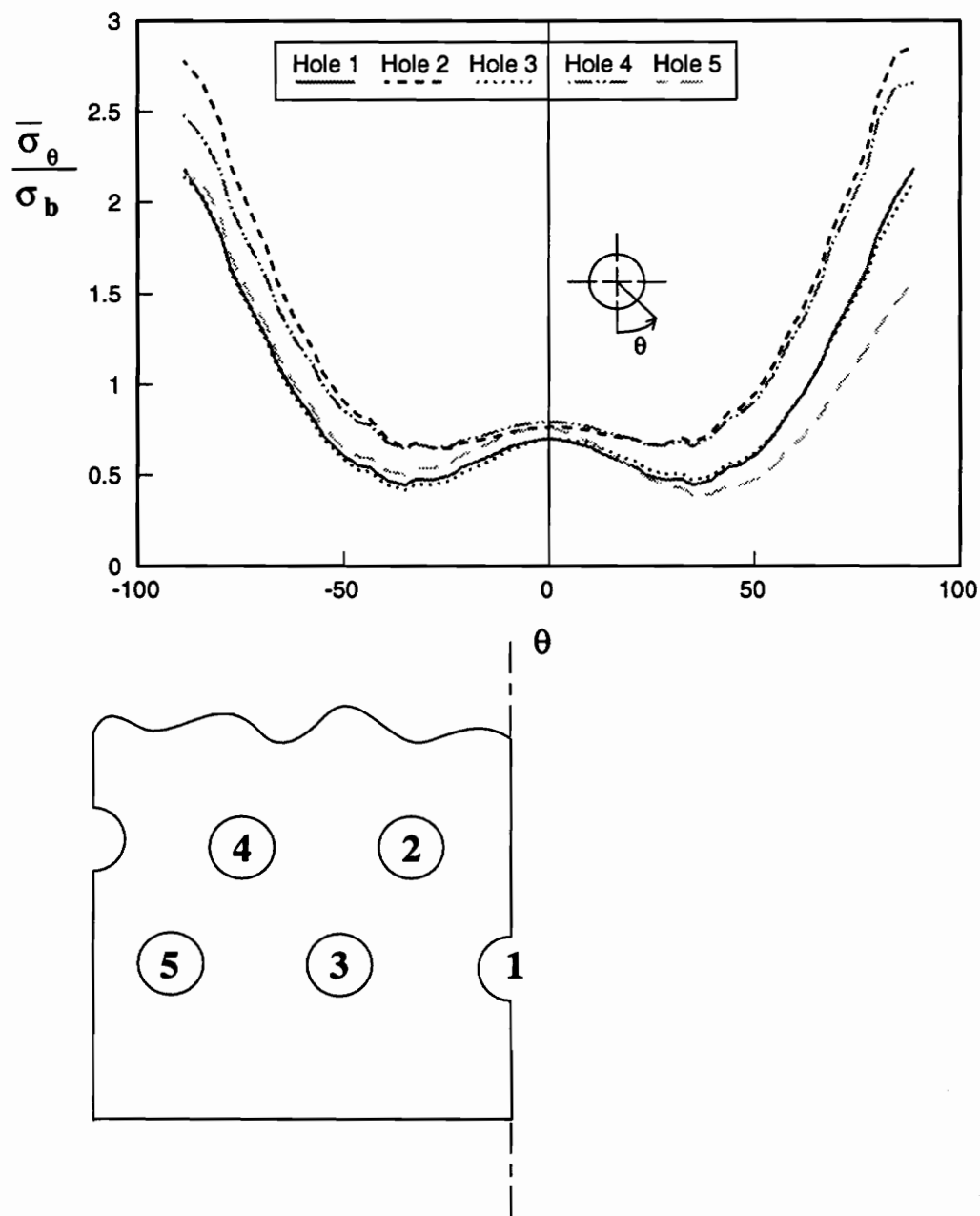


Figure 5.26. Distribution of circumferential stress $\bar{\sigma}_\theta$ for 9-hole T60 inboard specimen

a cosinusoidal - like distribution that is typical of an outboard hole. Second, the circumferential stresses always have a maximum value at the net-section. While the distributions of the circumferential stresses for the outboard holes tend to show a local maximum at the bottom of the hole, the distributions for the inboard holes tend to remain flat when they are straddled by two loaded outboard holes. However, in analogy to the earlier statements regarding the distribution of the radial stresses, the distribution of the circumferential stresses for the inboard holes that are not straddled by two outboard holes are more like the distribution of a typical outboard hole. The effect of the distribution decreasing at the bottom of the hole in case of radial stress distribution, and showing a local maximum in case of circumferential stress distribution, seems to be more pronounced as the material stiffness decreases in the loading direction.

6.0 SUMMARY AND RECOMMENDATIONS

As discussed in the first chapter, there are numerous issues to be addressed for having a complete understanding of behavior of multiple fastener composite joints. The present work can be categorized as a simple, yet positive beginning in that direction. The three primary objectives mentioned in Ch. 1 have been successfully accomplished. They can be summarized as follows.

1. A viable numerical procedure for studying joint response, using PATRAN and ABAQUS, has been established. The model has two independent finite-element meshes interacting through rigid circular surface acting as a pin. The model accurately accounts for interaction between different components of the model.
2. Numerical predictions have been successfully verified through experiments. Good correlation was found between numerical and experimental results with regard to percentage of total load carried by each pin. Strains in net-section region, where the strains gage measurements were believed to be accurate, agreed well with the numerical predictions. For strains around shear and bearing regions of the holes, where gages were in the vicinity of contact region and subjected to crushing, the agreement was fair.

Before addressing the third objective, it is appropriate to look at the other interesting and important findings of the current work. They can be combined as follows:

- a. As expected, for 3-hole specimens, the presence of unloaded half-hole resulted in severe distortion of adjoining loaded holes. This distortion seemed to be alleviated as the number of holes in the specimen increased.
- b. In general, the holes close to the vertical centerline tended to react lesser percentage load than the holes away from it. The centerline hole reacted the least percentage of the load and the percentage increased as the hole's distance from the centerline increased.
- c. Specimens with a half-hole on the inboard row were found to be stronger than the ones with half-hole on the outboard row. This reduction in strength was believed to occur due to shifting of load disproportionately to the inboard row. Also the load proportions reacted by individual holes in inboard specimens seemed to be closer to the uniformity expected in a complete cylindrical joint than the load proportions reacted by the individual holes in the outboard specimens, for similar reasons.
- d. Among the three different laminates considered, the laminate T45 was found to be strongest although it is less stiff in the loading direction than T30. The strength of T30 was a close second. The T60 specimens were found to be considerably weaker than the other two laminates.
- e. Although the laminate properties did not effect the load proportions substantially, there seemed to be some trend. Specifically, in case of T45 specimens the load seemed to be evenly distributed, with each row reacting about 50% of the total load. With the other two laminates load sharing between the rows was found to be more disproportionate. This could be one of the reasons for higher strength of T45 specimens compared to other two laminates.
- f. Net-section gages showed good repeatability and correlation with the numerical

predictions. Data from these strain gages confirmed the aforementioned trends, with the holes closer to the vertical centerline showing lesser strain than ones away from the centerline. They also confirmed that the holes on the inboard take more load than the ones on the outboard.

- g. No such conclusions could be drawn with confidence from the data obtained from gages at other locations, primarily due to poor repeatability of the measured values. However, in certain cases where repeatability was good, similar trends were observed.
- h. In general, the strains from T30 specimens were slightly higher than corresponding strains from T45. This difference can be related to the difference in the strength between these two laminates mentioned earlier. Similarly, the strains in T60 specimens were found to be significantly higher than the other two laminates in many cases, providing an explanation for the least strength of T60 specimens among the three lamination sequences considered in the study.
- i. Radial contact stresses around the holes seemed to follow a path significantly different from the prevalent assumption of cosinusoidal distribution in certain cases. For the inboard holes the stress distributions seemed to decrease at the bottom of the hole if the holes are straddled by two loaded outboard holes. The stresses for the inboard holes seem to follow a distribution closer to a cosine distribution when the holes have only one loaded hole to one side. The distribution for the outboard holes was somewhat cosinusoidal. Circumferential stresses also reflected similar effects, although not as clearly as the radial stresses.

Finally, coming to the third and final objective of the study,

- 3. Although there is a large difference in the absolute strengths of a 3-hole specimen

and a 9-hole specimen, gross strengths of the specimens, the strength that is important for transformation of results on to complete cylindrical joint, seem to change very little with the increase in the width of the specimen. In spite of severe distortions in 3-hole specimens due to high stress concentrations, the gross strength was found to be within 4% of that of 9-hole specimens. Obviously the reference here is to the inboard specimens. From the economic standpoint, a 3-hole specimen could be the best solution, as it requires less material than the other specimens, and gives the most conservative results. However, as discussed before, due to high stress concentrations and resulting distortions, the results could be misleading. Hence a 5-hole specimen may be a satisfactory compromise.

The following recommendations are made for future work.

1. A comprehensive failure criterion should be incorporated in to the analysis.
2. Nonlinear material behavior should be investigated as it possibly provides an explanation for some of the nonlinear behavior observed during present study.
3. It would be interesting to investigate into the effects of pin elasticity and friction on the response of the joint.
4. An experimental verification of the decrease in stress distributions at the bottom of the hole, in certain cases, could be carried out possibly using photomechanics.
5. Broad design issues such as hole diameter, hole spacing, number of rows, row spacing, etc., should be investigated.
6. Determining the influence of compliance of the double laps on the load proportions, and the stress distributions would be valuable. The limiting cases of infinite compliance and zero compliance would provide interesting bounds.
7. Other loading conditions, such as inplane bending, and reversing the load to study

compression, are also of interest for the application.

8. A detailed investigation should be carried out to translate the results obtained from the flat specimens to predict the response of a complete multiple fastener cylindrical joint

REFERENCES

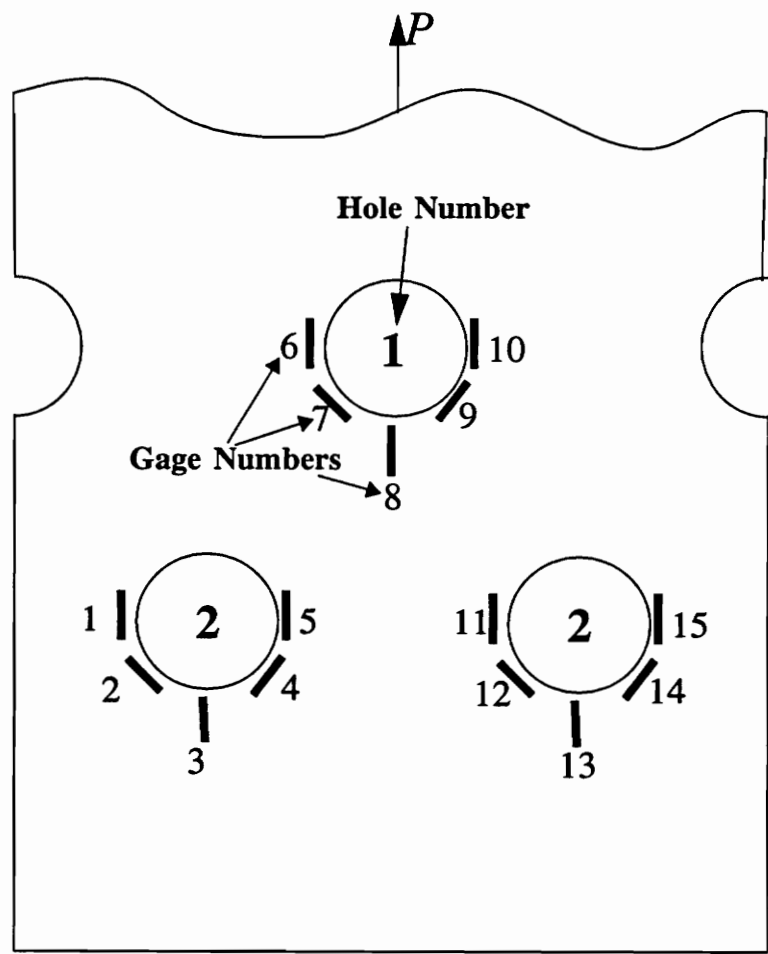
- 1 Kellas, S., and Morton, J., "Strength and Scaling in Fiber Composites," AIAA Paper No. 91-1144, *Proceedings of the 32nd AIAA/ASME/ASCE/AHS/ASC Structures, Structural Dynamics, and Materials Conference, Baltimore, MD, April 1991*, pp. 1181-1189.
- 2 ABAQUS version 4.8, available from Hibbitt, Karlsson, and Sorenson, Inc., Providence, RI.
- 3 Pyner, G. R., and Matthews "Comparison of Single and Multi-Hole Bolted Joints in Glass Fibre Reinforced Plastic," *J. Composite Materials*, Vol. 13, July 1979, pp. 232-237.
- 4 Hart-Smith, L.J., "Bolted Joints in Graphite-Epoxy Composites," NASA CR-144899, June 1976.
- 5 Hart-Smith, L. J., "Mechanically Fastened Joints for Advanced Composites-Phenomenological considerations and Simple Analysis," *Fibrous Composites in Structural Design*, Plenum Press, New York, 1980, pp. 543-574.
- 6 Wong, C. M. S. and Matthews F. L., "A Finite Element Analysis of Single and Two-Hole Bolted Joints in Fiber Reinforced Plastics," *J. Composite Materials*, Vol. 15, September 1981, pp. 481-491.
- 7 Godwin, E. W., Matthews, F. L., and Kilty, P. F. "Strength of Multi-Bolt Joints in GRP," *Composites*, Vol. 13, No. 3, July 1982, pp. 268-272.
- 8 Garbo, S. P., and Ogonowski, "Effect of Variances and Manufacturing Tolerances on the Design Strength and Life of Mechanically Fastened Composite Joints", AFWAL-TR-81-3041, Vols. 1-3, April 1981.
- 9 Whitney, J. M., and Nuismer, R.J., "Stress Fracture Criteria for Laminated Composites Containing Stress Concentrations", *J. Composite Materials*, 8, July 1974, pp. 253-259.
- 10 Rowlands, R. E., Rahman, M. U., et al, "Single-and Multiple-Bolted Joints in Orthotropic Materials," *Composites*, Vol. 13, No. 3, July 1982, pp. 273-278.
- 11 Collings, T. A., Strength of Bolted Joints in Multidirectional CFRP Laminates," *Composites*, Vol 15, Jan. 1984, pp. 33-38.
- 12 "Garbo, S. P., and Becker, M. L., "Carbon Epoxy Laminates Under Combined Fas-

- tener Bearing and Tension Bypass Loading," AIAA, Paper No. 83-0967, *Proceedings of the 24th AIAA/ASME/ASCE/AHS Structures, Structural Dynamics, and Materials Conference*, Lake Tahoe, Nevada, May 1983, pp. 499-509.
- 13 Crews, J.H. Jr., and Naik, R.A. "Bearing-Bypass Loading on Bolted Composite Joints," NASA-TM-89153, May 1987.
- 14 Chang, F.K., and Springer, G.S., "Strength of Mechanically Fastened Composite Joints," *J. Composite Materials*, 16, May 1982, pp. 470-493.
- 15 Chang, F.K., Scott, R.A., and Springer, G.S., "Failure of Composite Laminates Containing Pin-Loaded Holes-Method of Solution," *J. Composites Materials*, Vol. 18, May 1984, pp. 257-277.
- 16 Chang, F.K., Scott, R.A., and Springer, G.S., "Failure Strength of Nonlinearly Elastic Composite Laminates Containing a Pin-Loaded Hole," *J. Composites Materials*, Vol. 18, May 1984, pp. 464-477
- 17 Chang, F.K., Scott, R.A., and Springer, G.S., "A Progressive Damage Model for Laminated Composites Containing Stress Concentrations," *J. Composites Materials*, Vol. 21, Sept. 1987, pp. 843-855.
- 18 Hyer, M.W., and Chastain, P.A. "Effects of Load Proportioning on the Capacity of Multiple-Hole Composite Joints," NASA Contractor Report 178019, Nov. 1985.
- 19 Cohen, D., Norton, F.M., Hodgson, M.E., "Experimental Investigation of Failure Loads in Thick Composite Joints", *American Society for Composites, 4th Technical Conference on Composite Materials*, Oct. 1989, Blacksburg, VA. pp. 72-81, available Technomic Publishers, Lancaster, PA.
- 20 PATRAN Release 2.4, Available from PDA Engineering, Costa Mesa, California.
- 21 Hyer, M.H., Klang, E.C., and Cooper, D.E., "Effects of Pin Elasticity, Clearance, and Friction on the Stresses in a Pin-Loaded Orthotropic Plate", *J. Composite Materials*, vol. 21, Oct. 1987, pp. 190-206.
- 22 Hyer, M.H., Klang, E.C., "Contact Stresses in a Pin-Loaded Orthotropic Plates", *Int. J. Solids and Structures*, vol. 21, no. 9, 1985, pp. 957-975.
- 23 Griffin, O.H., Hyer, M.W., Yalamanchili, S.R, Cohen, D., Shuart, M.J., Prasad, C. B., "Analysis of Multiple Fastener Composite Joints", AIAA, paper No.92-2426, *Proceedings of the 33rd AIAA/ASME/ASCE/AHS Structures, Structural Dynamics, and Materials Conference*, Dallas, TX, April 1992, pp. 745-753.

- 24 Sun, C.T., Sankar, B.V., "Indentation of a Beam by a Rigid Cylinder", *Int. J. Solids Structures*, Vol 19, No. 4, 1983, pp. 293-303.
- 25 Sun, C.T., Sankar, B.V., "Smooth Indentation of an Initially Stressed Orthotropic Beam", *Int. J. Solids Structures*, Vol 21, No. 2, 1985, pp. 161-176.

APPENDIX A: STRAIN GAGE RESULTS FOR THE 3-HOLE SPECIMENS

The strain gage responses for the 3-hole specimens are presented in the following pages. They follow trends similar to those that were observed in case of the 5-hole specimens. The strain gage numbering scheme for the 3-hole inboard specimens, the only kind of specimen that was tested, is shown in fig. A.1. Also, only the T45 laminate was tested for the 3-hole specimens. The load vs. strain relations for net-section, shear, and bearing gages are shown in figs. A.2, A.3, and A.4 respectively. The strains for the net-section gages showed good repeatability, and they agreed well with predictions. As with the 5-hole specimens, the responses of shear and bearing gages were somewhat erratic.



3-Hole Inboard Specimen

Figure A.1. Strain gage numbering scheme for 3-hole T45 inboard specimens

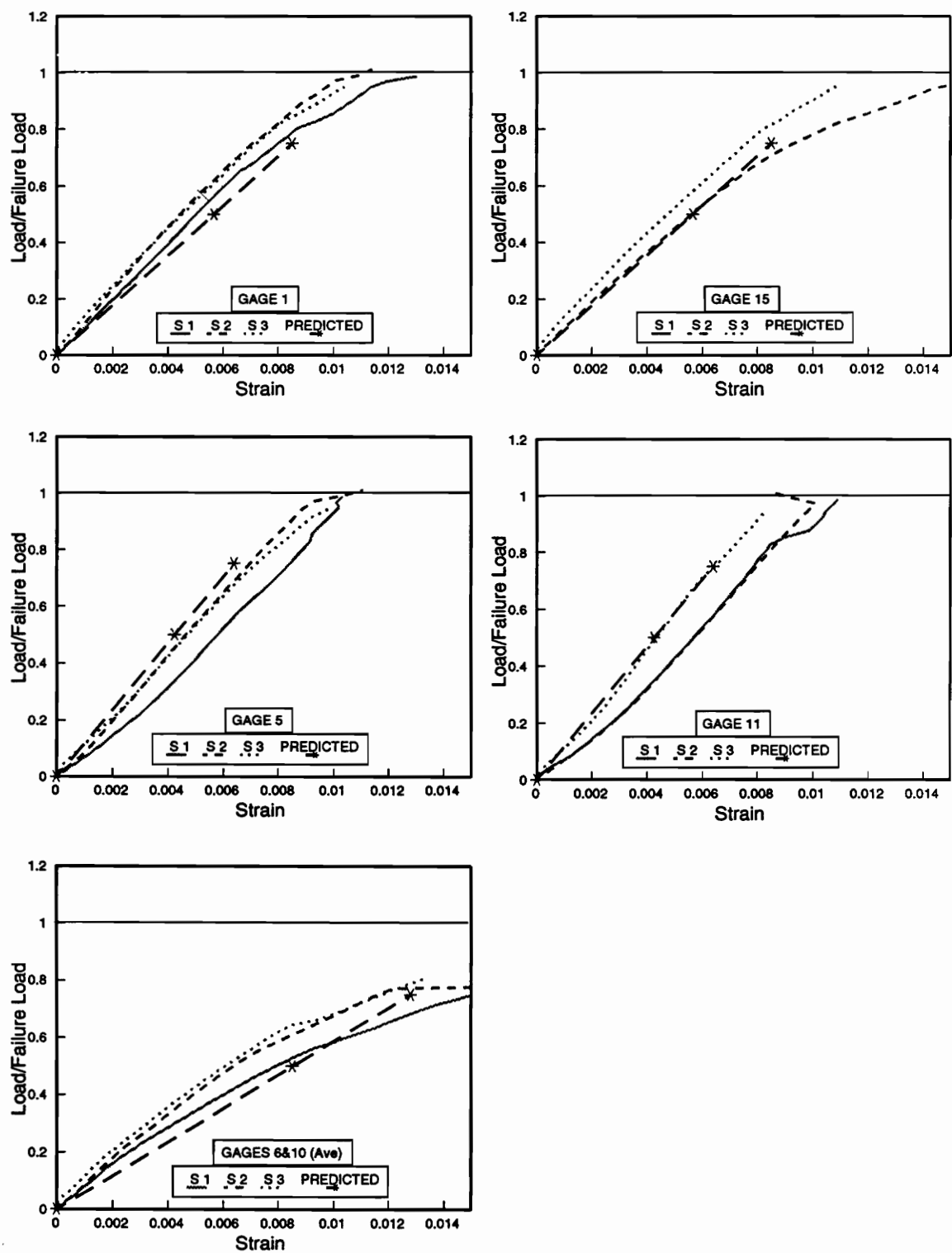


Figure A.2. Measured and predicted net-section gage strains for 3-hole T45 inboard specimens

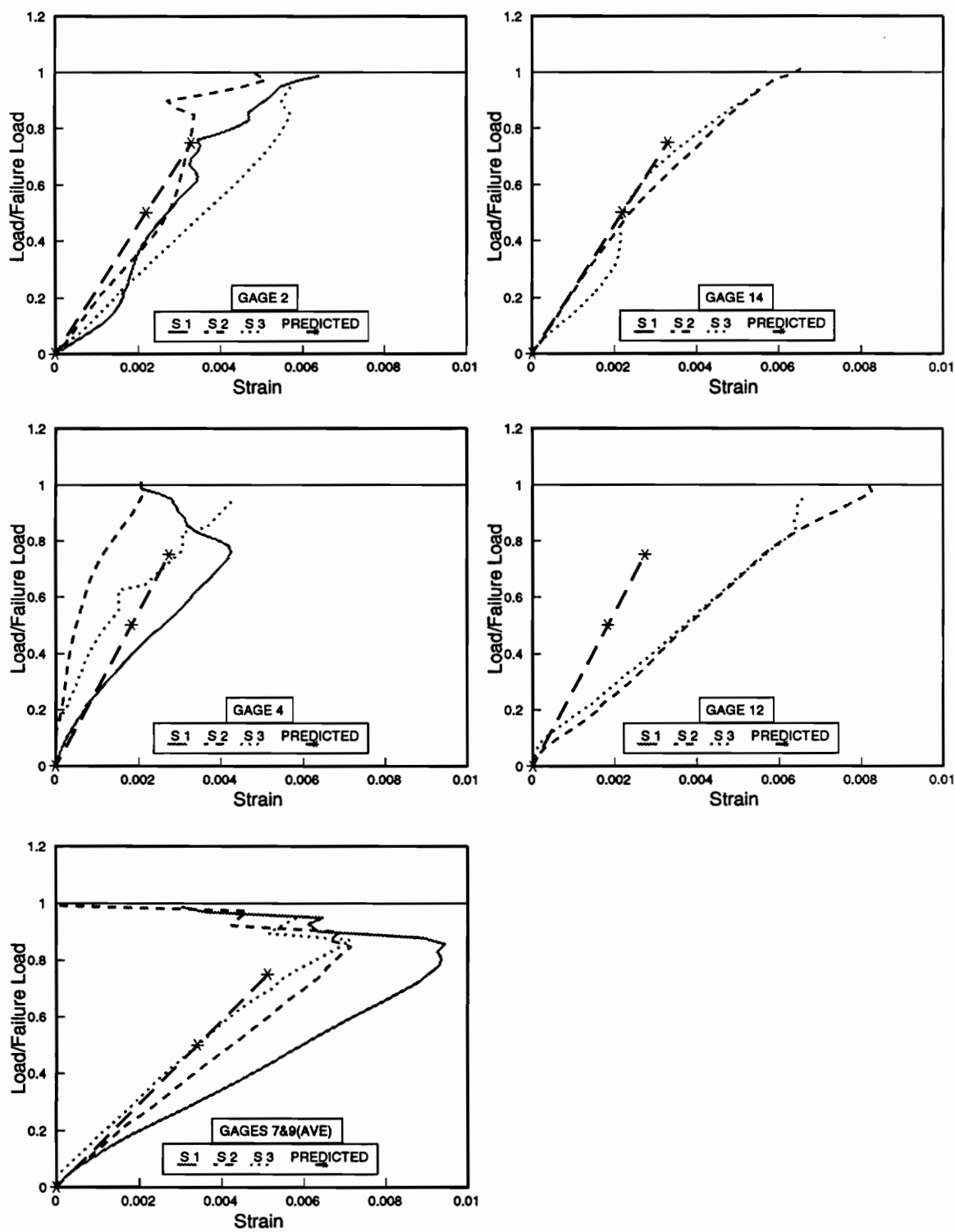


Figure A.3. Measured and predicted shear gage strains for 3-hole T45 inboard specimens

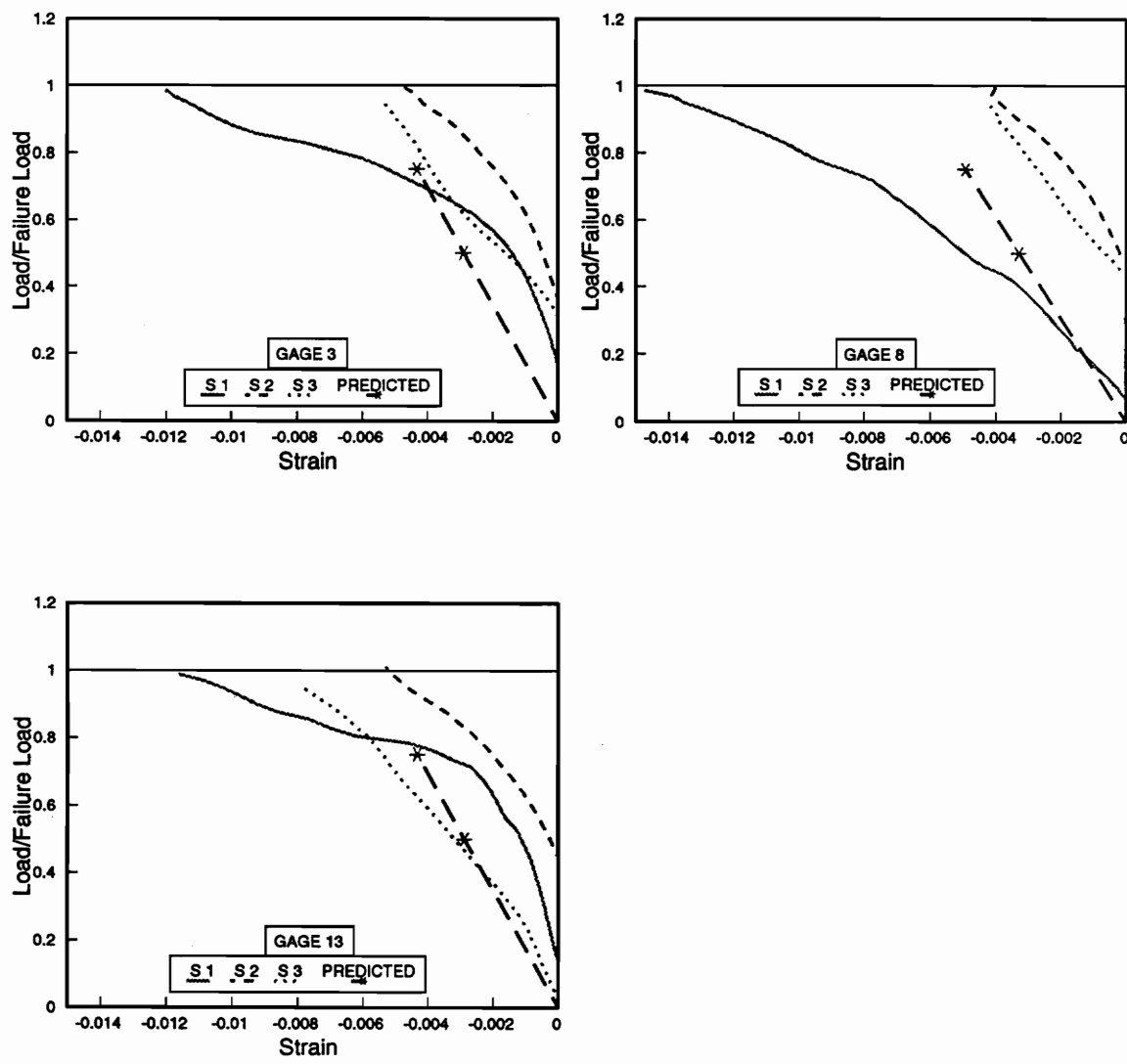


Figure A.4. Measured and predicted bearing gage strains for 3-hole T45 inboard specimens

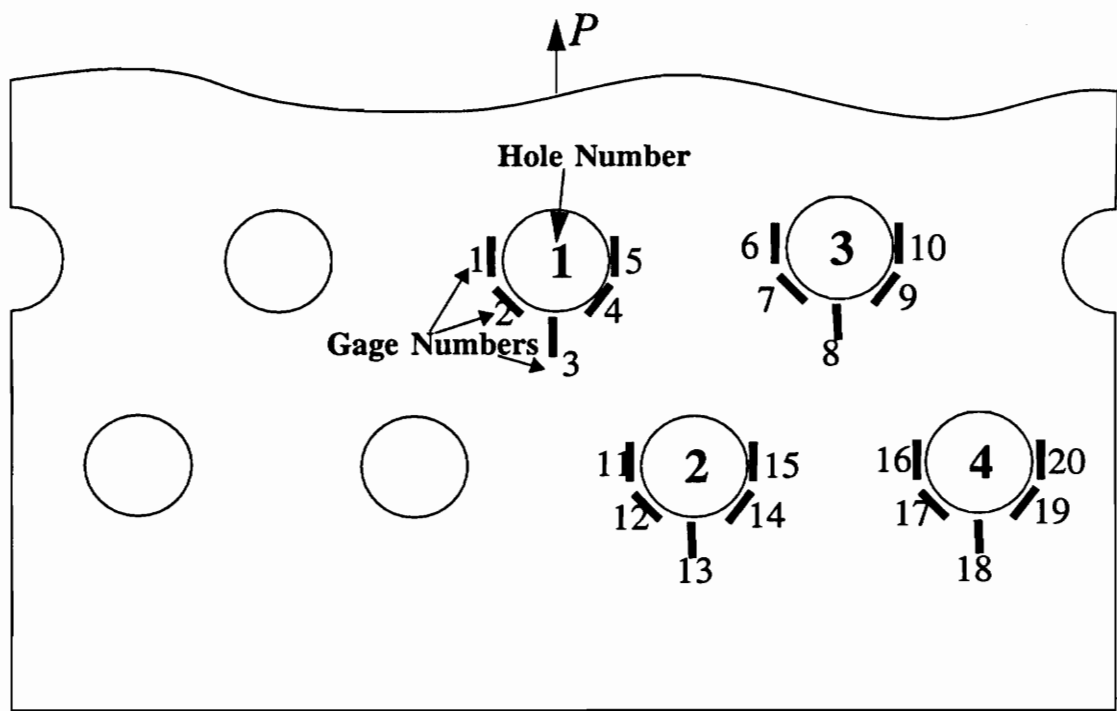
APPENDIX B: STRAIN GAGE RESULTS FOR THE 7-HOLE SPECIMENS

The strain gage responses for the 7-hole specimens are presented in the following pages. The strain gage numbering scheme for the 7-hole inboard specimens is shown in fig. B.1. One of the holes (hole 2L) in one of the T45 specimens was offset by a small fraction (about 0.002) of an inch. This resulted in complete distortion in load distribution among the holes. Naturally, this also resulted in unusual strain behavior. This will be obvious from the following figures. The other specimens followed the trends that were observed in 5-hole specimens. Hence for all practical purposes, the data from one T45 inboard 7-hole specimen (S1) can be ignored, while the data from S2 is somewhat reasonable. It should be noted that specimen S3 for this case was never tested. The load vs. strain relations for net-section gages for 7-hole T45 inboard specimens are shown in fig. B.2 and B.3. Similar relations for shear gages are shown in fig.s B.4 and B.5, while B.6 shows the data for the bearing gages.

Similarly, the plots for net-section gages of 7-hole inboard specimens of T30 and T60 laminates are shown in figs. B.7, B.8, and B.9, B.10 respectively. The data for shear gages for these laminates are shown in B.11, B.12, and B.13, B.14. The bearing gage plots are shown in fig.s B.15 and B.16 for T30 and T60 laminates, respectively.

The strain gage numbering scheme for the 7-hole outboard specimens is shown in fig. B.17. Data for net-section gages for the 7-hole T45 outboard specimens are shown in fig.s B.18, and B.19. The shear gage data for these specimens are shown in figs. B.20 and B.21,

while the data for bearing gages are shown in fig. B.22.



7-Hole Inboard Specimen

Figure B.1. Strain gage numbering scheme for 7-hole T45 inboard specimens

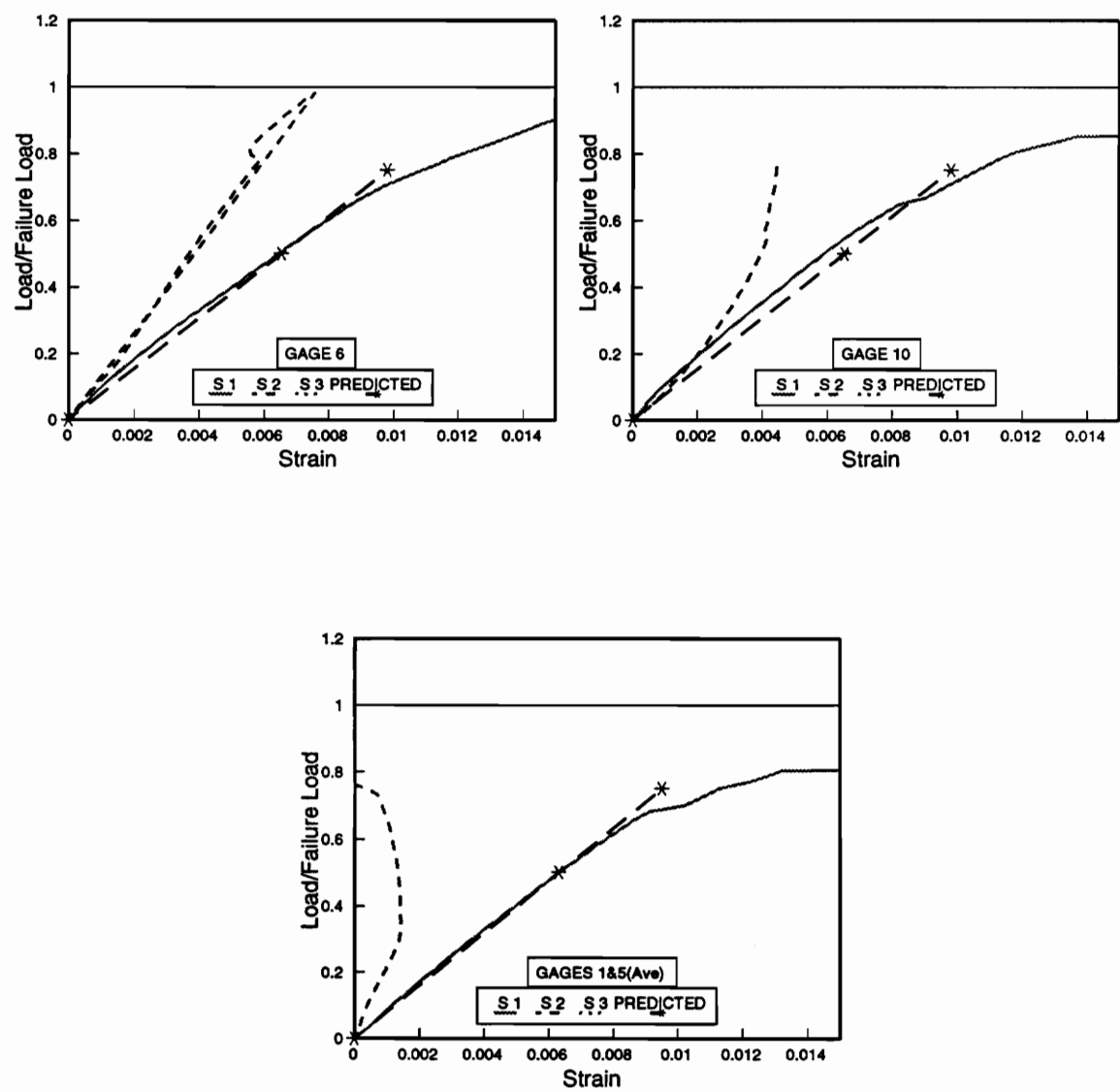


Figure B.2. Measured and predicted net-section gage strains for 7-hole T45 inboard specimens

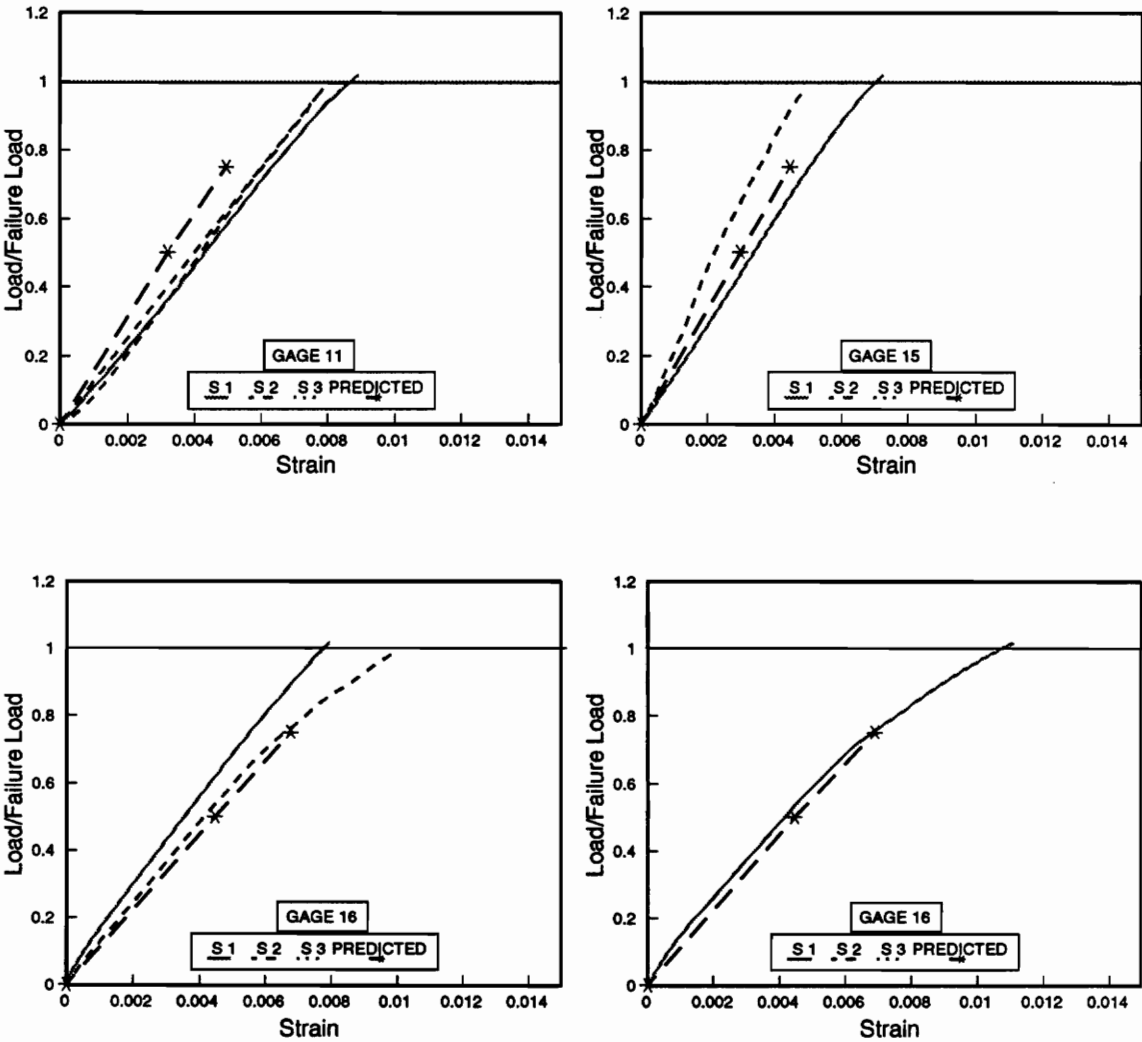


Figure B.3. Measured and predicted net-section gage strains for 7-hole T45 inboard specimens

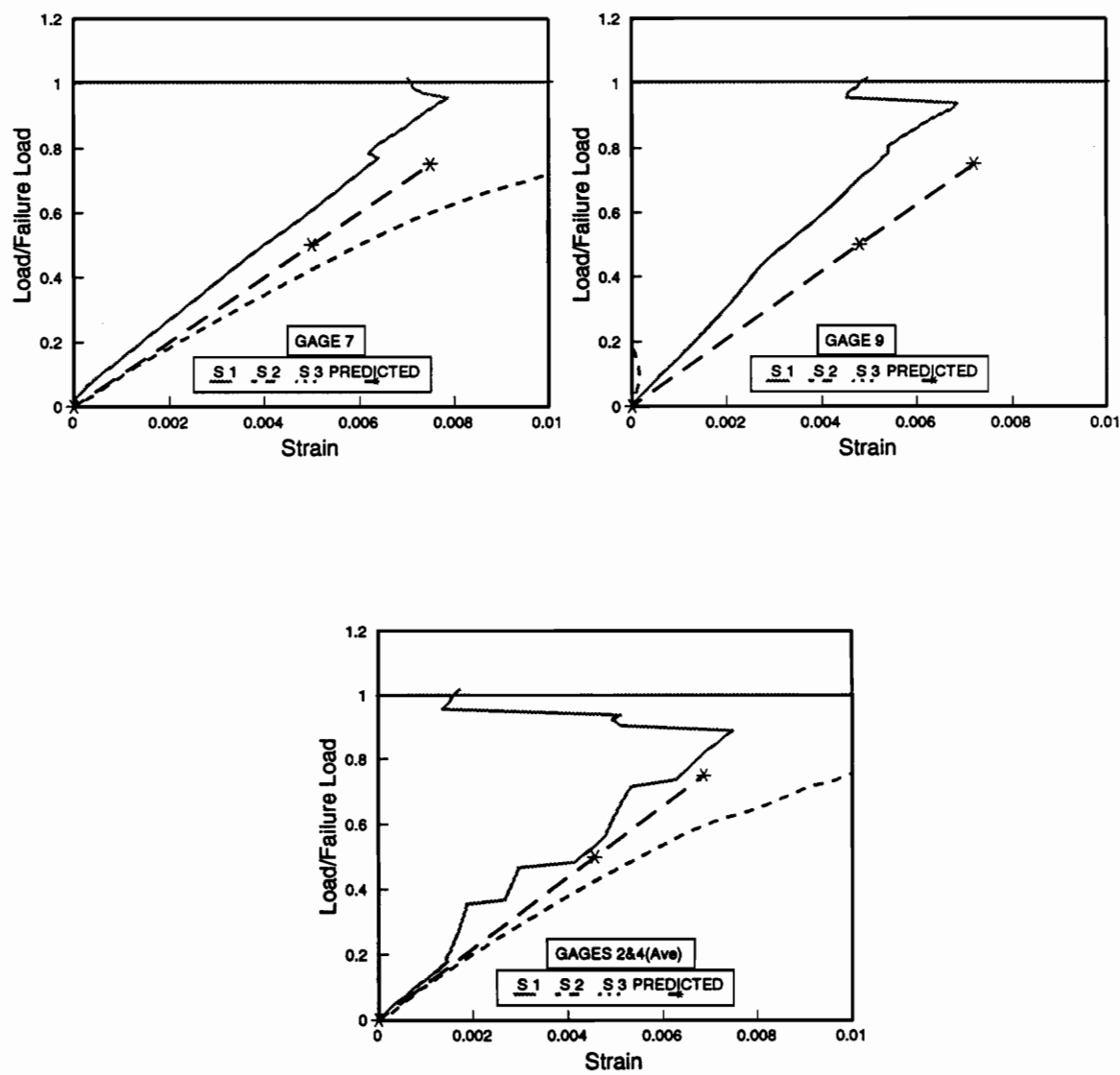


Figure B.4. Measured and predicted shear gage strains for 7-hole T45 inboard specimens

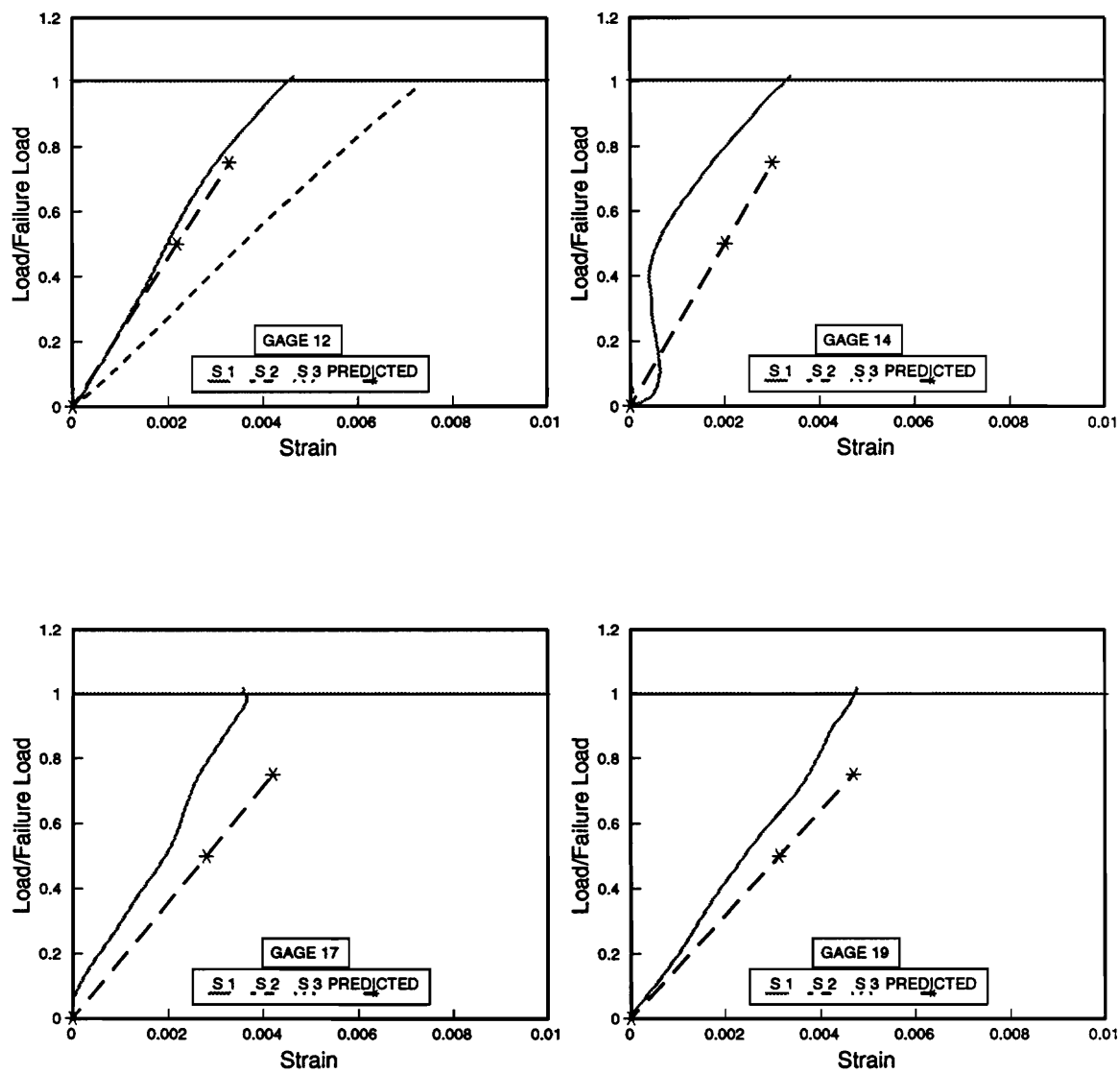


Figure B.5. Measured and predicted shear gage strains for 7-hole T45 inboard specimens

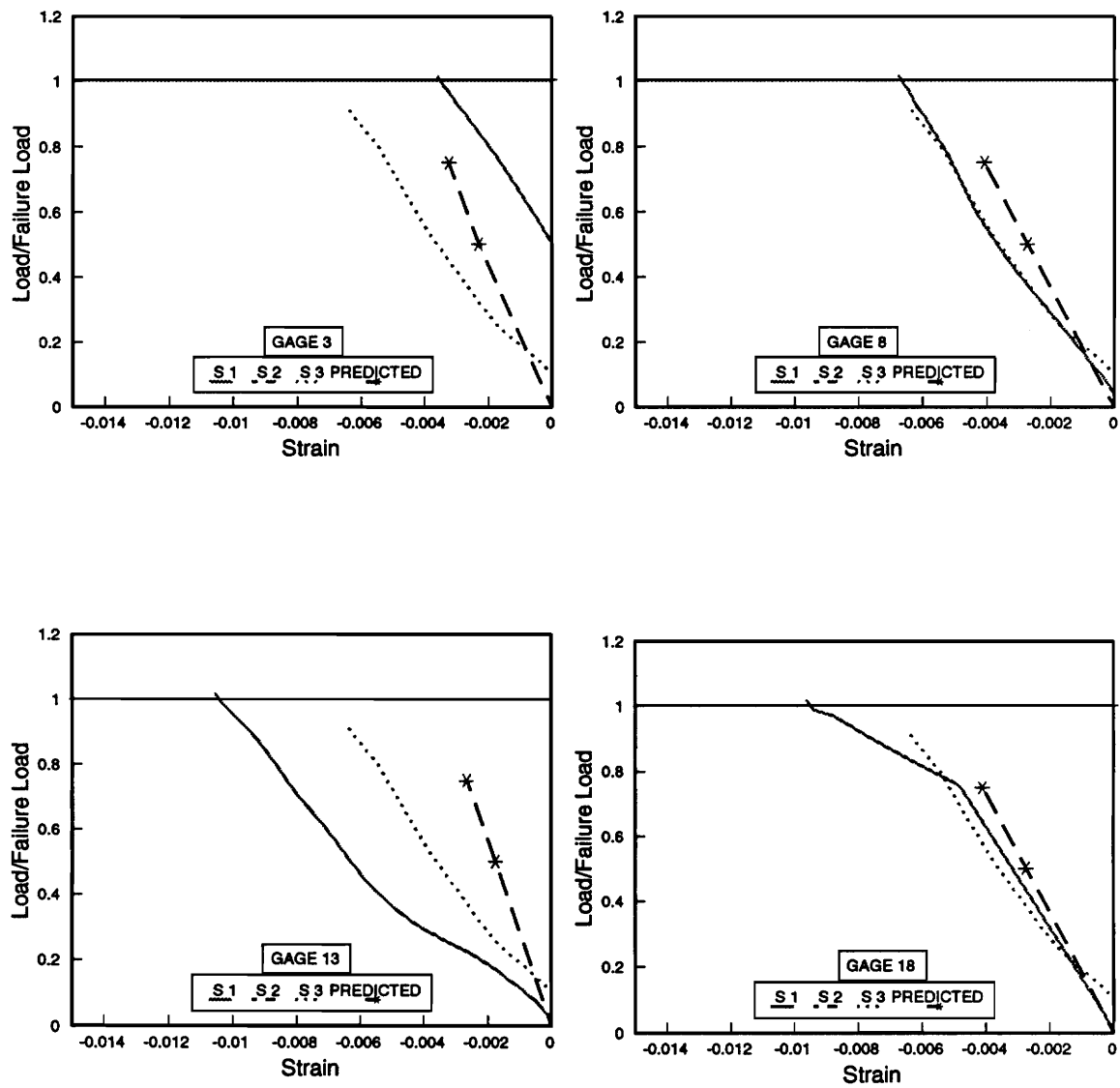


Figure B.6. Measured and predicted bearing gage strains for 7-hole T45 inboard specimens

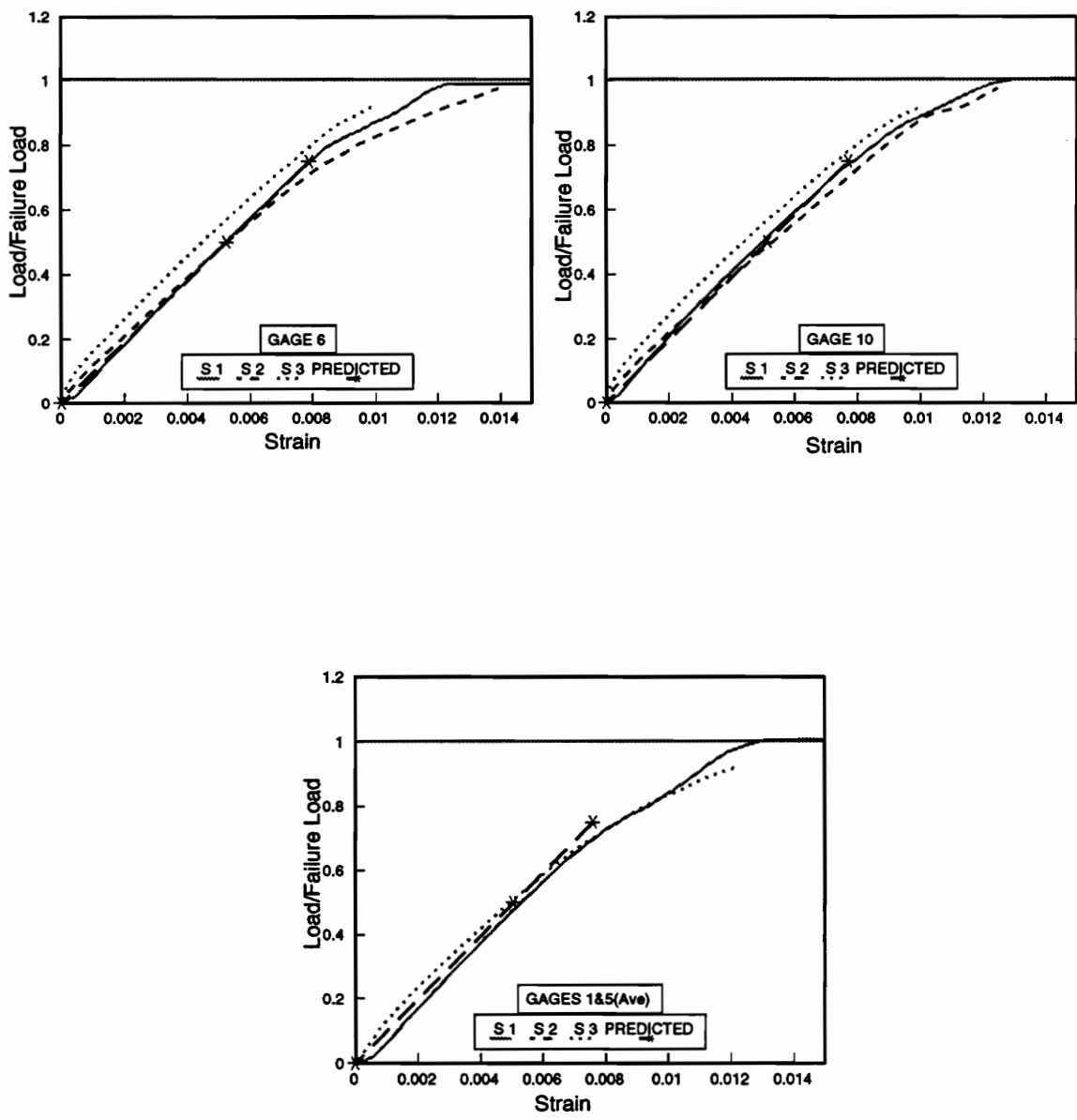
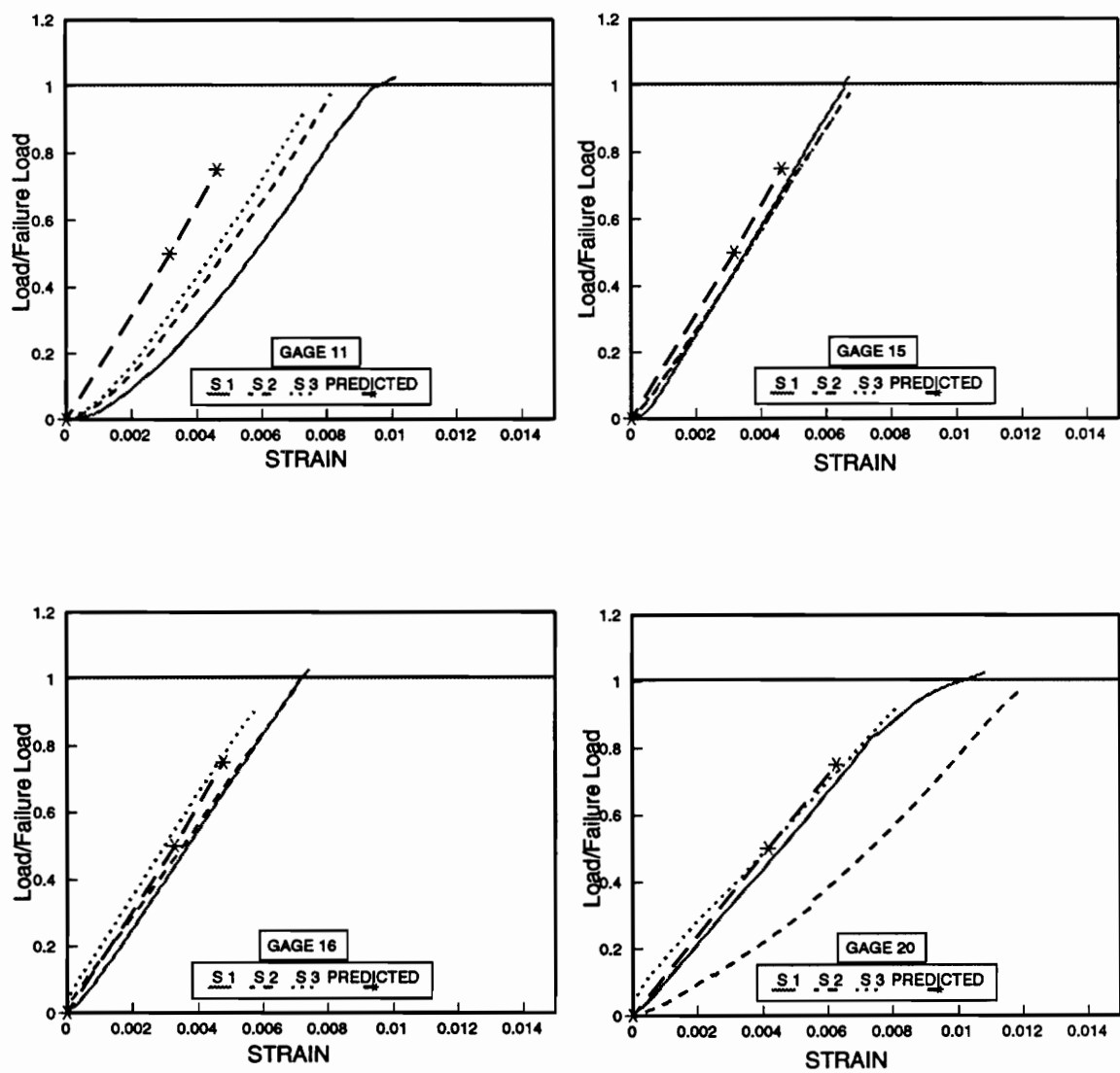


Figure B.7. Measured and predicted net-section gage strains for 7-hole T30 inboard specimens



730INet-Section Gages

Figure B.8. Measured and predicted net-section gage strains for 7-hole T30 inboard specimens

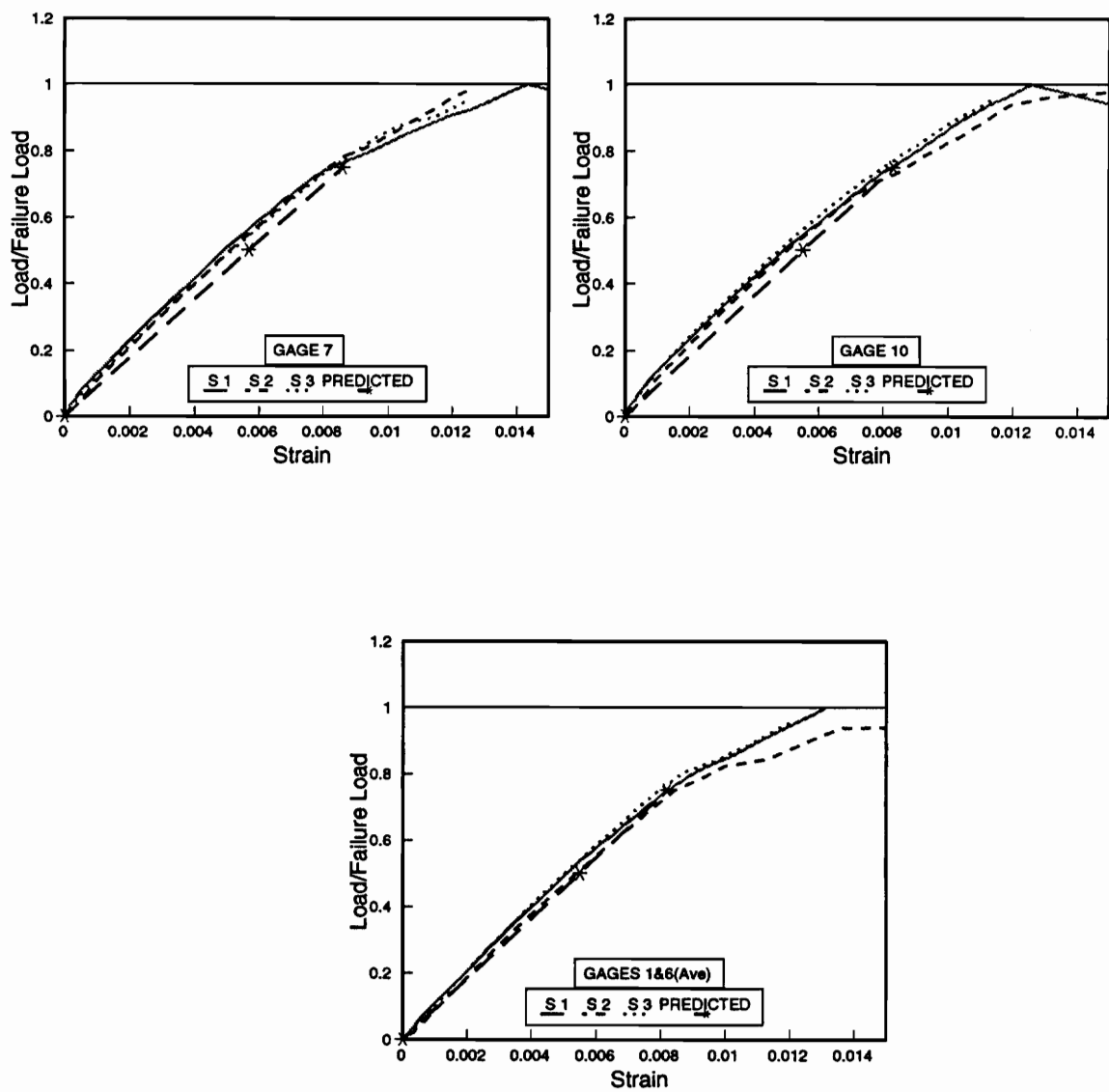


Figure B.9. Measured and predicted net-section gage strains for 7-hole T60 inboard specimens

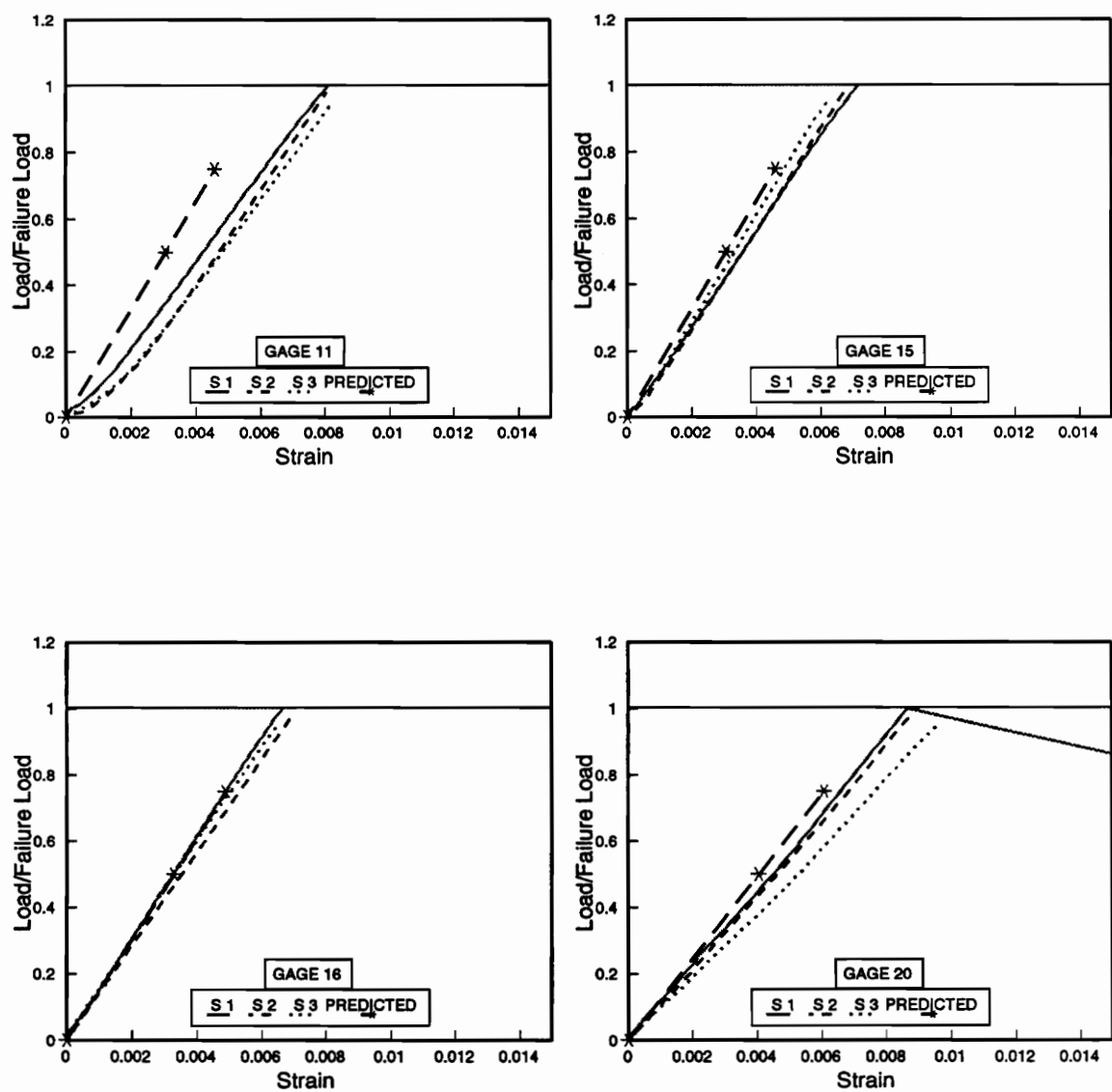


Figure B.10. Measured and predicted net-section gage strains for 7-hole T60 inboard specimens

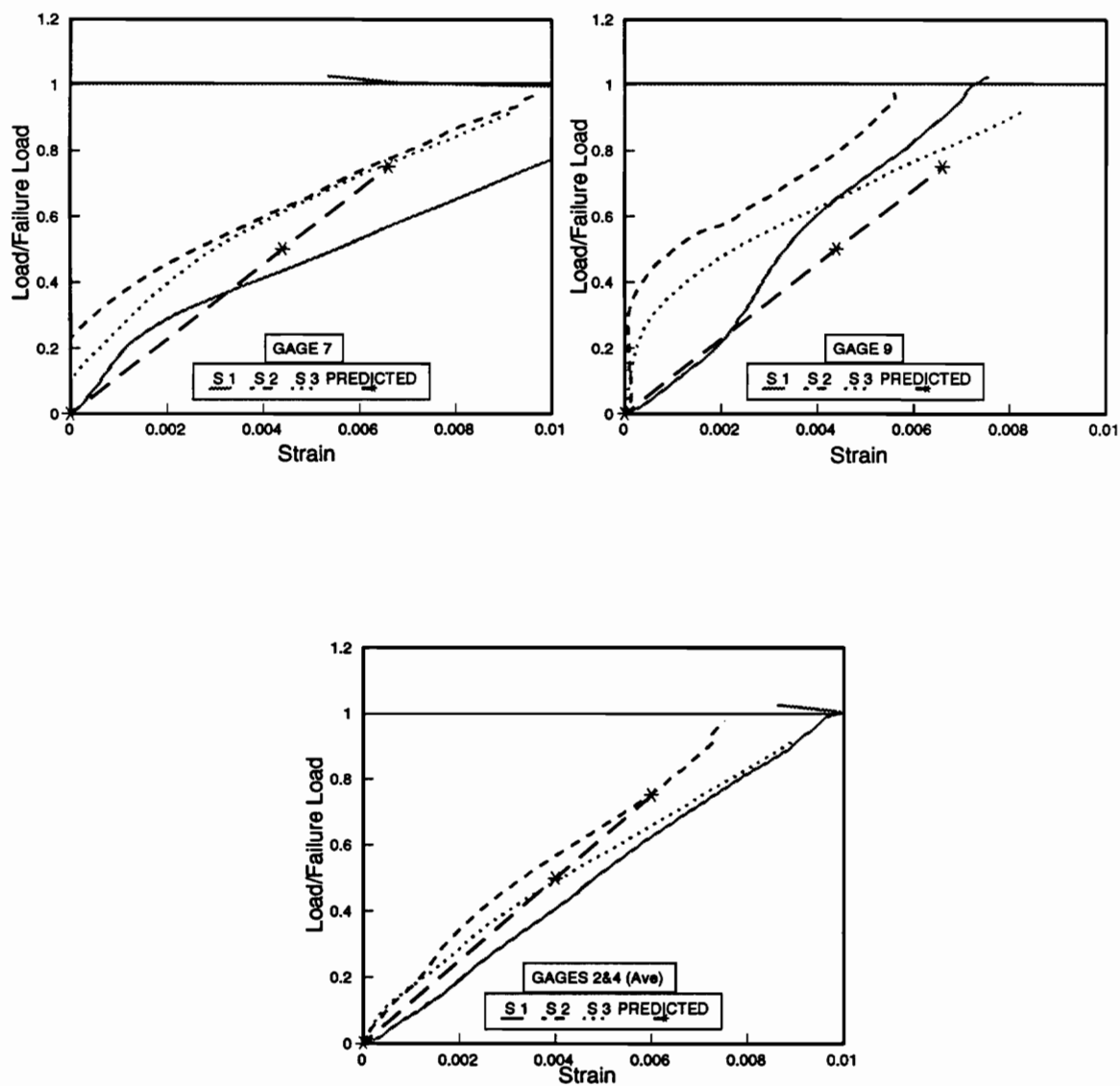


Figure B.11. Measured and predicted shear gage strains for 7-hole T30 inboard specimens

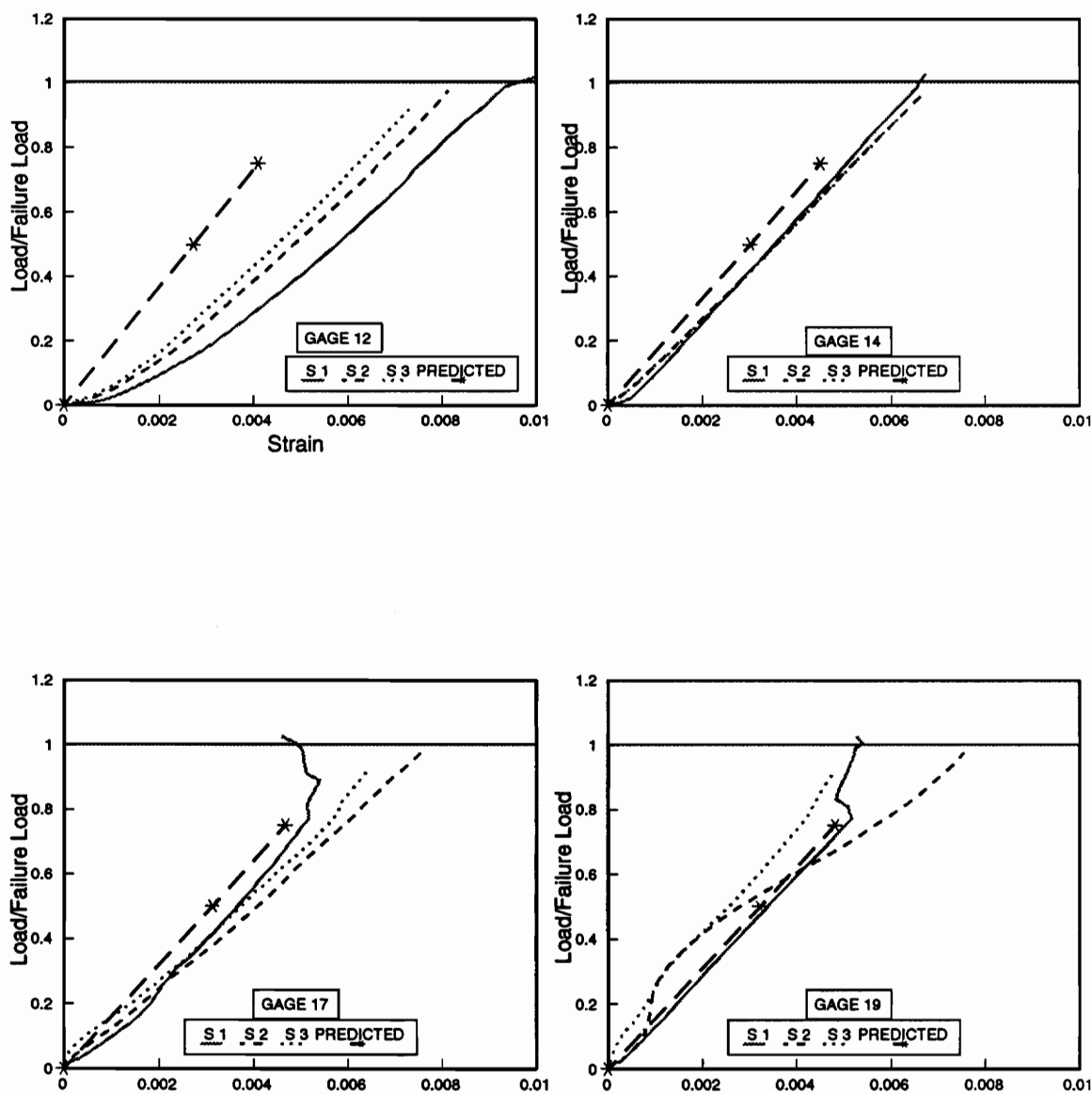


Figure B.12. Measured and predicted shear gage strains for 7-hole T30 inboard specimens

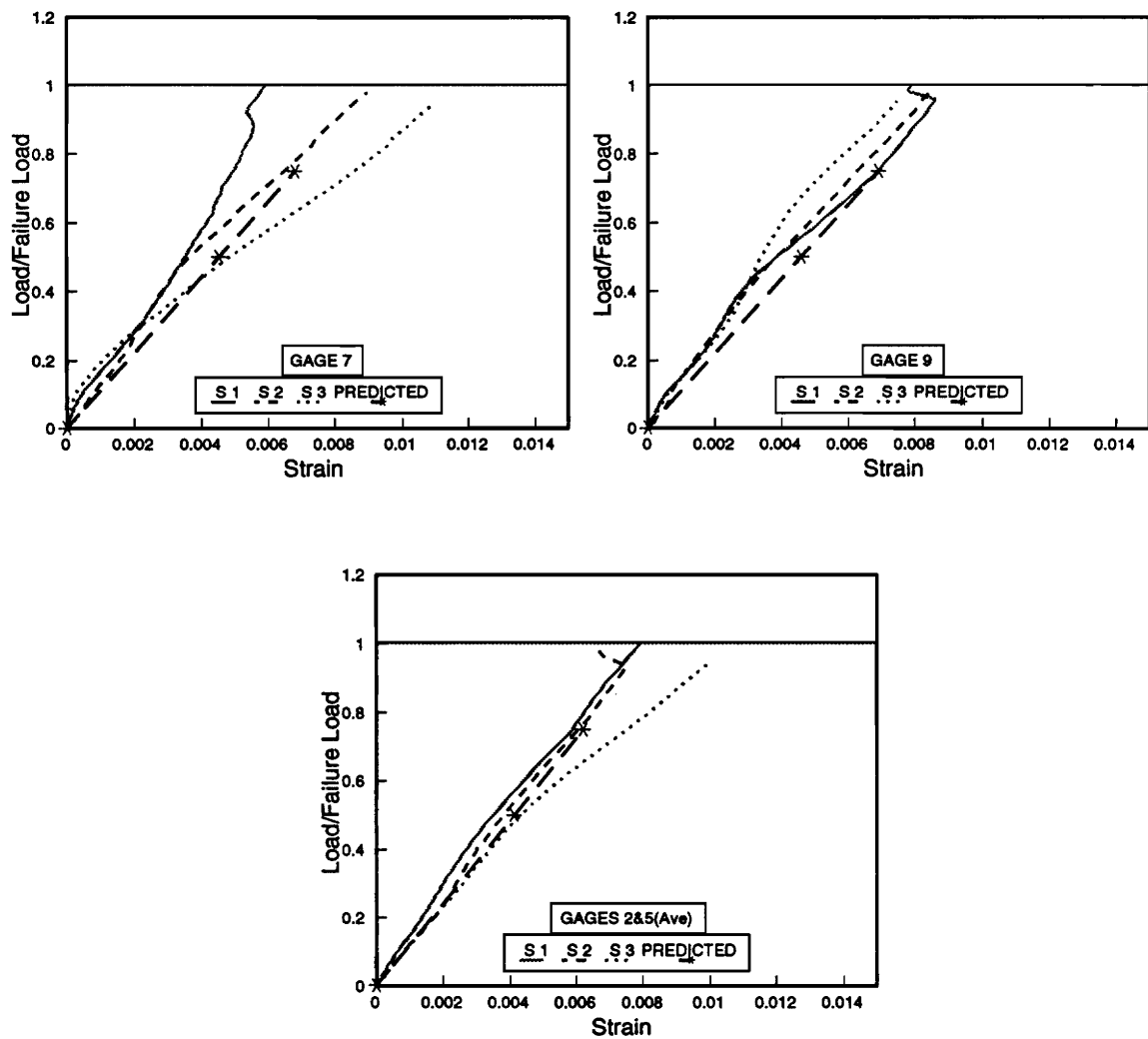


Figure B.13. Measured and predicted shear gage strains for 7-hole T60 inboard specimens

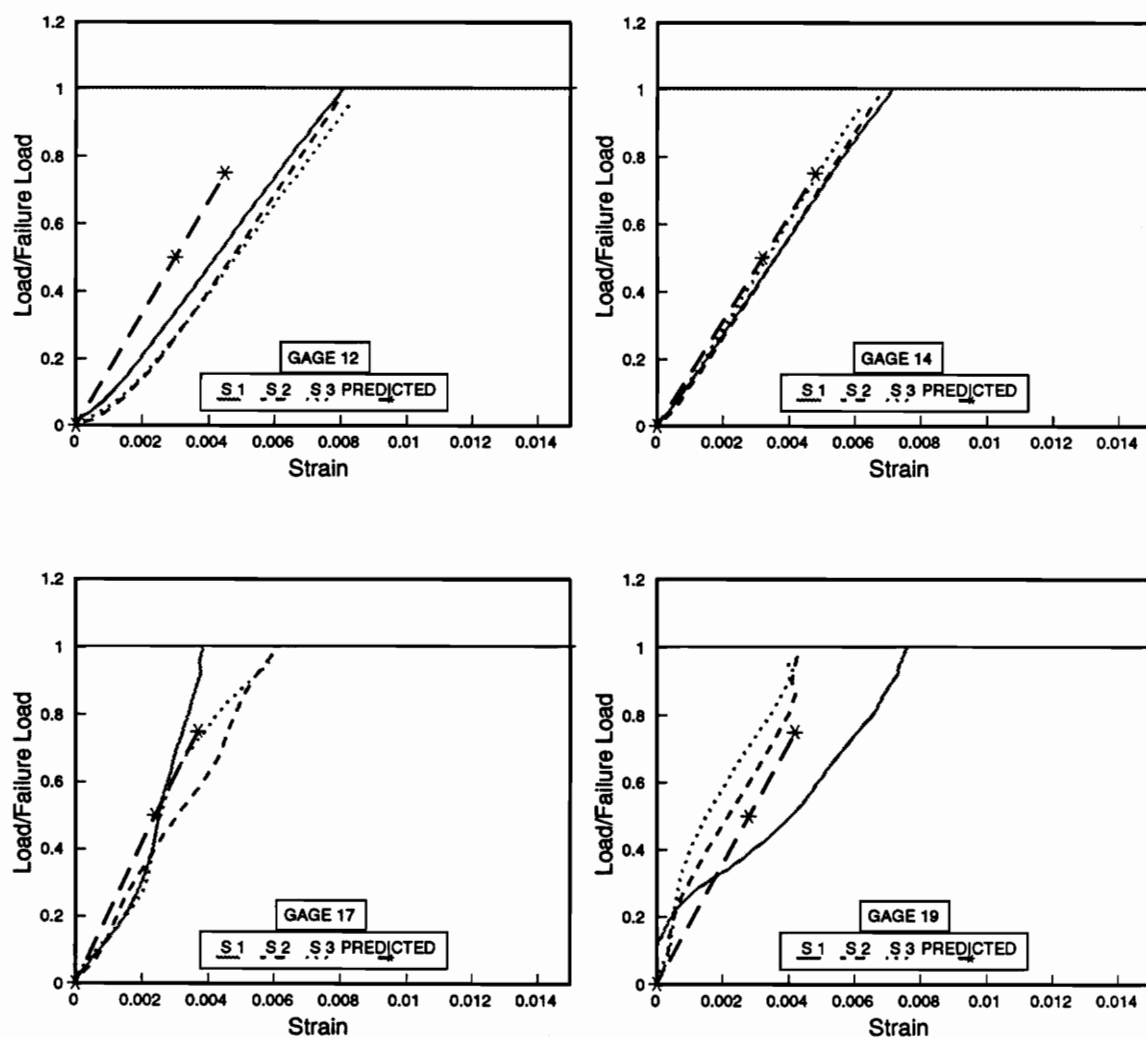


Figure B.14. Measured and predicted shear gage strains for 7-hole T60 inboard specimens

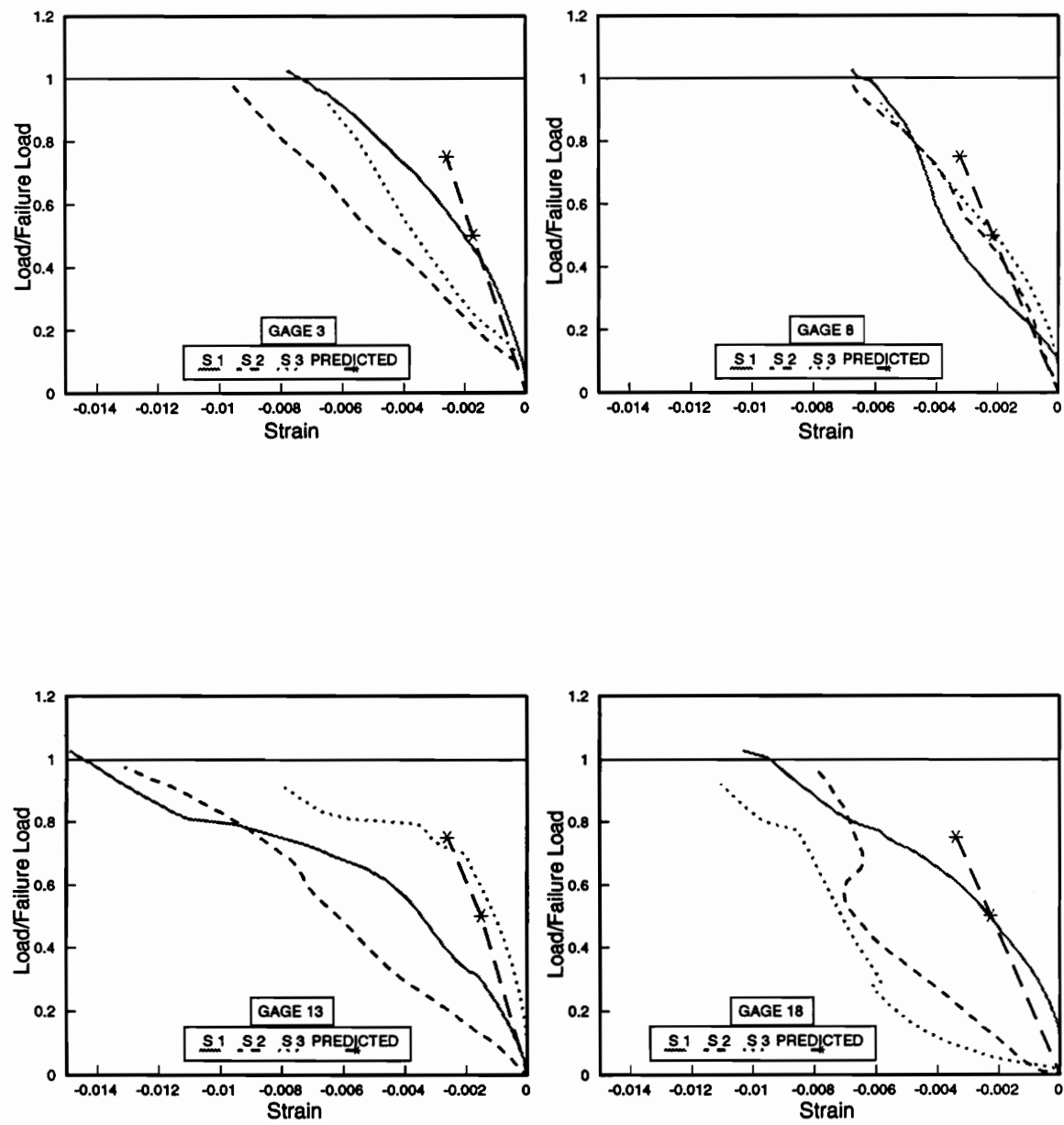


Figure B.15. Measured and predicted bearing gage strains for 7-hole T30 inboard specimens

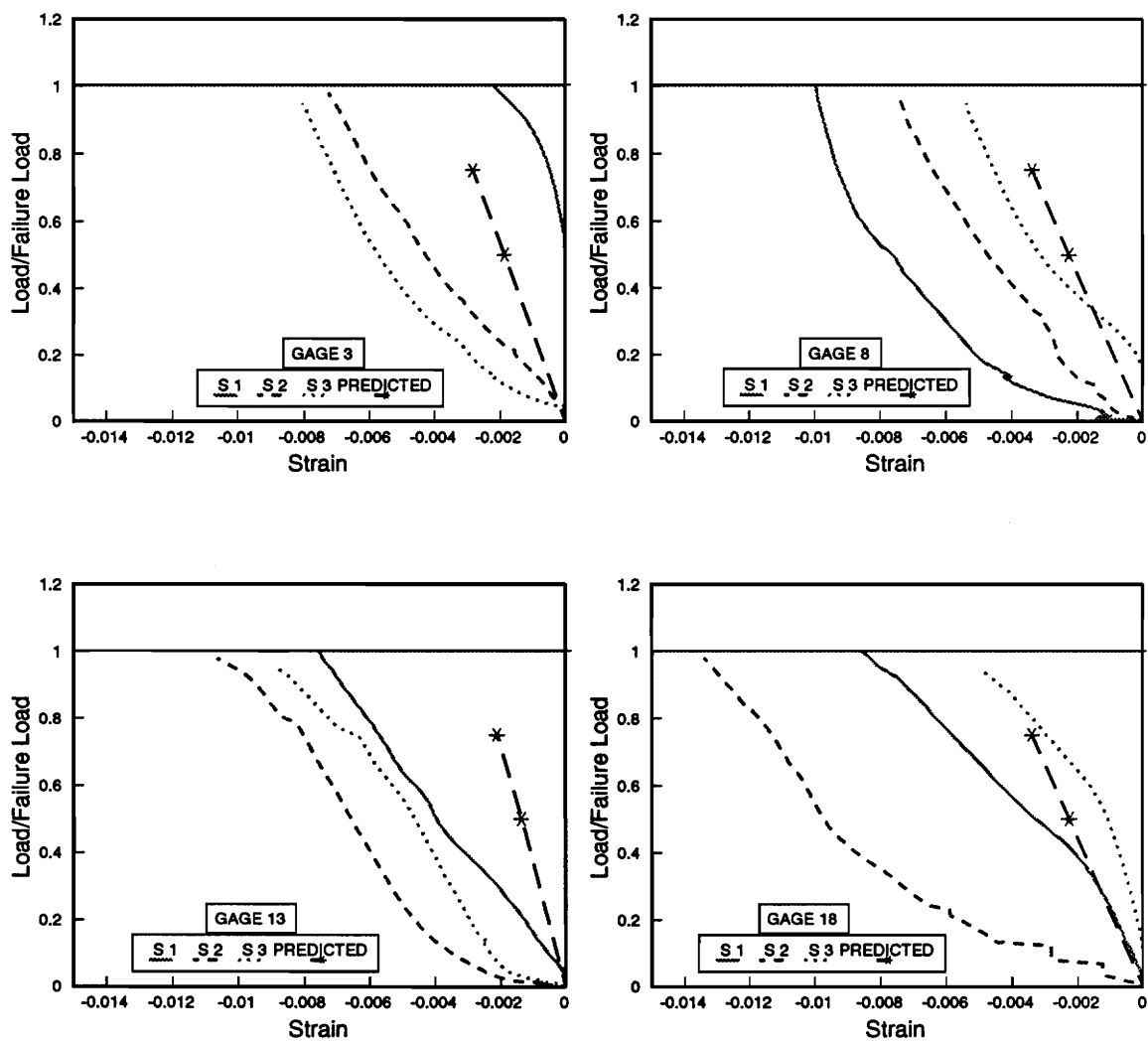
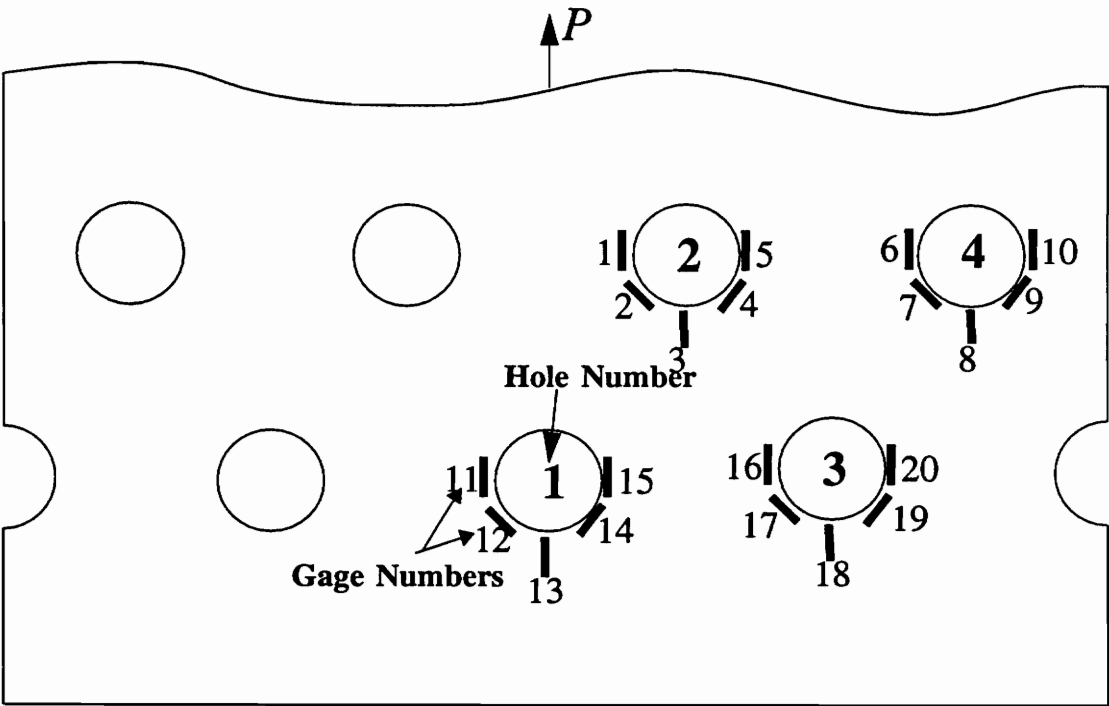


Figure B.16. Measured and predicted bearing gage strains for 7-hole T60 inboard specimens



7-Hole Outboard Specimen

Figure B.17. Strain gage numbering scheme for 7-hole outboard specimens

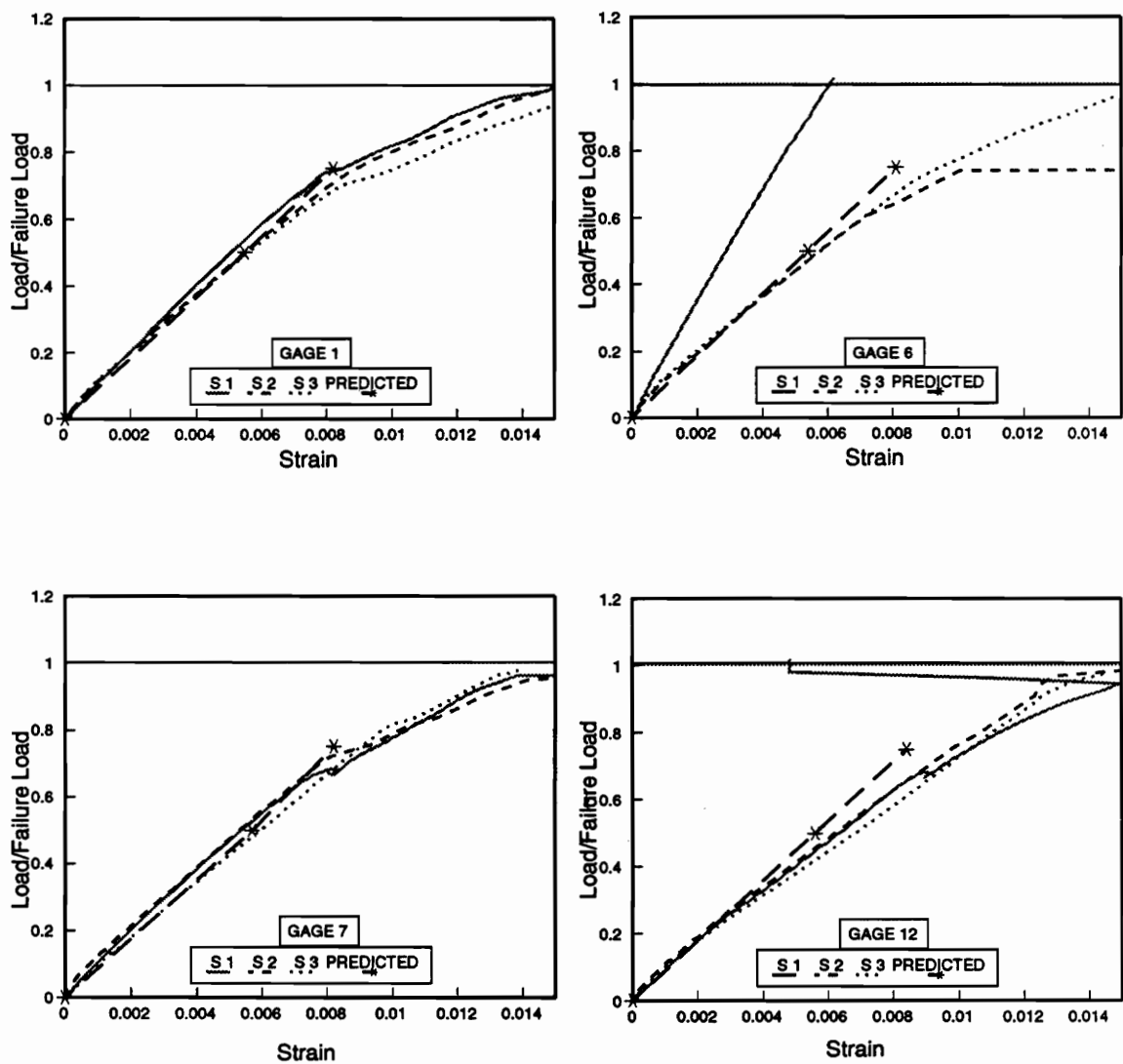


Figure B.18. Measured and predicted net-section gage strains for 7-hole T45 outboard specimens

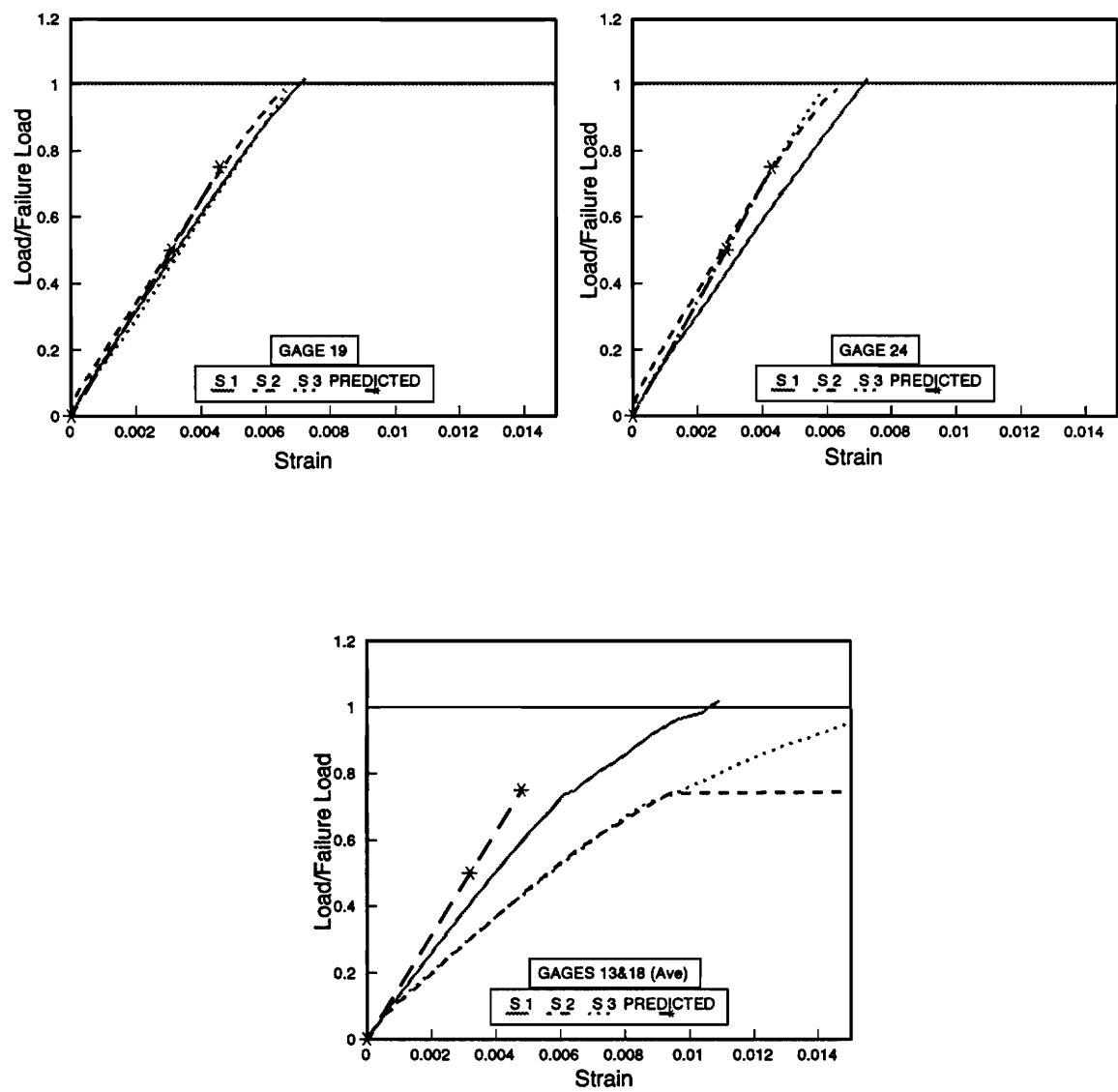


Figure B.19. Measured and predicted net-section gage strains for 7-hole T45 outboard specimens

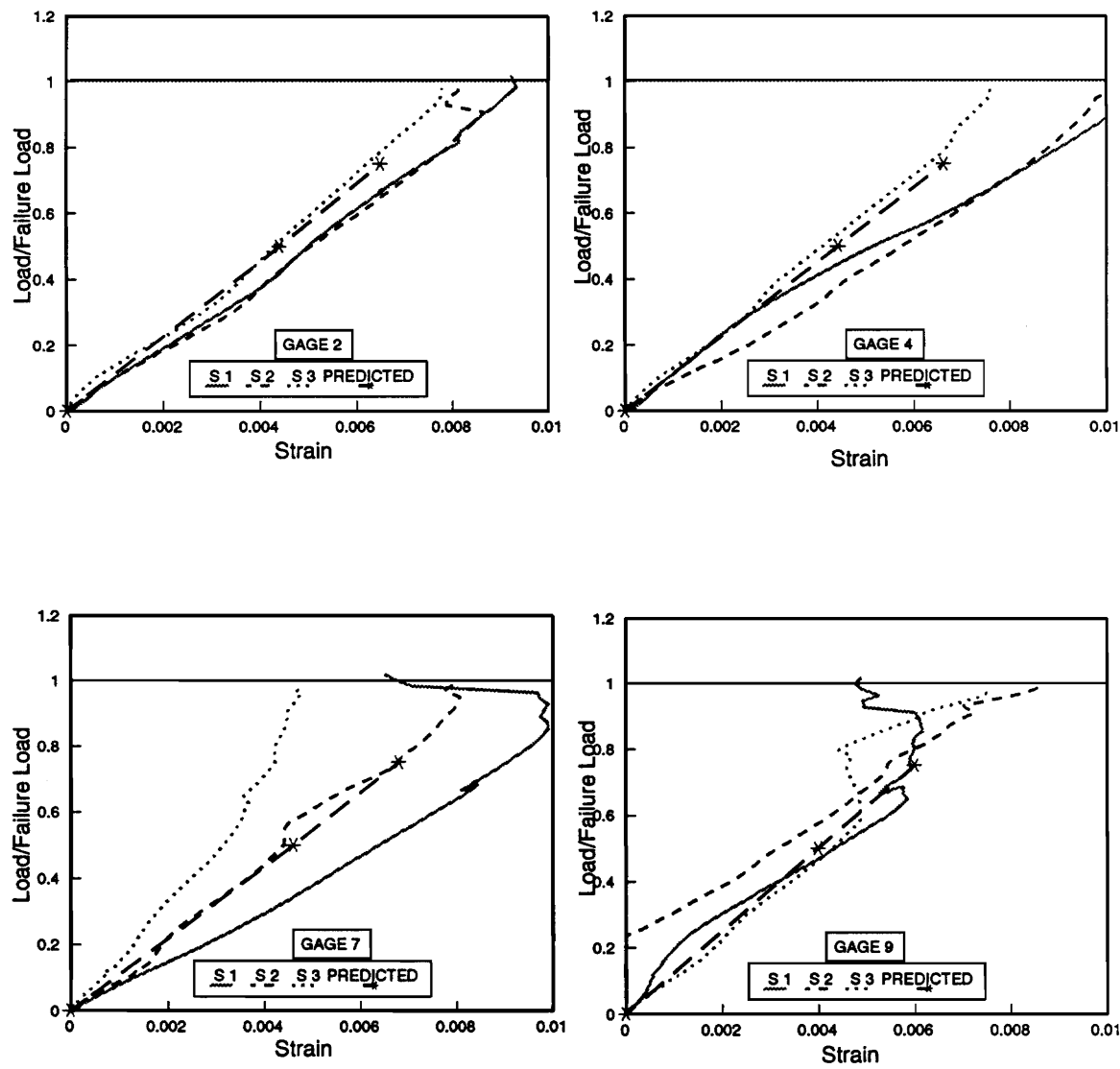


Figure B.20. Measured and predicted shear gage strains for 7-hole T45 outboard specimens

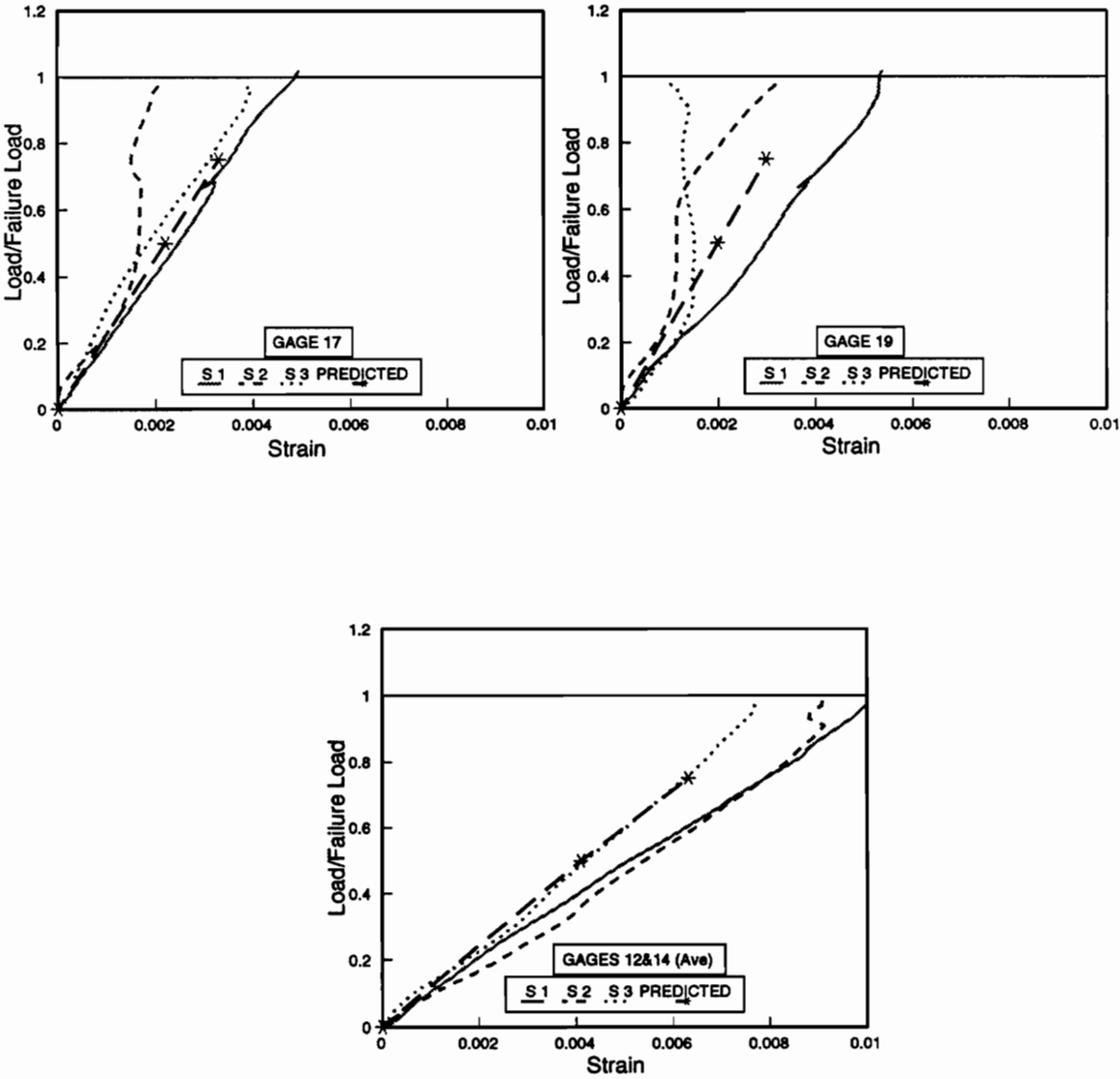


Figure B.21. Measured and predicted shear gage strains for 7-hole T45 outboard specimens

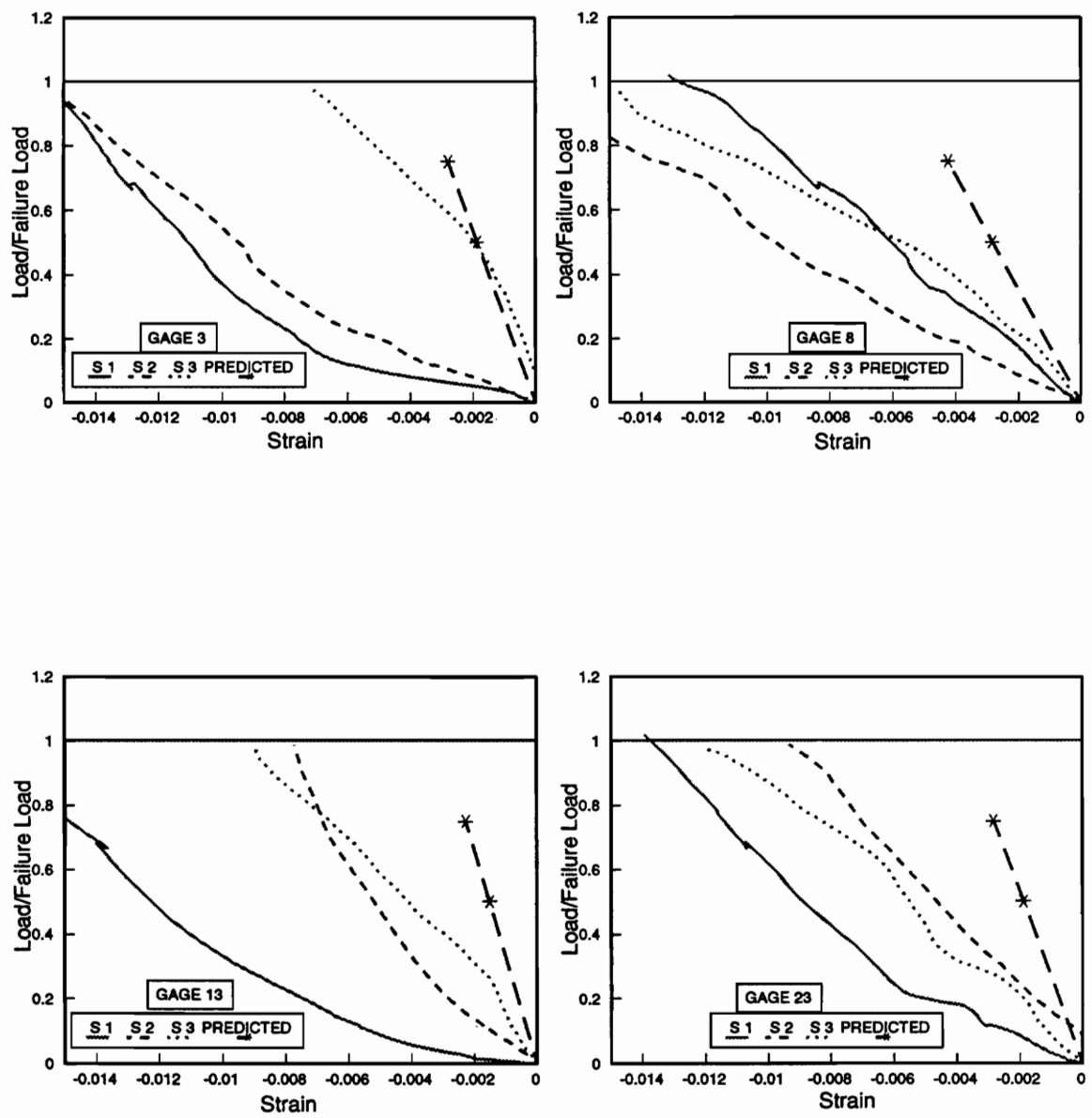
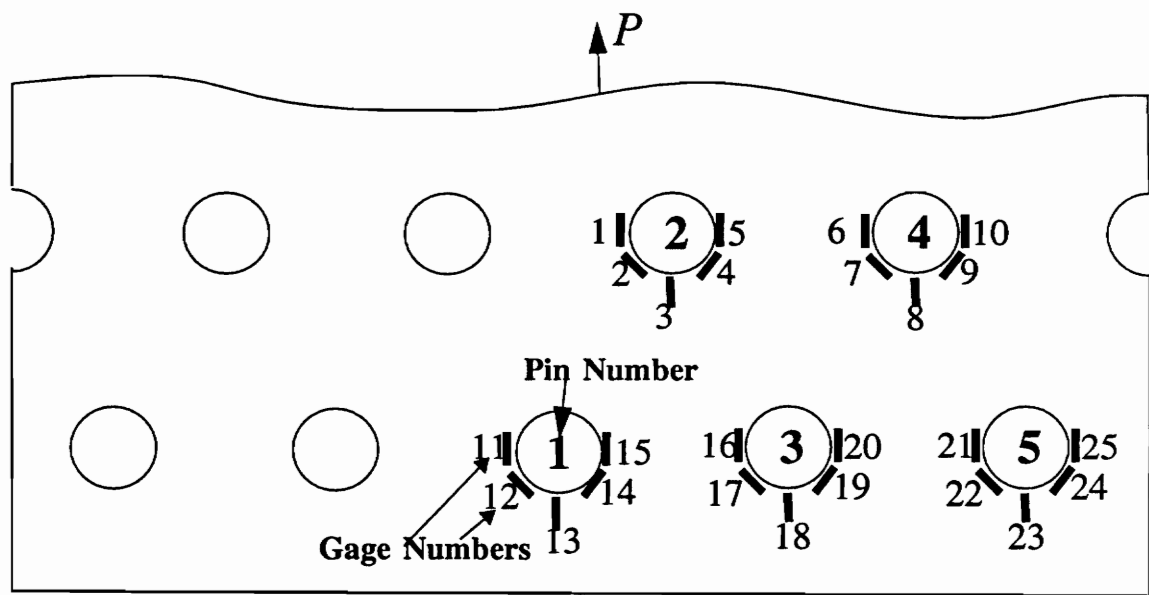


Figure B.22. Measured and predicted bearing gage strains for 7-hole T45 outboard specimens

APPENDIX C: STRAIN GAGE RESULTS FOR THE 9-HOLE SPECIMENS

The strain gage results for the 9-hole specimens are presented in the following pages. The strain gage numbering scheme for the 9-hole inboard specimens, the only kind of 9-hole specimen that was tested, is shown in fig. C.1. Also, only specimens of the T45 laminate were tested for the 9-hole joint. Hence the results shown here are only for T45 laminate. The load vs. strain relations for net-section gages are shown in fig.s C.2, C.3, while the same relations for shear gages are shown in figs. C.4 and C. 5. Finally the relations between strain and load for bearing gages are shown in fig. C.6.



9-Hole Inboard Specimen

Figure C.1. Strain gage numbering scheme for 9-hole T45 inboard specimens

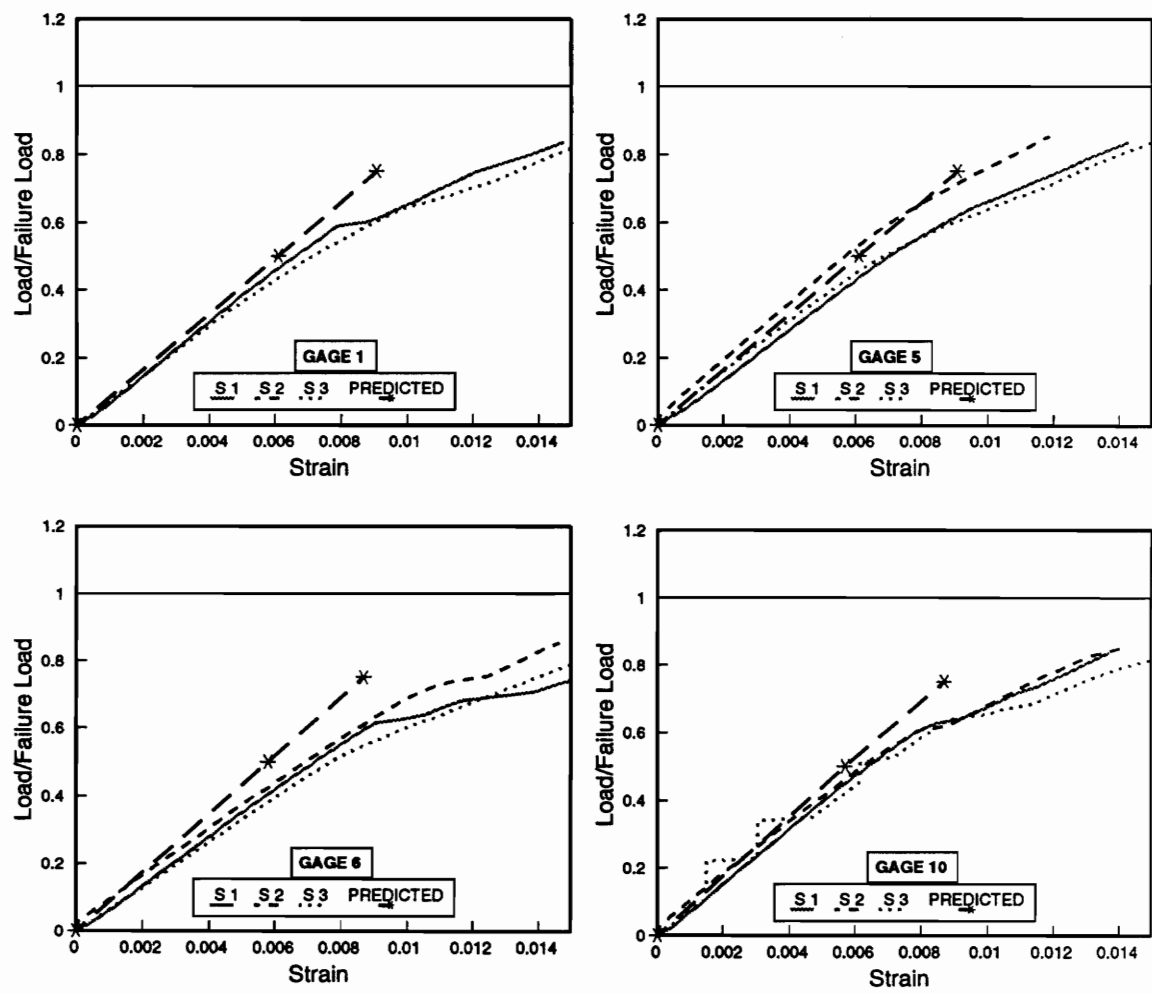


Figure C.2. Measured and predicted net-section gage strains for 9-hole T45 inboard specimens

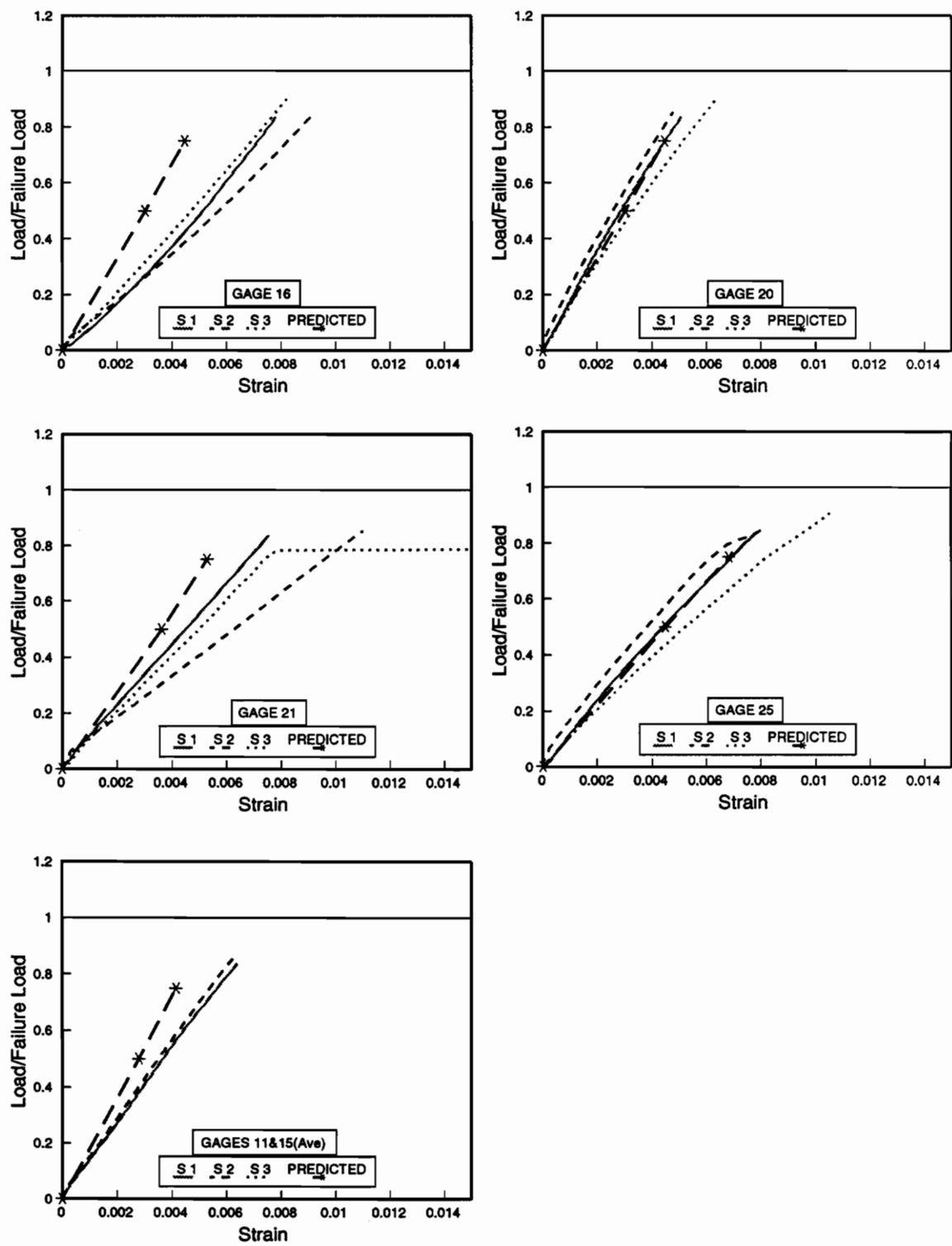


Figure C.3. Measured and predicted net-section gage strains for 9-hole T45 inboard specimens

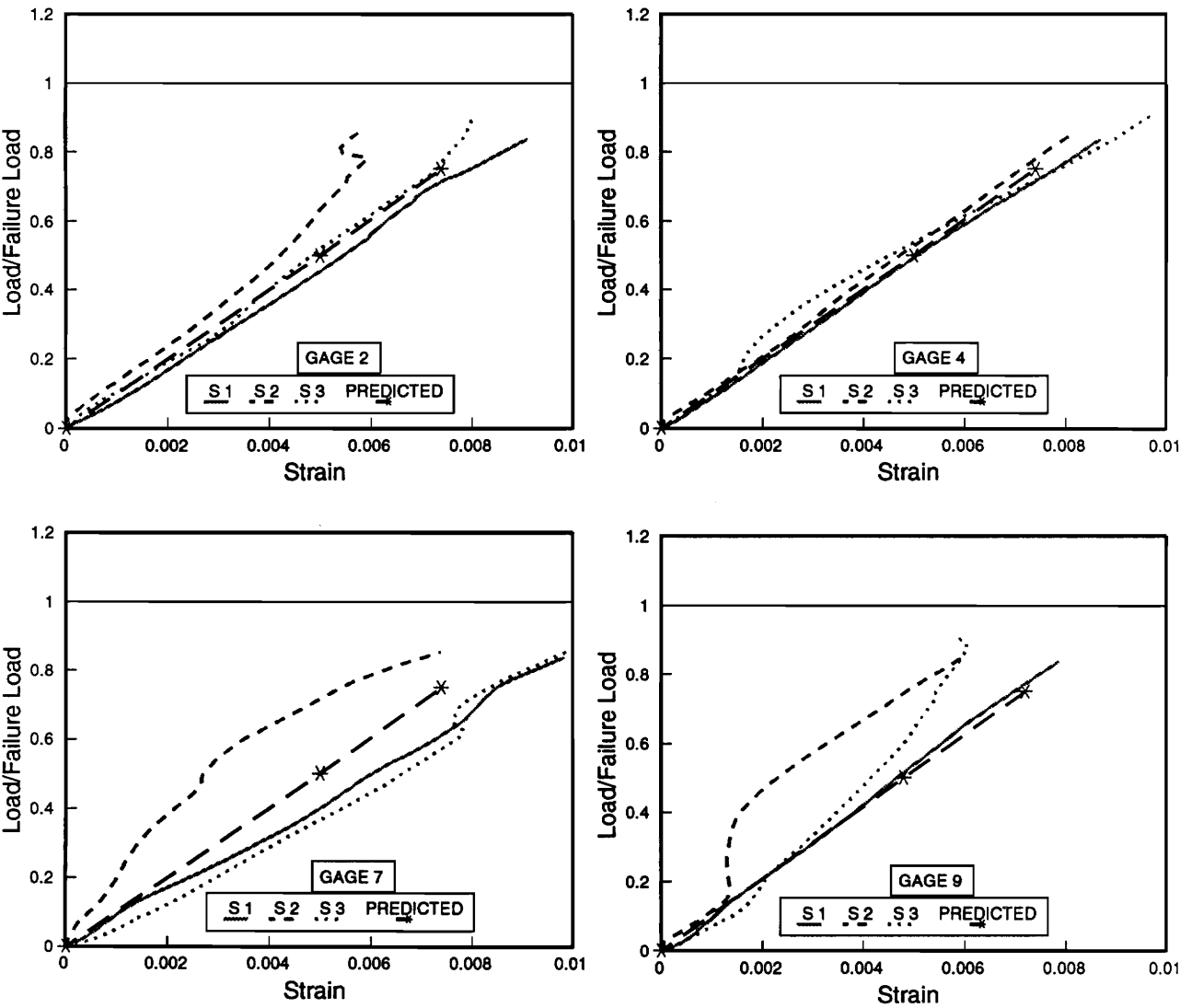


Figure C.4. Measured and predicted shear gage strains for 9-hole T45 inboard specimens

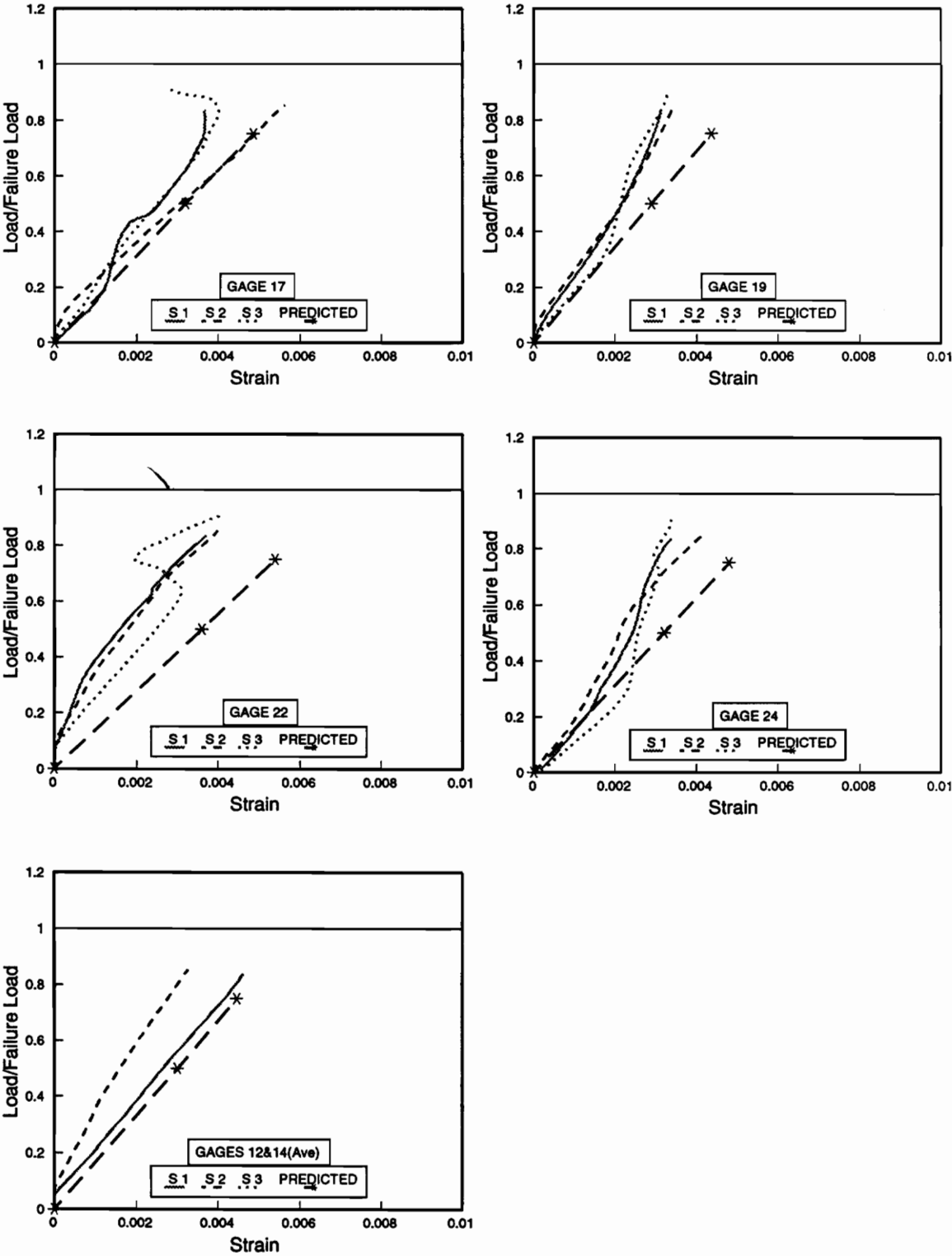


Figure C.4. Measured and predicted shear gage strains for 9-hole T45 inboard specimens

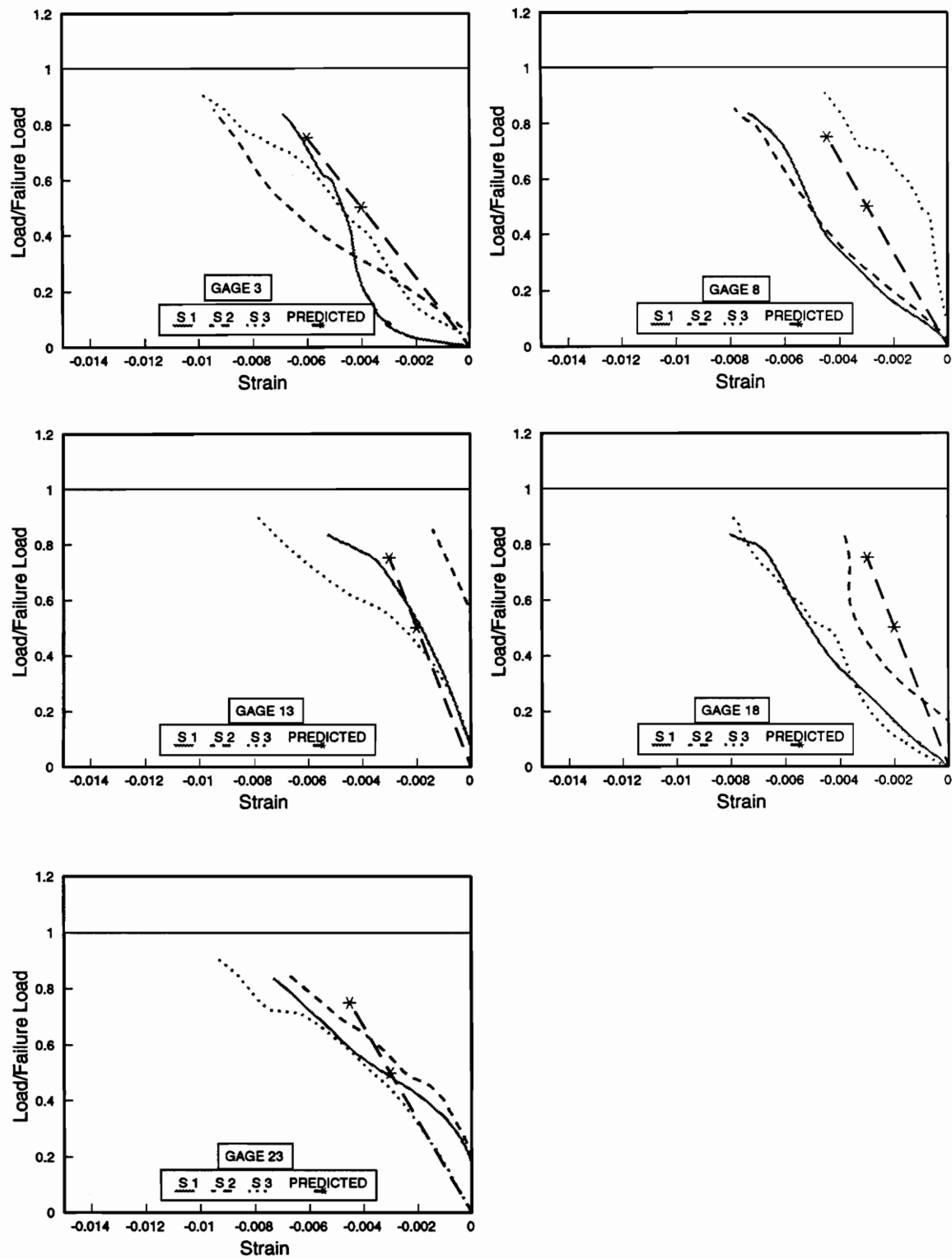


Figure C.5. Measured and predicted bearing gage strains for 9-hole T45 inboard specimens

Vita

Seshu Yalamanchili, the son of Dr. Seethambaram and Mrs. Kamala Yalamanchili, was born at Gudiwada in Andhra Pradesh, India on August 23, 1968. He graduated with a bachelor's degree in Mechanical Engineering from J. Nehru Technological University in Hyderabad, India in 1989. Mr. Yalamanchili received National Merit Scholarship in India for the entire period of higher education. He started his graduate study in Fall 1989 at Virginia Tech and graduated with M.S. in May 1992. He received an award for graduate research excellence from the College of Engineering of Virginia Tech in April 1992.

S.R. Yalamanchili